

Alma Mater Studiorum – Università di Bologna

DOTTORATO DI RICERCA IN  
**INGEGNERIA CIVILE, AMBIENTALE  
E DEI MATERIALI**

Ciclo XXVII

**Settore Concorsuale di afferenza:** 08/B3

**Settore Scientifico disciplinare:** ICAR/09

A LOW-DAMAGE RETROFITTING SOLUTION  
BASED ON CARBON-WRAPPED STEEL TUBES FOR BEAM-COLUMN  
FRICTION CONNECTIONS OF EXISTING PRECAST RC STRUCTURES

**Presentata da:**        **ANDREA VITTORIO POLLINI**

**Coordinatore Dottorato**

**Prof. Alberto Lamberti**

**Relatore**

**Prof. Claudio Mazzotti**

**Correlatore**

**Dr. Nicola Buratti**

**Esame finale anno 2016**

## ABSTRACT

The 2012 Emilia earthquakes caused significant damages to existing precast RC structures. These buildings were found being extremely vulnerable because, being designed for vertical loads only, they featured friction-based connections between structural elements, and in particular between beams and columns. Given the large diffusion of these structures as industrial buildings, and consequently the high social and economic impact of damages, their retrofit is critical. Various techniques have been proposed in the literature; in most of them friction-based connections are removed by inserting mechanical connectors that will make beam-column connections hinged. These approaches lead to a significant increase of the base shear and therefore often require strengthening of columns and foundations.

The research presents dissipative devices based on carbon-wrapped steel tubes to be used as an alternative low-damage solution for the retrofit of beam-column friction connections able to minimize structural damages.

Firstly, the study presents results of experimental tests on the devices and discusses their innovative energy absorption mechanism and dissipative behaviour.

Then, numerical analyses carried on to investigate the effectiveness of the introduction of dissipative devices in beam-column connections of precast structures are presented. Incremental Dynamic Analyses have been performed in order to evaluate an equivalent behaviour factor for structures with dissipative devices, by comparing the seismic response of simple frame structures with dissipative connections with equivalent elastic systems. Findings of numerical investigation show how the introduction of the dissipative devices in friction-based joints provides an effective connection between structural elements and, in addition, the capability to reduce forces transmitted to the columns, improving the seismic behaviour of the entire structure.

Finally, a simplified approach to evaluate an equivalent behaviour factor for a structure equipped with dissipative devices in friction-based beam-column joints is proposed.

### Keywords

Precast RC buildings, industrial buildings, friction connections, fuse restraint, dissipative device, energy absorption, anti-seismic device, carbon fibre, seismic retrofitting, low-damage, behaviour factor evaluation

## ACKNOWLEDGMENTS

First of all, I want to express my gratitude to Prof. Claudio Mazzotti for his continuous guidance and brilliant suggestions during the entire period of my research work. I want to thank him especially for the continuous encourage to pursuit new targets and for his technical and human skills that made me really appreciate the fascination to carry on a research activity. Special thanks to Nicola Buratti for his fundamental contribution in sharing ideas, discussing research results and for his constant help in solving research issues, especially concerning numerical investigations.

I want to sincerely thank Prof. Marco Savoia for his special contribution in terms of innovative ideas to the development of the research, especially at the beginning of the activities.

I'm thankful to all Department researchers at the University of Bologna to have let me experience working in a stimulating research environment.

I'm grateful to Eng. Dario Comand and Luca Pirazzini for the technical support provided, sharing their deep knowledge about composite materials, and for the confidence they relied on me about this research project.

Finally, really special thanks to my friends, my parents and my wife for their continuous support during all the new challenges of these last years and of all my life.

---

# TABLE OF CONTENTS

ABSTRACT .....	i
ACKNOWLEDGMENTS.....	ii
TABLE OF CONTENTS .....	iii
<b>1. INTRODUCTION .....</b>	<b>1</b>
1.1 Background and motivation .....	1
1.2 Aim of the research.....	3
1.3 Organisation of the dissertation .....	4
<b>2. SEISMIC BEHAVIOUR OF PRECAST RC STRUCTURES.....</b>	<b>6</b>
2.1 Wide use of single-storey precast RC structures in industrial buildings.....	6
2.2 Main typologies and characteristics of precast buildings.....	9
2.3 Connections between precast structural elements.....	19
2.4 Main sources of seismic vulnerability in precast structures.....	23
2.5 Code’s evolution concerning precast structures.....	30
<b>3. EMILIA EARTHQUAKES – REVIEW OF DAMAGES.....</b>	<b>35</b>
3.1 20 <sup>th</sup> and 29 <sup>th</sup> May 2012 events .....	35
3.2 Economic impact .....	42
3.3 Review of damages .....	47
3.4 Seismic behaviour of connections.....	53
3.4.1 Friction-based connections.....	54
3.4.2 Pinned connections.....	60
3.5 Seismic behaviour of columns .....	62
3.6 Seismic behaviour of precast panels .....	67
<b>4. FRICTION-BASED CONNECTIONS .....</b>	<b>72</b>
4.1 Seismic vulnerability of friction-based connections .....	72
4.2 Strengthening solutions.....	78
4.3 The proposed retrofitting solution.....	81
4.4 Dissipation energy mechanism .....	82

TABLE OF CONTENTS

---

5. EXPERIMENTAL TESTS .....	85
5.1 Materials and specimens .....	85
5.2 Quasi-static tests .....	86
5.2.1 Experimental setup.....	86
5.2.2 Dissipative behaviour under compressive loading .....	87
5.2.3 Experimental results.....	90
5.3 Cyclic tests.....	93
5.4 Impact tests .....	95
6. NUMERICAL MODELING .....	97
6.1 Behaviour of dissipative connection .....	97
6.2 Structural typologies of case studies .....	101
6.2.1 Ultimate chord rotation of columns.....	105
6.3 Seismic input definition .....	113
6.4 Preliminary nonlinear dynamic analyses .....	120
6.5 OpenSees structural model.....	124
7. EVALUATION OF BEHAVIOUR FACTOR USING IDA.....	137
7.1 Columns performing linear elastic behaviour .....	138
7.1.1 IDA results – 2012 Emilia earthquakes ground motions.....	138
7.1.2 IDA results - PEER database ground motions.....	143
7.2 Columns performing nonlinear behaviour .....	150
7.2.1 IDA results – PEER database ground motions.....	151
7.2.2 Comparison between dissipative and hinged connections.....	156
7.3 Simplified approach for behaviour factor evaluation.....	162
8. CONCLUSIONS.....	175
APPENDIX A .....	178
LIST OF FIGURES.....	209
LIST OF TABLES .....	219
REFERENCES.....	222

---

# 1. INTRODUCTION

## 1.1 Background and motivation

In Italy, precast structures have been widely used for industrial buildings since the 70s. According to the annual report of the Italian Revenue Agency (2012) on the Italian real estate market and stock of non-residential buildings, there are about 700.000 industrial buildings. Most of them are realised using precast reinforced concrete (RC) elements. As an example, Nuti and Vanzi (2014) showed that approximately 70% of the industrial buildings are precast RC structures. The most common typology of precast industrial buildings consists in single-storey statically-determined frame structures with socket foundations.

The behaviour under seismic actions of these structures (Bellotti et al. 2014), is typically characterised by great flexibility and large displacements. In fact, most of the mass is located at the roof level, columns are very slender and beam-column connections are at best hinged.

The earthquakes that struck the Emilia region (northern Italy) in May 2012 showed the large seismic vulnerability of Italian one-storey precast RC structures, designed and built without anti-seismic standards or criteria, and mainly used for industrial constructions.

Field reports after the 2012 Emilia earthquakes (Savoia et al. 2012, Liberatore et al. 2013, Bournas et al. 2013, Magliulo et al. 2014b) showed that most of the partial- and full-collapses observed were caused by the absence of effective mechanical connectors between structural elements (friction-based connections). Other vulnerabilities included insufficient longitudinal and transverse reinforcement of columns, inadequacy of the anchorages of precast cladding panels to structural elements, lack of rigid-diaphragm effect at the roof level and foundations without proper connections.

The vulnerability of structures with friction-based connections has been confirmed also by a parametric study provided by Magliulo et al. (2014b) and numerical studies (Biondini et al. 2013, Liberatore et al. 2013, Deyanova et al. 2014), showing that the vertical component of ground motion, together with the lack of connection between columns and beams, can play a significant role in the activation of collapses involving the unseating of beams.

Given the social and economic significance of industrial prefabricated structures, after May 2012, a great deal of research has been focused on developing strengthening solutions, in particular concerning the design of connections between structural elements. Most of investigated strengthening solutions are based on the introduction of steel ties, plates or cable

restraints in order to avoid sliding of the beams and therefore unseating failures (Ligabue et al. 2014, Muciaccia et al. 2014, Bournas et al. 2013, Magliulo et al. 2014a, Magliulo et al. 2014d). Since these techniques usually increase the base-shear, strengthening of the base of columns or of foundations is often required and the use of steel plates, bars or FRPs is suggested. Alternative solutions could be based on dampers (Marinini et al. 2011), but their introduction in existing precast industrial buildings can be difficult because of costs and interference with production plants.

Seismic protection of structures using anti-seismic devices is one of the most important goals of structural engineers in order to save lives and minimize damages to structures in case of earthquakes of high intensity. The possibility to reduce the effects of the seismic action and to minimize structural damages through the introduction of anti-seismic devices is particularly relevant in the seismic rehabilitation of existing industrial buildings where structural damage can determine high economic impact due to business interruption. Induced economic losses, due to the industrial business interruption, can be much more higher than direct structural damages and can have catastrophic consequences on production activities and warehouses, forcing a dislocation of business in other areas or even the bankruptcy of the business, both situations that obviously would cause a very negative economic and social impact on local territory. As an example, the Emilia earthquakes caused direct economic losses amounting to about €2.7 billion, while the induced economic damage, economic loss due to the industrial business interruption, accounted to about €3.1 billion (Regione Emilia-Romagna 2013).

The issue of seismic vulnerability of existing industrial buildings is of pristine importance for life safety, business continuity of activities and has relevant social and economic impact on territories.

## 1.2 Aim of the research

The study investigates the experimental and numerical behaviour of an innovative low-damage retrofitting solution for friction connections of existing precast structures able to reduce the effects of the seismic action on structural elements and to concentrate damages in predefined parts of the structures through the use of dissipative devices based on carbon-wrapped steel tubes.

Most of devices used to add damping to buildings in order to improve seismic response are based on yielding, friction or viscosity. The research activity focused on finding an innovative energy dissipation mechanism for civil structures, able to absorb a high amount of energy in small dimensions, performing a dissipative fuse behaviour.

A Collaboration between the Interdepartmental Centre for Industrial Research CIRI - Edilizia e Costruzioni of the University of Bologna and private companies led to the development of a device (*Sismocell*) based on carbon-wrapped steel tubes aimed at strengthening friction-based beam-column connections, derived from studies in automotive engineering and crash-tests (Song et al. 2000, Lima et al. 2011). The fuse behaviour researched in the innovative energy dissipation mechanism is linked to the aim of finding a strengthening solution able to connect structural elements and at the same time to limit forces transmitted between the structural elements connected through the devices. The device developed aim at providing an effective connection between structural elements and, in addition, the capability to dissipate a determined amount of energy, improving the seismic behaviour of the entire structure.

### **1.3 Organisation of the dissertation**

*Chapter 2* deals with seismic behaviour of precast RC structures. Firstly, the wide use of single-storey precast RC structures in industrial buildings is analysed. Main typologies and characteristics of precast buildings are briefly described, focusing on connections between precast structural elements. Then, main sources of vulnerability of precast structures design without anti-seismic provisions are discussed. Finally, an overview of code's evolution concerning precast structures is provided.

In *Chapter 3* the Emilia earthquakes of May 2012 consequences are critically discussed, analysing also economic impact on business activities. A complete review of damages occurred to precast structures is provided, taking into account seismic behaviour shown by connections (friction and pinned) between precast elements, columns and cladding panels.

*Chapter 4* focuses on the behaviour of friction-based connections of existing precast structures. State-of-the-practice for the assessment of existing precast structures is presented. The proposed low-damage retrofitting solution for friction-based connections is presented, describing the dissipation energy mechanism of the proposed device.

In *Chapter 5* results of an experimental campaign aimed at optimizing the design of the device on three different types of specimens are presented. For each different type of the device 25 specimens were tested, for a total of 75 tests performed. The experimental investigation allowed the characterization of the monotonic and cyclic behaviour of the device, evaluating also its dissipative capabilities.

*Chapter 6* aims to investigate the behaviour of connections equipped with dissipative devices under seismic action. Simple recommendations for the design of the introduction of the dissipative devices in beam-column friction connections are proposed.

The chapter provides then the description of main characteristics of structural models and the definition of seismic input considered for numerical analyses.

Results of nonlinear dynamic analyses performed on simple structures strengthened with the investigated devices are presented and discussed, in order to verify the effectiveness of their introduction in terms of reduction of forces transmitted to columns and improvement of the seismic behaviour of the structure.

*Chapter 7* presents Incremental Dynamic Analyses (IDA) performed in order to evaluate an equivalent behaviour factor for a structure equipped with dissipative devices. Results of various performed analyses are summarized. A simplified approach to evaluate the equivalent behaviour factor for structures with dissipative beam-column joints is finally proposed.

Finally, *Chapter 8* summarizes the main findings of previous sections. Recommendations for future research development are provided.

## **2. SEISMIC BEHAVIOUR OF PRECAST RC STRUCTURES**

### **2.1 Wide use of single-storey precast RC structures in industrial buildings**

Since the end of World War II, precast structures have been widely used in Italy due to the many advantages of the mass production of structural elements. Their diffusion has been supported by flexibility of structural net dimensions and by the economy and efficiency of the production process. Precast elements, produced in factories, are characterized by a more precise control, a better quality and a faster construction time than the cast-in-place RC elements. All over the world, particularly in Italy, precast structures are mainly used in the industrial field, where buildings require wide openings (e.g., large bays) and very regular plan configurations that are typically square or rectangular in shape (Magliulo et al. 2014c).

In Italy, precast structures have been widely used for industrial buildings since the 70s. According to the annual report of the Italian Revenue Agency (2012) on the Italian real estate market and stock of non-residential buildings there are about 700,000 industrial buildings. About 60% of the whole stock of industrial buildings is located in Northern Italy, while the other 40% is equally spread between Central and Southern Italy. Table 2.1 reports the distribution of industrial buildings by regions: Lombardia (19,6 % of the Italian stock), Veneto (12,5 %), Emilia-Romagna (11,9 %) and Piemonte (10,0 %) lead this ranking.

The concentration of industrial buildings in the area struck by 2012 Emilia earthquakes is evident in Figure 2.1. In Emilia-Romagna there are about 80,000 industrial buildings, one third of which are warehouses. The most frequent typology is reinforced concrete (85% of the total), more than two thirds of which realised using precast elements (Braga et al. 2014).

## 2. SEISMIC BEHAVIOUR OF PRECAST RC STRUCTURES

Area	Region	Stock [n°]	Stock [%]
North-East	Emilia-Romagna	83465	11.9%
	Friuli	15106	2.2%
	Veneto	87894	12.5%
<b>North-East</b>		<b>186465</b>	<b>26.6%</b>
North-West	Liguria	14283	2%
	Lombardia	137668	19.6%
	Piemonte	70228	10%
	Valle d' Aosta	1894	0.3%
<b>North-West</b>		<b>224073</b>	<b>31.9%</b>
Central	Lazio	35154	5%
	Marche	31031	4.4%
	Toscana	48852	7%
	Umbria	12639	1.8%
<b>Central</b>		<b>127676</b>	<b>18.2%</b>
South	Abruzzo	19527	2.8%
	Basilicata	5838	0.8%
	Calabria	15863	2.3%
	Campania	33229	4.7%
	Molise	4803	0.7%
	Puglia	36770	5.2%
<b>South</b>		<b>116030</b>	<b>16.5%</b>
Islands	Sardegna	17120	2.4%
	Sicilia	30614	4.4%
<b>Islands</b>		<b>47734</b>	<b>6.8%</b>
<b>Italy</b>		<b>701978</b>	<b>100%</b>

Table 2.1- Distribution of Italian industrial buildings by regions (Italian Revenue Agency 2012)

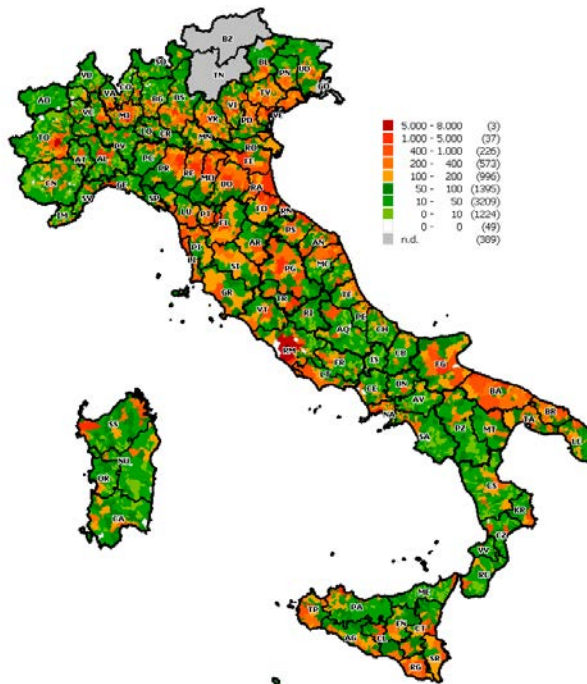


Figure 2.1- Distribution map of industrial buildings in Italy (Italian Revenue Agency 2012)

As an example, Nuti and Vanzi (2014) showed that approximately 70% of the industrial buildings are precast RC structures (Table 2.2).

Use	Stone/Masonry	Reinforced concrete		Steel	RC / steel	Other
		Cast in situ	precast			
<b>Agriculture</b>	13%	31.2%	30.4%	9.1%	8.2%	8%
<b>Industrial</b>	1.9%	18.6%	<b>67.4%</b>	4.4%	4.9%	2.8%
<b>Commercial and tourism</b>	2.7%	37.2%	51%	1.7%	5.4%	1.8%
<b>Transport, credit and insurance</b>	0.8%	19.5%	66.8%	0.3%	6.2%	6.4%
<b>Other</b>	4.9%	50.8%	30.2%	2.4%	7%	4.7%
<b>Total</b>	3.5%	25.1%	58%	4.4%	5.5%	3.5%

*Table 2.2- Distribution of non-residential buildings by structural typology and use (Nuti and Vanzi 2014)*

The most common typology used for the construction of precast industrial buildings in Italy consists in single-storey statically-determined frame structures with socket foundations, characterized by the use of precast reinforced concrete long-span roof girders supported over cantilever precast columns, which provides the large open spaces needed for manufacturing (Figure 2.2). The same typology is used in most seismic countries of the Southern Mediterranean region (e.g. Greece, Turkey, etc.).

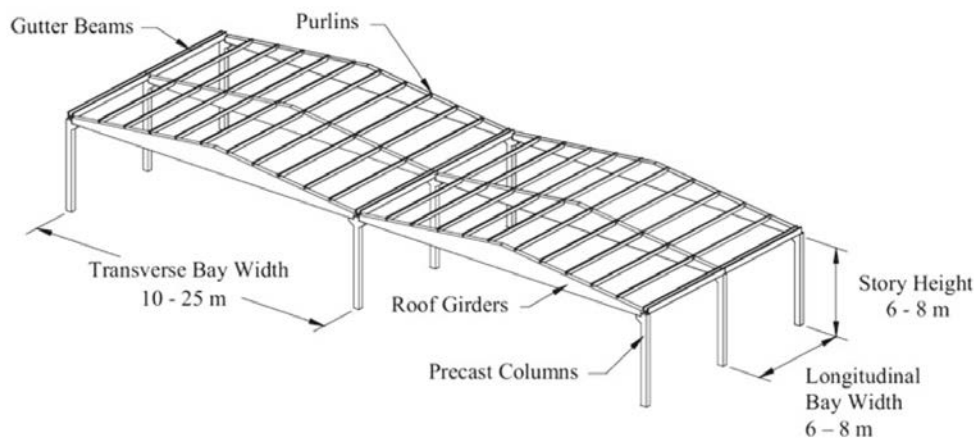


*Figure 2.2- Typical configuration of one-storey precast RC industrial buildings (Wood 2006)*

The buildings are typically rectangular in plan, with one or more bays in the transverse direction and several bays in the longitudinal direction. The most common structural configuration consists in a series of single bay portal frames. The transverse frame consists in

precast RC columns, supporting pre-stressed long-span beams. The depth of these girders often varies along the length, forming a triangular shape (double-slope beams). On top of the columns, precast RC beams connect the series of portal frames in the longitudinal direction. Beams oriented along the longitudinal axis of the building quite often have a U-shaped cross-section to function as gutters to collect water from the roof.

The width of the transverse bays ranges from 10 to 25 m, the width of the longitudinal bays ranges from 6 to 8 m, and storey height ranges from 6 to 8 m. The base of each precast column is typically grouted into a precast socket foundation to form a fixed connection. Many columns have also corbels in the transverse direction to support a bridge crane.

In buildings without seismic provisions, the beams in either direction are generally simply supported on the top of the columns or on column corbels and are held in position by shear key U-shaped or L-shaped extrusions of the column (forks).

For most of the structures, the roofing consists in precast elements (usually double-T prestressed elements or pre-stressed RC precast hollow slabs), spanning in the longitudinal direction. Purlins span between the roof girders at regular intervals. The precast roof girders, gutter beams, and purlins are usually simply supported at both ends. Older buildings can have a concrete-brick roof. Typically, lightweight materials are used to form the roof, which does not serve as a structural rigid diaphragm.

Masonry walls or precast RC panels (horizontal or vertical) are typically used for the exterior walls. If precast concrete wall panels are used, the connection details should be designed such that the panels do not contribute to the lateral stiffness of the building; however, this principle is not satisfied by the majority of the existing industrial precast concrete buildings. Some columns have an I-shaped cross section in order to support precast wall panels between successive columns. For rectangular columns, the precast RC cladding is connected using metal plate connectors and bolts (Bournas et al. 2013).

## **2.2 Main typologies and characteristics of precast buildings**

Precast buildings can be classified according to different variables:

- a) structural type;
- b) number of stories;
- c) roof type.

Three main structural types can be distinguished:

- panel structures;

- column structures;
- mixed structures.

Depending on the number of stories, precast structures can be:

- single-storey buildings (very common for industrial building);
- multi-storey buildings (used for commercial or office buildings).

Regarding roof types, roof elements supported by beams with variable sections (Figure 2.3), continuous plane roofs (Figure 2.4), discontinuous plane roofs (Figure 2.5), and shed roofs (Figure 2.6) can be found.

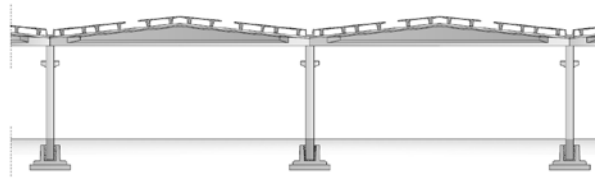


*Figure 2.3- Double-slope roof* (Bonfanti et al. 2008)

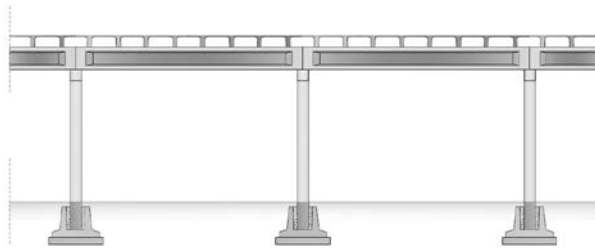


*Figure 2.4- Continuous plane roof* (Bonfanti et al. 2008)

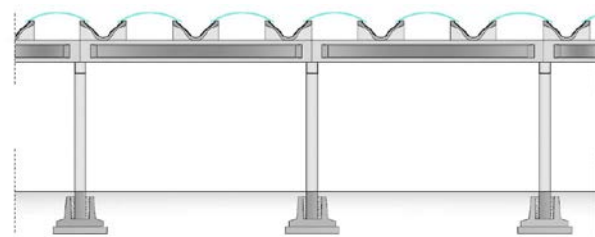


*Figure 2.5- Discontinuous plane roof* (Bonfanti et al. 2008)



*Figure 2.6- Shed roof* (Bonfanti et al. 2008)

In Italy, the most common precast buildings are column structures. They consist of socket footing foundations in which precast columns are placed and fixed in situ by cement mortar; the columns support ordinary or pre-stressed RC precast beams that can have different shapes. The most frequent beam cross sections are  $T$  or  $I$  section for beams with variable sections (double-slope beams) and  $Y$ ,  $H$ ,  $L$ ,  $I$  or rectangular section for plane beams. Reticular beams are also used, especially for very large spans. The main beams support roof elements: in multi-storey buildings, a cast-in-place slab is provided to cover corrugated elements of intermediate decks; in single-storey buildings, instead, a concrete slab is rarely used. Continuous or discontinuous roof elements solutions can be defined: in the first case, elements are put side by side (Figure 2.3 and Figure 2.4); in the second case, elements are spaced and alternated by light elements like translucent sheets (Figure 2.5) completed with sandwich or metal panels. An alternative solution is represented by a shed roof (Figure 2.6). Multi-storey buildings (Figure 2.7) have monolithic columns with corbels supporting beams, floor slabs and roof elements. Most common primary beams have  $T$ ,  $L$  or rectangular section. Precast elements used for intermediate floors are completed with a reinforced concrete casting, of thickness variable from 5 to 10 cm, in order to increase mechanical properties and distribute loads. Typical span lengths vary from 10 to 15 m. Intermediate floors are generally composed by corrugated precast elements, while roof floors are realised with systems used for single-storey buildings described in the following.

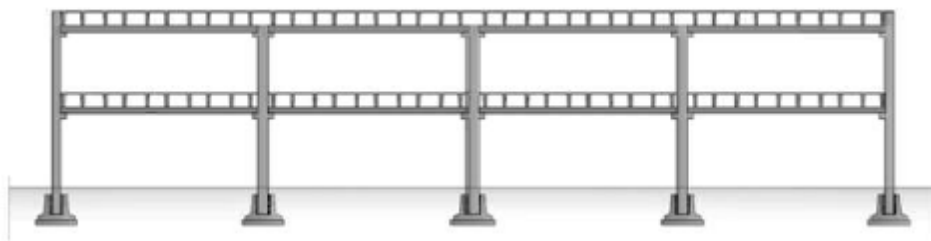


*Figure 2.7- Multi-storey precast building* (Bonfanti et al. 2008)

Among most common single-storey buildings there are structures with roofing realised using double-slope beams, very common until 90s (Figure 2.3). Double-slope beams can be used for span lengths of 10-40 m, with a distance between portal frames from 6 to 12 m. Roof elements can be ordinary or pre-stressed concrete precast elements, usually ribbed, ordinary or pre-stressed concrete or brick-concrete slabs with thickness of 12-20-24 cm. Roofing is completed with waterproof slabs. Slope of the roofing varies from 10% to 15% in order to

facilitate rainwater removal. Roofing can be with or without light elements or shed openings (Figure 2.8).

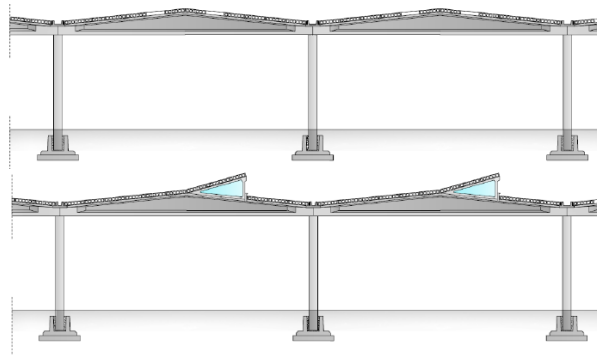


*Figure 2.8- Double-slope roof without and with shed openings* (Bonfanti et al. 2008)

In case of plane roofing, rectangular, *H*- or *I*-shaped beams are used for span lengths of 10-30 m, with a distance between portal frames from 6 to 30 m (Figure 2.9). Roof elements can be hollow-core pre-stressed concrete slabs, brick-concrete slabs, precast RC corrugated slabs, special shaped (*Y* section, small vaults, shed or micro-shed) precast RC elements ordinary or pre-stressed concrete precast elements, usually ribbed, ordinary or pre-stressed concrete or with thickness of 12-20-24 cm. Roofing precast elements can be put side by side in order to create continuous roof (Figure 2.4) or spaced and alternated by light elements like translucent sheets (Figure 2.5) completed with sandwich or metal panels in order to create discontinuous roof. Roofing is completed with insulation layers and waterproof slabs. Difference between plane roof and double-slope roof consist in different way of directing rainwater at roof level.

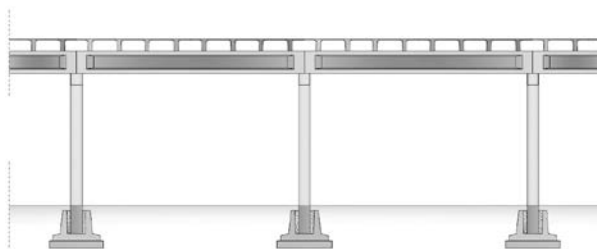


*Figure 2.9- Plane roof with corrugated tiles* (Bonfanti et al. 2008)

An alternative solution is represented by a shed roof; it can be built using reticular beams or discontinuous beams, known in Italy as “knee beams” (Figure 2.10), or by using inclined beams supported on columns at two different levels (Figure 2.11).

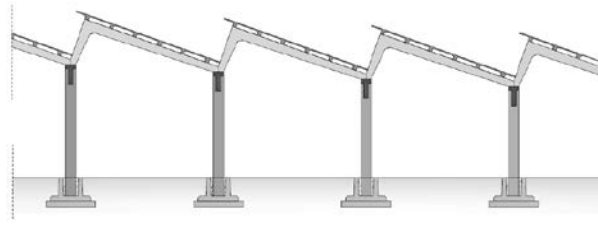


**Figure 2.10-** *Shed roof with knee beams* (Bonfanti et al. 2008)



**Figure 2.11-** *Shed roof with inclined beams* (Bonfanti et al. 2008)

Beam length varies from 12 to 16 m and spacing from 6 to 15 m. Roof elements supported on roof beams can be hollow-core concrete slabs, brick-concrete slabs or precast RC corrugated elements. Shed roofs developed in order to obtain a better natural lighting of spaces: the geometry of roof elements and the orientation of the building assure spread lighting. More recent micro-shed systems were studied to reduce transverse dimensions and to provide insulated elements.

Depending on the in-plane floor stiffness, Nascimbene and Bellotti (2013) classified (Figure 2.12) roofing of single-storey structures in:

- *rigid*: in-plane floor stiffness  $\gg$  vertical resistant system stiffness; in-plane deformability negligible respect to inter-story horizontal relative displacement and horizontal forces distribution is proportional to the stiffness of the vertical resistant system (frames, columns, walls);
- *flexible*: in-plane floor stiffness  $\ll$  vertical resistant system stiffness; in-plane deformability much greater than inter-story horizontal relative displacement and horizontal forces distribution is not dependent on the stiffness of the vertical resistant system, but on the area of influence of each column or wall;
- *semi-rigid*: intermediate situation where in-plane deformability of the floor and inter-story drift are comparable; horizontal forces distribution is influenced by both vertical system stiffness and area of influence of each column or wall.

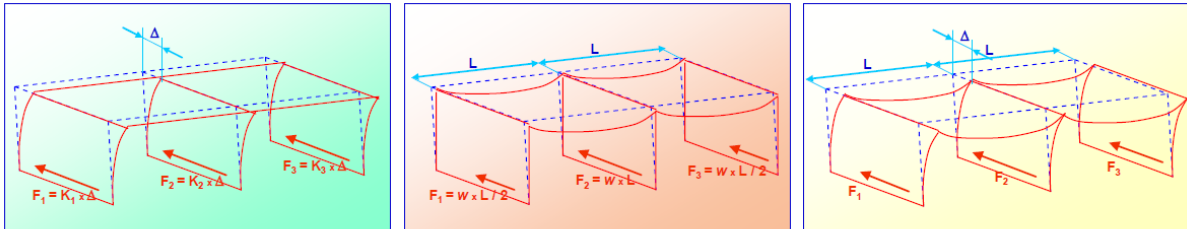


Figure 2.12- Classification of roof floor by in-plane stiffness: rigid, flexible and semi-rigid (Nascimbene and Bellotti 2013)

Exterior walls can consist in masonry infills or precast RC panels placed along the perimeter that can be inserted between columns or placed externally to the main structure. Infill systems using precast panels can provide different solutions: horizontal precast panels connected to columns, vertical precast panels attached to horizontal beams, and a mixed solution including horizontal and vertical panels are all used.

Main characteristics of most common precast elements listed by Bellotti et al. (2014) basing on information and materials provided by main Italian production factories are reported in the following figures.

Ordinary or pre-stressed precast RC beams present a great variability in typology, geometric dimension and length (Figure 2.13): most common beams are double-slope, *I*-, *T*-, *L*-, *H*-, *Y*-shaped, boomerang and reticular.

Tipologia: doppia pendenza p = 10%		
		
Tipo di impalcato	Copertura a doppia falda con tegoli	
Peso trave (kN/m)	5.5 ÷ 14.0	
Altezze massime in campata (m)	1.30 ÷ 2.90	
Luci correnti di impiego (m)	10 ÷ 40	

## 2. SEISMIC BEHAVIOUR OF PRECAST RC STRUCTURES

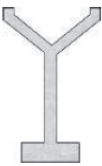
### Tipologia: I o doppio T di bordo con fondelli di vario spessore

			
Tipo di impalcato	Copertura con tegoli		
Peso trave (kN/m)	4.0 ÷ 9.0		
Altezze massime in campata (m)	0.80 ÷ 1.40		
Luci correnti di impiego (m)	8 ÷ 28		

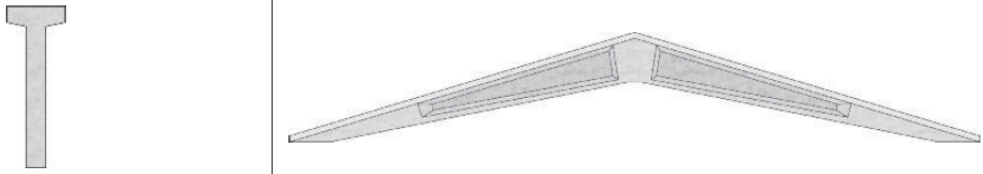
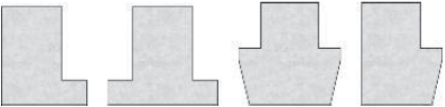
### Tipologia: ad H

			
Tipo di impalcato	Copertura con tegoli		
Peso trave (kN/m)	8.0 ÷ 12.0		
Altezze massime in campata (m)	0.80 ÷ 1.40		
Luci correnti di impiego (m)	8 ÷ 16		

### Tipologia: ad Y

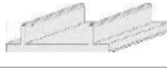
			
Tipo di impalcato	Copertura con voltine		
Peso trave (kN/m)	7.0 ÷ 11.5		
Altezze massime in campata (m)	0.60 ÷ 1.00		
Luci correnti di impiego (m)	10 ÷ 20		

## 2. SEISMIC BEHAVIOUR OF PRECAST RC STRUCTURES

Tipologia: Boomerang	
	
Tipo di impalcato	Copertura a doppia falda con tegoli a lastre
Peso trave (kN/m)	fino a 11.0
Altezze massime in campata (m)	1.30 ÷ 1.60
Luci correnti di impiego (m)	12 ÷ 20
	
Tipologia: Reticolare	
	
Tipo di impalcato	Copertura con estradosso piano o inclinato con tegoli o lastre
Peso trave (kN/m)	Variabile
Altezze massime in campata (m)	2.00 ÷ 2.50
Luci correnti di impiego (m)	15 ÷ 30
	
Tipologia: L e T rovescio o trapezio	
	
Tipo di impalcato	Coperture piane e solai piani con tegoli binervati o lastre
Peso trave (kN/m)	7.0 ÷ 17.0
Altezze massime in campata (m)	0.40 ÷ 1.20
Luci correnti di impiego (m)	8 ÷ 16
	

*Figure 2.13- Main characteristics of most common beams of current production (Bellotti et al. 2014)*

Precast roof floor elements (Figure 2.14) can be divided in partially or totally precast, which can be completed with in-situ grout injections. Roof elements can be spaced and alternated by light elements like translucent sheets.

Tipologia elemento	Sezioni tipiche	Dimensioni sagoma standard (m)		Peso totale (kN/m)	Luci correnti d'impiego (m)	Interasse (m)	
		base	altezza				
Solai totalmente prefabbricati (in c.a.p)	lastra alveolare		1.20	0.12 ÷ 0.80*	2.00 ÷ 8.50	6 ÷ 24	affiancati
	tegolo binervato		2.50	0.30 ÷ 1.20*	2.00 ÷ 5.00	8 ÷ 24	affiancati (o con lucernari in coperture piane)
	tegolo omega		2.25	0.40 ÷ 1.00*	2.50 ÷ 6.00	10 ÷ 20	affiancati
Solai parzialmente prefabbricati	tegolo binervato ad intradosso piano		1.20	0.50 ÷ 1.00*	3.5 ÷ 8.5	10 ÷ 20	0 ÷ 2.50
	lastra nervata		1.20	0.20 ÷ 0.30	1.50 ÷ 2.50	< 10	0 ÷ 2.50
	a travetti in c.a.p.		0.12 ÷ 2.50**	0.16 ÷ 0.24***	3.00 ÷ 15.00	4 ÷ 10	0 ÷ 0.80
	tralicciato (predalles)		1.20 ÷ 2.50	0.15 ÷ 0.60	-	3.5 ÷ 8	affiancati

\* escluso eventuale getto integrativo in c.a. di spessore 5 ÷ 10 cm;  
 \*\* relativa al singolo travetto;  
 \*\*\* relativa all'intero solaio, escluso il getto integrativo di 5 ÷ 6 cm all'estradosso.

Tipologia elemento	Sezioni tipiche	Dimensioni sagoma standard (m)		Peso totale (kN/m)	Luci correnti d'impiego (m)	Interasse (m)
		base	altezza			
Tegoli di copertura		2.50	1.00 ÷ 1.10	6.00 ÷ 8.00	16 ÷ 32	0 ÷ 6.00

Figure 2.14- Main characteristics of most common roof floor elements of current production (Bellotti et al. 2014)

Precast columns are usually realised using ordinary reinforced concrete and consist in monolithic elements fixed at their base. Pre-stressed precast columns are not frequent and used in case of high eccentricity of applied loads. A minimum dimension of column cross-section is typically a square section of 40-50 cm, depending on loads, column height, instability problems and presence of a drainpipe inside the column. Column can present rectangular sections with one side longer than 100 cm. Columns can have a *H*-shaped cross section in order to support precast wall panels between successive columns. Maximum height

is limited by following factors, related one to each other: instability, size of structural grid, structural scheme restraints, presence of braces, number of storeys. Maximum height of monolithic elements is about 12-14 m. Steel reinforcement is the same of ordinary RC elements. Columns are adequately shaped at the base to be inserted in socket foundations, while at the top they are shaped in order to support beams or other precast roof elements (Figure 2.15).

In correspondence of the connection with horizontal elements, columns are shaped or have corbels, in order to allow the support of beams, other structural elements or a bridge crane.

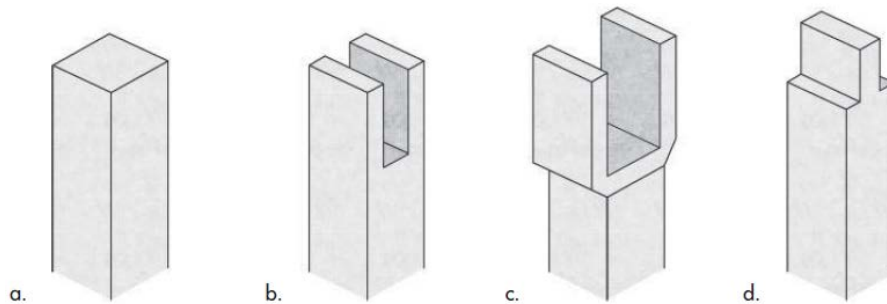


Figure 2.15- Different shapes of column tops: a) for rectangular or I-, L-, T-shaped beams; b) and c) with forks for double-slope beams; d) for H-shaped beams (Bellotti et al. 2014)

Precast panels can be classified in:

- *joist panels* with an outside frame and a system of horizontal and vertical reinforced joists completed with light materials like polystyrene. Standard thickness  $t$  of this kind of panels is 20 cm. Width  $L$  (longest side) is generally fixed by  $t > L/50$  or  $L < 10$  m, height (shortest side) is generally 2.5-3 m (4-4.5 m maximum). Weight is about 3.5-4 kN/mq. This kind of panel is characterized by a good insulation capacity and high ratio between out-of-plane resistant capacity and weight. Therefore they are often used as exterior walls.
- *sandwich panels* composed by a series of layers with different roles, able to guarantee very high insulation performances. Usually the sequence presents a structural bearing internal layer composed by a reinforced concrete slab, different intermediate layers with the aim to insulate and lighten the panel and an external layer for protection and surface finishing.
- *monolithic panels*, much heavier than other types of panels. Therefore, for panels of the same size of the other two typologies, thickness must be of 8-10 cm. They are used if very high mechanical performances are required or as fire-walls, loading directly on foundations. Insulation capacity is generally quite low.

Depending on orientation of installation (Figure 2.16), precast panels can be divided in:

- *vertical panels* supporting directly on horizontal foundation beam through a shaped mechanical connection and partially on socket foundation, while at the top there is only a restraint avoiding horizontal translation. The upper restraint is not necessarily placed at the maximum height of the panel. Vertical panels are necessarily placed at the external side of columns and are used to cover span length of more than 10-12 m.
- *horizontal panels*, hanged to columns through metallic fasteners or directly loading on foundations without any connection between panel and columns.

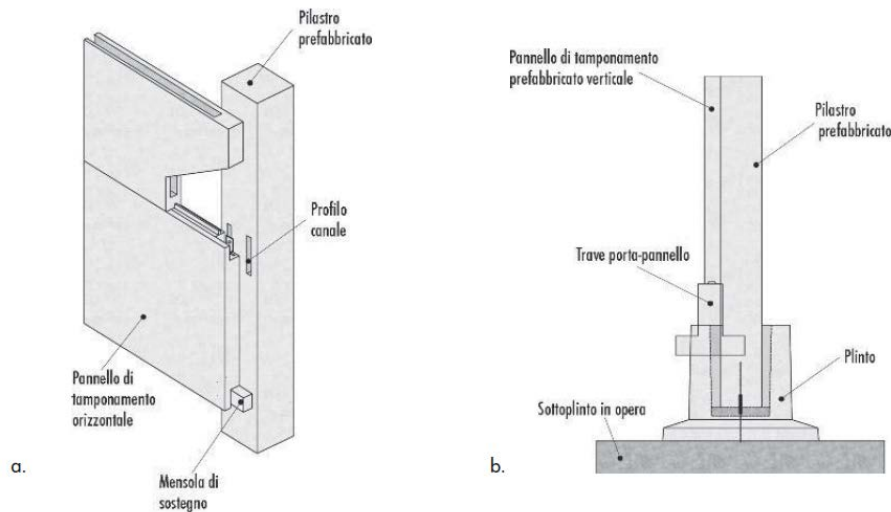


Figure 2.16- Precast panels: a) horizontal panels fixed to the columns; b) vertical panels supporting on foundation (Bellotti et al. 2014)

A more detailed review of the main typologies of precast structures used in Italy since the 70s is provided by Bonfanti et al. (2008) and Mandelli Contegni et al. (2008).

### 2.3 Connections between precast structural elements

The most crucial aspect of precast structures regards the connections between structural elements. The connections are made in situ and executed in order to reflect the calculation model assumed in the design phase. Depending on different realisation technologies, connection can statically be configured as different types of restraint.

A description of typical connections is presented by Magliulo et al. (2014c) and include:

- a) floor or roof adjacent elements connection;
- b) roof element-beam connection;

- c) beam-column connection;
- d) column-foundation connection;
- e) cladding panel-structural element connection.

The roof-adjacent elements connections (*a*) are generally made of steel angles and plates welded or bolted in order to ensure the slab continuity.

The roof element-beam connections (*b*) can be provided in different ways. The most common connection type provides a neoprene pad at the interface between the beam and the roof element, resulting in a friction connection. Another solution consists of steel angles bolted both to the roof element and to the beam defining a fixed connection (Figure 2.17 and Figure 2.18a). A fixed connection is also given by the presence of a dowel, inserted in the roof element and in the beam or by the presence of steel reinforcement and grout casting in-situ (Figure 2.18b).

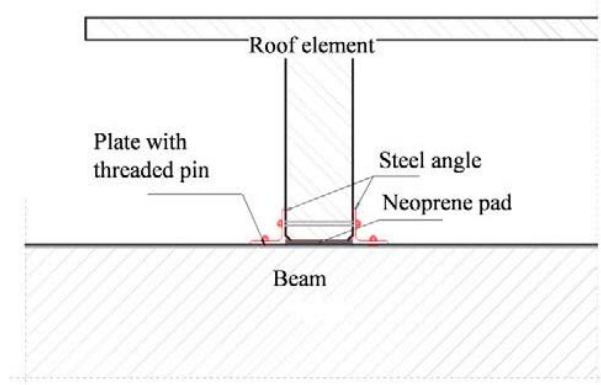


Figure 2.17- Roof element-beam connection using steel angles (Magliulo et al. 2014c)

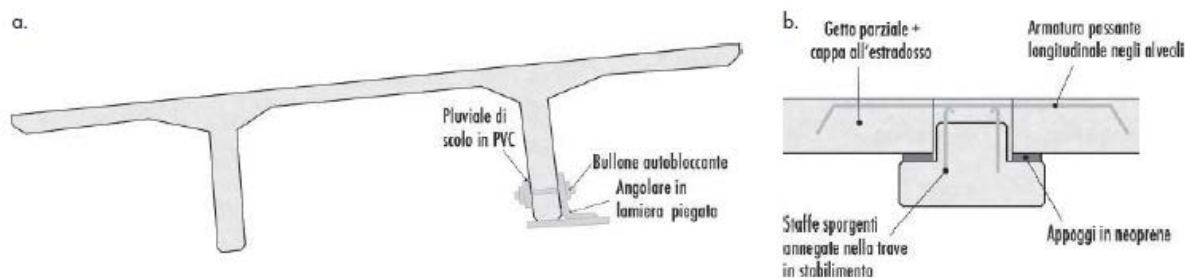


Figure 2.18- Roof element-beam connections: a) steel angles and bolts; b) steel reinforcement and grout casting in-situ (Bellotti et al. 2014)

A beam-column connection (*c*) can be a friction connection or a dowel connection (Figure 2.19). The former type is very common in existing precast structures and generally consists of a neoprene pad at the beam-to-column interface without providing any mechanical connectivity. It relies on friction to absorb resisting forces. In the latter type, a steel dowel is

inserted inside the column and anchored in predefined vertical holes in the beam (Figure 2.20); the connection requires a final grout casting. This solution defines a hinged support in the longitudinal direction of the beam.

The mechanical connection is provided using a vertical dowel, a metallic box inserted at the end of the beam and on the head of the column with one vertical bar (maximum two for each joint) 100 mm length and mean diameter of 24 mm or transversal bars connecting the end of the beam to forks or to the head of the column.

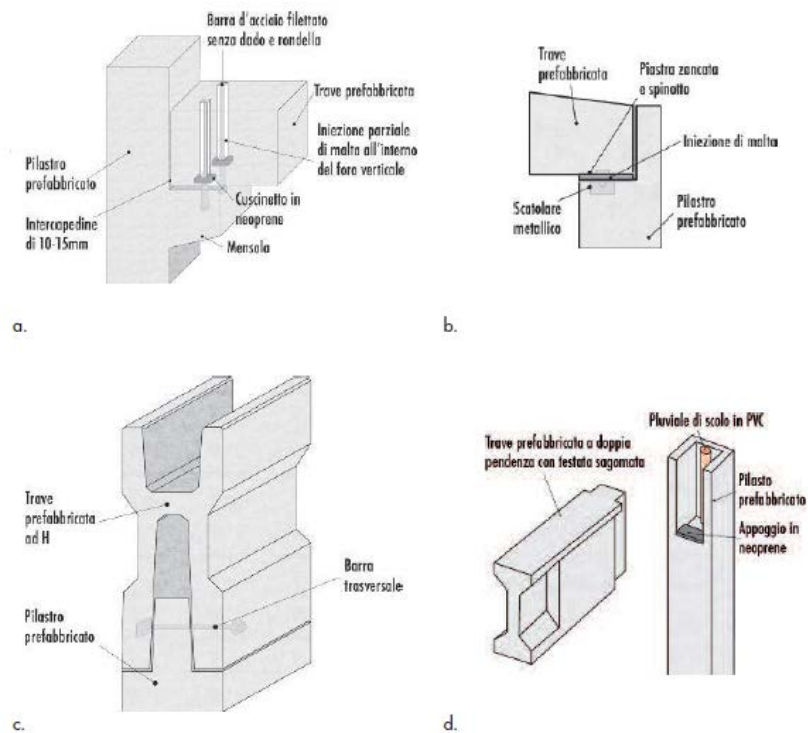


Figure 2.19- Most common beam-column connections (Bellotti et al. 2014)

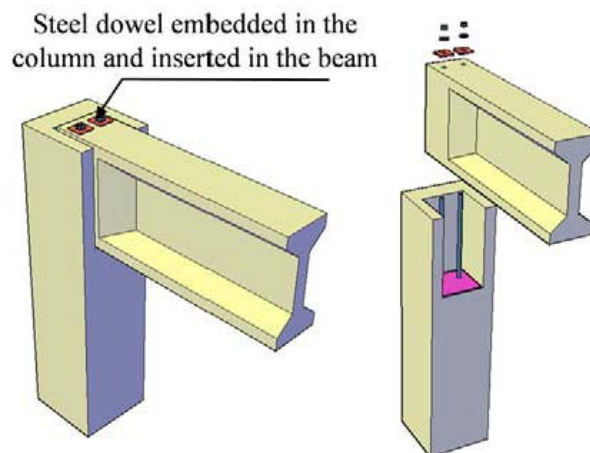


Figure 2.20- Dowel beam-column connection (Magliulo et al. 2014c)

The most common column-foundation connection (d) is the socket foundation (Figure 2.21). This type is characterized by a RC hollow-core body in which the column is inserted. Concrete or special mortar is poured to fill the gap between the column and the hollow-core body of the socket foundation. The socket foundation is generally modelled as a rigid connection, due to the study performed by Osanai et al. (1996), in which it is concluded that the connection is rigid if the column embedment depth is larger than 1.5 times the depth of the column cross section.

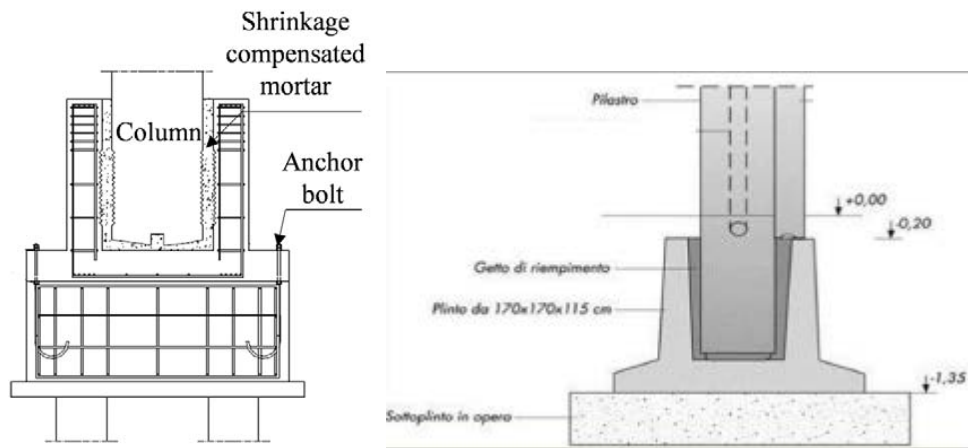


Figure 2.21- Socket column-foundation connection (Magliulo et al. 2014c)

Connections between cladding panels and structural elements (e) can provide different solutions, based on steel connectors such as channel bars, fasteners, angles, brackets, etc. (Figure 2.22).

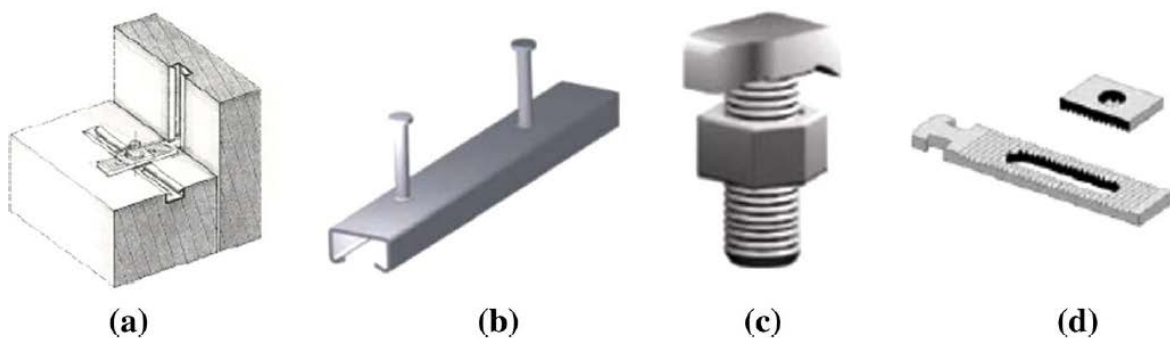


Figure 2.22- Connection between vertical precast panel and resistant structure (a), channel bar (b), interlock (c) and connector (d) (Magliulo et al. 2014b)

A detailed list of connections between precast structural elements used both in Italy and Europe is provided by Mandelli Contegni et al. (2007).

## **2.4 Main sources of seismic vulnerability in precast structures**

The use and development of precast RC structures in seismic zones have always suffered all over the world because of limited knowledge on their behaviour under seismic actions and because of absence of adequate standards. During past earthquakes, precast structures haven't always exhibited excellent performances and this contributed to increase a feeling of mistrust towards these structural schemes. It must be underlined that problems in seismic response of existing precast structures are not directly linked to intrinsic limits of precast technology, but rather to inadequacy in the design and in the quality of construction of details and connections, in the choice of the structural scheme or even to the absence in the design of seismic provisions.

In literature, there are evidences about the behaviour of precast structures during past earthquakes, such as Friuli - Italy (1976), Vrancea - Romania (1977), Montenegro (1979). More recently, experience has been gained in more modern structures after the earthquakes of Northridge – California U.S.A. (1994), Kobe – Japan (1995), Kocaeli –Turkey (1999), Wenchuan – China (2008), L'Aquila – Italy (2009). However, existing knowledge is rather incomplete and controversial. In fact, in most past earthquake events there is evidence of excellent behaviour of precast structures as well as reports of catastrophic collapses, which does not come as a surprise, since performance strongly depends upon the specific structural system, the type of connections, the adequacy of the design and the quality of construction. Also restricting the focus to precast frame structures (the typology which is most commonly used in Europe), evidences of very good structural behaviour go hand in hand with reports of collapses, as in the already mentioned cases of Friuli - Italy (1976) and Kocaeli –Turkey (1999) events. For this kind of structures, recent evidence after the 2009 L'Aquila earthquake seems to demonstrate that the behaviour of such structures is satisfactory, whereas some problems exist with the non-structural components connections, in particular with the heavy cladding elements, as was reported by Toniolo and Colombo (2012).



*Figure 2.23- Aerial photos of collapses of industrial precast buildings during 2012 Emilia earthquakes*

The main causes associated to the damage of the precast structures during past earthquakes were failure of connections, insufficient ductility of the columns, insufficient stiffness of the roof or slab system. Failure of the connections was the main factor leading to most of the collapses, which took place typically because of loss of support of precast elements due to too high relative displacement values. The poor connections between beams and columns or even the absence of mechanical connections between precast elements make this kind of structures very vulnerable particularly to lateral loads induced by the earthquake. As a result, the most common type of failure mechanism observed during past earthquakes events consisted in the collapse of transverse and longitudinal beams slipped off the columns. Plastic hinges were also observed at the base of the columns. In most cases, the shear key also failed. It was observed that the latter was not adequately detailed with reinforcement, and no redundancy provisions were provided to make a monolithic connection.

The behaviour under seismic actions of these structures, as highlighted by Bellotti et al. (2014), is typically characterised by great flexibility and large displacements. In fact, most of the mass is at the roof level, columns are very slender, and beam-column connections are at best hinged.

Since precast structures have usually large spans, and since most of the elements are pin connected, they often have long fundamental periods of vibration. In addition the ground conditions can amplify considerably the ground shaking particularly at lower frequencies, and hence industrial warehouses can be subjected to large acceleration values.

The connections between precast elements are the key element in determining the seismic performance of industrial precast buildings. The main issue relates to the capacity of beam-column connections by either allowing for relative displacements without losing beam seating (i.e. for buildings designed for vertical forces only), or for adequately transferring lateral

horizontal forces to the column and down to the foundation without losing capacity (Bournas et al. 2013).

Precast structures have been widely used in Italy for industrial buildings since the 70s (see Section 2.1). The use of this structural typology in last decades brought to the born of whole industrial districts composed by precast buildings assemblies or isolated precast buildings realised with different age of construction and consequently designed according to different codes. It is also necessary to add to the temporal variability, also the spatial variability related to the building site of these structures.

Seismic hazard of the site have influenced both design provisions and construction technologies of precast RC structures. Actually, historical seismicity didn't caused differences only between different building sites, but also caused differences among buildings of the same area but with different age of constructions because of continuous updating of seismic hazard and zonation maps (Gruppo di Lavoro Agibilità Sismica dei Capannoni Industriali 2012).

Despite of spatial and temporal variability described above, some deficiencies common to most existing single-storey precast RC industrial buildings can be found and can be identified as the main sources of seismic vulnerability of these structures:

- absence of mechanical connection between precast structural elements (roof elements-to-beam and beam-to-column connections) able to assure the transfer of forces under seismic action, relying only on friction to resist to horizontal forces and making structures very sensitive to loss-of-support collapses and unseating;
- inadequacy of mechanical connection between precast structural elements (roof elements-to-beam and beam-to-column connections), because of limited distance of the dowels from the edge and insufficient transverse reinforcement in structural elements;
- inadequacy of mechanical connection between exterior cladding precast panels and structural elements;
- interaction with masonry infills distributed non-uniformly across the structure because of windows;
- deficiencies in terms of strength and/or ductility in vertical resistant systems (e.g. inadequacy of confinement at the base of the columns) and in foundations, usually composed by socket foundations, because of design procedures according to past standards without anti-seismic provisions;

- steel racking systems not able to resist to horizontal forces because of the absence of adequate bracing elements, causing interaction with the structure and important economic consequences due to the loss of their contents.

Existing precast structures are usually characterized by a low robustness, therefore the collapse of only few, even one, connection can cause the collapse of the whole structure.

Bonfanti et al. (2008) identified main issues that can strongly influence behaviour under seismic action of precast framed structures:

- connections between structural elements able to transfer horizontal forces (Figure 2.24);
- rigid-diaphragm effect at roof level able to distribute forces (Figure 2.25);
- restraints able to assure stability against lateral collapses of precast elements (Figure 2.26);
- short column shear failure due to partial-height masonry infills;
- classification of the area as seismic zone at the age of construction;
- use of seismic design standards and provisions.

These aspects are not so relevant for gravitational vertical loads, but are key issues in order to define behaviour of the structure under seismic action.

Lessons learned from past earthquakes, especially 2012 Emilia earthquakes, show that it is not possible to rely on friction mechanism for the transferring of horizontal seismic loads. The combination between horizontal and vertical components of acceleration can easily lead to loss of support of precast simply supported elements, for both beam-column connections and roof elements-beam connections (Figure 2.24). Friction-based connections must be avoided in seismic zones and it is necessary to provide adequate mechanical connections between structural elements.

Most existing precast RC structures designed and built without anti-seismic provisions in areas only recently classified as seismic zones presents this kind of vulnerability, because codes allowed friction connections in non-seismic zones (see Section 2.5).

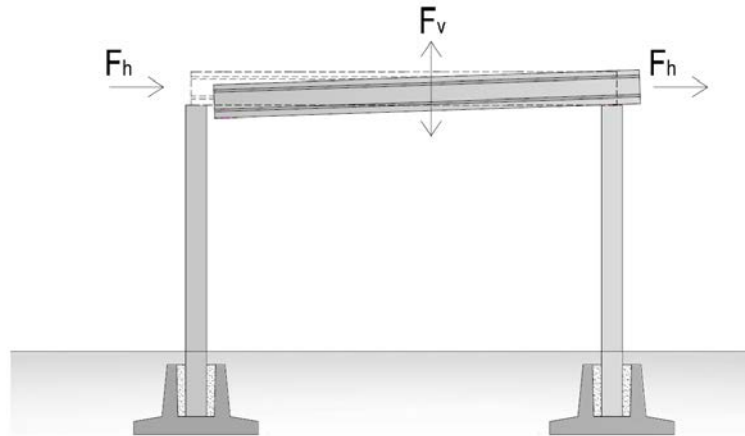


*Figure 2.24- Typical mode of collapse of single-storey precast structures due to loss of support in beam-column connections based on friction (Bonfanti et al. 2008)*

A rigid-diaphragm effect at roof level is necessary in order to guarantee an adequate seismic response of structural elements, distributing forces uniformly on different resistant elements and avoiding dangerous non-synchronous displacements between different parts of the same structures (Figure 2.25).

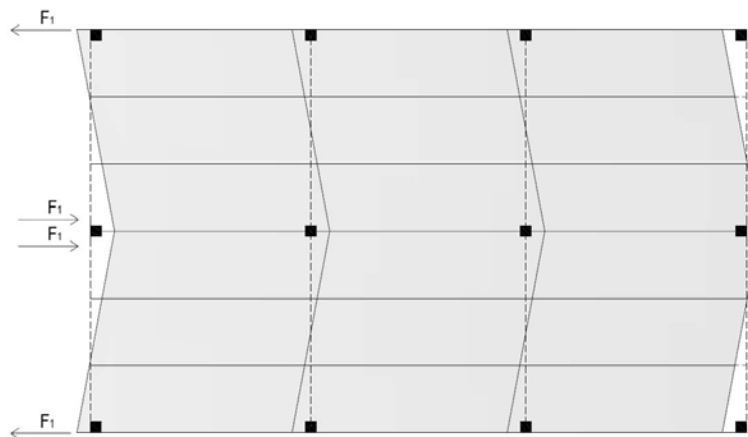


*Figure 2.25- Mode of vibration in absence of rigid-diaphragm effect (Bonfanti et al. 2008)*

The presence of lateral restraints is very important in order to assure stability against lateral collapses of precast elements (Figure 2.26).

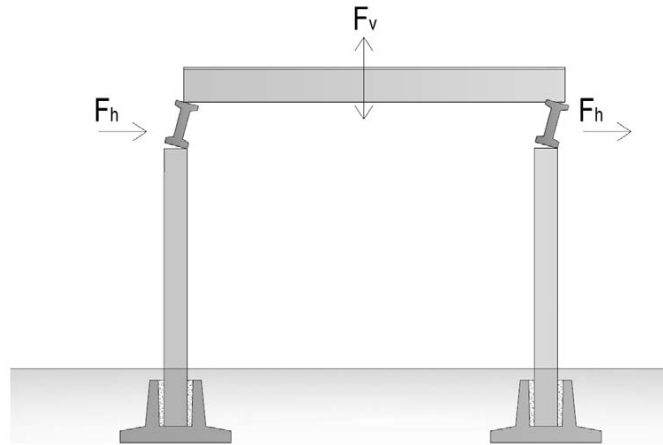


*Figure 2.26- Beam collapse due to absence of adequate lateral restraints* (Bonfanti et al. 2008)

Another important vulnerability consists in the activation of short-column shear failure mechanism due to interaction with partial-height masonry infills. This kind of damage was observed in several past earthquakes, like Kocaeli – Turkey (1999) or Emilia – Italy (2012).

Industrial precast RC structures, particularly those built during 70s and 80s, are characterised by very slender columns and great flexibility respect to horizontal loads. Therefore, in-plane stiffness of masonry infills or cladding panels influences significantly seismic response.

Current design practice for precast industrial buildings is based on a bare frame model, where the external cladding panels or masonry infills enter only as masses, without considering any stiffness contribution. The interaction with masonry panels distributed non-uniformly across the structure often led to non-synchronous displacements at the top of columns, thus contributing to unseating of the beams. Masonry panels, when not covering the full length of the column, led in many cases to the formation of short-column failures.

Figure 2.27 represents the situation of a masonry infill not covering the full length of the column, because of the presence of continuous windows. The upper part of the column not interacting with masonry infills is very short, with a higher stiffness that induces higher seismic actions and a local behaviour of shear failure. Without interaction with masonry infills, slenderness of such columns would have a better ductile flexural behaviour.

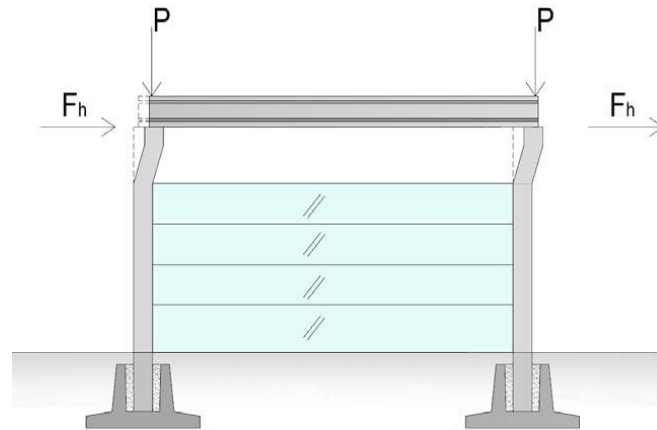


*Figure 2.27- Shear failure due to short-column mechanism* (Bonfanti et al. 2008)

The evolution of anti-seismic codes (see Section 2.5) and the continuous updating in classification of seismicity of sites and hazard maps increased the entity of design seismic actions to be considered. Therefore structures designed and built tens of years ago, can be now not able to resist to seismic actions according to current knowledge and standards.

Review of damages after major past national and international seismic events permitted to focus sources of vulnerabilities and to develop solutions and criteria in order to improve seismic behaviour of precast RC structures.

## 2.5 Code's evolution concerning precast structures

In order to give an idea of the reason of seismic vulnerability of existing precast concrete buildings, a brief overview of the code's evolution is given by Magliulo et al. (2014c), focusing on the code provisions regulating the design of elements and connections in precast structures (Table 2.3).

Code	Acronym	Precast structures requirements	Friction connection forbidden	Compulsory
Legge 25 Novembre 1962, n.1684	Legge 1684	No	-	Yes
Legge 5 Novembre 1964, n.1224	Legge 1224	No	-	Yes, integrates Legge n.1684
Circolare del Ministero dei Lavori Pubblici n.1422 del 6 Febbraio 1965	Circ. M.LL.PP. n.1422	No	Yes, if $T/N > 0.35$	Yes, integrates Legge n.1224
Legge 2 Febbraio 1974, n.64	Legge 64	Yes	-	Yes, replaces previous codes
Decreto Ministeriale del 3 Dicembre 1987	D.M. 3/12/1987	Yes	In seismic zones	Yes, integrates Legge n.64
Ordinanza del Presidente del Consiglio dei Ministri n.3274 del 30 Marzo 2003	O.P.C.M. n.3274	Yes	Yes	Yes, only for infrastructures and strategic buildings
Eurocode 8	Eurocode 8	Yes	Yes	No
Decreto Ministeriale del 14 Gennaio 2008	D.M. 14/01/2008	Yes	Yes	Yes, integrates Legge n.64 and replaces previous integrations

Table 2.3- Italian Building Code evolution overview (Magliulo et al. 2014c)

Legge n. 1684 (1962) and its integration Legge n.1224 (1964) only specify the horizontal actions to consider in seismic zones in Italy, without any particular requirement for precast structures. A noteworthy code was published in 1965 (Circolare M.LL.PP. n. 1422), forbidding the use of horizontal joints without mechanical devices if the ratio  $T/N$  was larger than 0.35 (where  $T$  is the maximum value of the shear force,  $N$  is the expected axial compression force, and, implicitly, 0.35 is the friction coefficient of the connection).

In 1974, the code (Legge n. 64) introduced specific indications for the seismic design of structures. Concerning precast structures, however, the code gives only a few general indications and these are for load-bearing precast panels structures.

The first specific regulations for precast structures were in the D.M. 3/12/1987, which already point out the role of the connections, considering also the transition phases of construction.

The requirements for structural elements and for the design of connections are still limited, but for the first time it is forbidden in seismic zones to use beam-column connections that transfer horizontal forces by friction alone. The only prescriptive provision is given for the width of the beam-to-column and roof floor element support: “For floor elements or similar it must be guaranteed a width of the support not smaller than 3 cm if a continuity of the connection is provided in situ, otherwise not smaller than 5 cm. For discontinuous supports, like corrugated or ribbed elements, previous values must be doubled. For the beams, the end support must be not smaller than  $8 + l/300$  [cm], where  $l$  is the clear beam span length in centimetres. Values must be considered net of tolerances and structural deformations.

Concerning design forces, a conventional horizontal force equal to a percentage of total vertical load (at least 1.5% during transition phases of construction and 2% at the end of construction) had to be considered in order to prevent instability, without any combination with other lateral loads (wind or seismic action) (D.M. 3/12/1987).

More detailed suggestions on precast structures are given in O.P.C.M. n. 3274 (2003). According to the Italian government, the application of this code is compulsory only in the case of infrastructure and strategic buildings. Multi-storey framed structures and single-storey structures with isostatic columns are taken into consideration, according to the number of stories and the capability of the connections in transferring bending moments. Specific behaviour factors (i.e., 5.0 and 3.75, respectively) are assigned to the two structural types. Moreover, the significant influence of the connections on the static and dynamic behaviour of the whole structure is recognized.

In the case of framed structures, the code, referring to Eurocodes, distinguished three possible conditions concerning connection types:

- a) connections located well outside critical regions with inelastic behaviour not affecting the energy dissipation capacity of the structure respect to monolithic systems;
- b) connections located within critical regions (at the ends of beams and columns) but adequately over-designed with respect to the rest of the structure, so that in the seismic design situation they remain elastic while inelastic response occurs in adjacent regions of elements;
- c) connections located within critical regions (at the ends of beams and columns) and properly designed in terms of ductility and quantity of dissipated energy.

For single-storey structures with isostatic columns, the beam-column connections may be fixed or free to slide horizontally. The connections must transfer the seismic design horizontal forces, without taking into account the friction strength. For the fixed connection, the capacity

---

design approach is considered, that is, its strength must be larger than the horizontal force that produces the ultimate resistant bending moment at the base of the column.

In Europe, precast concrete structures are regulated by Eurocode 8 (EC8), which underlines the importance of the connections. It requires friction resistance to be ignored in evaluating the resistance of a connection for both the beam-to-column connections and for the primary seismic elements-to-diaphragm horizontal joints. However, it should be noted that the Eurocode 8 is not compulsory in Italy. Concerning the structural types, the following five systems are considered for precast concrete structure: (i) frame structures, (ii) wall structures, (iii) dual structures (mixed precast frames and precast or monolithic walls), (iv) wall panel structures (cross wall structures), and (v) cell structures (precast monolithic room cell systems). The behaviour factor for one-storey framed systems ranges from a maximum of 4.95 to a minimum of 1.65, which corresponds to connections not regulated by the code.

The current Italian building code (D.M. 14/01/2008) gives more attention to precast structures than has been given in past Italian codes. It takes the main framework of O.P.C.M. n. 3431 (2005), adopting some provisions of EC8. Concerning the precast column systems, the two structural categories defined in O.P.C.M. n. 3431 (2005) are provided, that is, (i) framed structures and (ii) isostatic column structures; the former include structures with continuous or hinged joints, while the latter concern one-storey buildings with beams hinged at one side and with a sliding support at the other one.

The current Italian building code (D.M. 14/01/2008) identifies:

- *framed structures with continuous joints* (force and moment continuity in correspondence of joints similar to monolithic connections), following rules of connections type *c*). Plastic hinge formation is possible in beams of all intermediate floors and in both top and base joints of columns.

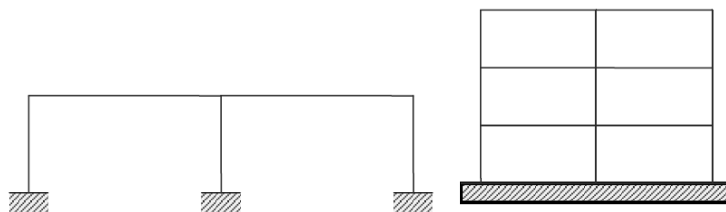
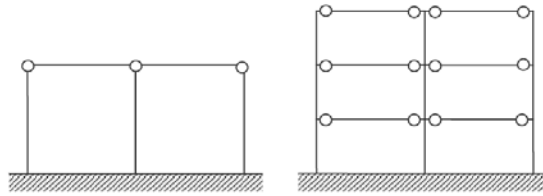


Figure 2.28- Framed structure with continuous joints (Circolare n. 617 2009)

- *framed structures with hinged joints between beams and columns* (force continuity in correspondence of joints) following rules of connections type *a*), while the column-to-foundation joint must be a fixed restraint and follow rules of connections type *b*).

Plastic hinge formation is possible only at the base of the columns.

Framed structures with hinged connections are the most common typology of precast technology.



*Figure 2.29- Framed structure with hinged joints* (Circolare n. 617 2009)

- *isostatic column structures* allow roof expansions because of the presence of roller connections and concentrate horizontal seismic actions only on determined columns. Plastic hinge formation is possible only at the base of the columns without roller restraints.

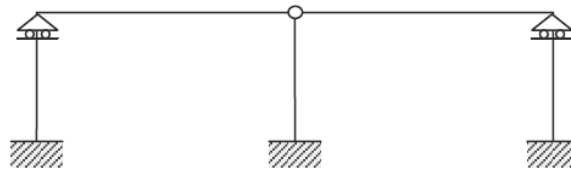


*Figure 2.30- Isostatic column structure* (Circolare n. 617 2009)

Furthermore, the connections have to transfer the horizontal forces under the design seismic load without taking into account the friction strength; this last rule also applies to roof-to-beam connections. The code forces a reduction of 50% in the behaviour factor, if some of the specific requirements concerning the connections are not followed.

As highlighted by the previous overview on the code's evolution concerning precast structures, design provisions and criteria for precast RC structures in non-seismic zones referred only to safety towards vertical loads till 2003. Wind, together with bridge crane if present, was the only horizontal load considered. Standards indicated minimum dimensions for elements, but there weren't limits for beam dimensions respect to column ones. There were provisions on minimum reinforcement for columns, but it was very poor compared to provisions for seismic zones. Beam-column connections usually relied on friction, or in some cases, metallic bars were used but only in order to facilitate construction phases (Savoia et al. 2012).

Several activities of research focused in last years on the development and the definition of standards and provisions on the anti-seismic design of precast RC structures, particularly concerning the detailing of connections between structural elements. Among them, the research project *SAFECAST* (Performance of innovative mechanical connections in precast buildings structures under seismic conditions), financed by the Seventh Framework Program and carried out at the European Laboratory for Structural Assessment (ELSA) of the Joint Research Centre (JRC) of the European Commission at Ispra (Italy), had the aim to fill the gap in the knowledge of the seismic behaviour of the mechanical connections used in precast concrete structures. A set of guidelines for the design of connections of precast structures in seismic areas was finally delivered in the framework of *SAFECAST* (Negro and Toniolo 2012).

A rational procedure for the seismic design and proper detailing of pinned beam-to column connections was proposed by Negro and Toniolo (2012). Following the concept of EC8, the connections are overdesigned with respect to the strength of beam and column. The prevailing energy dissipation mechanism of the structure relies on the formation of plastic hinges within the critical regions of the columns, with the connections remaining elastic. The design of the columns is based on a prescribed force reduction factor  $q$ , whereas the design of the connections follows the capacity design rule: the design shear force  $E_d$  for the connection is obtained assuming that the ultimate flexural resistance is developed at the base of the column, calculated by multiplying its flexural resistance  $M_{Rd}$  by the over-strength factor  $\gamma_{Rd}$  (suggested general safety factor  $\gamma_{Rd}$  is equal to 1.30 as proposed by Federation International du Beton). Verification for the shear resistance of the connection  $R_d$  is made, namely by satisfying the inequality  $E_d \leq R_d$ .

## 3. EMILIA EARTHQUAKES – REVIEW OF DAMAGES

### 3.1 20<sup>th</sup> and 29<sup>th</sup> May 2012 events

At the end of May 2012, a seismic sequence struck the Emilia region (Northern Italy), with two main events of local magnitude  $M_L = 5.9$  and  $5.8$  (Table 3.1).

On 20 May 2012 at 02:03:52 (UTC), local time 04:03:52, a  $M_L$  5.9 earthquake occurred interesting a huge area of Pianura Padana in Emilia, Veneto and Lombardia, particularly the Province of Ferrara, Modena, Reggio Emilia, Bologna, Mantova and Rovigo.

The epicentre of the earthquake was located by the National Strong Motion Network of INGV (National Institute of Volcanology and Geophysics of Italy) at coordinates Lat.  $44.89^\circ$  N, Lon.  $11.23^\circ$  E, between the towns of Mirandola and Finale Emilia in Province of Modena, near the limits with the Province of Ferrara. A series of aftershocks interested the area, two of which with magnitude  $M_L > 5.0$  in the same day.

On 29 May 2012 at 07:00:03 (UTC), local time 09:00:03, a new  $M_L$  5.8 earthquake occurred interesting the same area with epicentre between the towns of Medolla (MO) and San Felice sul Panaro (MO), only 12 km far from the epicentre of first event. Even the May 29<sup>th</sup> main event was followed by many aftershocks, two of which with magnitude  $M_L > 5.0$  in the same day.

A last strong seismic event of magnitude  $M_L = 5.1$  took place on 03 June 2012 at 17:20:43 (UTC), local time 19:20:43, with epicentre in Province of Modena.

Date	Local time (UTC+2)	Latitude [ $^\circ$ N]	Longitude [ $^\circ$ E]	Deepness [km]	Magnitude $M_L$
<b>20/05/2012</b>	<b>04:03:52</b>	<b>44.889</b>	<b>11.228</b>	<b>6.3</b>	<b>5.9</b>
20/05/2012	04:07:31	44.863	11.370	5.0	5.1
20/05/2012	15:18:02	44.831	11.490	4.7	5.1
<b>29/05/2012</b>	<b>09:00:03</b>	<b>44.851</b>	<b>11.086</b>	<b>10.2</b>	<b>5.8</b>
29/05/2012	12:55:57	44.888	11.008	6.8	5.3
29/05/2012	13:00:25	44.879	10.947	5.4	5.2
03/06/2012	21:20:43	44.899	10.943	9.2	5.1

*Table 3.1- Seismic events with  $M_L > 5$  recorded during 2012 Emilia sequence (QUEST INGV Working Group 2012)*

The whole area affected by the seismic sequence, including all epicentres, is approximately 60 km (East-West) x 30 km (North-South) with more than 2200 aftershocks and 7 main events of magnitude  $M_L > 5$ , showing a progressive move of epicentres westward. Two main shocks of 20<sup>th</sup> and 29<sup>th</sup> May were perceived in a very huge area including Northern and Central Italy, Switzerland, Slovenia, Croatia, Austria, South-Eastern France and Southern Germany.

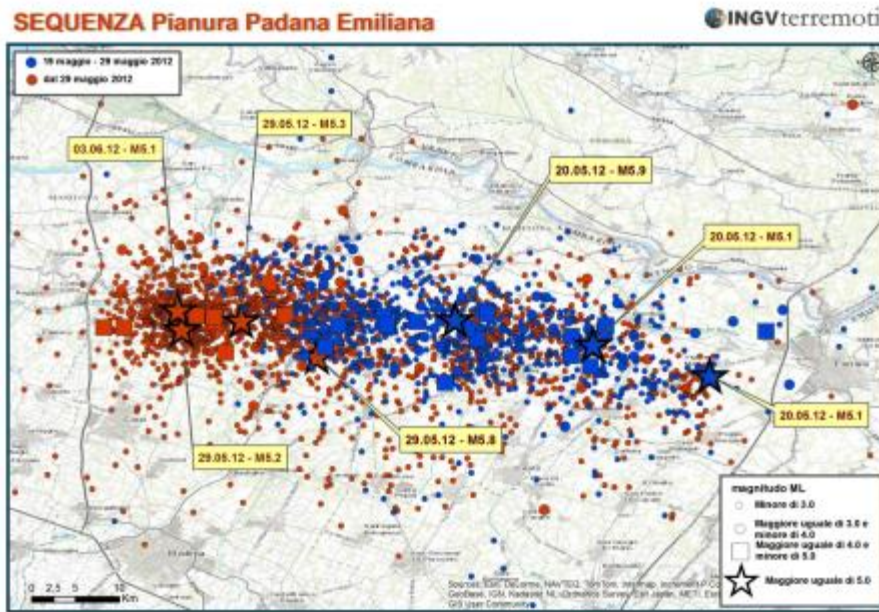


Figure 3.1- Map of the area affected by Emilia earthquakes of May 2012 showing westward progressive move of epicentres (INGV 2012a)

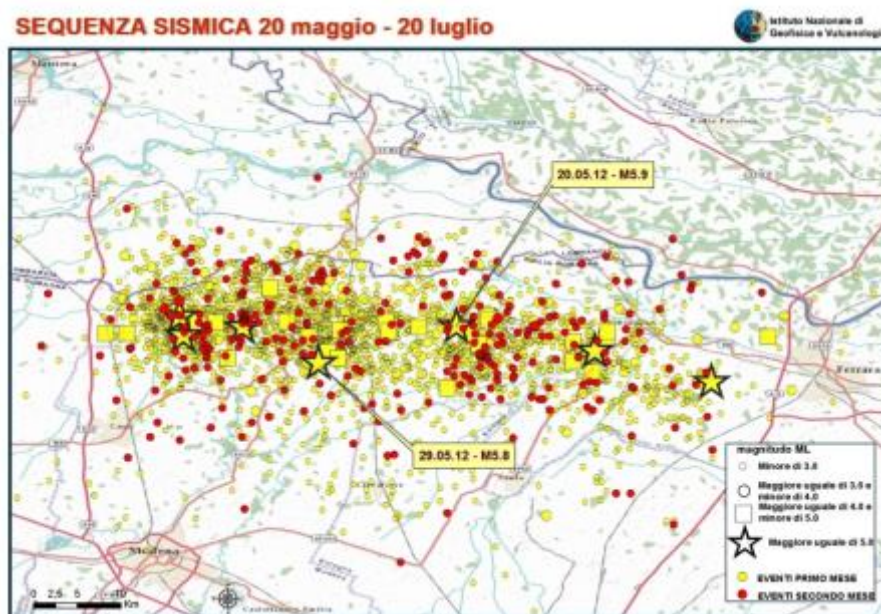


Figure 3.2- Map of seismic sequence of Emilia earthquakes from 20<sup>th</sup> May to 20<sup>th</sup> July 2012 (INGV 2013)

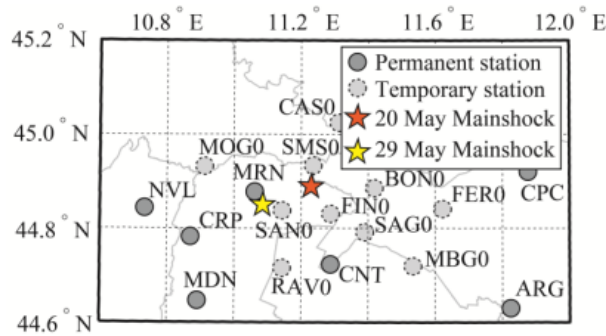


Figure 3.3- Permanent and temporary (installed after 20<sup>th</sup> May 2012) stations of Strong Motion Network

Following Figure 3.4 shows ground motion recordings of horizontal (*N-S* e *E-W*) and vertical component of acceleration at Mirandola station (*MRN* in Figure 3.3) on 20<sup>th</sup> May 2012.

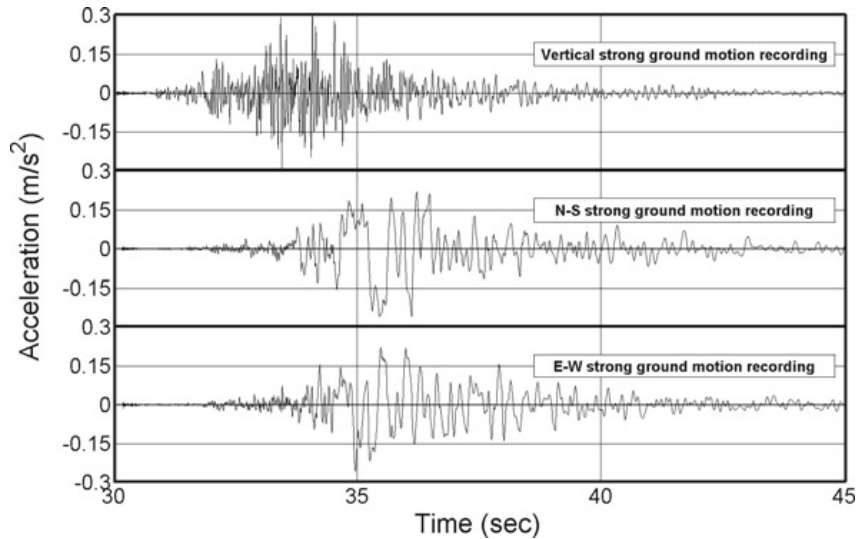


Figure 3.4- Vertical, *N-S* and *E-W* recordings at Mirandola station during 20<sup>th</sup> May 2012 event (Bournas et al. 2013)

Table 3.2 presents a summary of the maximum recorded accelerations for each orthogonal component obtained from Mirandola station, the permanent station closest to the epicentre, during the main events of 20<sup>th</sup> and 29<sup>th</sup> May.

Station	Date	Direction	Magnitude $M_L$	Distance [km]	PGA (cm/sec <sup>2</sup> )	PGV (cm/sec)	PGD (cm)
MRN	20 <sup>th</sup> May	Vertical	5.9	17	303	5.9	2.3
MRN	20 <sup>th</sup> May	E-W	5.9	17	256	30	9.2
MRN	20 <sup>th</sup> May	N-S	5.9	17	260	47	14
MRN	29 <sup>th</sup> May	Vertical	5.8	2	900	28	11
MRN	29 <sup>th</sup> May	E-W	5.8	2	220	29	9.2
MRN	29 <sup>th</sup> May	N-S	5.8	2	290	57	18

Table 3.2- Maximum recorded PGA, PGV and PGD at Mirandola for 20<sup>th</sup> and 29<sup>th</sup> May 2012 events (Bournas et al. 2013)

Maximum recorded peak ground acceleration (*PGA*) recorded by RAN (National Strong Motion Network) during the main events of 20<sup>th</sup> and 29<sup>th</sup> May 2012 was respectively equal to 0.265 g and 0.296 g, both values referred to N-S direction and recorded at Mirandola station.

Mirandola station recorded maximum vertical *PGA* values equal to 0.306 g for 20<sup>th</sup> May event and 0.917 g for 29<sup>th</sup> May event.

Historical seismicity of the Pianura Padana area interested by seismic sequence is quite low. Historical catalogues of the events in the area did not indicate relevant seismic phenomena in a radius of 30 km away from the epicentre, excepted for the strong earthquake that hit the town of Ferrara on 17<sup>th</sup> November 1570. Recently, most important seismic events have been on 11st July 1987,  $M_L = 5.4$  between Bologna and Ferrara and on 17<sup>th</sup> July 2011,  $M_L = 4.7$  in the Reggio Emilia district (QUEST INGV Working Group 2012).

In order to understand the damages recorded after the Emilia earthquakes, a brief description on code's evolution concerning seismic zone classification is provided.

Defining seismic zones in Italy began in 1909 following the Reggio Calabria and Messina earthquake in 1908 that caused about 80,000 fatalities. The regions in southern Italy that suffered from this earthquake were defined as seismic zones. Since then, the map has been refreshed, enlarging the zones defined as "seismic" after each significant Italian earthquake.

The Emilia region that was struck by the recent earthquakes (the black dot in Figure 3.5) was still outside of the seismic zones in the 1984 map (Figure 3.5a).

Finally, in 2003 (O.P.C.M. n. 3274/2003) the whole Italian territory was classified as seismic (Figure 3.5b), distinguishing among four seismic zones: Zones 1, 2, 3, and 4, corresponding to design peak ground acceleration at the bedrock equal to 0.35 g, 0.25 g, 0.15 g, and 0.05 g, respectively. The updated seismic zonation is compulsory since 23<sup>rd</sup> October 2005.

The area struck by the 2012 Emilia earthquakes was located in Zone 3 of medium-low seismicity, with expected peak ground acceleration *PGA* on rigid soil equal to 0.15 g for a return period of 475 years.

Hence, it is expected that all structural types in the Emilia region, designed up to 2003, do not take into account seismic design at all, strongly increasing the seismic vulnerability of structures built in that region. In particular, precast structures built up to 2003 typically provide beam-to-column friction connections because friction connections were forbidden only in seismic zones since 1987 (see Section 2.5).

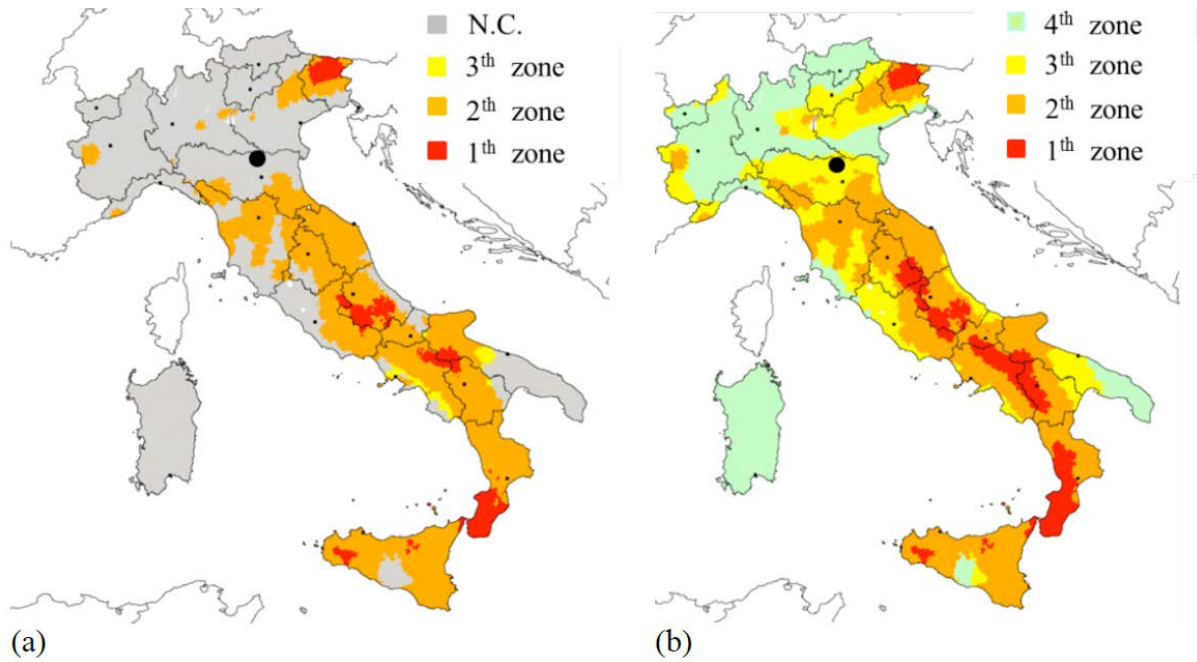


Figure 3.5- Seismic zone classification in Italy (a) in 1984 and (b) in 2003; the black dot indicates the Emilia earthquakes epicentral zone (INGV 2012b)

Deyanova et al. (2014) highlighted that 85% of investigated buildings in Emilia-Romagna were designed and constructed before 2003 (indicated in Figure 3.6 with the vertical dashed line), when the Emilia region was not classified as seismic zone. Figure 3.6 shows also that 40% of investigated buildings in Emilia-Romagna were designed and constructed after 1996 when the code provisions in Italy started implementing capacity design and performance-based design principles. Yet, the beam-column connections did not undergo conceptual changes.

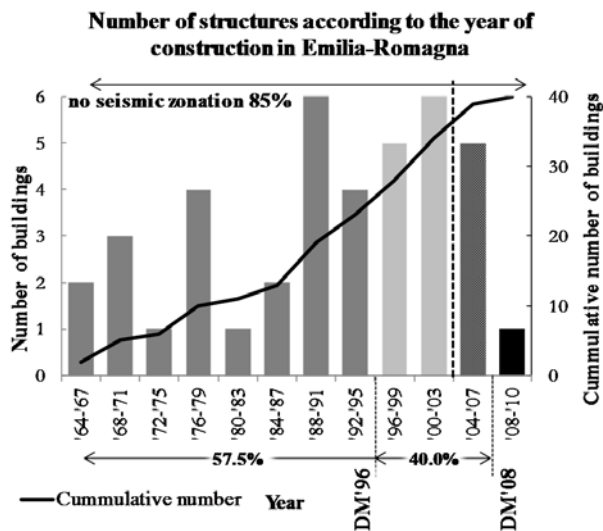


Figure 3.6- Number of structures according to the year of construction in Emilia-Romagna (Deyanova et al. 2014)

Lastly, the current Italian code (D.M. 14/01/2008) defines hazard parameters continuously for the whole national territory, without distinguishing different seismic zones. In particular, for the area struck by 2012 earthquakes, *PGA* values for a return period of 475 years are equal to 0.14 g – 0.17 g for rigid soil and 0.22 g – 0.26 g for soil *C*.

Figure 3.7 plots the spectra of the *N-S* component of the two strongest records of 20<sup>th</sup> and 29<sup>th</sup> events at Mirandola station as compared with the current Italian code, for ground type *B* and 5% viscous damping. It can be observed that the spectra from the recorded ground motions are consistently larger than the 475 years spectrum currently specified by the Italian norms.

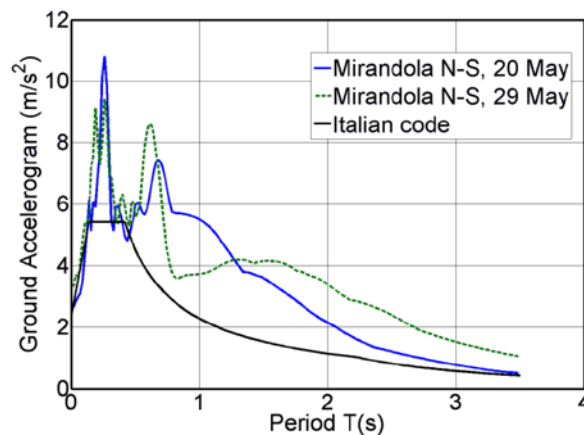


Figure 3.7- Spectra of the *N-S* component of the 20<sup>th</sup> and 29<sup>th</sup> May 2012 events compared to the Italian code spectrum (Bournas et al. 2013)

An explanation of extensive damages to precast structures can be found analysing recorded response spectra and acceleration values for different period of vibration.

It should be noted here that the fundamental period of a typical single-storey industrial precast RC building, calculated following a benchmark design study among Italy, Greece, Slovenia and Turkey, ranges between 0.8 and 1.4 s (Olgiati et al. 2011).

In order to establish the spectral accelerations in the precast structures during the investigated Emilia seismic events, a correct evaluation of the period of vibration is necessary. Two different period ranges can be distinguished according to the extensive parametric study provided by Magliulo et al. (2014b) on single-story precast structures designed according to the current Italian code in low-to-high seismic zones. The bare precast structures exhibit an elastic fundamental period ranging from 0.54 sec to 1.45 sec, while infilled precast structures range from 0.09 sec to 0.40 sec, due to the presence of cladding panels.

In Figure 3.8, the recorded spectra at Mirandola station on 20<sup>th</sup> May 2012 are compared with the design spectra provided by Italian building code in the epicentral zone for return periods equal to 475 and 2475 years (*C* soil and  $T_I$  surface), assuming a damping ratio equal to 5%.

The comparison demonstrates the rarity of the event for typical period of vibration of precast structures, according to the actual Italian seismic hazard maps and the historical data they are based on. The  $N-S$  component spectrum is generally included between the two considered design spectra for a low period range (i.e., before 0.6 sec), and it exceeds the spectrum with the higher return period for high period range (i.e., beyond 0.6 sec). No significant difference between the spectral ordinates for bare and infilled structures for  $N-S$  component is evidenced; on the contrary, in the case of  $E-W$  component, the 0.09 sec–0.40 sec range provides larger spectral ordinates (Magliulo et al. 2014c).

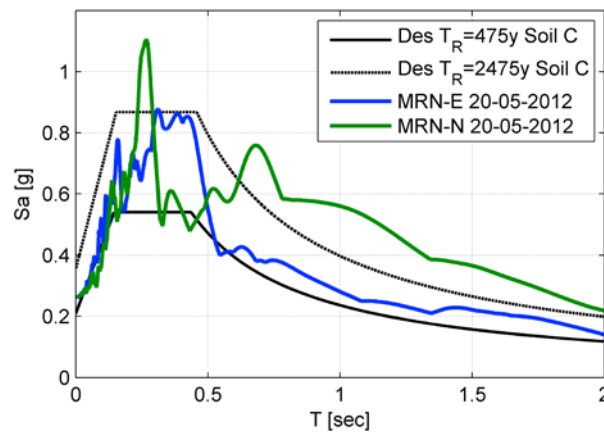


*Figure 3.8- Elastic response spectra recorded on 20th May 2012 in Mirandola: N-S (green) and E-W component (blue) compared to elastic response spectra provided by Italian building code (Magliulo et al. 2014c)*

The same conclusion can be reached observing Figure 3.9 that shows the response spectra of the  $N-S$  and  $E-W$  components of the ground motions recorded at Mirandola station for both events of 20<sup>th</sup> and 29<sup>th</sup> May. As it can be observed, beyond the peak value of acceleration which occurred for low periods, only the  $N-S$  component of the response spectra in both earthquakes shows high accelerations for higher periods. In particular, Bournas et al. (2013) notices how for periods in the range of 0.7–1.8 s, the spectral acceleration of the  $N-S$  component of the 29<sup>th</sup> May earthquake is approximately equal to half of its peak spectral value.

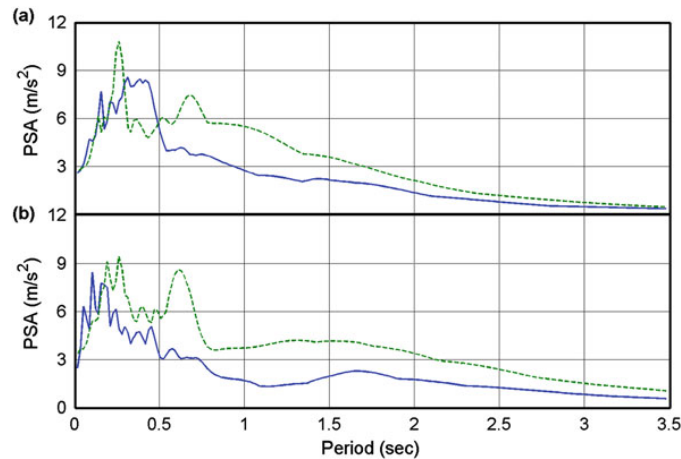


Figure 3.9- Response spectra at Mirandola station of N-S (green dashed line) and E-W (blue line) components for the earthquakes of (a) 20<sup>th</sup> May and (b) 29<sup>th</sup> May 2012 (Bourmas et al. 2013)

The low frequency content of recorded acceleration, particularly of the N–S component, may have contributed to the high levels of damage experienced by structures with high periods of vibration, such as the very flexible precast industrial buildings.

## 3.2 Economic impact

Past international experiences have shown that, especially in very industrially developed zones, earthquakes can threaten local economies. Since the solution cannot rely only on insurance for consequences, a systematic prevention is the only method to guarantee owners as well as employees and in general the regional community.

Induced economic losses, due to the industrial business interruption, can be much more higher than direct structural damages and can have catastrophic consequences on production activities and warehouses, forcing a dislocation of business in other areas or even the bankruptcy of the business, both situations that obviously would cause a very negative economic and social impact on local territory.

The issue of seismic vulnerability of industrial plants is of pristine importance for life safety, for business continuity of activities and for social and economic consequences on territories. In other terms dealing with industrial buildings, the protection of exposed value (machinery and stocked goods) and business continuity issues must be added to life safety.

The seismic risk is very high in zones with significant exposure, due to concentration of industrial activities, only recently classified as seismic-zones, where vulnerability of existing structures built without anti-seismic provisions is particularly high, like the Emilia region of Northern Italy.

Referring to 2012 Emilia earthquakes, the main shock of May 20<sup>th</sup> caused seven casualties, of which four were caused by the collapse of the industrial plants of three different firms. The number of casualties was limited due to the earthquake occurring in the night between Saturday and Sunday when most people were in their homes, which were less damaged when compared to industrial plants. A main shock during working hours would probably have resulted in a far greater number of victims. The May 29<sup>th</sup> event caused a total of 20 further casualties, most of them being workers involved in the rescue of equipment and goods. Totally, the Emilia seismic sequence of 2012 caused 27 deaths, about 400 injured and about 15,000 homeless.

In the area:

- 500 factories with severe structural damages;
- 3,000 factories with banned access;
- 15,000 workers laid off or lost their jobs (5,000 engineering sector, 4,000 food production, 4,000 biomedical production, 2,000 ceramics);
- 60,000 firms interested by the earthquakes.

The Emilia earthquakes caused direct economic losses (due to damages) amounting to about € 2.7 billion, while the induced economic damage, the loss due to the industrial business interruption, amounts to about €3.1 billion (Regione Emilia-Romagna 2013).

The area struck by the Emilia earthquakes is one of the most industrialized regions of Europe (Figure 3.10) and is characterized by a high density of precast structures. The area produces about 2% of national GDP.

Indeed, referring to 2001 data of Italian National Institute of Statistics (Istituto Nazionale di Statistica, or ISTAT), the percentage of commercial, industrial, transportation, communication, office, and hotel buildings that are precast structures in the whole of Italy is 3,65%. Considering the locations hit by the seismic events - for example, Medolla, Mirandola, and San Felice sul Panaro - this percentage increases to 9%; this illustrates both the high incidence of precast buildings and the influence that the vulnerability of this structural type has on the seismic risk of the area (Magliulo et al. 2014c). Most of precast industrial buildings are single-storey buildings, while commercial and office buildings can be also multi-storey precast buildings.

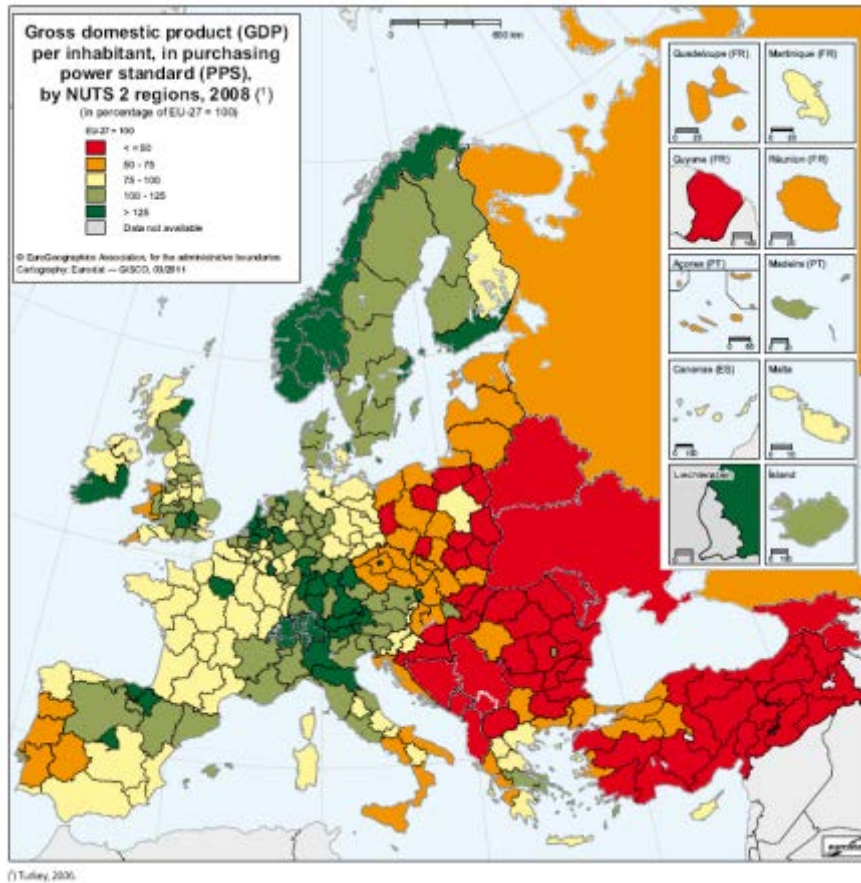


Figure 3.10- Gross domestic product (GDP) per inhabitant, in purchasing power standard (PPS), by NUTS 2 regions (Eurostat regional yearbook 2011)

In the following, considerations about economic impact of earthquakes on business activities are introduced.

With reference to 2012 prices estimated in the annual report of the Italian Revenue Agency (2012), structural construction costs are estimated, on average,  $100 \text{ €m}^2$ ; the market value is equal to about  $600 \text{ €m}^2$ . Market value is the mean value of samples excerpted by official (registered sale contracts) and non-official (estimations of local officials) data. Considering a mean surface of about  $1,000 \text{ m}^2$  (most of industrial activities are small factories with less than 10 employees), the mean value  $V$  of an industrial building in Emilia-Romagna can be calculated as  $V = 600 \text{ € m}^2 \times 1,000 \text{ m}^2 = 600,000 \text{ €}$

The annual industrial production of Emilia-Romagna region, based on official data, is 19.6 billion € (about 20% of whole annual GDP of the region). Therefore, given the total number of industrial buildings in Emilia Romagna region (see Section 2.1), the yearly production  $P$  per industrial building is  $P = 19.6 \text{ billion €} / 83,465 = 234,829 \text{ €}$ . The yearly cost of business interruption is much larger than the yearly lost due to failure, which can be subdivided in about 30 years ( $V = 600,000 \text{ €} / 30 \text{ years}$ ):  $P = 234,829 \text{ €/year} \gg V = 20,000 \text{ €/year}$ .

The obvious conclusion is that the value of contents is much greater than the value of the building.

Furthermore, past experiences, and in part also the recent one, have shown that due to the general failure in the epicentral area, there is also the risk that industries leave instead of rebuild their structure, to be able to restart the production in short time (Nutti and Vanzi 2014). In addition, enormous social and economic implication must be considered.

The high social and economic impact of 2012 Emilia earthquakes respect to not so high seismic events intensity is mainly due to the combinations of following aspects:

- high exposure of the area due to high concentration of industrial activities in one of the most industrialized region of Europe (Figure 3.10);
- high seismic vulnerability of existing industrial precast structures designed without anti-seismic standards, due to only recent classification as seismic-zone (Section 3.1);
- spectral characteristics of recorded acceleration that affected especially structures with high periods of vibration, such as the very flexible precast industrial buildings (Section 3.1).

The severe damage that affected industrial precast buildings is probably the most controversial issue raised by the Emilia earthquakes, because of the high exposure in terms of human life, building content (both equipment and goods) and importance of production process continuity. Due to the deficiencies observed in the damaged buildings, the building occupancy assessment procedure was modified with reference to the ordinary one. The ordinary Italian procedure is to consider the building safe if, based on a visual survey, it can be expected to survive another shock of the same intensity as the main shock which has occurred, but in the case of industrial buildings such a procedure has now been made much more stringent. Due to the frequent inadequacy of the fastenings between non-structural and structural elements, the common absence of connections between the structural elements and the recurrent lack of any redundancy even in the main structure, an engineering appraisal is required stating that the building does not suffer from main deficiencies. This more strict approach has raised discussions because it ensures human life, but may cripple the business by interrupting production even in undamaged buildings (Liberatore et al. 2013).

Social and economic impact of 2012 Emilia earthquakes showed how post-earthquakes measures and strengthening solutions can't be based only on technical considerations.

Braga et al. (2014) underlines that disaster management authorities had to cope with the high damage observed in industrial structures, the uncertainties on the information gained from the surveys, public safety, and necessity of a rapid recovery of activities with the least possible impact on social and economic life.

Two main regulations were issued, the first one on June 6<sup>th</sup> 2012 by the Italian Government (Decreto Legge n. 74 6 giugno 2012), the second one on August 1<sup>st</sup> 2012 by the Italian Chambers (Legge n. 122 1 agosto 2012); both concerned only the region struck by the earthquakes (part of the Emilia Romagna region, plus small parts of the confining regions of Lombardy and Veneto).

The first regulation was issued a few days after the events of May 2012 and was based on a post-earthquakes assessment process divided in two phases, aiming at rapid socio-economic recovery in the short term and a higher generalized safety level in the medium term.

For precast structure it was required to follow a procedure that provides two main phases:

- the *first phase*, in which the elimination of the most important structural deficiencies must be guaranteed;
- the *second phase*, in which a series of extensive actions must be provided in order to achieve a given performance level.

The common deficiencies that must be solved during the first phase are:

- a) the lack of mechanical connection devices between vertical and horizontal elements and between horizontal elements;
- b) the presence of cladding panels not adequately connected to the main structure;
- c) the presence of not braced storage-rack structures that may involve the main structures in their failure.

Then, within a determined period, in fact, all industrial structures had to be verified and retrofitted with the provisions of the current Italian building code (D.M. 14/01/2008), namely using chapter 8 concerning existing structures. The seismic verification required was lower with respect to the one used for new structures; this lower level was subjectively set at 0.6 times the seismic load used for the design of new structures.

The short term checks entitled to temporary occupancy permission: if no evidence of heavy structural deficiencies were found, or if they were solved for, the structure could be normally used, although for a limited period. The checks on structural deficiencies were minimal, in order to make them simple and timely. If either:

- i. no connections between vertical and horizontal structural elements, or between horizontal elements was found;
- ii. pre-cast infill elements were not adequately connected to the structure;
- iii. shelf systems (carrying heavy materials whose collapse may result in damage or collapse of the structure) were unbraced;

the deficiencies had to be solved before using, even temporarily, the structure.

---

i., ii. and iii. are in fact the most frequent causes of seismic collapses and damages; clearly they do not cover all possible vulnerabilities. The short term provision tried in fact to compromise between timely recovery and safety, accepting a lower level in the short term.

The provisions in the longer term (verify or retrofit at 60% the seismic load for new structures) were however incoherent with the safety level accepted elsewhere in Italy. In fact, existing structures, designed with older structural codes and often not satisfying the requirements of new ones, are compelled to upgrading at the newer code requirements only if there is load or usage change; in all other cases, the usage of the structure can continue unchanged. What appears a compromise between the initial requirement of Decreto Legge n. 74 6 giugno 2012 and what was customarily accepted elsewhere in Italy (and generally in all countries) was found within the second regulation by the Italian Chambers (Legge n. 122 1 agosto 2012).

This one, in short, made use of the recorded earthquakes as a test: if the industrial building had undergone a strong enough earthquake without any damage, both for the structural and non-structural and installations parts, this information was used as a test to prove (or disprove) acceptability of the structural safety level. Since the first regulation (Decreto Legge n. 74 6 giugno 2012) set the seismic load with which to verify (and retrofit, if the verifications were not satisfied) the structures at 0.6 times the seismic load (defined via the elastic response spectrum) for new structures, the strong enough earthquakes were similarly defined. More precisely, if the local elastic earthquake response spectrum was higher than 0.7 times the design response spectrum, and the structure had well performed, then the regulation (Legge n. 122 1 agosto 2012) stated there was no obligation to verify (and possibly retrofit) with 0.6 times the seismic load for new structures. Good performance was conservatively defined as a stress and deformation state with the linear elastic field, both for the structural, non-structural and installations building components (Braga et al. 2014).

### **3.3 Review of damages**

Industrial single-storey precast RC buildings are the structural type that suffered the most damage during the Emilia earthquakes. Magliulo et al. (2014c) reported that more than a half of the existing precast structures exhibited significant damage.



*Figure 3.11- Aerial photo of collapses of industrial precast buildings during 2012 Emilia earthquakes*

As described in previous sections, the huge damage experienced by single-storey precast structures can be explained by the exclusion of the epicentral region from the seismic areas recognized by the Italian building code up to 2003, so that it is expected that almost all existing industrial precast buildings in the Emilia region were designed and built without seismic design at all.

According to standards compulsory at the age of construction, most of the precast industrial buildings in the affected area were designed for gravity loads only. Precast structures designed and built without anti-seismic standards proved to be completely inadequate to resist to seismic action. Deficiencies observed in seismic response of existing precast RC structures are generally due to inadequate seismic design of detailing or, more frequently, to a complete absence in the design of anti-seismic provisions.

A small number of buildings were designed and constructed during the last 5–7 years, presumably conforming to the updated seismic zoning of the area (Bournas et al. 2013).

In addition another reason of high damages may be found in the high content of low frequencies recorded in Emilia earthquakes, that affected particularly structures with long fundamental periods of vibration, as precast structures typically have.

Most common observed damages concerned:

- unseating of horizontal structural elements, particularly in case of friction-based connections between roof elements and beams and between beams and columns;
- damage to columns;
- cladding precast panels detachment, after panel-structure connection failure.

The main vulnerability of industrial buildings designed without seismic provisions concerns the absence or the inadequacy of the connections between precast elements. Other

deficiencies include insufficient seating in case of friction-based connections, insufficient longitudinal and transverse reinforcement of columns, insufficient splice and anchorage lengths, inadequacy of the anchorages of precast cladding panels to structural elements, lack of rigid-diaphragm effect at the roof level and isolated unconnected column foundations. The floor/roof system and the beams, where most of the masses are concentrated, were not tied together and there were no means of transferring the inertial seismic loads to the lateral load resisting system, namely the columns (Bournas et al. 2013).

In addition, large displacements that caused unseating of the beams from the column supports have been often increased by other phenomena, like interaction with non-structural elements, especially irregular cladding panels or partial-height masonry infills (Savoia et al. 2012).

After Emilia earthquakes of May 2012, many field survey activities and damage observations have been carried on in the affected area by reconnaissance teams of technic, volunteers, institutions and researchers. These activities produced many field reports and research papers, with the aim to observe and understand damages in order to find strengthening solutions able to reduce vulnerabilities showed by these structures.

Field reports after the Emilia earthquakes showed that most of the partial- and full-collapses observed were caused by the absence of effective mechanical connectors between structural elements (Savoia et al. (2012), Liberatore et al. (2013), Bournas et al. (2013), Magliulo et al. (2014c)).

In particular, Bournas et al. (2013) reported that approximately 75% of the precast concrete industrial buildings designed with non-seismic provisions that they analysed in the affected area presented damage and detachment of the exterior cladding elements, with 25% of the total presenting partial or total collapse of the roof, mainly due to the loss of seating of the main girder.

The key element that influenced the behaviour of the structure under seismic action consists in the typology of beam-column connection. Precast industrial buildings designed with seismic provisions generally presented no damage to the structural elements. The damage on non-structural elements, which typically comprised the detachment of cladding panels from the main structure due to insufficient capacity of the connections, instead were not significantly reduced in the buildings designed with seismic provisions.

Liberatore et al. (2013) presented a synopsis (Figure 3.12) of the damage surveyed on more than 30 buildings, where tentative damage levels (from slight damage to severe damage) are proposed together with their frequency of occurrence.

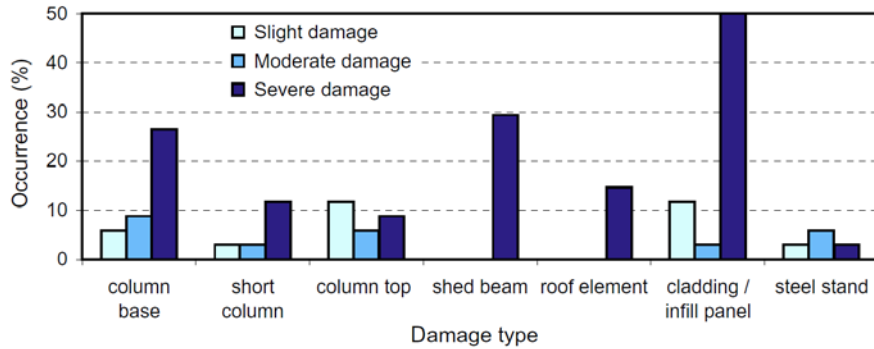


Figure 3.12- Synopsis of damages observed in more than 30 surveyed industrial buildings (Liberatore et al. 2013)

Figure 3.12 highlights the high percentage (50%) of severe damage suffered by cladding elements and infill panels. In cladding panels, the damage is related mainly to the failure of fastening elements and to the consequent out-of-plane overturning. Occurrence of severe damage to columns amounts to almost 50% as well (considering together the damage at the base, at the top and the short-column mechanism).

Damage to shed beams was due, in almost 30% of the buildings surveyed, to their unseating: the vertical component of ground motion, together with the lack of connection between column and beam, played a significant role in the activation of this kind of collapse. In Figure 3.12 damage of the roof caused by the unseating of the beams has not been reported: the damage to roof panels in the figure is related to their unseating alone. Finally, it should be noted that, because it was not always possible to survey the interior of the buildings, the occurrence of non-structural damage might have been higher than reported in Figure 3.12.

Analysing damages of existing precast structures, Savoia et al. (2012) distinguished the behaviour of buildings built during 70s and 80s and more recent buildings. Even there is a great variability among different structures, in order to simplify the understanding of seismic behaviour and to identify some common characteristics and vulnerabilities, Savoia et al. (2012) proposed a classification of surveyed precast RC buildings in two different types:

- precast RC structures built during 70s and 80s (*Type I*), characterized by great deformability, slender columns (40x40 cross-section), friction-based beam-column connections and masonry infills as exterior walls (Figure 3.13);



*Figure 3.13- Precast RC structure built during 70s-80s (Type 1) with double-slope beams and masonry infills (Savoia et al. 2012)*

- precast RC structures built after 1990 (Type 2), characterized by large spans, beams and columns with big dimensions, precast roof elements alternated with light elements with high roof in-plane deformability, exterior cladding precast panels (horizontal or vertical) connected to the structure (Figure 3.14).



*Figure 3.14- Precast RC structure built after 1990 (Type 2) with pre-stressed precast roof elements and precast cladding panels (Savoia et al. 2012)*

Savoia et al. (2012) observed that the high values of relative displacement between structural elements that determined collapse of simply supported roof beams can have been increased by interaction with non-structural elements, in particular partial-height masonry infills masonry or precast concrete cladding panels with irregular distributions across the structure.

Considering behaviour in transverse direction of the building, in the plane of frames, regular masonry infills play the role of shear walls and their strength can generally prevent from significant damages. During 2012 Emilia earthquakes for example, buildings with a regular distribution of masonry panels suffered few damages (Figure 3.15).



*Figure 3.15- Lightly damaged regular masonry infills (Savoia et al. 2012)*

In some cases, just the presence of regular masonry infills permitted to avoid damages in correspondence of head portal frames, while all intermediate frames collapsed (Figure 3.16).



*Figure 3.16- Damages in head portal frames avoided by regular masonry infills (Savoia et al. 2012)*

On the contrary, in case of masonry infills not covering the full length of the column, because of the presence of continuous windows, typically under the precast beam, interaction between partial-height masonry infills and columns caused significant damages to the columns, with short-column shear failure mechanism leading to the unseating of the beam (see Section 2.4). The unseating of the beam typically interested only head portal frames, but in some cases also the following frame. In following Figure 3.17 some examples of short-column mechanism of failure leading to the unseating of the beam are shown.



*Figure 3.17- Unseating of the beam due to short-column mechanism because of interaction with partial-height masonry infills (Savoia et al. 2012)*

Observations of damages of past earthquakes show how the effect of masonry infills in the plane of the frames can be positive if they have a regular distribution across the structure and behave as shear walls, negative if they don't cover the full length of the columns.

In next sections damages that occurred to precast structures during the Emilia earthquakes are presented through photographic documentation, subdividing seismic behaviour of connections (friction-based and pinned), columns and external cladding panels.

### **3.4 Seismic behaviour of connections**

Most common observed damage concerned unseating of horizontal structural elements (beams and roof elements), from their support elements (beams and columns, respectively). The loss of support can be caused by:

- Absence of mechanical connections (friction-based connections)
- Inadequacy of existing mechanical connections (limited distance of the dowels from the edge and insufficient transverse reinforcement in structural)

(Gruppo di Lavoro Agibilità Sismica dei Capannoni Industriali 2012).

Most of existing precast RC structures present connections with transferring of horizontal forces that relies only on friction, without any mechanical device. The vulnerability and consequent damages recorded in precast structures during Emilia earthquakes of 2012 is certainly larger than the vulnerability exhibited by similar precast structures in past earthquakes, (e.g. 1999 Kocaeli earthquake in Turkey). The main reason is just the common presence of connections relying on friction in the Emilia region, contrasting with the doweled connections used in other countries, like Turkey.

Seismic behaviour exhibited by connections between existing precast structural elements during 2012 Emilia earthquakes is described in the following, distinguishing the behaviour of friction-based connections and pinned connections.

### ***3.4.1 Friction-based connections***

Most of damaged precast RC buildings presented friction-based connections. As described in Section 3.1, the area struck by the 2012 Emilia earthquakes was classified as seismic zone (zone 3 of medium-low seismicity) only in 2003 (O.P.C.M. n. 3274). The D.M. 3/12/1987 and previous standards according to which most of existing precast RC buildings were designed, allowed the use of friction-based connections in non-seismic zones. Consequently, most of existing precast RC industrial structures built in zones only recently classified as seismic were realised without any mechanical connection between structural elements, both in roof elements-beam connections and beam-column connections.

In this connection typology, the capacity of transferring lateral loads depends entirely on the static coefficient of friction between the supporting surfaces of beam and column and on the length of the beam seating when the friction forces are exceeded by the earthquake force demands. Just the lack of mechanical connection devices between structural elements, especially beam-column joints, was the main cause of local and global damages and collapses in single-storey precast RC structures.

The weak link in the vast majority of the industrial buildings visited was the absence of mechanical connections between roof-girders and columns. The low strength towards lateral loads given by friction mechanism caused losses of support of both roof elements from beams and beams from column, with disastrous consequences (Figure 3.18).

The most common collapse mechanism in precast buildings with friction-based connections consists in the loss of support of structural elements, especially in beam-column connections. It is clear that the reliance on friction alone is not sufficient to prevent unseating of structural elements, especially when a significant vertical component of ground motion can be expected. Because of any lack of redundancy, a catastrophic collapse of all roof elements has usually followed the failure of one or more main beams (Liberatore et al. 2013).



*Figure 3.18- Collapses due to unseating of roof precast beams* (Bournas et al. 2013) (Liberatore et al. 2013)

One of the most common typology of connection corresponded to double-slope beams, simply supported over special openings (forks) at the top of columns. This typology was used in Italy during the 60s and 70s for agricultural buildings, now being replaced by the more common flat-roof systems. The collapse of most of the precast buildings was due to unseating of the transverse girders from the column forks. Concerning the loss of seating of beams and columns, it is noted that the flat and the sloped roof systems are equally vulnerable. The main difference between the two systems is that the sloped roof corresponds to a generally older design, where the girder has a smaller width (due to its higher section height) that leads more easily to out-of-plane failures.

In following figures a series of damages and collapses due to unseating of double-slope roof beams are shown (Gruppo di Lavoro Agibilità Sismica dei Capannoni Industriali 2012).



*Figure 3.19- Unseating of roof beams* (Gruppo di Lavoro Agibilità Sismica dei Capannoni Industriali 2012)



*Figure 3.20- Relative beam-column displacements without reaching loss of support*

Unseating of the roof elements or panels has been observed in a few cases, although less frequently than that of the main beams. Of course collapse of the beams has systematically induced that of the roof elements. Older clay-block RC slabs usually performed better, being able to behave as rigid diaphragms (Liberatore et al. 2013).

Figure 3.21 shows the loss of support of a main beam from the column and consequent collapse of precast roof panels, causing the inhabitability of the whole building.



*Figure 3.21- Unseating of main beam and consequent collapse of roof panels* (Gruppo di Lavoro Agibilità Sismica dei Capannoni Industriali 2012)

In some cases (Figure 3.22) the presence of friction-based connections induced loss of support only of roof elements from the main beam and didn't involve beam-column joint.



*Figure 3.22- Collapse of precast roof elements due to unseating* (Gruppo di Lavoro Agibilità Sismica dei Capannoni Industriali 2012)

In buildings with multiple bays, the seating loss was in the majority of the cases observed in the central column, where the seating length of the girders was rather limited and the relative displacement between the column and girder exceeded the available width.

As described in Section 2.4, in many cases exterior walls significantly influenced structural behaviour. Particularly, the interaction with partial-height masonry infills often led to non-synchronous displacements at the top of columns, thus contributing to unseating of the beams and causing local behaviour of shear failure of column, as shown in Figure 3.23.



*Figure 3.23- Unseating of the beam due to interaction with partial-height masonry infills and short-column shear failure (red arrow indicates the direction of seismic action) (Bournas et al. 2013)*

In some cases, because of inadequacy of beam-column restraint, permanent rotations took place in the out-of-plane direction of the roof girder (Figure 3.24).



*Figure 3.24- Rotation of the beam in the out-of-plane direction (Gruppo di Lavoro Agibilità Sismica dei Capannoni Industriali 2012)*



*Figure 3.25- Rotation of the beam in the out-of-plane direction* (Liberatore et al. 2013)

Very often the only restraint towards lateral displacements and rotations consists in the presence of forks at the top of the column, usually with few or without any reinforcement. In other cases the collapse of the girders took place in the out-of-plane direction of the girder, after failure at the base of the forks. Figure 3.26 and Figure 3.27 illustrate the out-of-plane collapse of a double-slope precast beam after unseating, following failure of the lateral restraints of the fork at the seat pocket.



*Figure 3.26- Out-of-plane collapse of a double-slope precast beam after unseating following shear failure of the fork*  
(Bournas et al. 2013)



*Figure 3.27- Out-of-plane collapse of a double-slope precast beam after unseating following shear failure of the fork (Saitta et al. 2012)*

### ***3.4.2 Pinned connections***

The main feature of precast industrial buildings constructed with seismic provisions lies in the type of beam-column connections. When horizontal forces are taken into consideration in design, the most common connection system for the construction of single-storey industrial buildings in Europe comprises hinged beam-column connections by means of dowel bars (shear connectors). This type of connection is able to transfer shear and axial forces resulting from the seismic actions. Practically, the horizontal beam-column connection is established by means of vertical steel dowels (typically one or two) which are protruding from the column into special beam sleeves, as shown in Figure 2.20. This pinned beam-column connections are constructed by seating the beams on the column capitals and by holding the beam ends in place by the use of these vertical steel dowels.

In general, recently constructed precast concrete buildings, which most probably incorporated steel dowels in the beam-column joints, exhibited apparent good performance.

Even in presence of mechanical connection between structural elements, failure of beam-column connections were observed, mainly due to the absence of specific anti-seismic provisions. It is worth mentioning that a building completed in 2010 showed partial collapse, in spite of having been designed (according to information provided by the owner) with pinned beam-column connections following the new Italian building code. Visual inspection revealed failure at the top of one of the central column beam-column connections. This failure was followed by loss of the girder seating and its subsequent collapse (Figure 3.28). The rather limited distance of the dowels from the edge of the column and the limited amount of transverse reinforcement might have resulted into the formation of a shear crack across the

concrete cover, followed by the loss of the dowels anchorage and consequently the loss of the girder seating. The strength of the pin connection is designed referring to the failure of the dowel, but in this case the spalling of concrete occurred before the yielding of the dowel, due to the small size of the cover and to the lack of dense stirrups close to the supporting zones. This failure reveals the lack of specific provisions for detailing the beam-to-column connections of precast RC buildings in the current Italian construction standards and the as well as in the Eurocodes (Bournas et al. 2013).



*Figure 3.28- Collapse due to failure of the pinned beam-column connection* (Bournas et al. 2013)



*Figure 3.29- Relative beam-column displacement, in spite of probable presence of mechanical connection device but without adequate transverse reinforcement* (Gruppo di Lavoro Agibilità Sismica dei Capannoni Industriali 2012)

### 3.5 Seismic behaviour of columns

In Italian single-storey precast existing structures, columns are generally precast elements connected, at the bottom, to a socket foundation and, at the top, by a horizontally sliding or hinged support to the beams not able to transfer seismic loads. Therefore the columns can be assumed to act as cantilevers fixed at the base. The formation of plastic hinges at the column base represents the main source of energy dissipation of these buildings due to the absence of bilateral connection between columns and beams.

Finally, precast columns have suffered different types of damages:

- loss of verticality, due to a rotation in the foundation element caused by a possible inadequate column-to-foundation connection (even if this cause is not easily ascertainable unless a direct inspection of foundation is made) or by the impact of collapsed horizontal elements (roof precast elements and beams), after their unseating (Figure 3.30, Figure 3.31, Figure 3.32);
- plastic hinge development at the column base (Figure 3.34-Figure 3.35);
- short-column shear failure due to the interaction with partial-height masonry infill systems (Figure 3.36);
- damages at the top of the columns due to concrete spalling at the beam support (Figure 3.37) or failure of lateral forks (Figure 3.38 and Figure 3.39).

In some cases the rotation of the columns has been substantial, showing out-of-plumb values of even 3%. The high top displacements values reached by the columns may have induced the unseating of supported beams in absence of mechanical connections between structural elements.



*Figure 3.30- Loss of verticality of columns* (Gruppo di Lavoro Agibilità Sismica dei Capannoni Industriali 2012)



*Figure 3.31- Rotation of columns increased by the impact of a fallen roof beam* (Liberatore et al. 2013)



*Figure 3.32- Loss of verticality of a column and consequent reduction of beam seating length* (Gruppo di Lavoro Agibilità Sismica dei Capannoni Industriali 2012)

The activation of a plastic hinge at the base of a column has been observed by Liberatore et al. (2013) in more than 40% of the buildings investigated. In some cases columns showed only cracking of the base section (Figure 3.33), in others concrete spalling and rebar buckling

occurred because of lack of transverse reinforcement in the critical region of the column (Figure 3.34 and Figure 3.35).



*Figure 3.33- Cracking of the base section of the column* (Gruppo di Lavoro Agibilità Sismica dei Capannoni Industriali 2012)



*Figure 3.34- Plastic hinge at column base after substantial rotation of the column* (Liberatore et al. 2013)



*Figure 3.35- Plastic hinge at column base with concrete spalling and longitudinal bar buckling because of the lack of adequate transverse reinforcement in critical region (Gruppo di Lavoro Agibilità Sismica dei Capannoni Industriali 2012)*

Masonry panels, when not covering the full length of the column, led in many cases to the formation of short-column failures (Figure 3.36).



*Figure 3.36- Short-column failure due to interaction with masonry infills*

A frequent damage at the top of the columns consisted in failure of lateral forks of the pocket supports, that didn't manage to act as lateral restraints and to avoid out-of-plane direction

---

collapses. Another type of damage at the top of the columns, of less gravity, consisted in spalling of the concrete directly supporting the beam, especially in absence of rubber pads between the two structural elements.



*Figure 3.37- Concrete spalling at beam-column support due to absence of rubber pads* (Liberatore et al. 2013)



*Figure 3.38- Failure of lateral forks at the top of the column* (Liberatore et al. 2013)



*Figure 3.39- Damaged lateral forks at the top of the column* (Savoia et al. 2012) (Nascimbene and Bellotti 2013)

### 3.6 Seismic behaviour of precast panels

Exterior wall systems of single-storey precast buildings, especially of more recent structures, in the Emilia region are mostly constituted by precast cladding panels. Horizontal (Figure 3.40a) and vertical (Figure 3.40b) panels collapse is one of the most frequent damage in precast buildings. Liberatore et al. (2013) observed that almost two factories out of three of surveyed building after 2012 Emilia earthquakes suffered such damage.



*Figure 3.40- Collapse of horizontal (a) and vertical precast panels (b)*

Both horizontal and vertical panels can be anchored to columns and beams through different kinds of connections. During 2012 Emilia earthquakes, failure of many panels connections was observed, inducing the collapse of heavy cladding panels. The vertical external cladding panels generally have shown a better performance, because they are embedded in the thick ground flooring.

Magliulo et al. (2014c) identified causes of collapses in:

- The lack of seismic design in cladding panel-to-structural element connection devices, designed only for gravitational loads and wind actions;
- The pounding of roof elements, columns or other precast panels;
- The panel-structure interaction that causes additional lateral forces in the connection devices, not considered during the design process.



*Figure 3.41- Failure of horizontal precast panels connections* (Magliulo et al. 2014c)



*Figure 3.42- Failure of vertical precast panels connections* (Magliulo et al. 2014c)

Most of the inspected buildings, designed with or without seismic provisions, presented failure of the connections of the cladding elements due to their insufficient displacement capacity that led to overturning of the cladding elements. The panel connections were designed to transfer the vertical (self-weight) load of the panel, as well as any out-of-plane loading, to the main elements of the precast structure (beams and columns). For small drifts of the structure, the connections do not provide any in-plane stiffness interaction with the panels. However, during the earthquake the precast buildings might have been subjected to excessive inter-storey drifts, as well as high out-of-plane inertial lateral forces, for which these connections were not designed for.

The excessive drifts which were experienced by the precast building exhausted the displacement capacity of the connections of the panels, leading to the development of high forces that led to failure of the connections and unseating of the horizontal panel.



*Figure 3.43- In-plane detachment of an exterior cladding element after failure of the connections with the main structure*  
(Bournas et al. 2013)

Current design practice for precast industrial buildings is based on a bare frame model, where the peripheral cladding panels enter only as masses, without any stiffness contribution. This also leads to a higher-than-real period of vibration and thus to a reduced spectral acceleration Magliulo et al. (2014c). In addition, some designers introduce only the inertial mass contribution of the walls orthogonal to the plane of the walls. The panels are then connected to the structure with fastenings devices which are dimensioned by means of a local calculation, with anchorage forces orthogonal to the plane of the panels computed based on their mass and design spectral acceleration.

The connecting devices are expected to allow for all other relative deformations. However, when the free relative deformation capacity of the connection is exceeded, the panels become an integral part of the resisting system, conditioning its seismic response. The high in-plane stiffness of this resisting system leads to much higher forces than those calculated from the frame model. These forces are related to the global mass of the floors and are primarily resisted in the plane of the walls. Furthermore, the seismic force reduction considered in precast structures relies on the energy dissipation resulting from the formation of plastic

hinges at the columns bases. Due to the large flexibility of precast structures, very large drifts of the columns are typically needed to activate the energy dissipation mechanism assumed in design. However, the capacity of the connections between the cladding elements and the structure is typically exhausted well before such large drifts can develop (Bournas et al. 2013).

The design of the claddings connections proved to be insufficient also in the orthogonal direction. The out-of-plane inertial effects of the panel led to the development of high out-of-plane lateral forces that induced failure in the panel-to-frame and panel-to-panel connections (Figure 3.44). Generally is quite difficult from a survey of the damaged buildings to understand if the connections failed due to in-plane or out-of- plane forces.



*Figure 3.44- Out-of-plane detachment of horizontal cladding due to high inertial forces that caused failure of fastenings*  
(Bournas et al. 2013)

In other cases, the high out-of-plane inertial effects led to the development of high rotations (especially when more than two horizontal panels were used), which together with vertical inertia effects, led to unseating and loss of the panel connection (Figure 3.45).



*Figure 3.45- Out-of-plane overturning of exterior horizontal claddings* (Bournas et al. 2013)

Seismic behaviour of external masonry infills of single-storey precast buildings of less recent construction was already described in previous sections (see Section 2.4).

## 4. FRICTION-BASED CONNECTIONS

### 4.1 Seismic vulnerability of friction-based connections

As described in Chapter 3 (particularly Section 3.1), the extensive damages occurred to precast RC industrial buildings in the area affected by the 2012 Emilia earthquakes may be explained considering that, until October 2005, the Italian Building Code classified that area as non-seismic. Magliulo et al. (2014c) provided an overview of the Italian building code evolution over time, focusing on the design of connections in precast structures, and highlighted that friction-based connections were forbidden since 1987, but only in seismic zones (see Section 2.5). Therefore, in all the areas classified as non-seismic until 2005 friction-based connections were widely adopted. Bellotti et al. (2014) presented a review of the precast structural typologies and construction practice in Northern Italy, analysing 650 industrial buildings, 40 of which located in the Emilia region. Deyanova et al. (2014) reported that more than 85% of the 40 buildings of the Emilia region were built without seismic design rules, before seismic classification of the area of 2003 (see Section 3.1). More than 70% of them featured friction-based connections (45.2% with forks + 26.2% without forks at the top of the column).

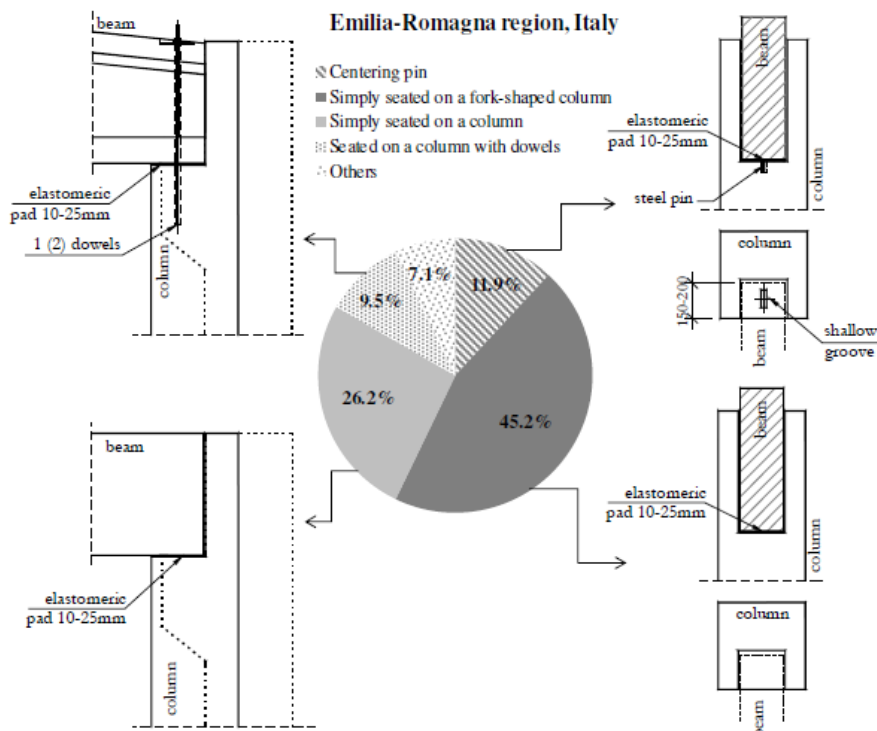
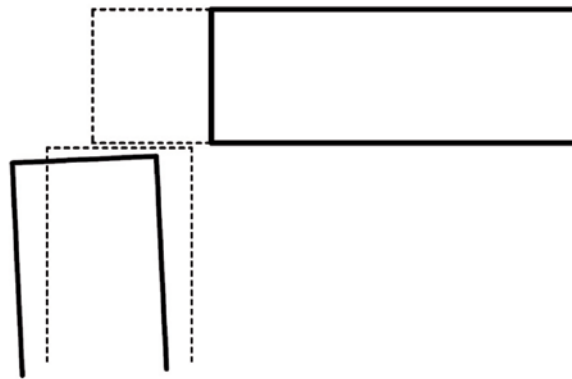


Figure 4.1- Beam-column connections from a database of 40 precast RC industrial buildings from Emilia region in Italy (Deyanova et al. 2014)

In many cases, the length of the bearing was too short to allow the beam-column relative displacement (Figure 4.2) under the seismic action.



*Figure 4.2- Scheme of possible relative displacement between the beam and the column* (Saitta et al. 2012)

Each portal frame, from a structural point of view, can be schematized as shown in Figure 4.3, where the equilibrium exists only if the horizontal forces acting on the beam-column joint do not overcome the friction forces.

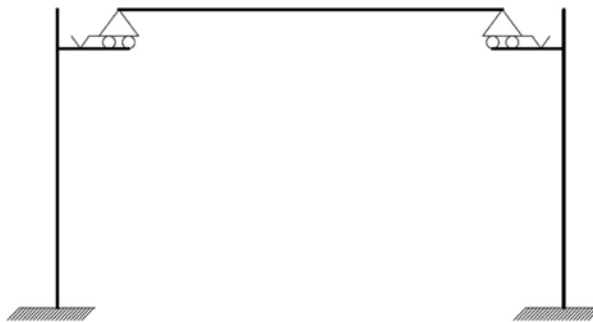


*Figure 4.3- Structural scheme of typical portal frame with simply supported beam over the columns* (Saitta et al. 2012)

In Chapter 3 it has been highlighted that loss of support has been the main cause of collapses in precast RC structures in the Emilia region during 2012 earthquakes. This can be deduced also upon simple considerations on the recorded spectra, as reported by Magliulo et al. (2014c). Assuming that the rigid-diaphragm effect is not ensured, as commonly is found in precast buildings in the Emilia region, the total horizontal seismic force  $F_{tot}$  is divided among the columns using a criterion based on influence area, i.e. proportionally to the ratio between the dead loads  $W_i$  acting on the considered column and the total weight of the structure  $W_{tot}$ . Considering that the participating mass ratio is 100% for the translational modes, the seismic force  $V_{Ed}$  acting on a beam-column connection, equal to the base shear of the considered

column, can be evaluated starting from the total base shear  $F_{tot}$  and dividing it among the columns as follows:

$$V_{Ed} = F_{tot} \cdot \frac{W_i}{W_{tot}} \quad (1)$$

As suggested by guidelines prepared by Gruppo di Lavoro Agibilità Sismica dei Capannoni Industriali (2012), referring to the fundamental period of vibration of the structure, the total base shear  $F_{tot}$  can be easily calculated as:

$$F_{tot} = W_{tot} \cdot S_a(T_1)/g \quad (2)$$

with

$T_1$  fundamental period of vibration of the structure

$S_a(T_1)$  spectral acceleration of design response spectrum for the site, calculated at the fundamental period of vibration of the structure  $T_1$

Substituting equation (2) in (1):

$$V_{Ed} = W_i \cdot S_a(T_1)/g \quad (3)$$

The strength of a friction connection  $V_{Rd}$  can be evaluated multiplying the vertical force acting on the connection and the friction coefficient  $\mu$ :

$$V_{Rd} = \mu \cdot W_i \quad (4)$$

Based on these considerations, the loss of support mechanism is immediately checked comparing the friction coefficient with the acceleration spectral ordinates in  $g$ , as shown in Figure 4.4. Thus, a safety factor  $SF$  can be evaluated and plotted (Figure 4.5) versus the fundamental period for the recorded spectra:

$$SF = \frac{V_{Rd}}{V_{Ed}} = \frac{\mu}{S_a(T_1)/g} \quad (5)$$

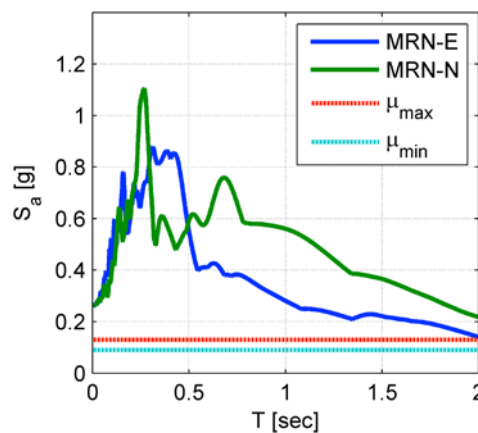


Figure 4.4- Acceleration spectral ordinates recorded in Mirandola (Emilia - Italy) during the event of 20<sup>th</sup> May 2012 compared to the friction coefficient (upper and lower bounds) evaluated by Magliulo et al. (2011) (Magliulo et al. 2014c)

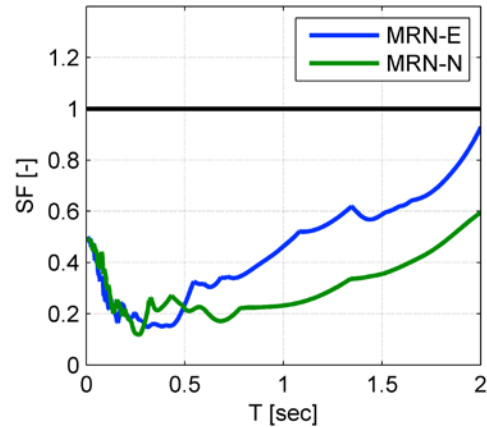


Figure 4.5- Safety factor of loss of support plotted versus fundamental periods for recorded acceleration time histories in Mirandola (Emilia – Italy) during the event of 20<sup>th</sup> May 2012, assuming  $\mu=0.13$  (Magliulo et al. 2014c)

According to the experimental studies conducted by Magliulo et al. (2011) on neoprene-concrete connections, the friction coefficient varies in the range of 0.09 - 0.13 for compressive stress varying between 1.7 MPa and 5.3 MPa. In Figure 4.4 these limits are compared to the recorded spectral ordinates at Mirandola station during 2012 Emilia earthquakes. Figure 4.5 shows the safety factor  $SF$ , evaluated considering  $\mu$  equal to 0.13. The safety factor  $SF$  is much below 1 for a wide range of periods and confirms the vulnerability due to friction connections of precast structures.

It should be noted that the simple considerations presented above neglect both the vertical component of the seismic action and the bi-directionality of the input motion. Obviously, if the two phenomena had been taken into account, lower safety factors would have been found. Even in the case of larger friction coefficients had been considered (for example, Caltrans (1994) suggests a coefficient ranging from 0.2 to 0.4 in case of neoprene-concrete interface for bridge applications) the loss of support would not have been avoided for a wide range of structural periods.

The use of an unreduced elastic spectrum for the evaluation of the force acting on beam-column friction connections may be questioned, since precast structures may dissipate energy developing plastic hinges. However, inelastic action in the concrete elements will not occur if the frictional strength of the connection is lower than the plastic shear, that is, the force that causes the formation of the plastic hinge at the column base. Indeed, in this case, no plastic sources are exploited, and, hence, the unreduced elastic spectrum must be used for the evaluation of the seismic actions.

It is concluded that if the shear failure of the connection comes before the flexural hinging in the column, precast structures with neoprene-concrete friction connections will exhibit a loss

of support of their horizontal elements under the recorded seismic excitation. Magliulo et al. (2008) anticipated this evidence, demonstrating that precast structures with friction connections suffer from loss of support due to the sliding of the beam from the column.

Precast structures hit by the Emilia earthquakes were designed according to different codes, depending on the construction time. As described in Section 3.1, most of the precast structures in Emilia were designed without taking into account seismic forces, based on the above-mentioned considerations on the seismic hazard map evolution in Italy; however, horizontal forces, such as wind and crane actions, were also considered.

Since the wind horizontal forces imply lateral loads on the connections, the use of friction connections may be questioned. For this reason, Magliulo et al. (2014c) provided a parametric study in order to justify a similar widespread design choice. In the parametric study, the horizontal shear demand in the connections caused by the wind actions is evaluated according to different past Italian codes and compared to the friction strength. In particular, the wind action is evaluated according to CNR Instructions (CNR-UNI 10012 1967) and D.M. 16/1/1996, as shown in Figure 4.6. The current building code (D.M. 14/01/2008) is not taken into account because Emilia region has been a seismic zone since 2003 and, according to the current code, friction connections are forbidden in seismic areas.

Code	Parameter	Unit	Description	Formula
CNR 1967	$p$	N/m <sup>2</sup>	Wind velocity pressure	$p = c \cdot k \cdot q$
	$c$	[-]	External exposure and shape coefficient	0.8
	$k$	[-]	Slenderness coefficient	$f(H/(2 \cdot B))$
	$q$	N/m <sup>2</sup>	Wind kinetic pressure	600
DM 1996	$p$	N/m <sup>2</sup>	Wind velocity pressure	$p = q_{ref} \cdot c_e \cdot c_p \cdot c_d$
	$q_{ref}$	N/m <sup>2</sup>	Kinetic pressure	$q_{ref} = v_{ref}^2 / 1.6$
	$v_{ref}$	m/sec	Wind speed	25
	$c_e$	[-]	External exposure coefficient	$f(H)$
	$c_p$	[-]	Shape factor (upstream facades)	0.8
	$c_d$	[-]	Dynamic factor	1.0

Figure 4.6- Evaluation of the wind equivalent forces according to past Italian building codes (Magliulo et al. 2014c)

The ratios between the design shear demand in the beam-column connection induced by wind and the connection friction strength are evaluated for the different case studies (Figure 4.7). In particular, the shear demand is evaluated according to CNR Instructions and D.M. 16/1/1996 and the shear strength is calculated according to friction coefficient equal to 0.35, 0.13 and 0.09. It is found that if the friction coefficient  $c = 0.35$  is used, as recommended by past

Italian code (Circolare M.LL.PP. n. 1422 1965), the shear demand will be always much smaller than the capacity. This outcome justifies the use of friction connections in existing structures. Conversely, if the experimental coefficients proposed by Magliulo et al. (2011) are considered ( $c = 0.13 - 0.09$ ), the capacity decreases, and in 25% cases, it can be exceeded by the shear demand. The authors concluded that an unrealistic high friction coefficient for the evaluation of the shear capacity of the connections in the past Italian codes allowed the use of friction connections.

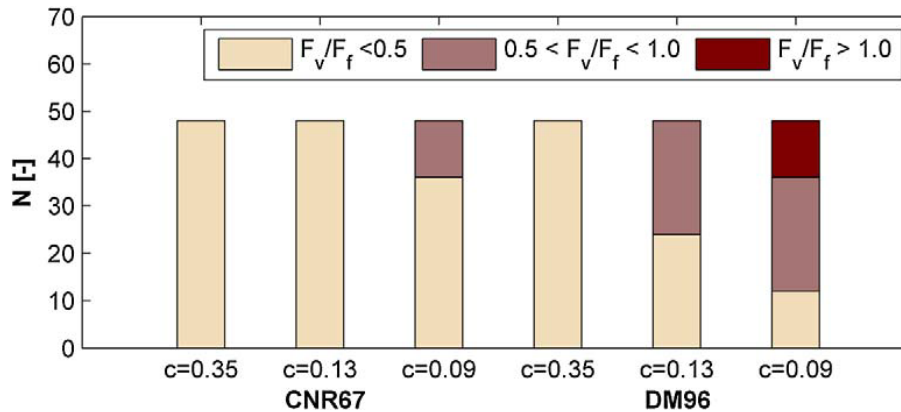


Figure 4.7- Ratios between the design shear demand  $F_v$  in beam-column connection induced by wind, evaluated according to CNR 1967 (CNR67) and D.M. 1996 (DM96), and the connection friction strength  $F_f$ , evaluated according friction coefficient  $c$  equal to 0.35, 0.13, and 0.09, for the different case studies (Magliulo et al. 2014c)

The seismic vulnerability of structures with friction-based connections has been confirmed also by numerical studies.

Biondini et al. (2013) investigated the seismic behaviour of friction-based connections performing incremental dynamic analyses, considering different values of friction coefficient and taking into account also the vertical component of ground-motions.

Liberatore et al. (2013) performed numerical analyses showing that the vertical component of ground motion, together with the lack of connection between column and beam, played a significant role in the activation of collapses due to unseating of elements. Their analyses, performed using as seismic input accelerograms recorded in Mirandola on May 20<sup>th</sup> and 29<sup>th</sup> 2012 and assuming a coefficient of friction equal to 0.4, showed large relative horizontal displacements between beam and column, if vertical component is considered.

Finally, Deyanova et al. (2014) noticed that the failure of a beam-column connection that relies only on friction can occur before the plastic hinge at the base of the column is activated, leading to a very brittle failure mode.

These evaluations also lead to the obvious conclusion that it is not possible to perform a seismic verification of the structural safety level on precast RC structures with friction connections. If mechanical connections between structural elements are not present, losses of support collapses can occur. This kind of collapse is very difficult to be evaluated because it is based on friction mechanisms, strongly depending on the unpredictable combination of horizontal and vertical components of seismic acceleration. Precast structures with friction connections are not able to resist to horizontal seismic actions, and the evaluation of their structural safety level is very difficult because it is not possible to schematize friction-based joints as hinged connections.

## **4.2 Strengthening solutions**

Given the economic significance of prefabricated structures, after May 2012 Emilia earthquakes, a great deal of research has been focused on developing strengthening solutions, in particular concerning the design of connections between structural elements. Various retrofitting proposals for friction connections of existing precast industrial buildings have been proposed.

Guidelines for rapid assessment and repairing of existing precast RC industrial facilities prepared by Gruppo di Lavoro Agibilità Sismica dei Capannoni Industriali (2012) and Consiglio Superiore dei Lavori Pubblici (2012) provided to designers some instructions and examples of technical solutions for local and global intervention on existing precast structures. The guidelines highlight the importance of realizing interventions in order to reduce relative beam-column displacements through the insertion of mechanical connections. These guidelines are supposed to be the reference for precast industrial building retrofitting all over Italy. The Italian government has in fact disposed relevant benefits for whoever will retrofit building for seismic action (Nutti and Vanzi 2014).

Ligabue et al. (2014) investigated the experimental behaviour of steel plates for the connection of precast concrete elements, performing also a parametric study in order to find normalized force-displacement curves for the design of the geometric characteristics of the steel element.

Muciaccia et al. (2014) provided a study on the use of post-inserted metal anchors and fastenings for use in concrete under seismic action.

Bournas et al. (2013) proposed for the strengthening of existing industrial building a scheme which is used for the seismic retrofit of simply supported bridges: to reduce the likelihood of

collapse due to unseating, cable restrainers are used between the girders and the piers/abutments of the bridge. The strengthening configuration proved to be effective in cases where seat widths were very small and relative displacements needed to be limited. For the retrofit of industrial buildings with beams simply supported at the top of columns, the restrainers would be anchored at the column and beam ends (Figure 4.8), where the bending moment is minimum, with the advantage that their installation would not significantly disturb the functioning of the building.

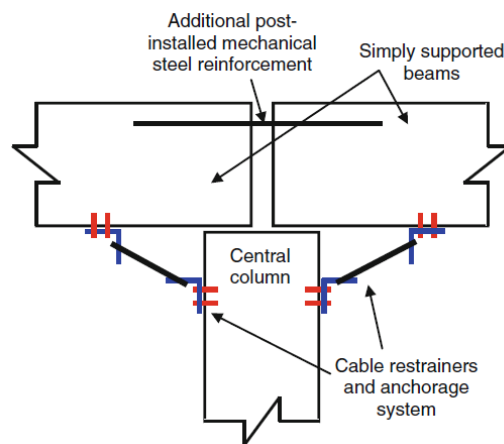


*Figure 4.8- Scheme of a retrofitting solution for beam-column connections using cable restrainers* (Bourmas et al. 2013)

Magliulo et al. (2014d) proposed beam-to-column steel connections able to avoid the loss of support of the beam, not inducing additional bending moment at the column top (Figure 4.9). The effectiveness of the solution proposed for beam-column joints was verified performing cyclic shear tests on real scale concrete elements under displacement control, as described in (Magliulo et al. 2014a).

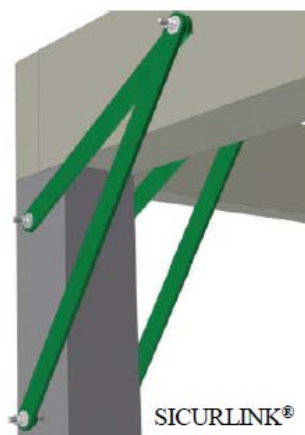


*Figure 4.9- Retrofitting solution for beam-column connections* (Magliulo et al. 2014d)

Most of investigated strengthening solutions are based on the introduction of steel ties, plates or cable restraints in order to avoid sliding of the beams and therefore unseating failures. Since these techniques usually increase the base shear, strengthening of the base of columns or of foundations is often required and the use of steel plates, bars or FRPs is suggested. Alternative solutions could be based on the introduction of dampers, as suggested in Marinini et al. (2011), but their introduction in existing precast industrial buildings can be difficult because of costs and interference with production processes. In addition, usually these devices are designed for higher level of forces to be used in other typologies of RC buildings or bridges.

Nuti and Vanzi (2014) identified the possibility to adopt three basic strategies of interventions:

- i. guarantee a sufficient ductility to the main structural system;
- ii. reduce seismic demand increasing available dissipation;
- iii. reduce seismic demand increasing the period (base isolation at roof level or other).

The idea of the third strategy (*iii*) is to introduce isolation between the head of the columns and the roof, once this has been rendered sufficiently rigid in its plane. This technique become feasible if one can intervene without large supporting interventions in the phase of cut between column and roof to insert isolators.

The second strategy (*ii*) is more popular for this kind of structures. There are two ways of increasing dissipation:

- using dissipative bracings. This permits to stiffen the structure without a substantial increase of base shear, thanks to brace yielding and large cyclic dissipation;
- introducing dissipative connections wherever possible.

The first strategy (*i*), meant to increase ductility, is usually the most common among the three options. In fact this implies typical solutions to connect elements each other and to increase ductility for example by confining elements with FRP wrapping. One key point is always the retrofitting of the roof precast elements: they must be fixed each other to obtain a slab of sufficient strength and stiffness.

The choice of the most suitable retrofitting technique must be evaluated basing on specificities of the single building and designed according to the global strategy of improvement of the seismic behaviour of the existing structure, that can be achieved increasing strength, stiffness or ductility of structural elements or adding supplemental damping through anti-seismic devices.

### 4.3 The proposed retrofitting solution

The research activity aimed at finding an innovative low-damage retrofitting solution for friction connections of existing precast structures able to reduce the effects of the seismic action on structural elements and to concentrate damages in predefined parts of the structures through the use of dissipative devices.

As highlighted in Section 4.2, the realization of rigid connections using steel plates anchored to structural elements can determine a high increase of forces transmitted to the rest of the structure, typically the columns. Consequently this may imply the need of intrusive and expensive strengthening interventions on columns and foundations. These interventions are particularly difficult to carry out on industrial buildings because they often interfere with the production process. Seismic protection of structures using anti-seismic devices is one of the most important goals of structural engineers in order to save lives and minimize damages to structures in case of earthquakes of high intensity. The possibility to reduce the effects of the seismic action and to minimize structural damages through the introduction of anti-seismic devices is particularly relevant in the seismic rehabilitation of existing industrial buildings where structural damage can determine high economic impact due to business interruption.

The study started exploring different mechanisms of energy absorption and various possibilities to dissipate the energy of the seismic action using supplemental damping devices. By equipping a building with additional devices with high damping capacity, the seismic energy entering the building can be greatly reduced. Most of systems and devices used to add damping to buildings in order to improve seismic response and reduce damages are based on yielding, friction or viscosity.

Some important aspects guided the activity of research for an innovative energy dissipation mechanism for civil structures:

- i. the need to develop a device able to absorb a high amount of energy in small dimensions;
- ii. the aim to obtain a device with a dissipative fuse behaviour;
- iii. the need of ease of replacement of devices.

These requirements were considered in order to design an effective and low-damage solution for connections of existing one-storey precast structures designed and built without anti-seismic standards. The fuse behaviour researched for the retrofitting solution is linked to the aim of finding a strengthening solution able to connect structural elements and at the same

time to limit forces transmitted between the structural elements connected through the devices. The retrofitting solution should have in fact a two-fold purpose:

- i. the capacity to provide an effective mechanical connection for beam-column friction joints, preventing the possible unseating of beams from columns,
- ii. the capacity to limit the forces transferred between structural elements, acting as a dissipative fuse able to reduce the effects of seismic actions on structural elements and to concentrate damage.

Collaboration between the Interdepartmental Centre for Industrial Research CIRI - Edilizia e Costruzioni of the University of Bologna and private companies led to the development of a device (*Sismocell*) based on carbon-wrapped steel tubes, derived from studies in automotive engineering.

#### **4.4 Dissipation energy mechanism**

A series of studies on structural crashworthiness, carried out for many years in automotive engineering (Lima et al. 2011), have shown that the combination of metals and composite materials in thin-section circular tubes provides excellent properties in terms of energy absorption under axial compressive loads. The circular shape is the most suitable because of symmetry and because it is associated to a regular buckling, which is controlled by the tube length, its diameter and its thickness.

In general, a circular metallic tube under compressive loading will buckle and fold, experiencing extensive plastic deformations. On the other hand, composite materials typically feature high strengths and brittle failure modes. The combination of the two materials to form a composite-wrapped metallic tube proved to be a good solution for catching the benefits of both: it increases energy absorption and ensures a stable behaviour (Lima et al. 2011). This latter is of prime importance for the reliability of such an application. Among composite materials, carbon fibres with high values of strength and stiffness maximize the axial loading and the absorption of energy, keeping geometric dimensions limited (Song et al. 2000).

The mode of collapse of such a device under compressive load is characterized by the formation of a series of folds along its section after the onset of buckling (Figure 4.10).

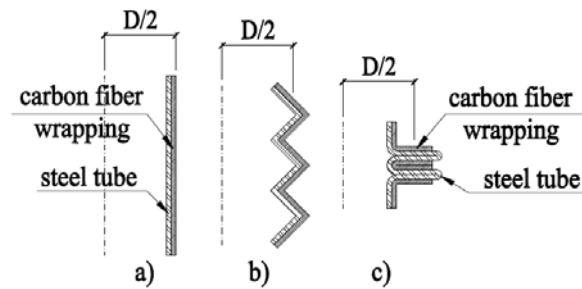


*Figure 4.10- Characteristic mode of collapse of carbon-steel thin section: (a) before buckling, (b) during buckling, (c) final shape*

As the compressive load increases, the wall of the circular inner metallic section begins to bend partially outwards and partially inwards and the applied force falls sharply until the complete formation of the first fold. When the fold is completely smashed, the force reaches its minimum and then starts to increase again. The new force increase produces a new buckling pattern, this time rotated with respect to the previous one: i.e. the portion of perimeter bended outwards is overlapped to the portion previously bended inwards. Correspondingly, the force decreases again and the pattern is repeated.

The mode of collapse described above is shown in Figure 4.11 for a steel tube with and without carbon fibres external wrapping.



*Figure 4.11- Mode of collapse of steel tubes with and without carbon fibre external wrapping*

The external composite wrapping by carbon fibres limits the outwards movement of the steel wall, until the tensile failure of carbon fibres. Because of the high strength properties of carbon fibres, their use increases significantly the value of force in correspondence of which the plastic deformation of the device takes place. Carbon fibres, by means of their confinement action, assure a regular behaviour during buckling and increase the strength of the device, increasing, consequently, the capacity to dissipate energy. The effect of fibres is maximum when they have a  $90^\circ$  inclination with respect to the axis of the cylinder (i.e. fibres run in the circumferential direction) as already verified by Song et al. (2000). Finally, the

compressive strength of the tubes, and consequently the amount of dissipated energy, increases as the number of carbon fibre layers increases.

The effectiveness of the dissipation energy mechanism described above was investigated and verified performing experimental tests on specimens with different configurations in order to identify an optimum design of the device.

Figure 4.12a shows one of the specimens manufactured. The wrapped cylinders have steel heads with a central hole to allow the insertion of a threaded bar. The function of the threaded bar is to provide a guide during the plastic deformation of the devices and a support for the anchor of the system to existing precast structural elements. Given the monotonic behaviour of the device (it is effective under compression only), in real-world applications they will always be installed in couples because of the cyclic nature of seismic actions (Figure 4.12b).



*Figure 4.12- Proposed device made of carbon-wrapped steel tubes*

## 5. EXPERIMENTAL TESTS

This chapter describes the experimental campaign performed on the devices developed in order to evaluate their mechanical behaviour in terms of force, deformation and energy dissipation capacities under axial compressive loading.

### 5.1 Materials and specimens

Specimens were manufactured using stainless steel AISI 304 for the inner tube (Figure 5.1). High strength carbon fibres (tensile strength of about 4800 MPa) were used for the external wrapping. Bond between fibres and steel is obtained by using epoxy, which plays the role of an adhesive in order to assure the effectiveness of external composite wrapping.

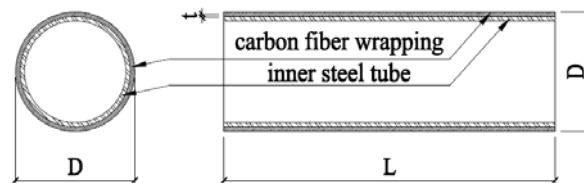


Figure 5.1- Typical configuration of the steel tube wrapped by carbon fibre

Different specimens were prepared by considering different diameters of the cylinder ( $D = 50$  mm and  $D = 60$  mm), thickness of the tube (from 1 to 2 mm), carbon fibre orientations ( $\pm 45^\circ$  and  $90^\circ$ , where the  $0^\circ$  direction is the tube longitudinal direction), number of FRP layers (3, 4, 6 and 8 layers). The length of all specimens was selected to be 150 mm in order to avoid Euler buckling.

Results presented in the following refer to three different combinations of the above parameters, identified as type A, B and C in Table 5.1.

	Type A	Type B	Type C
length $L$ [mm]	150	150	150
diameter $D$ [mm]	50	60	60
steel tube thickness $t$ [mm]	1	1.2	1.5
carbon fibre layers [ $n^\circ$ ]	3	6	6

Table 5.1- Dimensions and characteristics of tested specimens of type A, B and C

These three parameters combinations were defined in order to obtain different energy dissipation capacities. Preliminary experimental tests showed that in order to obtain a given

maximum “plastic” shortening of the device, its length should be about twice that dimension. Since the length of all the specimens was 150 mm, they all were expected to provide for a maximum deformation capacity of about 75 mm. For each of the three combinations in Table 5.1, 25 specimens were tested, for a total of 75 tests performed.

## 5.2 Quasi-static tests

### 5.2.1 Experimental setup

Quasi-static tests of axial compressive loading were conducted on three different specimens of the device designed to work in compression under the seismic action.

Tests were performed using a 600 kN electro mechanical machine. Tests were carried out under displacement control, applying an axial compressive loading until maximum plastic deformation capacity of the specimens. During the tests the force and the vertical displacement of the machine head were measured.

Specimens were tested according to the setup of Figure 5.2. Most of tests were performed applying a monotonic compressive loading at different displacement rates (from 1 mm/sec to 10 mm/sec). The load was applied on a flanged threaded bar, inserted in the central holes of the steel heads of the device, which slide inside a hole located in the base plate of the machine. This bar provided transverse restraint during the buckling process and is similar to what is used to install the devices on structures.

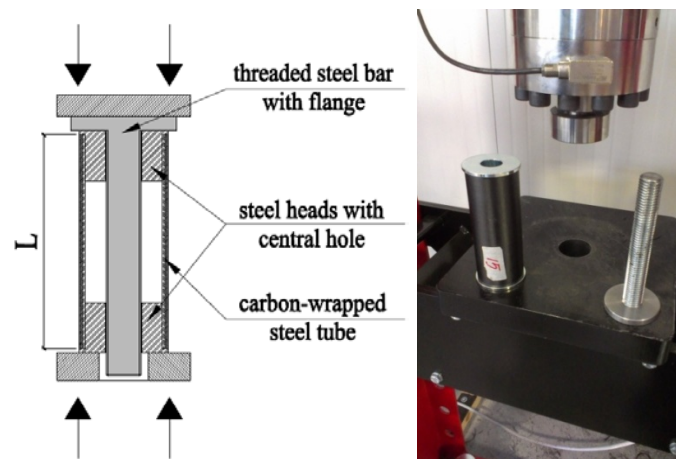


Figure 5.2- Scheme of experimental setup

### 5.2.2 Dissipative behaviour under compressive loading

The application of a compressive load on the device determines the collapse mechanism described in Section 4.4, which involves the buckling of the steel tube.

Figure 5.3- shows the failure sequence observed during the tests. Buckling starts at one of the two ends of the specimen and continues progressively until the maximum deformation capacity ( $S_{max}$ ). Energy dissipation takes place during the development of plastic deformations of the steel tube, accompanied by the tensile failure of carbon fibres.



Figure 5.3- Sequence of frames of experimental test showing the progression of the plastic deformation of the device

The contribution of carbon fibres in terms of increasing dissipation capacity of the device is shown in Figure 5.4, where the comparison between the experimental load-displacement curves of specimens fabricated with and without external wrapping is reported. Fibres allow to significantly increase the capacity to dissipate energy of the devices, to obtain a regular mechanism of collapse guiding the development of buckling, and to keep geometric dimensions limited.

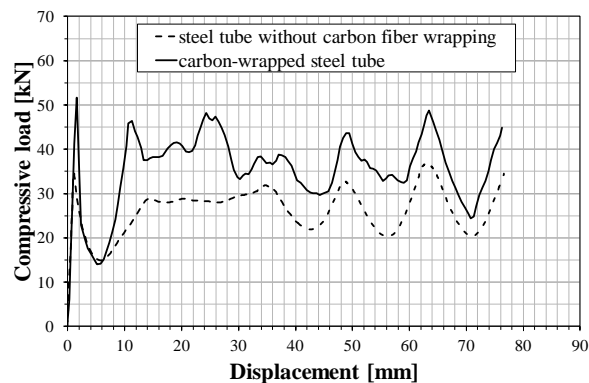


Figure 5.4- Comparison of load-displacement curves between specimens with and without carbon fibre external wrapping showing contribution of carbon fibres in terms of increasing dissipation capacity

Typical load-displacement curves obtained from first tests performed are reported in Figure 5.5. They present an initial elastic branch, followed by the buckling phase, during which the curves feature an alternation of peaks and valleys corresponding to the formation of the outward and inward parts of the folds along the section of the device. When the two steel heads at the extremities of the device get in contact, the device reaches its maximum plastic deformation capacity and its energy dissipation capacity runs out. After this point, the device works as a very stiff element leading to a strong increment of force.

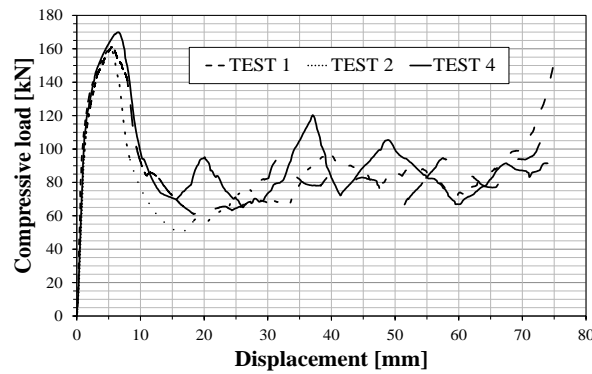


Figure 5.5- Experimental load-displacement curves of a steel tube simply wrapped with carbon fibre showing a high initial elastic peak load value

In order to summarise the behaviour of the devices tested, their experimental load-displacement curves, will be simplified with a trilinear model, as shown in Figure 5.6. The first branch has the same slope of the experimental curve, while the plateau (second horizontal branch –  $F_{eq}$ ) is defined so to have, in the range 0 to  $S_{max}$ , the same area under the curve of the experimental case. This area corresponds to the dissipated energy. After reaching the maximum deformation capacity, the third branch has the same slope of the first one, as observed experimentally.

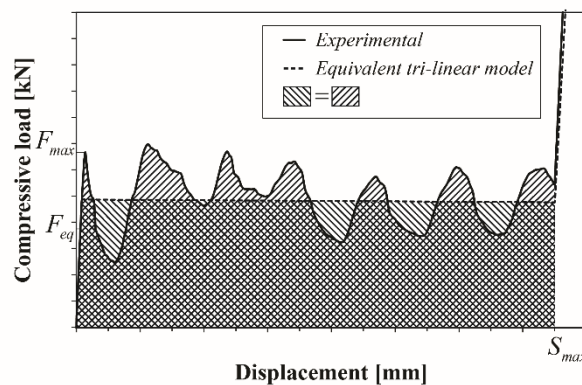


Figure 5.6- Experimental and trilinear equivalent curve in terms of absorbed energy

It is important to notice that the load-displacement curves in Figure 5.5, obtained from first tests performed, feature a high first peak strength ( $F_{max}$ ) before the onset of buckling, after which the following load-peaks are always smaller. The value of force of initial elastic peak ( $F_{max}$ ) is about twice the value of force applied to the device during its plastic deformation. This first initial peak force is necessary to trigger buckling and is characteristic of the compressive failure of carbon-wrapped steel tubes (Lima et al. (2011) and Song et al. (2000)), while the following peaks and valleys are related to the plastic folding of the tube. To quantify this behaviour, a parameter named Plasticization Force Efficiency ( $PFE$ ), was defined as the ratio  $F_{eq} / F_{max}$ .

The plasticization force efficiency  $PFE$  for first specimens tested is quite low, about 0.5. These low  $PFE$  values don't allow schematizing the experimental behaviour with the trilinear model introduced above, equivalent in terms of absorbed energy. In addition the presence of a high initial peak in the value of force doesn't satisfy the requirement to obtain a fuse effect in order to limit forces transmitted between the structural elements connected through the devices.

In order to maximize the fuse effect, since the introduction of the devices aims to limit forces transmitted between structural elements,  $PFE$  should be as close as possible to one. In fact, a device can be able to dissipate a high amount of energy but it may be impractical because the load required to initiate the plastic deformation may be too high. To overcome this issue, the manufacturing process of the steel tubes was modified and an effective trigger mechanism was implemented in the fabrication process in order to facilitate the onset of buckling and reduce the first peak load. Improving the literature behaviour of steel tubes wrapped with carbon fibre under compressive loading permitted to increase the plasticization force efficiency  $PFE$  reaching values of about 0.7 and to better satisfy the initial purposes of the research to obtain a dissipative fuse behaviour.

Table 5.2 shows  $PFE$  values obtained from standard and weakened specimens of geometry type C.

	standard specimens		weakened specimens	
	Fmax [kN]	PFE	Fmax [kN]	PFE
TEST 1	160	0.53	101	0.70
TEST 2	162	0.53	99	0.74
TEST 3	154	0.52	107	0.65
TEST 4	170	0.54	103	0.66
TEST 5	163	0.51	96	0.68
TEST 6	166	0.51	108	0.66

Table 5.2- Results of experimental tests on standard and weakened specimens of type C

In the following only the results for the weakened tubes will be presented. In particular, for each test performed, the following parameters are reported in Table 5.3: maximum load ( $F_{max}$ ); maximum deformation ( $S_{max}$ ); dissipated energy ( $E_{diss}$ ); and equivalent force of plasticization ( $F_{eq}$ ).

### 5.2.3 Experimental results

In general, the experimental tests showed a very regular behaviour during the buckling stage (Figure 5.7) and a very good repeatability of energy dissipation characteristics.



Figure 5.7- Specimens after quasi-static tests of compression

Figure 5.8 (a, b and c) shows the experimental load-displacement curves for some of the specimens of type A, B and C.

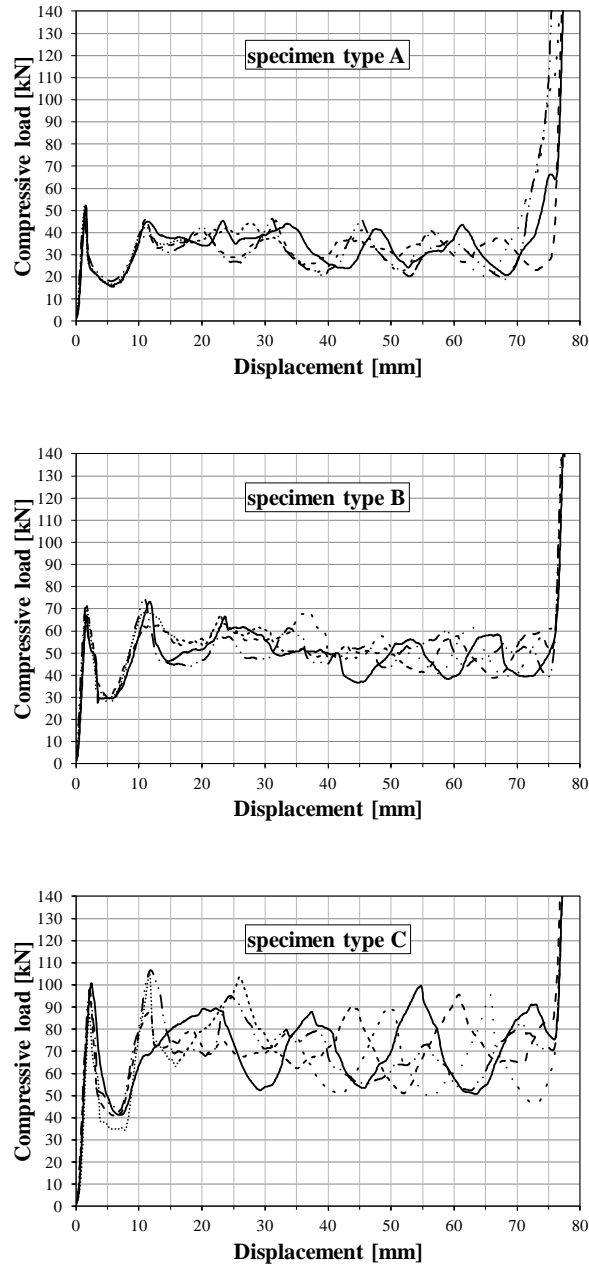


Figure 5.8- Experimental load-displacement curves for specimens of type A, B and C

Table 5.3 summarizes the results of the 75 tests carried out. The three different device geometries (type A, B and C) are characterized by different values of total dissipated energy  $E_{diss}$  and equivalent plasticization force  $F_{eq}$ . The mean value of equivalent force of plasticization  $F_{eq}$  is 33 kN, 53 kN, and 72 kN, respectively for specimens of type A, B and C. The mean values of total dissipated energy  $E_{diss}$  are 2511 J, 3955 J and 5426 J. Experimental tests showed a limit elastic-deformation (i.e. deformation at the end of the first branch) of the devices varying from 1 mm for specimens of type A to 2 mm for specimens of type C. The slope of the first elastic branch is almost independent from the specimen type and corresponds

5. EXPERIMENTAL TESTS

to a stiffness of about 40 kN/mm. The coefficient of variation of experimental results is in general low and spans from 8% to 12%. The maximum plastic deformation capacity  $S_{max}$  was, as designed, equal to 75 mm for all the specimen groups. The *PFE* presents for all the device types a mean value of 64%.

	type A				type B				type C			
	Feq [kN]	Ediss [J]	Fmax [kN]	PFE [%]	Feq [kN]	Ediss [J]	Fmax [kN]	PFE [%]	Feq [kN]	Ediss [J]	Fmax [kN]	PFE [%]
<b>TEST 1</b>	33	2481	53	63%	52	3919	71	73%	73	5445	110	66%
<b>TEST 2</b>	33	2462	52	63%	52	3872	71	72%	67	5033	114	59%
<b>TEST 3</b>	33	2490	52	64%	49	3654	73	67%	69	5179	112	62%
<b>TEST 4</b>	31	2359	54	58%	50	3718	75	66%	66	4918	96	68%
<b>TEST 5</b>	36	2736	55	66%	49	3658	75	65%	70	5231	125	56%
<b>TEST 6</b>	32	2418	47	69%	50	3723	77	65%	71	5327	106	67%
<b>TEST 7</b>	33	2508	58	58%	49	3712	72	69%	72	5410	106	68%
<b>TEST 8</b>	32	2391	45	71%	49	3688	89	55%	63	4762	111	57%
<b>TEST 9</b>	32	2458	51	63%	52	3895	74	70%	71	5326	107	66%
<b>TEST 10</b>	34	2546	56	60%	51	3862	69	74%	73	5492	99	74%
<b>TEST 11</b>	32	2392	46	69%	48	3652	71	68%	71	5288	101	70%
<b>TEST 12</b>	32	2407	57	56%	56	4204	87	64%	70	5222	107	65%
<b>TEST 13</b>	30	2222	57	52%	52	3919	90	58%	68	5113	108	63%
<b>TEST 14</b>	32	2424	57	55%	52	3934	89	59%	72	5379	110	65%
<b>TEST 15</b>	33	2506	55	60%	54	4040	89	61%	66	4977	109	61%
<b>TEST 16</b>	30	2224	45	67%	54	4044	88	61%	73	5448	111	66%
<b>TEST 17</b>	28	2072	40	69%	51	3800	88	57%	71	5313	108	66%
<b>TEST 18</b>	36	2729	55	66%	52	3935	82	64%	70	5251	132	53%
<b>TEST 19</b>	36	2719	53	68%	51	3850	89	57%	68	5105	103	66%
<b>TEST 20</b>	36	2668	52	69%	56	4166	84	66%	66	5083	107	62%
<b>TEST 21</b>	36	2732	55	66%	56	4209	89	63%	77	5777	111	69%
<b>TEST 22</b>	37	2751	55	67%	58	4355	92	63%	84	6268	139	60%
<b>TEST 23</b>	37	2777	56	66%	57	4273	92	62%	90	6753	135	67%
<b>TEST 24</b>	35	2624	50	71%	57	4272	77	74%	82	6187	131	63%
<b>TEST 25</b>	36	2691	51	71%	60	4516	75	80%	85	6363	138	61%
<b>Mean</b>	<b>33</b>	<b>2511</b>	<b>52</b>	<b>64%</b>	<b>53</b>	<b>3955</b>	<b>81</b>	<b>64%</b>	<b>72</b>	<b>5426</b>	<b>113</b>	<b>64%</b>
<b>Standard deviation</b>	<b>2.5</b>	<b>186</b>	<b>4.6</b>	<b>5.3%</b>	<b>3.3</b>	<b>244</b>	<b>8.1</b>	<b>6.1%</b>	<b>6.6</b>	<b>485</b>	<b>12.4</b>	<b>4.8%</b>
<b>Coefficient of variation</b>	<b>7.6%</b>	<b>7.4%</b>	<b>8.8%</b>	<b>8.3%</b>	<b>6.2%</b>	<b>6.2%</b>	<b>9.9%</b>	<b>9.4%</b>	<b>9.1%</b>	<b>8.9%</b>	<b>10.9%</b>	<b>7.4%</b>

Table 5.3- Results of performed tests for specimens of type A, B and C

Data distribution was analysed as well; the Anderson–Darling test suggested that data could be described by a log-normal distribution. Figure 5.9 shows, as an example, the distribution of the dissipated energy values for the type C specimens.

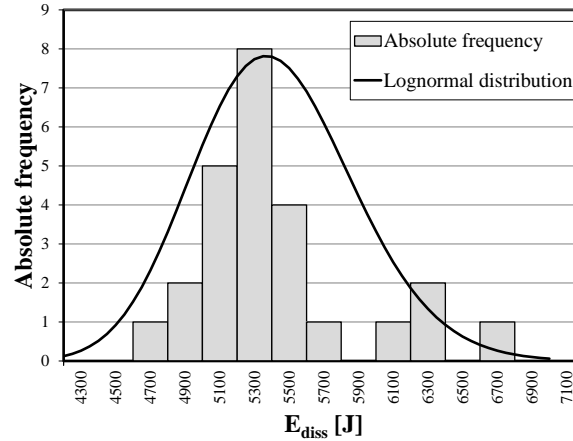


Figure 5.9- Frequency distribution for  $E_{diss}$  for specimens type C

The experimental load-displacement behaviour satisfies the requirement to obtain a fuse effect in order to limit forces transmitted between the structural elements connected through these devices. Modifying the characteristics of the carbon-steel circular thin section the behaviour of specimens under compressive loading doesn't change qualitatively but only quantitatively and it is possible to obtain devices with different values of equivalent force of plasticization  $F_{eq}$  and different energy dissipation capacities.

### 5.3 Cyclic tests

Quasi-static cyclic tests were performed applying displacement-controlled cyclic compressive-loads to the specimens (each device works in compression only). Each cycle started and ended at a displacement equal to zero. The hysteresis cycle of the devices has the characteristic to accumulate progressive damage; as the maximum deformation increases, a gap, along the axis of deformation, opens because of the residual deformation of the tubes (Figure 5.10). Therefore, considering a general cycle  $i$ , the force in the device is zero until the displacement is smaller than the displacement at the end of the unloading phase of cycle  $i-1$ . In fact, loading and unloading cycles showed that, in the tube-buckling phase, the reloading branch intersects the load-displacement monotonic curve exactly at the value of force in correspondence of which the unloading had started. Furthermore, unloading and reloading are linear with a stiffness corresponding to the initial one.

## 5. EXPERIMENTAL TESTS

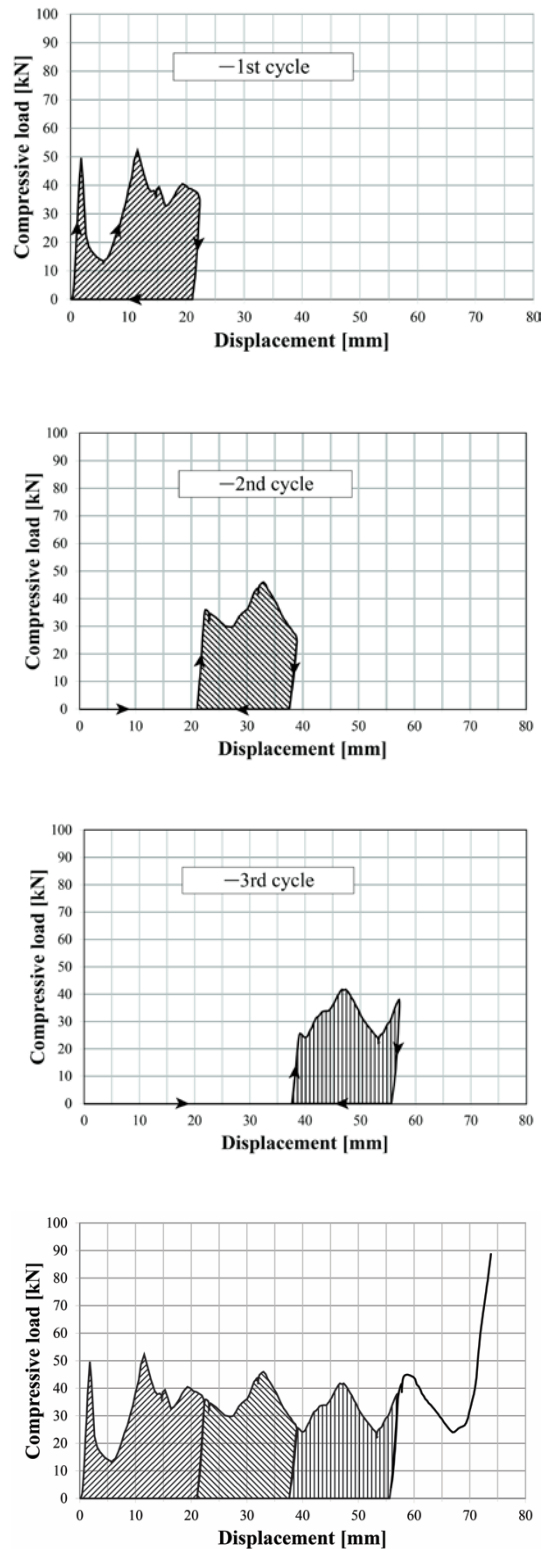


Figure 5.10- Cyclic loading experimental test of compression on specimen type A

According to this behaviour, energy can be dissipated only because of the monotonic progression of the plastic deformation (buckling). Figure 5.10a to c show the amount of energy dissipated after each loading-unloading cycle (shaded area) and the corresponding

residual permanent deformation of the device. Figure 5.10d shows the complete curve. The device is able to dissipate the energy identified by the monotonic curve, even when cyclic loading is considered. As a consequence, the dissipated energy is a direct function of the actual plastic deformation and it is independent from the number of cycles performed.

## 5.4 Impact tests

In order to verify results of quasi-static experimental tests described in Section 5.2 under dynamic conditions, shock tests under compression of the device were performed by using a drop weight impact system (Figure 5.11).

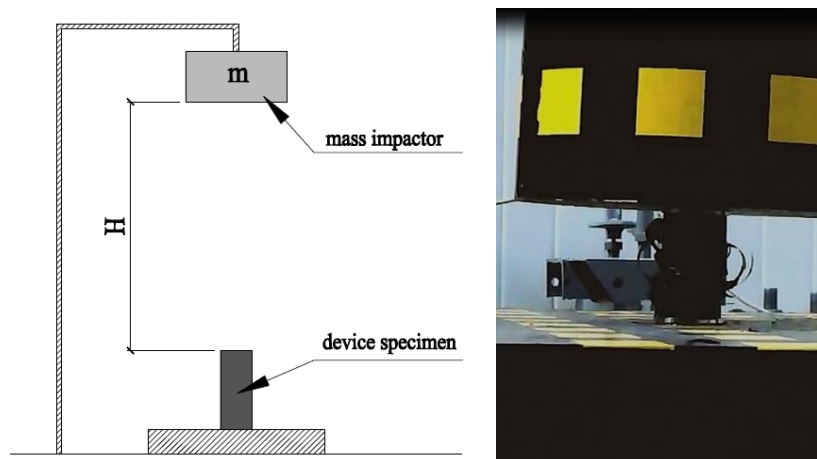


Figure 5.11- Shock experimental tests performing using a drop weight impact system

The impact energy for an impactor of mass  $m$  freefalling from a height  $H$  can be easily calculated as  $E_{impact} = mgH$ . Starting from the results of quasi-static tests, three different impact energies were considered: respectively 2200, 3600 and 5000 J. A mass impactor of 105 kg falling free under the action of gravitational acceleration was used for all the tests. The freefall height  $H$ , i.e. the distance between the upper surface of the device and the lower surface of mass impactor, was varied in order to produce the desired impact energy. Freefall heights  $H$  of 2.1, 3.5 and 4.8 m were used to obtain the desired energies, respectively.

After the tests, the residual deformation of the devices was measured in order to verify that they did not reach the ultimate static deformation capacity  $S_{max}$ . The measured mean deformations (under dynamic impact) of type A, B and C specimens were 68, 61 and 57 mm, respectively. Therefore, they were lower than maximum deformation capacity  $S_{max}$  of 75 mm. Mean values of dissipated energy  $E_{diss}$  of quasi-static experimental tests, calculated at the deformations measured under dynamic impact, are 2164, 3154 and 4020 J, respectively for

type *A*, *B* and *C* specimens, showing a dynamic behaviour comparable to the one shown during quasi-static tests, with even better energy dissipation capacity.

## 6. NUMERICAL MODELING

The study then focused on the design of the introduction in beam-column friction connections of existing precast RC structures of the devices with the dissipative behaviour investigated through experimental campaign described in previous chapter. The behaviour of the dissipative connection respect to the seismic behaviour of the entire structure was investigated. Some recommendations concerning the design of the anchoring system to precast elements are provided.

The effectiveness of the introduction of carbon-wrapped steel tubes in the beam-column connections of existing precast structures has been investigated with numerical analyses.

Different types of nonlinear dynamic analyses have been performed on simple structures reinforced with the device to verify its dissipative fuse effect. Performing nonlinear dynamic analyses permits to investigate the dynamic behaviour of the device during ground motions and its effects in terms of reduction of relative beam-column displacement and forces transferred to the column.

Characteristics of structural models identified as representative of the most common existing precast RC structures are illustrated.

Analyses have been carried out using firstly the FEM software *SAP2000* for nonlinear dynamic analyses, then the FEM software *OpenSees* for Incremental Dynamic Analyses (IDA) described in Chapter 7.

Numerical analyses expect to prove a reduction of stresses at the base joint of the column, comparing this dissipative connection with a hinged beam-column connection.

### 6.1 Behaviour of dissipative connection

The device developed provides an effective connection between simply supported structural elements and, in addition, the capability to dissipate a determined amount of energy. The purpose of the introduction of the devices is to cut the effect of the main peaks of the seismic acceleration and to reduce the effects of the earthquake on structural elements. In addition, in this way it is possible to concentrate damages in predefined parts of the structures.

Since each single device works and dissipates energy only under compressive loading, two devices must be inserted in each joint. The carbon-wrapped steel tubes of the dissipative device have at their ends steel heads with a central hole to allow the insertion of a threaded

bar. The function of the threaded bar is to provide a guide during the plastic deformation of the devices and a support for anchoring the system to existing structural elements.

The design of the anchoring system to existing structural elements requires a particular attention in order to make the devices work properly. The threaded bar must be fixed to the column using a first anchoring element. The anchorage to the beam must be provided by a second element placed between the two devices with adequate strength and stiffness, in order to transfer forces from the roof horizontal elements to the devices and at the same time to slide through the threaded bar. The anchoring elements to the beam and to the column can be designed using common steel plates, threaded bars and anchor dowels (see Figure 6.1).

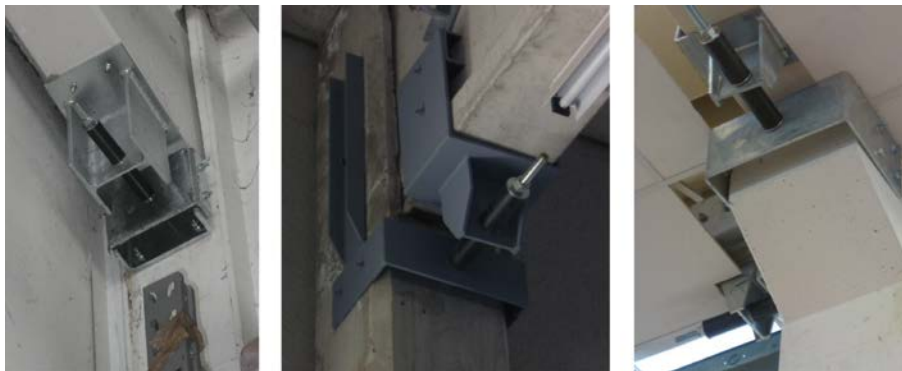


*Figure 6.1- Examples of the introduction of dissipative devices in precast structures with different anchoring elements to the structure*

The dissipative device provides that, up to a target value, the relative displacement between structural elements, occurring once overcome friction forces, determines the compression of the devices, dissipating energy during their plastic deformation (Figure 6.2). Therefore, the relative displacement between the beam and the column takes place at a controlled value of force. The device avoids relative displacement between the structural elements below a certain pre-established force threshold. Above this pre-set force threshold, the plastic deformation of the device takes place, accompanied by energy dissipation.

In this way it is possible to avoid the realization of a rigid hinged joint that can determine considerable transfer of forces to the columns.



*Figure 6.2- Behaviour of the dissipative connection under seismic action*

Considering the experimental behaviour of the devices, the theoretical behaviour of a retrofitted beam-column joint under a monotonically increasing horizontal force (originating from the beam) can be described as follows (Figure 6.3):

- *Phase 1*: the horizontal force is larger than the friction force but lower than the buckling force of the device: the force is entirely transmitted to the column. The relative beam-column displacement is extremely small thanks to the high initial stiffness of the devices.
- *Phase 2*: as the force increases, one of the two devices (that under compression) begins to buckle and dissipate energy during the progression of plastic deformation. The force transmitted to the column through the threaded bar and the anchoring elements is limited until the device reaches its maximum deformation capacity  $S_{max}$ . Beam-column relative displacement is now apparent and it corresponds to the axial deformation of the device.
- *Phase 3*: the device reaches its maximum deformation capacity  $S_{max}$ , providing for a rapidly increasing horizontal force but preventing from further relevant increment of relative displacement, acting now as an effective connection between structural elements through the threaded bar.
- *Phase 4*: the column, facing this high value of force, yields and subsequently reaches its ultimate deformation capacity.

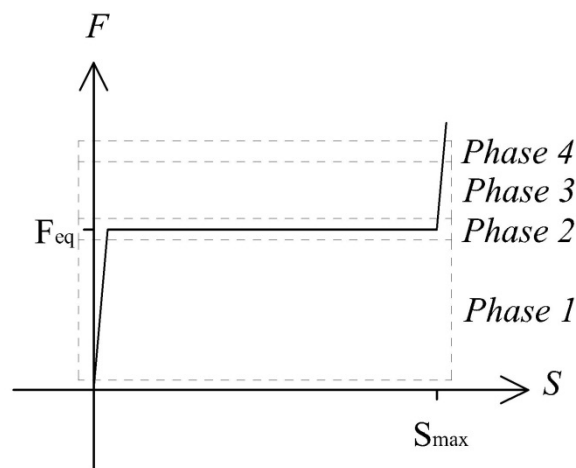


Figure 6.3- Subsequent phases of the behaviour of the device under compressive loading

When considering cyclic loadings of the connections, the two devices are engaged alternatively; in particular, if the load reversal takes place during *phase 2*, there is an initial sliding of the system with zero force, necessary to close the gap produced by the irreversible deformation. After that the steel element anchored to the beam is put in contact with the second device, phases identical to those already described can be repeated (Figure 6.4).

Relative beam-column displacements smaller than  $S_{max}$  are therefore allowed and are associated to energy dissipation. This behaviour expects to mitigate the effects of main acceleration peaks of ground-motions.

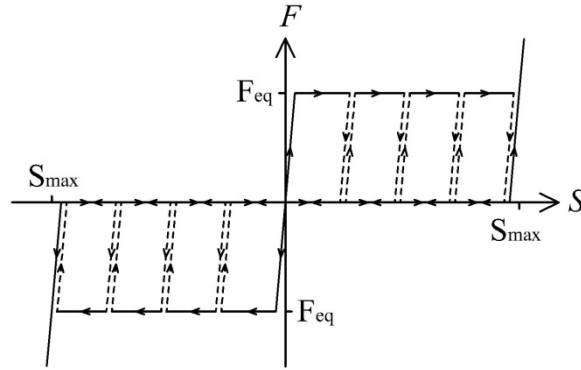


Figure 6.4- Hysteretic cycle of the system composed by two devices

Considering that the sliding of beams over columns is required in order to dissipate energy, it is mandatory to limit friction forces, in order to: *i)* allow sliding and therefore energy dissipation and; *ii)* to control the shear transferred to the columns. For these reasons, when designing the retrofit interventions with the proposed devices, it is important take provisions (e.g. by using PTFE pads) in order to control and/or reduce the friction coefficient between beams and columns. Limiting the friction coefficient will also reduce the sensitivity of the system to variations of the axial load in the columns, which may be produced by the vertical component of ground-motions.

Furthermore, in order to maximize the dissipated energy, it is, in general, convenient to maximize the two main parameters that characterize the dissipative devices:

- maximum deformation capacity  $S_{max}$
- equivalent force of plasticization  $F_{eq}$

The largest usable values for these parameter are related, respectively, to the maximum allowable beam-column relative displacement (in order to avoid loss-of support failures) and to the strength of the column, which must fail after the devices.

The design of the device required a particular attention to the limit deformation control. The deformation of the device and consequently the energy dissipation is due to the slide of the beam over the column, once overcome the friction force in correspondence of the joint section. For this reason in order to avoid collapses it is necessary to limit the deformation of the device, making the joint work like a rigid hinged connection after a limit value of relative displacement (*phase 3* and *phase 4*). The maximum relative displacement allowed between

the beam and the column is controlled by the maximum deformation of the device. Therefore, the deformation of the device must be defined as a function of the size of the beam-column support in order to prevent loss-of-support collapses of structural elements. The deformation of the device is in fact coincident to the relative displacement value between the beam and the column.

The value of the equivalent force of plasticization  $F_{eq}$  of the device should be related to the capacity of the column and its reinforcement steel bars. The  $F_{eq}$  value should be designed as the maximum value of force that, added to friction forces, can be transferred to the top of the column before reaching the yield moment at its base. This provision permits to respect the hierarchy resistance criterion introduced above describing subsequent phases and to have column performing linear elastic behaviour until the devices have not reached their maximum deformation capacity.

## **6.2 Structural typologies of case studies**

Parameters characterising structural models used for numerical analyses were defined through an analysis on most widespread typologies of existing precast concrete structures. This preliminary analysis was based on design guidelines and standards, original structural designs, precast manufacturers documents, post-earthquake reports after the 2012 Emilia earthquakes and a literature review on the same theme.

Deyanova et al. (2014) investigated 60 buildings (40 from the Emilia-Romagna region and 20 from other regions), summarizing their main properties in terms of span length, column aspect ratio and beam-column connections. Figure 6.5 shows that the most common beam span length is between 14 and 20 m and column aspect ratio (column height / cross-section width) is greater than 10.

Bellotti et al. (2014) presented a review of precast structural typologies and construction practice in Northern Italy, and, for industrial buildings partly located in Emilia (and struck by the 2012 earthquake sequence) and partly in Tuscany, analysed the probabilistic distribution of some geometrical characteristics, such as span length of main girders and roof slab elements, and column height. The total number of precast RC buildings included into that study is 670, whose 40 are located in Emilia.

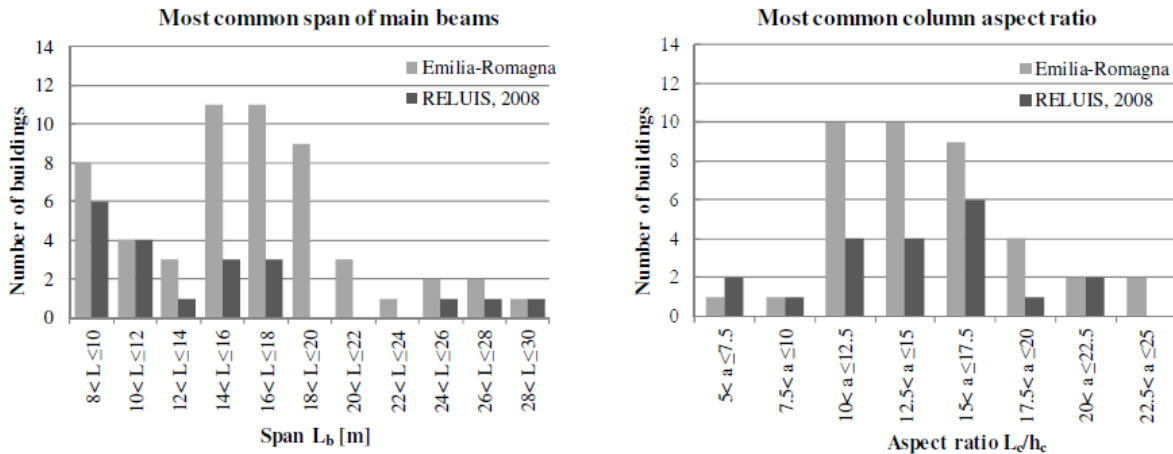


Figure 6.5- Beam span length and column aspect ratio for 60 precast RC industrial buildings from Italy (40 from the Emilia-Romagna region and 20 from other regions) (Deyanova et al. 2014)

Particularly, the selection of case studies considered in the present work was based on a report by Mandelli Contegni et al. (2008) on different types of precast structures in Italy since 1970, collecting information about existing buildings provided by ASSOBETON, a consortium of several construction companies, manufacturers of precast elements, in Italy.

Main geometrical and structural characteristics derived by typological analysis have been collected in a database with the aim to identify some significant examples of industrial buildings built in Italy starting from 1960 (Figure 6.6). The database concerned those structures designed and realized without anti-seismic standards with structural elements simply supported without mechanical connections. Main parameters considered are span length, column height, geometry of structural elements, masses and loads, materials characteristics and steel reinforcement of columns.

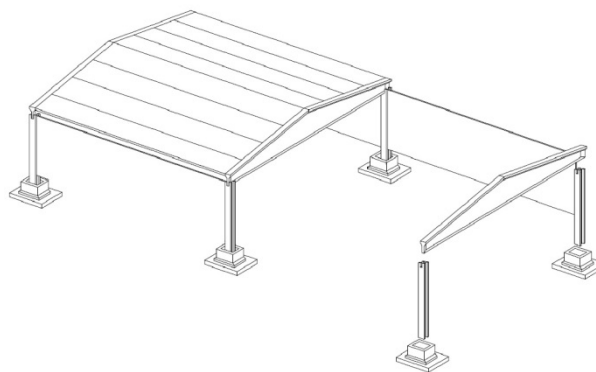


Figure 6.6- Scheme of most widespread typology of one-storey precast buildings

Three different structural typologies have been identified as representative of the most common existing precast structures with friction-based connections. Building typology

considered consists of cantilever columns forming frames in the transverse direction and no additional lateral resisting system in the longitudinal direction.

Main geometrical parameters assumed for structural models (Model A, B and C) of the three identified case studies are span lengths of 12, 20 and 25 m and column heights of 8, 7 and 6 m, respectively for Model A, B and C. Columns have a 50x50 or 45x45 cm<sup>2</sup> rectangular cross-section and the beam has a 30 x 110 cm<sup>2</sup> rectangular cross-section. The gravity load on the roof, computed as the sum of dead and variable loads, is equal to approximately 6.93, 5.46 and 7.03 kN/m<sup>2</sup>, respectively for Model A, B and C.

Numerical analyses have been performed on simple structural models (Model A, B and C) schematizing the three identified case studies with columns performing both linear elastic behaviour and nonlinear behaviour.

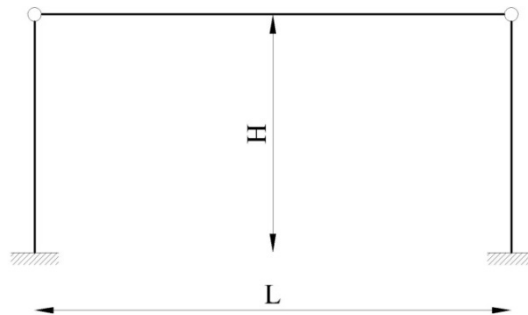


Figure 6.7- Scheme of typical portal frame of structural models

Some parameters of structural models have been modified in analyses depending on the two different behaviour of columns, i.e. linear elastic and nonlinear, as reported in the following tables.

Characteristics of structural models (Model A, B and C) of the three identified case studies used for analyses with columns performing linear elastic behaviour are reported in Table 6.1.

		Model A	Model B	Model C
Span Length $L$	m	12	20	25
Column Height $H$	m	8	7	6
Interaxis between frames	m	6	7	8
Column Section	m	0.5 x 0.5	0.5 x 0.5	0.45 x 0.45
Beam Section	m	0.3 x 1.1	0.3 x 1.1	0.3 x 1.1
Beam Load (without beam self-weight)	kN/m	33.33	30	48
Total Beam Load (dead + variable)	kN/m	41.58	38.25	56.25
Total Roof Load (dead + variable)	kN/m <sup>2</sup>	6.93	5.46	7.03
Total Joint Load (dead + variable)	kN	249	383	703

Table 6.1- Parameters of the three structural models with columns performing linear elastic behaviour

Characteristics of structural models (Model A, B and C) of the three identified case studies used for analyses with columns performing nonlinear behaviour are reported in Table 6.2.

		Model A	Model B	Model C
Span Length $L$	m	12	20	25
Column Height $H$	m	8	7	6
Interaxis between frames	m	6	7	8
Column Section	m	0.5 x 0.5	0.5 x 0.5	0.5 x 0.5
Beam Section	m	0.3 x 1.1	0.3 x 1.1	0.3 x 1.1
Beam Load (without beam self-weight)	kN/m	33.33	30	48
Total Beam Load (dead + variable)	kN/m	41.58	38.25	56.25
Total Roof Load (dead + variable)	kN/m <sup>2</sup>	6.93	5.46	7.03
Total Joint Load (dead +variable)	kN	249	383	703
Column longitudinal steel reinforcement $A_{s,sup}$		3 Ø24	4 Ø24	4 Ø26
	cm <sup>2</sup>	13.57	18.10	21.24
Column longitudinal steel reinforcement $A_{s,med}$		-	-	2 Ø26
	cm <sup>2</sup>	-	-	10.62
Column longitudinal steel reinforcement $A_{s,inf}$		3 Ø24	4 Ø24	4 Ø26
	cm <sup>2</sup>	13.57	18.10	21.24
Column transverse steel reinforcement		Ø6	Ø6	Ø8
Column transverse steel reinforcement spacing	cm	15	15	15

Table 6.2- Parameters of the three structural models with columns performing nonlinear behaviour

For analyses performing nonlinear behaviour of columns, a cubic characteristic compressive strength of 50 MPa for the concrete (C40/50) and a yield strength of 430 MPa and ultimate strength of 540 MPa (FeB44k steel bars) for the steel reinforcement are assumed.

The three case studies identified during the preliminary typological analysis were schematized modelling simple portal frames with fixed base joints and different kinds of beam-column connections.

Different configurations of beam-column joints have been considered: (i) beam pinned to the columns; (ii) beam simply supported on the column tops, assuming different values of friction coefficients for beam-column joints. The friction coefficient depends on the type of interface that supports the beam (concrete, rubber pads or steel plates). The definition of this parameter is a controversial matter. Values of friction coefficient considered in analyses are based on experimental studies conducted by Magliulo et al. (2011) on neoprene-to-concrete connections, showing friction coefficients in the range of 0.09 - 0.13.

In some of the analyses performed it was decided not to introduce friction models in the beam-column joint. This choice respects international standards according which it is not possible to rely on friction in the design of precast connections for new structures. As shown

by records of Emilia earthquakes of May 2012 (see Section 3.1), the vertical component of acceleration can reduce or nullify the friction effect, determining losses of support of structural elements without mechanical connections (Biondini et al. 2013). In addition, in order to have a better control of the transfer of horizontal forces induced by seismic actions, rehabilitations of existing precast structures with the presented device should be accompanied by interventions that permit to control and, if necessary to reduce, the presence of friction. An accurate friction control permits to maximize the effectiveness and the benefits associated to the introduction of the dissipative device. The very low coefficient of friction supposed to be present consequently to this assumption, was conservatively not taken into account in some of the analyses, not considering its positive dissipative effect.

The choice of the characteristics of the dissipative device for each of the three models is related to the capacity of the column and its reinforcement steel bars. The value of the equivalent force of plasticization  $F_{eq}$  of the device considered in the analyses is designed as the maximum value of force that, added to friction forces, can be transferred to the top of the column before reaching the yield moment at its base.

### ***6.2.1 Ultimate chord rotation of columns***

As described in previous sections, in this type of structures the lateral resisting capacity typically relies mainly on the cantilever columns, considered fixed into their socket foundations with plinths. As highlighted by Deyanova et al. (2014), these columns are expected to have different behaviour under horizontal loading compared to the most investigated and tested column types, to which the existing analysis methodologies are calibrated. The main reason is the combination between slenderness and low transverse reinforcement ratio. The aspect ratio (column height / cross-section width), typically greater than 10, would suggest flexural failure as a predominant failure mechanism. At the same time, the low amount of transverse reinforcement classifies these columns in the group of columns with expected shear failure. Post-yielding behaviour and ultimate capacity do not necessary follow well-known empirical models and procedures for columns with a very low shear aspect ratio (Fischinger et al. 2008). Therefore, engineers face the difficulty to predict their performance and expected deformation/rotation capacity when assessing existing precast RC structures.

In the present work, the definition of the ultimate chord rotation of precast cantilever columns was based on recommendations for yielding curvature, ultimate curvature and plastic hinge

---

length described by Priestley et al. (2007), typical of “DDBD (Direct Displacement-Based Design) procedure” (Figure 6.8 - Figure 6.10).

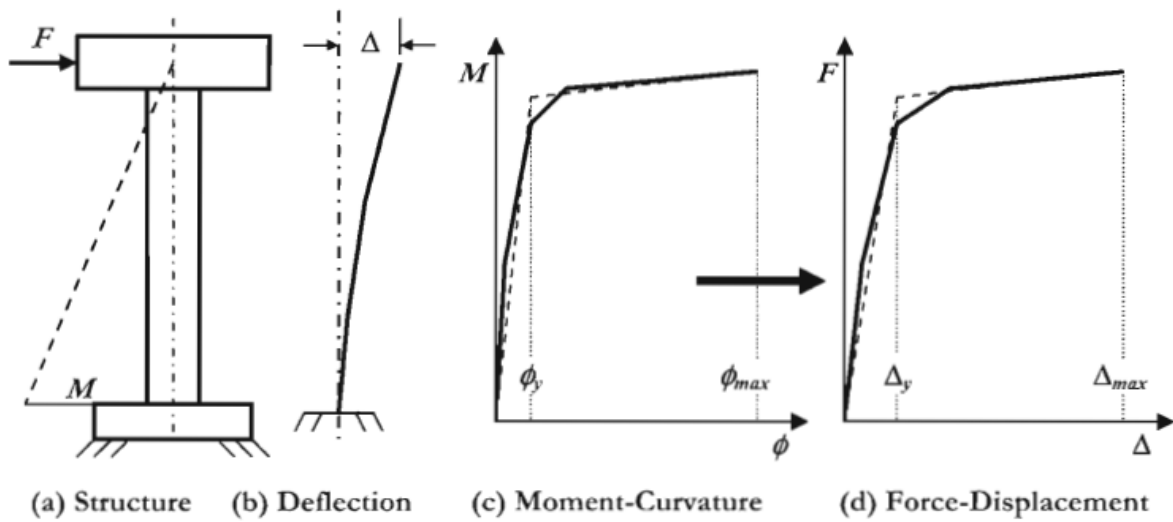


Figure 6.8- Force-displacement response of cantilever columns (Priestley et al. 2007)

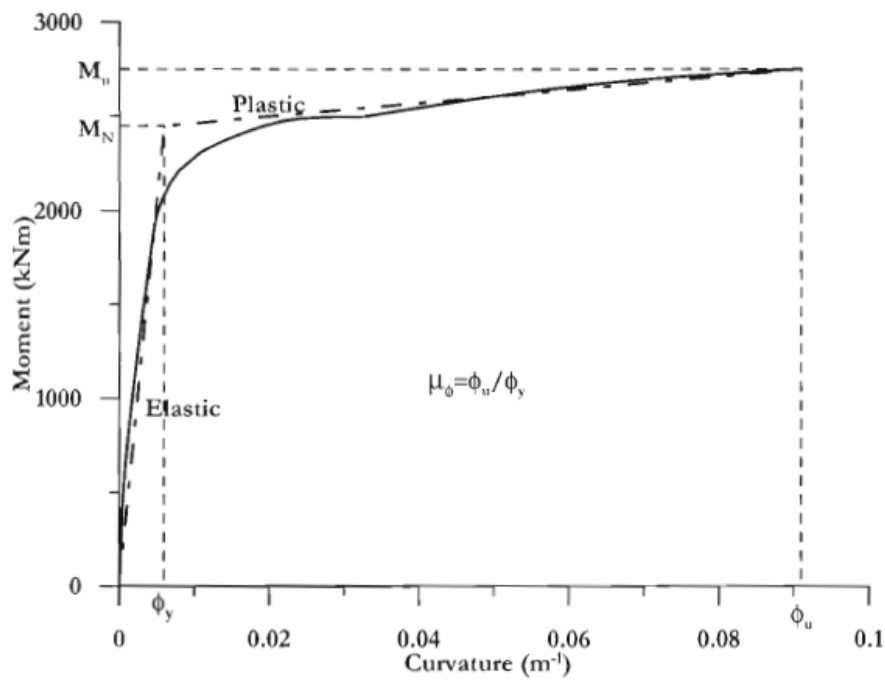


Figure 6.9- Moment-curvature response (Priestley et al. 2007)

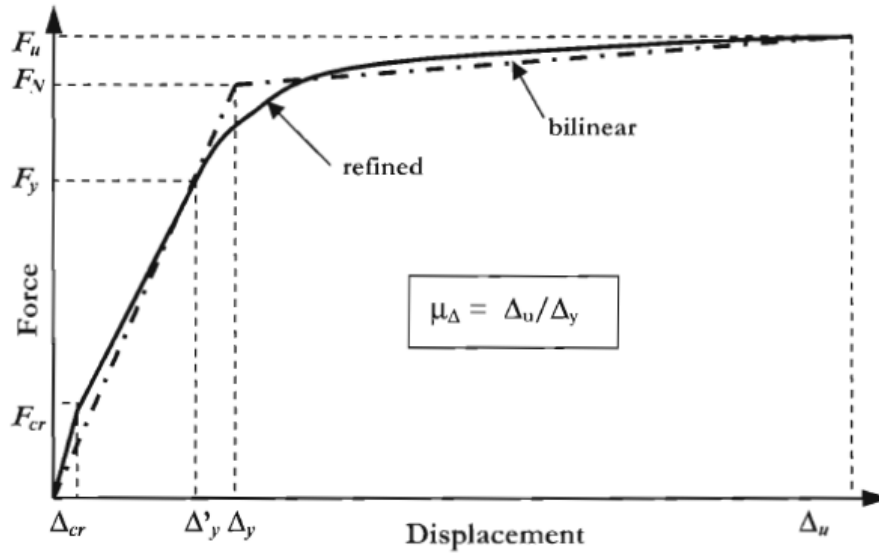


Figure 6.10- Force-displacement response (Priestley et al. 2007)

Referring to recommendations of Priestley et al. (2007), plastic hinge length  $L_P$ , i.e. length over which strain and curvature are considered to be equal to the maximum value at the column base, is given by:

$$L_P = k \cdot L_C + L_{SP} \geq 2 \cdot L_{SP}$$

where

$$k = 0.2 \cdot \left( \frac{f_u}{f_y} - 1 \right) \leq 0.08$$

$$L_{SP} = 0.022 \cdot f_{ye} \cdot d_{bl}$$

with

$L_C$  length from the critical section to the point of contraflexure in the member

$\frac{f_u}{f_y}$  ratio of ultimate tensile strength to yield strength of the flexural reinforcement (if this value is high, plastic deformations spread away from the critical as the reinforcement at the critical section strain hardens, increasing the plastic hinge length)

$f_{ye}$  yield strength of the longitudinal reinforcement

$d_{bl}$  diameter of the longitudinal reinforcement

$L_{SP}$  strain penetration length over which the curvature may be considered constant and equal to the column base curvature

According to this simplified approach proposed by Priestley et al. (2007), the plastic hinge incorporates the strain penetration length  $L_{SP}$  and the curvature distribution higher up the

column is assumed to be linear, in accordance with the bilinear approximation to the moment-curvature response, as shown in Figure 6.11.

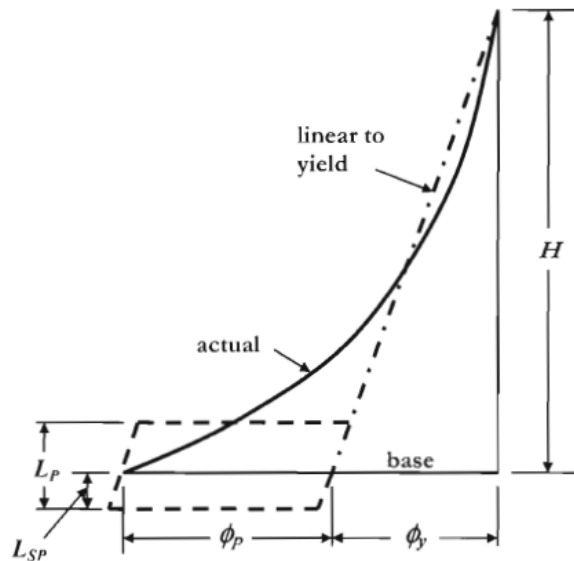


Figure 6.11- Plastic hinge length and idealization of curvature distribution (Priestley et al. 2007)

In structural models used to perform analyses  $L_c = H$  (column height),  $\frac{f_u}{f_y}$  ratio is equal to 1.25 (540/430 MPa for FeB44k steel bars),  $f_{ye}$  is 430 MPa for FeB44k steel bars.

First yielding and ultimate curvatures and moments were calculated using the software *Cumbia*. *Cumbia* is a *Matlab*-based moment-curvature software, developed by Priestley et al. (2007), which provides information for different limit states. The software is a set of *Matlab* codes to perform monotonic moment-curvature analysis and force-displacement response of reinforced concrete members of rectangular or circular section. The section analysis is performed by tabulating moment and curvature of the member section for increasing levels of concrete strain. The member response is obtained from the section moment-curvature results along with an equivalent plastic hinge length.

The software *Cumbia* also calculates the displacement at expected buckling according to two methodologies: Moyer and Kowalsky (2003) denoted as M-K buckling, for which it assumes that the longitudinal reinforcement yields between stirrups; and Berry and Eberhard (2005) denoted as B-E buckling. In the present work Moyer and Kowalsky buckling model was considered.

Default constitutive models for concrete and steel stress-strain relationships have been used. The defaults models for the unconfined and confined concrete are those proposed by Mander

et al. (1988). The default stress-strain relationship of the steel is the model proposed by King et al. (1986).

In the following figures stress-strain relations for confined and unconfined concrete and reinforcing steel, moment-curvature and force-displacement relations calculated with the software *Cumbia* are reported for reinforced concrete rectangular column sections of Model A, B and C.

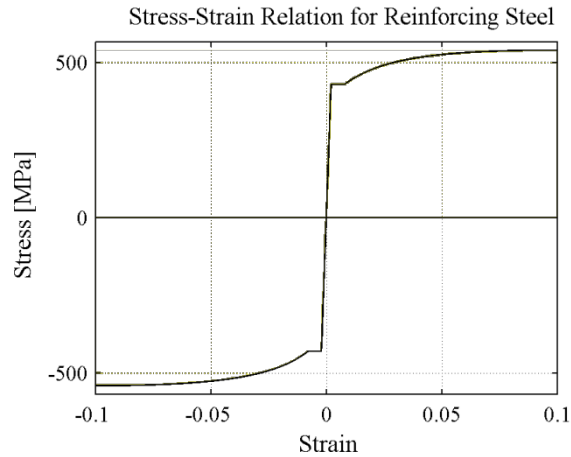


Figure 6.12- Stress-strain relation for reinforcing steel for Model A, B and C

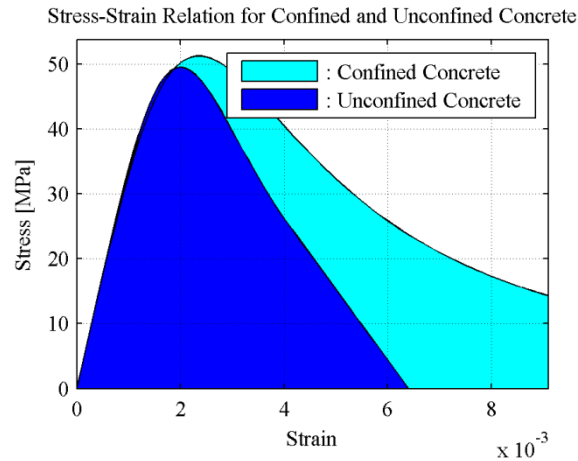


Figure 6.13- Stress-strain relation for confined and unconfined concrete for Model A

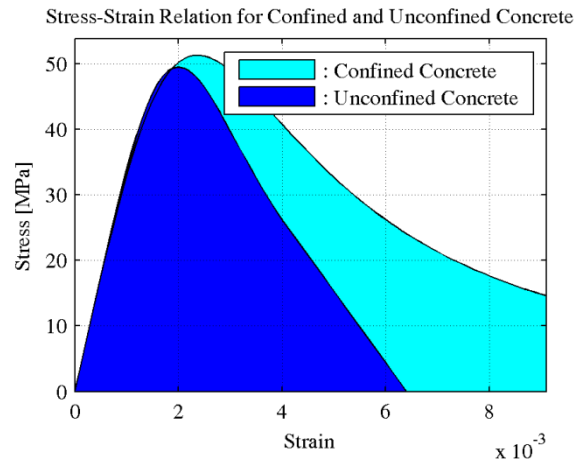


Figure 6.14- Stress-strain relation for confined and unconfined concrete for Model B

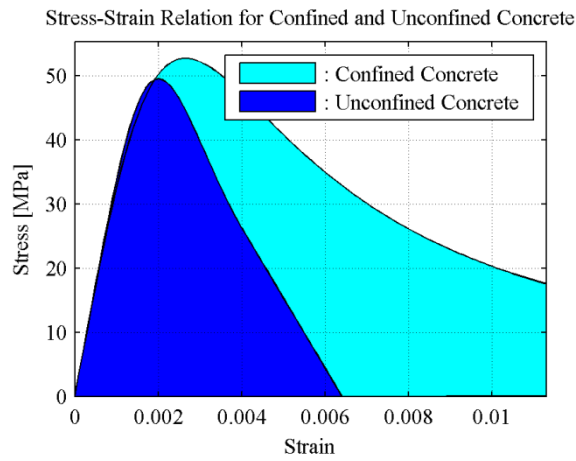


Figure 6.15- Stress-strain relation for confined and unconfined concrete for Model C

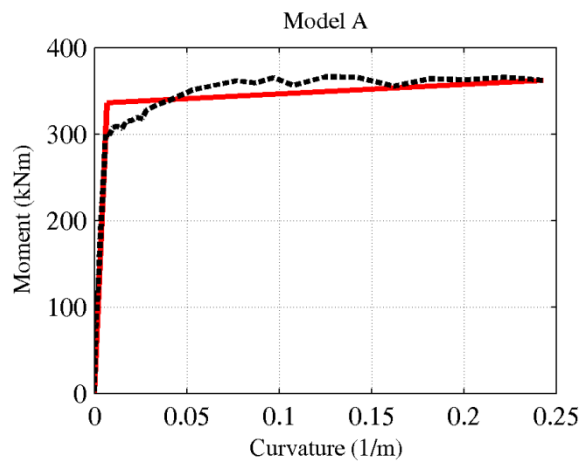


Figure 6.16- Moment-curvature relation for Model A

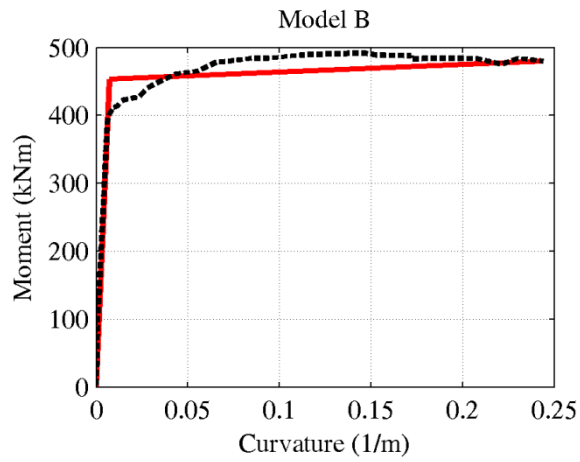


Figure 6.17- Moment-curvature relation for Model B

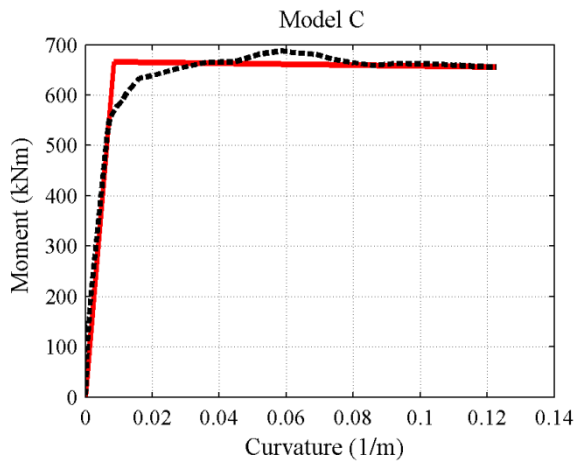


Figure 6.18- Moment-curvature relation for Model C

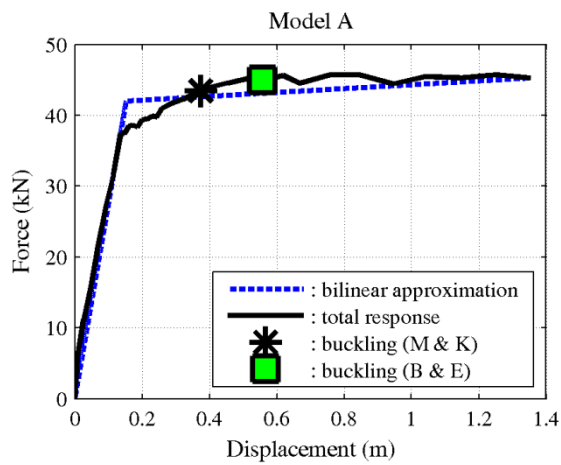


Figure 6.19- Force-displacement relation for Model A

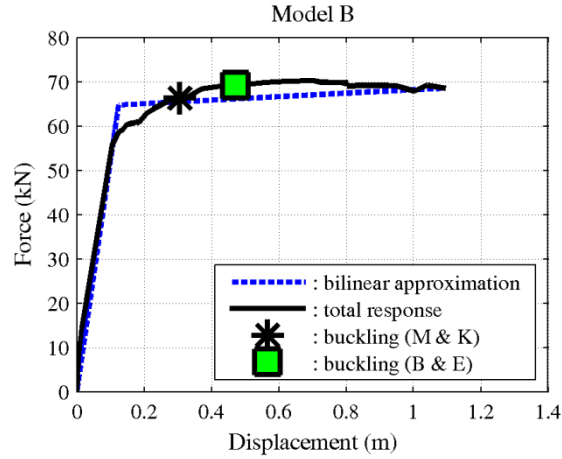


Figure 6.20- Force-displacement relation for Model B

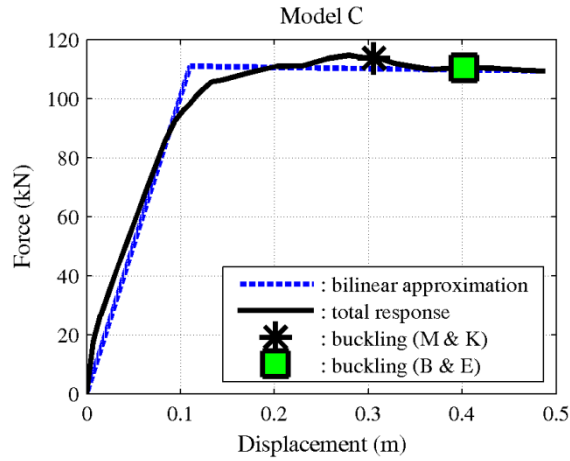


Figure 6.21- Force-displacement relation for Model C

Basing on first yielding and ultimate curvature values of column rectangular section calculated using the software *Cumbia*, first yielding displacement  $\Delta_y$  and ultimate displacement  $\Delta_u$  values for columns were computed according to Priestley et al. (2007).

$$\Delta_y = \phi_y \cdot (H + L_{SP})^2 / 3$$

$$\Delta_u = \Delta_y + \Delta_p = \Delta_y + \phi_p L_P H = \Delta_y + (\phi_u - \phi_y) L_P H$$

with

$\phi_y$  curvature for first yield

$\phi_p$  plastic hinge curvature

$\phi_u$  ultimate curvature

$L_{SP}$  strain penetration length

$L_P$  plastic hinge length

$H$  column height

For cantilever columns, horizontal force  $F$  can be calculated as:

$$F = M/H$$

Therefore, first yielding force  $F_y$  and ultimate force  $F_u$  are:

$$F_y = M_y/H$$

$$F_u = M_u/H$$

Chord rotation of columns  $\theta$  can be calculated as:

$$\theta = \Delta/H$$

Therefore, first yielding chord rotation  $\theta_y$  and ultimate chord rotation  $\theta_u$  are:

$$\theta_y = \Delta_y/H$$

$$\theta_u = \Delta_u/H$$

In Table 6.3 plastic hinge length, yielding and ultimate moment, curvature, force, displacement and chord rotation values of columns for Model A, B and C are resumed.

		<b>Model A</b>	<b>Model B</b>	<b>Model C</b>
Plastic hinge length $L_p$	mm	636	585	553
Curvature for First Yield $\phi_y$	1/m	0.0061	0.0063	0.0069
Ultimate Curvature $\phi_u$	1/m	0.0497	0.0506	0.0667
Moment for First Yield $M_y$	kNm	300	392	535
Ultimate Moment $M_u$	kNm	348	463	682
Displacement for First Yield $\Delta_y$	mm	137	110	89
Ultimate Displacement $\Delta_u$	mm	359	291	288
First Yielding Force $F_y$	kN	38	56	89
Ultimate Force $F_u$	kN	43	66	114
First Yielding Chord Rotation $\theta_y$	%	1.72	1.57	1.49
Ultimate Chord Rotation $\theta_u$	%	4.49	4.16	4.80

*Table 6.3- Nonlinear column capacity parameters of Model A, B and C*

### 6.3 Seismic input definition

Different input seismic were considered depending on the kind of nonlinear dynamic analysis performed: (i) combinations of seven real records selected using the software *REXEL* and compatible in the average with the reference spectra according to current Italian building code criteria; (ii) recorded acceleration time histories from 2012 Emilia earthquakes; (iii) recorded

acceleration time histories from *PEER* database selected in order to have three classes of motions belonging to three different Magnitude-Distance scenarios.

(i) *Spectrum-compatible ground motions*

The seismic input considered for nonlinear dynamic analyses performed with the software *SAP2000* was a set of seven spectrum-compatible ground-acceleration time histories selected using the software *REXEL* (Iervolino et al. 2010 – Figure 6.22). The 5% damped pseudo-acceleration response-spectra of the records match, on average, the life-safety spectrum (475 years return period) defined according to the current Italian building code for the site of Finale Emilia (MO) – one of the municipalities severely hit by the 2012 Emilia earthquakes - Longitude 11.17°E, Latitude 44.50°N, soil class C according to Eurocode 8.

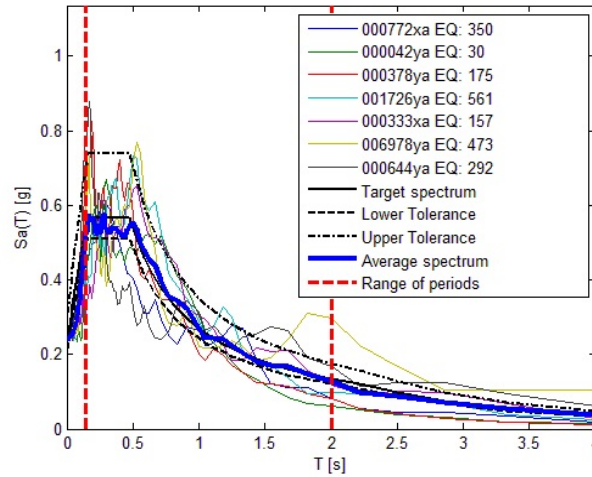


Figure 6.22- Set of time histories selected using *REXEL* spectrum-compatible for the site of Finale Emilia (MO) - Italy

Main characteristics of selected ground motions are reported in the following table.

TH-ID	EqID	EqName	EqDate	Distance [km]	$M_w$	PGA_X [m/sec <sup>2</sup> ]	PGA_Y [m/sec <sup>2</sup> ]
772xa	350	Umbria Marche (aftershock)	03/10/1997	20	5.3	0.5673	0.405
42ya	30	Ionian	04/11/1973	15	5.8	5.1459	2.4983
378ya	175	Lazio Abruzzo	07/05/1984	16	5.9	1.4437	1.1158
1726ya	561	Adana	27/06/1998	30	6.3	2.1575	2.6442
333xa	157	Alkion	24/02/1981	20	6.6	2.2566	3.0363
6978ya	473	Izmit (aftershock)	13/09/1999	25	5.8	1.3873	0.7001
644ya	292	Umbria Marche (aftershock)	14/10/1997	29	5.6	0.5383	0.3256

Table 6.4- Characteristics of ground motions selected using *REXEL*

**(ii) Records from 2012 Emilia earthquakes**

The input seismic considered for time history analyses are recorded acceleration time histories from 2012 Emilia earthquakes. Two main events struck the region: a 5.9  $M_w$  earthquake on the 20<sup>th</sup> May and a 5.8  $M_w$  earthquake on the 29<sup>th</sup> May with epicentre 15 km northwest of the first one.

For each main event the North-South (which is the strongest one) component of acceleration recorded in the stations closest to the epicentre was used. The Mirandola station (MRN) is the permanent station closest to the epicentre that recorded both main events. After the 20<sup>th</sup> May event temporary stations were installed in the area of the epicentre, as shown in Figure 6.23.

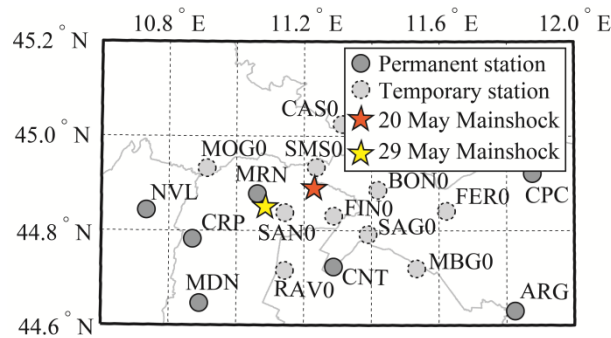


Figure 6.23- Ground-motion recording stations during Emilia earthquakes (temporary stations were installed after the event of May 20<sup>th</sup> 2012)

Time history acceleration records used for analyses are from the MRN permanent station for both 20<sup>th</sup> May and 29<sup>th</sup> May events and from SAN0 and SMS0 temporary stations for the 29<sup>th</sup> May event.

Main characteristics of recorded ground motions are reported in the following table.

TH-ID	EqDate	Station	Station type	Distance [km]	$M_L$	PGA [m/sec <sup>2</sup> ]
20May-MRN	20th May 2012	MRN	Permanent	13.32	5.9	3.85
29May-MRN	29th May 2012	MRN	Permanent	3.55	5.8	2.93
29May-SAN0	29th May 2012	SAN0	Temporary	4.72	5.8	2.41
29May-SMS0	29th May 201298	SMS0	Temporary	14.93	5.8	1.82

Table 6.5- Characteristics of records from 2012 Emilia earthquakes

**(iii) Records from PEER database with 3 different Magnitude-Distance scenarios**

Recorded acceleration time histories from PEER database were selected in order to have three classes of motions belonging to three different Magnitude-Distance scenarios:

- Large Magnitude – Large Distance;
- Large Magnitude – Small Distance;
- Small Magnitude – Small Distance.

The definition of three different Magnitude-Distance scenarios has the aim to evaluate the dependence of dynamic behaviour of dissipative devices from the characteristics of the seismic input, particularly to evaluate the presence of near-source effects using ground motions recorded during 2012 Emilia earthquakes used for initial time history analyses performed using the model created with the software *OpenSees* .

For each Magnitude-Distance scenario from *PEER* database were selected ground motions to perform time history analyses using the following criteria:

- For a range of period of vibration of 1-1.5 seconds, typical values of fundamental period of vibration for precast RC structures, spectral acceleration values must be greater than  $1.5 \text{ m/sec}^2$  in order to have seismic actions on beam-column connections similar to the equivalent forces of plasticization  $F_{eq}$  of the dissipative devices to avoid the use of too high scaling factor for acceleration records during time history analyses to be performed. In following tables maximum spectral acceleration values for the range of period of vibration 1-1.5 seconds are reported (column *SpectralAcc*);
- Maximum four acceleration records from the same seismic event.

Therefore, referring to three different Magnitude-Distance scenarios introduced above, the following number of recorded ground motions have been selected:

- 35 ground motions for the Large Magnitude – Large Distance scenario;
- 33 ground motions for the Large Magnitude – Small Distance scenario;
- 29 ground motions for the Small Magnitude – Small Distance scenario.

Impulsive and non-impulsive motions have been distinguished.

In following tables main characteristics of selected ground motions are reported for each Magnitude-Distance scenario.

**Large Magnitude – Large Distance scenario**

<b>TH-ID</b>	<b>EqID</b>	<b>RecSeq</b>	<b>Pulse</b>	<b>Distance [km]</b>	<b>Magnitude</b>	<b>PGA [m/sec<sup>2</sup>]</b>	<b>SpectralAcc [m/sec<sup>2</sup>]</b>
<b>1</b>	28	36	0	45.12	6.63	1.28	2.15
<b>2</b>	30	68	0	22.77	6.61	2.06	1.73
<b>3</b>	50	169	0	22.03	6.53	3.44	3.38
<b>4</b>	116	729	0	23.85	6.54	2.03	3.46
<b>5</b>	116	724	0	22.24	6.54	1.82	1.87
<b>6</b>	118	758	0	76.87	6.93	2.55	5.17
<b>7</b>	118	776	0	27.67	6.93	3.63	5.12
<b>8</b>	118	777	0	27.33	6.93	2.11	4.55
<b>9</b>	118	759	0	43.77	6.93	2.89	4.14
<b>10</b>	123	826	0	40.23	7.01	1.75	2.40
<b>11</b>	125	900	0	23.62	7.28	2.40	3.86
<b>12</b>	125	888	0	79.76	7.28	0.76	1.79
<b>13</b>	125	850	0	21.78	7.28	1.51	1.72
<b>14</b>	125	882	0	26.84	7.28	1.31	1.71
<b>15</b>	127	963	0	20.1	6.69	5.04	4.12
<b>16</b>	127	1003	0	21.17	6.69	4.30	1.91
<b>17</b>	127	987	0	20.36	6.69	3.15	1.80
<b>18</b>	127	985	0	23.51	6.69	1.65	1.61
<b>19</b>	129	1107	0	22.5	6.9	3.38	3.18
<b>20</b>	129	1110	1	24.78	6.9	2.10	2.18
<b>21</b>	129	1121	1	27.77	6.9	1.55	2.10
<b>22</b>	129	1100	1	24.85	6.9	2.30	1.55
<b>23</b>	136	1147	0	68.09	7.51	1.81	3.64
<b>24</b>	136	1166	0	30.74	7.51	1.34	2.90
<b>25</b>	136	1155	0	60.43	7.51	1.06	2.10
<b>26</b>	137	1264	0	50.51	7.62	1.39	3.17
<b>27</b>	137	1542	0	25.44	7.62	1.17	3.11
<b>28</b>	137	1329	0	81.7	7.62	0.94	3.07
<b>29</b>	137	1419	0	97.69	7.62	1.04	3.00
<b>30</b>	144	1640	0	93.3	7.37	1.34	2.21
<b>31</b>	144	1634	0	75.58	7.37	2.05	2.07
<b>32</b>	144	1637	0	63.96	7.37	0.84	1.83
<b>33</b>	158	1762	0	41.82	7.13	1.78	2.00
<b>34</b>	158	1792	0	74	7.13	1.21	1.71
<b>35</b>	158	1794	0	31.06	7.13	1.43	1.68

*Table 6.6- Large Magnitude – Large Distance scenario ground motions*

**Large Magnitude – Small Distance scenario**

<b>TH-ID</b>	<b>EqID</b>	<b>RecSeq</b>	<b>Pulse</b>	<b>Distance [km]</b>	<b>Magnitude</b>	<b>PGA [m/sec<sup>2</sup>]</b>	<b>SpectralAcc [m/sec<sup>2</sup>]</b>
<b>1</b>	6	6	0	6.09	6.95	2.11	2.11
<b>2</b>	30	77	0	0	6.61	12.03	7.95
<b>3</b>	41	126	0	3.92	6.8	5.97	4.34
<b>4</b>	46	143	0	1.79	7.35	8.20	5.92
<b>5</b>	46	139	0	0	7.35	3.98	1.81
<b>6</b>	50	171	0	0.07	6.53	2.90	5.03
<b>7</b>	50	182	1	0.56	6.53	4.54	4.64
<b>8</b>	68	292	1	6.78	6.9	2.46	3.00
<b>9</b>	68	285	0	8.14	6.9	1.98	2.91
<b>10</b>	97	495	0	2.48	6.76	9.59	2.27
<b>11</b>	111	587	0	16.09	6.6	2.51	1.66
<b>12</b>	116	723	0	0.95	6.54	4.46	9.52
<b>13</b>	116	728	0	13.03	6.54	2.07	3.21
<b>14</b>	118	779	1	0	6.93	9.48	7.99
<b>15</b>	118	3548	0	3.22	6.93	4.24	5.85
<b>16</b>	121	821	1	0	6.69	5.05	6.89
<b>17</b>	123	828	1	0	7.01	6.50	4.72
<b>18</b>	123	825	1	0	7.01	14.69	3.98
<b>19</b>	125	879	0	2.19	7.28	7.13	4.53
<b>20</b>	125	864	0	11.03	7.28	2.79	3.70
<b>21</b>	127	1063	1	0	6.69	8.10	9.67
<b>22</b>	127	1086	0	1.74	6.69	8.27	7.95
<b>23</b>	129	1114	1	3.31	6.9	3.09	8.51
<b>24</b>	129	1106	0	0.94	6.9	8.06	7.02
<b>25</b>	136	1158	0	13.6	7.51	3.51	5.27
<b>26</b>	136	1176	1	1.38	7.51	3.42	4.42
<b>27</b>	137	1517	0	0	7.62	11.35	15.91
<b>28</b>	137	1492	0	0	7.62	4.11	9.79
<b>29</b>	138	1605	1	0	7.14	5.25	4.87
<b>30</b>	138	1602	1	12.02	7.14	8.07	4.03
<b>31</b>	144	1633	0	12.56	7.37	4.87	4.06
<b>32</b>	158	1787	0	10.35	7.13	3.30	3.89
<b>33</b>	169	2114	1	0.18	7.9	3.13	6.90

*Table 6.7- Large Magnitude – Small Distance scenario ground motions*

**Small Magnitude – Small Distance scenario**

<b>TH-ID</b>	<b>EqID</b>	<b>RecSeq</b>	<b>Pulse</b>	<b>Distance [km]</b>	<b>Magnitude</b>	<b>PGA [m/sec<sup>2</sup>]</b>	<b>SpectralAcc [m/sec<sup>2</sup>]</b>
<b>1</b>	25	29	0	6.27	6.19	4.67	4.59
<b>2</b>	31	95	0	3.51	6.24	3.31	1.74
<b>3</b>	48	150	0	0.42	5.74	4.26	2.46
<b>4</b>	48	147	0	8.47	5.74	3.33	1.92
<b>5</b>	56	230	0	1.1	6.06	4.09	2.09
<b>6</b>	64	265	0	13.8	6.33	6.09	2.88
<b>7</b>	64	266	0	18.53	6.33	1.47	2.06
<b>8</b>	69	300	0	8.81	6.2	1.74	2.78
<b>9</b>	73	319	1	6.18	5.9	3.61	4.00
<b>10</b>	73	316	1	16.54	5.9	2.37	2.23
<b>11</b>	76	368	0	7.69	6.36	5.80	3.42
<b>12</b>	76	367	0	7.69	6.36	3.72	2.64
<b>13</b>	90	451	1	0.18	6.19	12.74	3.77
<b>14</b>	90	459	0	9.85	6.19	2.86	2.82
<b>15</b>	101	529	0	0	6.06	5.83	4.26
<b>16</b>	101	527	0	3.67	6.06	2.14	4.12
<b>17</b>	103	558	0	6.44	6.19	4.38	2.85
<b>18</b>	108	569	1	3.71	5.8	3.99	4.14
<b>19</b>	108	568	1	2.14	5.8	8.58	3.88
<b>20</b>	134	1141	0	0	6.4	3.45	4.53
<b>21</b>	172	2655	0	18.1	6.2	1.97	1.79
<b>22</b>	172	2457	0	18.47	6.2	1.83	1.71
<b>23</b>	173	2734	0	6.02	6.2	3.17	2.95
<b>24</b>	175	3475	1	0	6.3	5.27	1.65
<b>25</b>	48	149	0	4.79	5.74	2.66	1.71
<b>26</b>	48	148	0	6.75	5.74	2.24	1.65
<b>27</b>	90	461	0	3.45	6.19	3.06	1.85
<b>28</b>	90	458	0	11.53	6.19	2.20	1.52
<b>29</b>	172	2658	0	10.95	6.2	9.33	1.68

*Table 6.8- Small Magnitude – Small Distance scenario ground motions*

## 6.4 Preliminary nonlinear dynamic analyses

Firstly, the effectiveness of the dissipative devices in strengthening beam-column joints of precast structures was investigated by means of nonlinear time-history analyses on a simple portal frame structure, modelled with the FEM software *SAP2000*.

Nonlinear dynamic analyses permit to evaluate the stress and deformation time histories of structural elements and the nonlinear behaviour of the dissipative device.

The aim of performed analyses was to evaluate the effects of the introduction of the dissipative devices in terms of relative beam-column displacement control and base shear reduction respect to systems with hinged connections.

The case-study structure considered in these analyses is the scheme of Model *B* (see Table 6.1) with column performing linear elastic behaviour.

These analyses were performed according to three different configurations of beam-column joints:

- System *a*: Hinged connections
- System *b*: Connections based on the dissipative devices with no friction
- System *c*: Connections based on the dissipative devices and beam-column friction.

System *a* was considered as representative of traditional retrofitting solutions based on the introduction of steel plates in order to avoid relative beam-column displacements and was used as reference for evaluating the variation of performance of the dissipative devices.

Since numerical studies (Biondini et al. 2013) showed that the vertical ground-motion component can reduce or even cancel the friction effect, present analyses were carried out considering two different values for the friction coefficient: 0.1 (System *c*) and 0.0 (System *b*). The 0.1 friction coefficient value considered in System *c* was based on Magliulo et al. (2011) considerations.

The most significant part of the model (Figure 6.24) concerns the definition of the properties of the *Non Linear Links (NLLink)* used for the simulation of the nonlinear behaviour of the dissipative devices connected to beam-column joints (CSI Computers and Structures Inc. 2013). In particular, each beam-column joint was modelled using a *NLLink* able to simulate friction plus a combination of *NNLinks* and *Joint Constraints* in order to simulate the behaviour of the investigated devices under cyclic loads and to reproduce the configuration of the real beam-column joint strengthened with the devices (see Figure 6.1).

---

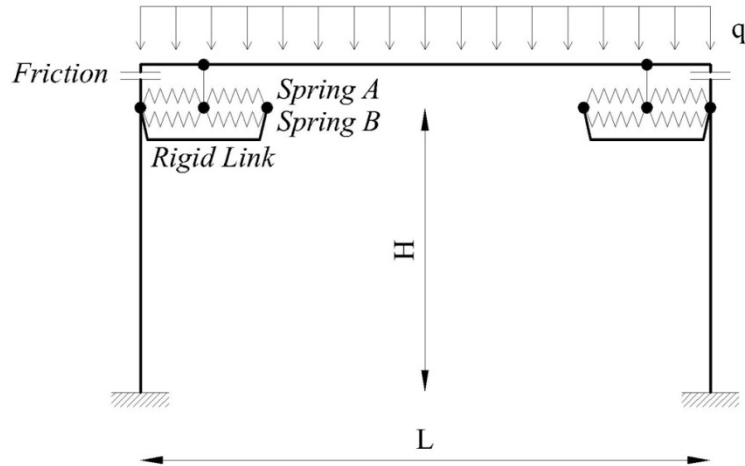


Figure 6.24- Scheme of structural model used for SAP2000 numerical analyses

The devices considered in the model had an equivalent plasticization force  $F_{eq}$  of 20.0 kN and a maximum deformation capacity  $S_{max} = 75$  mm (see Figure 6.4).

Each carbon wrapped tube is modelled by two links as shown in Figure 6.24:

- i. a *NLLink* based on a modified Takeda hysteresis rule (Figure 6.24 – Spring A and Figure 6.25) in order to simulate the cyclic behaviour. The adopted hysteresis rule features an elastic-perfectly plastic load-displacement behaviour in compression and unloading and reloading stiffness equal to the initial elastic stiffness. Zero strength and stiffness were assigned for tensile loads, in order to simulate the increasing axial gap. The numerical parameters used in the model were based on experimental test results and were defined using the criteria described in previous sections.

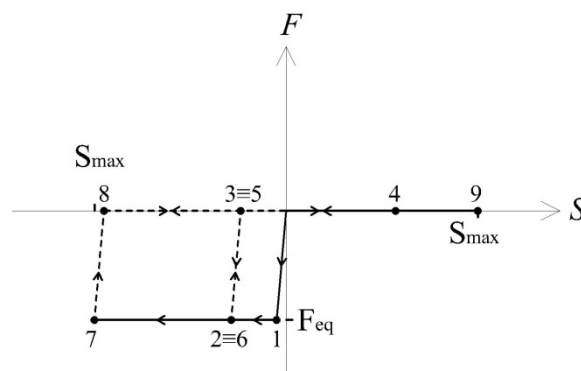


Figure 6.25- Modified Takeda hysteretic rule

- ii. an elastic link (Figure 6.24 – Spring B) with an initial gap in compression equal to the maximum deformation capacity of the device  $S_{max}$  (see Figure 6.4), in order to simulate the behaviour when the plastic deformation capacity is extinguished. The

loading stiffness for axial displacements greater than  $S_{max}$  corresponds to the initial elastic stiffness.

Concrete of beam and columns was assumed as elastic with an elastic modulus  $E_c=25000$  MPa. A 5% Rayleigh damping ratio was adopted in all the analyses.

The seismic input considered for nonlinear dynamic analyses of all the three systems was a set of seven spectrum-compatible ground-acceleration time-histories selected using the software *REXEL* (Iervolino et al. 2010), as introduced in Section 6.3. The 5% damped pseudo-acceleration response-spectra of the records match, on average, the life-safety spectrum (475 years return period) defined according to the Italian building code (NTC 2008) for the site of Finale Emilia (MO) – one of the municipalities severely hit by the 2012 Emilia earthquakes - Longitude 11.17°E, Latitude 44.50°N, soil class C according to Eurocode 8.

In the analyses carried out, only the horizontal component of acceleration was considered.

For each analysis, the relative beam-column displacement, the hysteretic behaviour of the devices and the column base shear were evaluated. As an example, Figure 6.26 shows the cyclic behaviour for the couple of carbon-wrapped tubes in one beam-column connection, obtained from System *b* and time history *42ya*. It is worth noticing that, according to experimental results, once a given equivalent plastic-deformation is achieved for the first time along one direction, a gap is created and therefore, in the following cycles, the reaction force of the devices along that same direction will be zero until the actual displacement becomes larger than the gap. This behaviour creates an effect of isolation/disconnection between beam and column that allows reducing base shear.

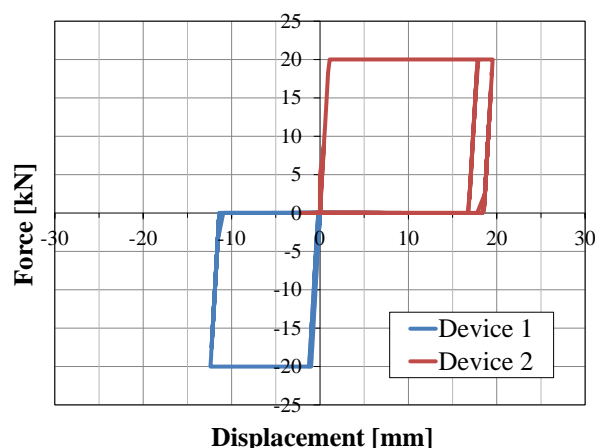


Figure 6.26- Hysteresis cycle of the dissipative device (System *b*, Time history *42ya*)

Figure 6.27 shows, from the same analysis, the relative beam-column displacement versus time.

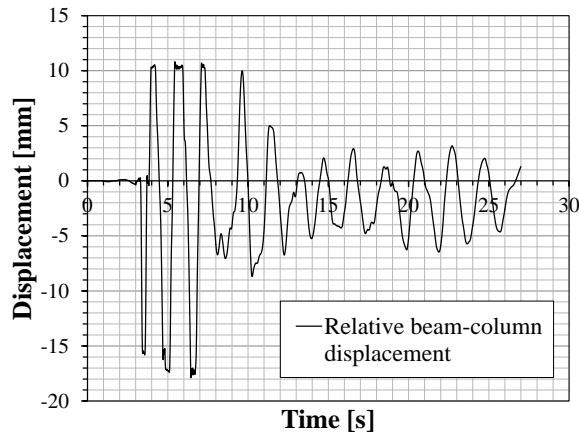


Figure 6.27- Relative beam-column displacement (System *b*, Time history 42ya)

Figure 6.28 shows, from the same recorded time history 42ya, the reduction of the column base shear passing from System *a* with hinged connections to System *b* with connections based on the dissipative devices with no friction.

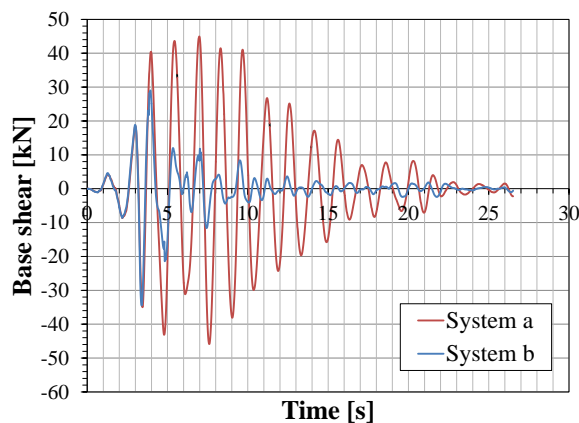


Figure 6.28- Base shear reduction with dissipative connections (Time history 42ya)

Table 6.9 reports, for each time history analysis, the maximum value of shear force and bending moment at the base of the column and the maximum residual deformation of the devices, corresponding to the relative beam-column displacement. Comparing the behaviour of the model with hinged connections (System *a*) with the models with dissipative devices (Systems *b* and *c*), it is possible to observe a significant reduction of base shear: of 31% and 47% in case of friction coefficient equal to 0.1 and 0.0, respectively. A reduced friction coefficient led, on one hand, to a smaller base shear, and on the other hand to an increase in the maximum deformation of the devices (on average 30 mm in System *b* and 24 mm in System *c*). In the present case study, the maximum deformation capacity of the devices ( $S_{max}$  of 75 mm) was never exceeded.

Time History	42ya	1726ya	378ya	333xa	644ya	6978ya	772xa	mean
<b>System a - Hinged connection</b>								
Column shear [kN]	46	68	46	85	85	66	62	<b>66</b>
Column bending moment [kNm]	325	473	319	597	598	464	433	<b>458</b>
<b>System b - Connection based on the dissipative devices with no friction</b>								
Column shear [kN]	36	33	34	34	39	41	28	<b>35</b>
Column bending moment [kNm]	249	223	232	235	261	276	190	<b>238</b>
Device deformation [mm]	19	22	17	33	37	66	18	<b>30</b>
<b>System c - Connection based on the dissipative devices with friction</b>								
Column shear [kN]	37	42	38	45	55	62	37	<b>45</b>
Column bending moment [kNm]	254	290	259	307	377	422	254	<b>309</b>
Device deformation [mm]	14	18	14	25	35	48	15	<b>24</b>

Table 6.9- Results of time history analyses for Systems a, b and c

Numerical simulations of the behaviour of a simple portal frame structure were carried out in order to verify the effectiveness of the introduction of the devices to improve the seismic behaviour of existing structures. Results were compared with those provided by equivalent elastic systems with simple hinged beam-column connections. A significant reduction of base shear was recorded for the system with dissipative connections respect to hinged connections, respectively of 31% and 47% in case of friction coefficient equal to 0.1 and 0.0.

## 6.5 OpenSees structural model

Performing a high number of time history analyses with the aim to provide a parametric study in order to verify the effectiveness of the introduction of the presented dissipative devices in beam-column connections is not practical using a commercial software like *SAP2000*. For this reason a new code was developed using the software *Matlab* and analyses have been carried out using the FEM software *OpenSees* (Mazzoni et al. 2006).

Analyses have been performed according to the model schematized in Figure 6.29.

The scheme is a simple 2D portal frame with three degree of freedom portal frames, with fixed base joints and different kinds of beam-column connections. The code was developed in order to perform time history analyses having the possibility to easily vary some significant parameters of the structure and of the dissipative devices to identify the correct behaviour of the model under seismic action.

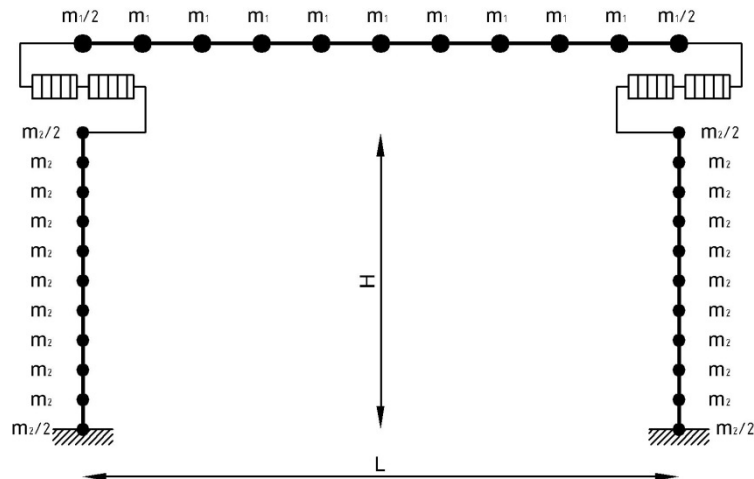


Figure 6.29- Scheme of structural model used for analyses performed using OpenSees

Particularly, concerning the structure, main variables are:

- span length  $L$ ;
- column height  $H$ ;
- roof loads and masses;
- column steel reinforcement.

Concerning the dissipative devices, the two main variables are:

- equivalent force of plasticization  $F_{eq}$ ;
- maximum deformation capacity  $S_{max}$ .

Two different values of flexural stiffness of columns were assumed depending on behaviour, linear elastic or nonlinear, of columns.

An elastic modulus  $E_c=25000$  MPa was assumed for the concrete of elements performing linear elastic behaviour.

For concrete columns performing nonlinear behaviour the flexural stiffness of cracked sections was considered and derived by the moment-curvature relationship of column section calculated using the software *Cumbia* for each model (Model A, B and C).

Distributed masses and loads have been defined through a discretization of structural elements in multiple segments. Each element, i.e. the beam and the columns, have been divided into 10 segments.

The most significant part of the models concerns the definition of the properties for the simulation of the nonlinear behaviour of the dissipative devices and of the friction mechanism in the beam-column joint.

Mechanical properties and cycling behaviour of the device are based on experimental test results. The trilinear curve derived by experimental load-displacement curves (see Figure 5.6), was implemented in the models. The first branch of the trilinear curve has the same slope of the experimental curve while the plateau (second horizontal branch –  $F_{eq}$ ) is defined so to have, in the range 0 to  $S_{max}$ , the same area under the curve of the experimental case. This area corresponds to the dissipated energy. After reaching the maximum deformation capacity  $S_{max}$ , the third branch has a slope similar to the first one, as observed experimentally.

The dissipative devices are modelled in *OpenSees* using a combination of “ZeroLength” elements (element objects defined by two nodes at the same location) with the uniaxial material “Elastic-Perfectly Plastic Gap” to reproduce the correct force-deformation relationship of the device. The material is able to simulate an elastic-perfectly plastic behaviour and to accumulate the progressive damage for each cycle of loading and unloading, increasing the gap along the axis of deformation.

The *OpenSees* command for the “Elastic-Perfectly Plastic Gap Material” is:

```
uniaxialMaterial ElasticPPGap $matTag $E $Fy $gap <$eta> <damage>
```

**\$matTag** integer tag identifying material  
**\$E** tangent  
**\$Fy** stress or force at which material reaches plastic state  
**\$gap** initial gap (strain or deformation)  
**\$eta** hardening ratio ( $=E_h/E$ ), which can be negative  
**\$damage** an optional string to specify whether to accumulate damage or not in the material. With the default string, “noDamage” the gap material will re-centre on load reversal. If the string “damage” is provided this re-centring will not occur and gap will grow.

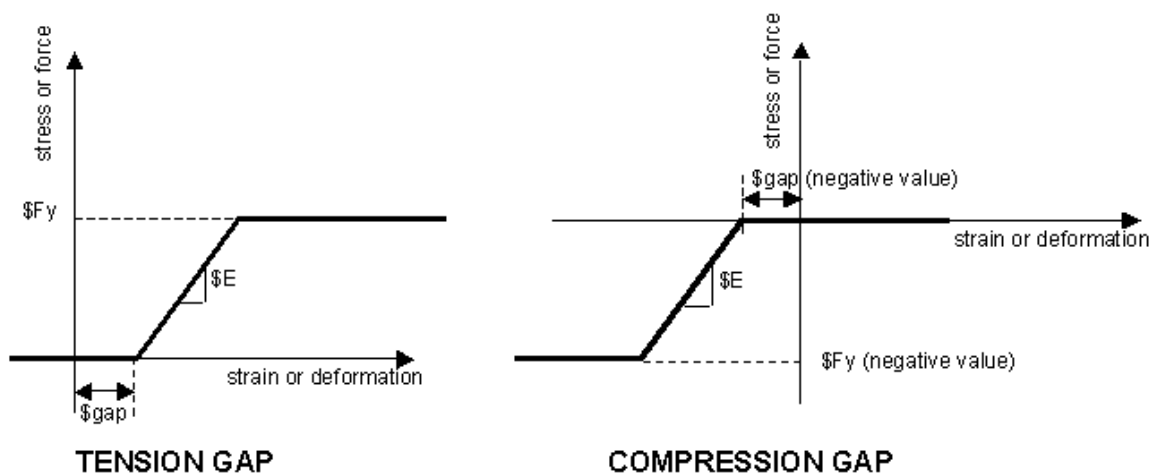


Figure 6.30- Elastic-Perfectly Plastic Gap Material in *OpenSees*

In the model the material was used providing an initial gap and a hardening ratio both equal to zero and activating the option “damage”. The  $F_y$  requested by the material command, i.e. the stress or force at which material reaches plastic state, is the equivalent force of plasticization  $F_{eq}$  of the device.

The correct hysteresis cycle is implemented using two elements with this type of relationship: one element works in compression, the other one in tension. In this way the model can simulate the possibility to dissipate energy in both direction of the seismic action.

In order to avoid some numerical errors, present in first analyses performed and probably due to the combination of the option “damage” of the *OpenSees* material and a hardening ratio equal to zero, the uniaxial material “Elastic” was used in parallel with the material “Elastic-Perfectly Plastic Gap”, providing a very low stiffness value equal to 1 N, not affecting results of analyses.

The *OpenSees* command for the “Elastic Material” is:

```
uniaxialMaterial Elastic $matTag $E <$eta>
```

\$matTag	unique material object integer tag
\$E	elastic stiffness
\$eta	damping stiffness (optional, default=0.0)

Friction mechanism is modelled in *OpenSees* using a “ZeroLength” element with the uniaxial material “Elastic-Perfectly Plastic”.

The *OpenSees* command for the “Elastic-Perfectly Plastic Material” is:

```
uniaxialMaterial ElasticPP $matTag $E $sepsyP <$sepsyN $seps0>
```

\$matTag	integer tag identifying material
\$E	tangent
\$sepsyP	strain or deformation at which material reaches plastic state in tension
\$sepsyN	strain or deformation at which material reaches plastic state in compression (optional, default is tension value)
\$seps0	initial strain (optional, default: zero)

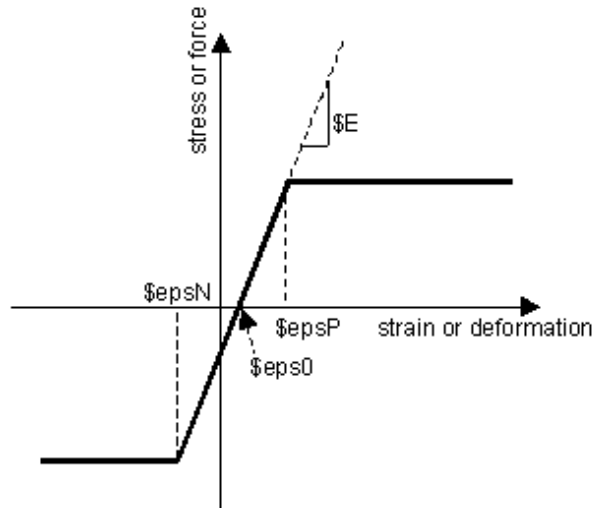


Figure 6.31- Elastic-Perfectly Plastic Material in OpenSees

Main parameters characterizing friction mechanism are the slope of the initial elastic branch and the friction force.

The slope of the initial elastic branch of friction relationship should be as high as possible in order to simulate the rigid-plastic behaviour of friction. Stiffness of initial elastic branch of friction was defined making various attempts with the aim to provide a high value, but without numerical errors related to the damping of the model. Stiffness of initial elastic branch of friction must be in any case much more higher, at least 1 order of magnitude as shown by numerical attempts, than stiffness of initial elastic branch of trilinear relationship of dissipative devices. Since stiffness of initial elastic branch of dissipative devices, as observed experimentally, is about  $4 \times 10^7$  N/m, a stiffness of  $1 \times 10^9$  N/m was used for the initial elastic branch of friction.

Friction force in the model is computed as a percentage of vertical gravitational loads and masses, multiplying their value with the considered friction coefficient.

In order to limit the axial deformation of the devices, the material “Elastic-Perfectly Plastic Gap” was used and combined in parallel with the same material “Elastic-Perfectly Plastic Gap” used to reproduce the dissipative behaviour of the devices (phases 1 and 2 of Figure 6.3). The slope of the initial elastic branch for the material used to simulate the rigid behaviour of the devices once they have reached maximum deformation capacity (phases 3 and 4 of Figure 6.3) is similar to the initial elastic branch of force-deformation relationship of the devices. The material was used providing an initial gap equal to maximum deformation capacity  $S_{max}$  of the devices, a hardening ratio equal to zero and not activating the option “damage”. The use of such a material with the possibility to assign an initial gap permits to

easily define the maximum deformation capacity  $S_{max}$  of the device and make it vary for each different analysis performed. The maximum deformation of the device is in general a design parameter, defined as a function of the size of the beam-column support in order to prevent loss-of-support collapses of structural elements. In the model the maximum deformation of the device is in fact coincident to the relative displacement value between the beam and the column.

The “Geometric Transformation” command is used to construct a coordinate transformation (CrdTransf) object, which transforms beam element stiffness and resisting force from the basic system to the global-coordinate system.

“Linear Transformation” is used to construct a linear coordinate transformation (LinearCrdTransf) object, which performs a linear geometric transformation of beam stiffness and resisting force from the basic system to the global-coordinate system.

“PDelta Transformation” is used to construct the P-Delta Coordinate Transformation (PDeltaCrdTransf) object, which performs a linear geometric transformation of beam stiffness and resisting force from the basic system to the global coordinate system, considering second-order P-Delta effects.

In the model a linear coordinate transformation was used for columns performing linear elastic behaviour, while for columns performing nonlinear behaviour second-order P-Delta effects were considered.

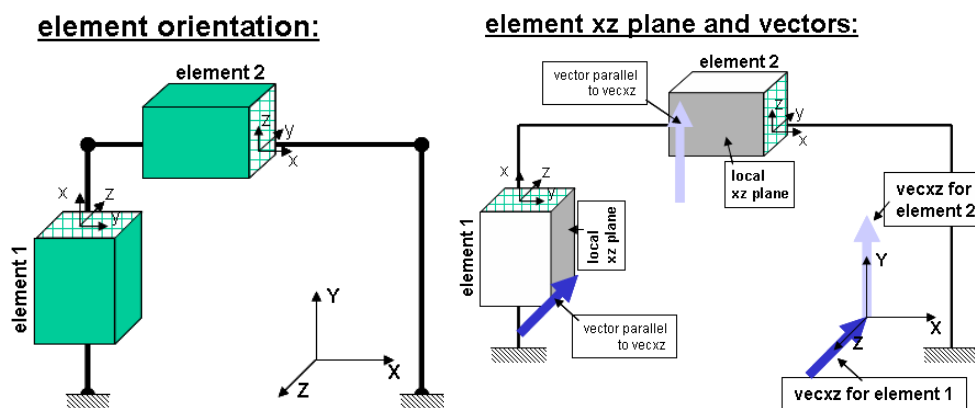


Figure 6.32- Geometric coordinate transformation in OpenSees

Structural elements performing a linear elastic behaviour were modelled in *OpenSees* using the element “Elastic Beam Column” for each beam or column segment.

The arguments for the *OpenSees* command “Elastic Beam Column Element” depend on the dimension of the problem and for a two-dimensional problem are:

```
element elasticBeamColumn $eleTag $iNode $jNode $A $E $Iz $transfTag
```

---

\$eleTag	unique element object tag
\$iNode \$jNode	end nodes
\$A	cross-sectional area of element
\$E	Young's Modulus
\$Iz	second moment of area about the local z-axis
\$transfTag	identifier for previously-defined coordinate-transformation (CrdTransf) object

Since the beams are pre-stressed precast members designed to remain elastic under the gravity loads, and the hinge connections do not allow the additional moments in the columns produced by the seismic action to be transmitted to the beams, for the sake of simplicity it was decided to represent them with elastic elements.

Structural elements performing a nonlinear behaviour were modelled in *OpenSees* using a lumped plasticity model. Concerning lumped plasticity model definition, two different column sections typologies created using the *OpenSees* command “Section Aggregator” were used in order to define characteristics of plastic hinges at the ends of the column and of the remainder central part of column with linear elastic behaviour.

The command “Section Aggregator” aggregates previously-defined UniaxialMaterial objects into a single section force-deformation model. Each UniaxialMaterial object represents the section force-deformation response for a particular section degree-of-freedom (dof). There is no interaction between responses in different dof directions.

The *OpenSees* command “Section Aggregator” is:

```
section Aggregator $secTag $matTag1 $dof1 $matTag2 $dof2 .....
```

\$secTag	unique section tag
\$matTag1 \$matTag2 ...	tag of previously-defined UniaxialMaterial objects
\$dof1 \$dof2 ...	the force-deformation quantity to be modelled by this section object

One of the following section degree-of-freedom (dof) may be used:

P	Axial force-deformation
Mz	Moment-curvature about section local z-axis
Vy	Shear force-deformation along section local y-axis
My	Moment-curvature about section local y-axis
Vz	Shear force-deformation along section local z-axis
T	Torsion Force-Deformation

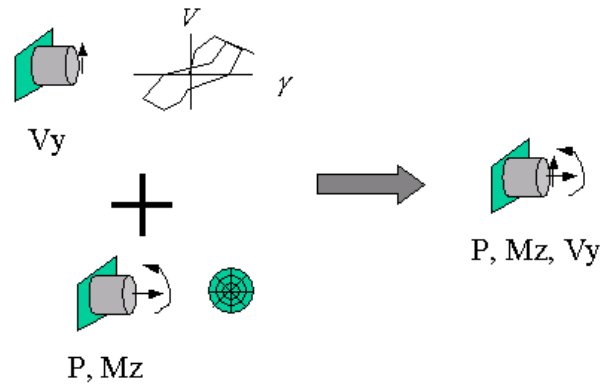


Figure 6.33- Section degree-of-freedom for the command “Section Aggregator” in OpenSees

The column section response in the model is defined combining axial force-deformation response and moment-curvature about section local z-axis response.

Column sections for plastic hinges and for linear elastic central height of columns have the same axial force-deformation response, calculated using the *OpenSees* uniaxial material “Elastic” with an elastic stiffness equal to  $E_c \cdot A$  (with  $E_c$  concrete elastic modulus,  $A$  cross-section area of the column), while moment-curvature response is different for the linear elastic and nonlinear parts of columns.

For plastic hinge sections, moment-curvature response is assigned using the uniaxial material “Hysteretic”.

The *OpenSees* command for the “Hysteretic Material”, used to construct a uniaxial bilinear hysteretic material object with pinching of force and deformation, damage due to ductility and energy, and degraded unloading stiffness based on ductility, is:

```
uniaxialMaterial Hysteretic $matTag $s1p $e1p $s2p $e2p <$s3p $e3p> $s1n $e1n $s2n
    $e2n <$s3n $e3n> $pinchX $pinchY $damage1 $damage2 <$beta>
```

\$matTag integer tag identifying material

\$s1p \$e1p stress and strain (or force & deformation) at first point of the envelope in the positive direction

\$s2p \$e2p stress and strain (or force & deformation) at second point of the envelope in the positive direction

\$s3p \$e3p stress and strain (or force & deformation) at third point of the envelope in the positive direction (optional)

\$s1n \$e1n stress and strain (or force & deformation) at first point of the envelope in the negative direction

\$s2n \$e2n stress and strain (or force & deformation) at second point of the envelope in the negative direction

\$s3n \$e3n stress and strain (or force & deformation) at third point of the envelope in the negative direction (optional)

\$pinchx	pinching factor for strain (or deformation) during reloading
\$pinchy	pinching factor for stress (or force) during reloading
\$damage1	damage due to ductility: $D1(\mu-1)$
\$damage2	damage due to energy: $D2(E_{ii}/E_{ult})$
\$beta	power used to determine the degraded unloading stiffness based on ductility, $\mu$ -beta (optional, default=0.0)

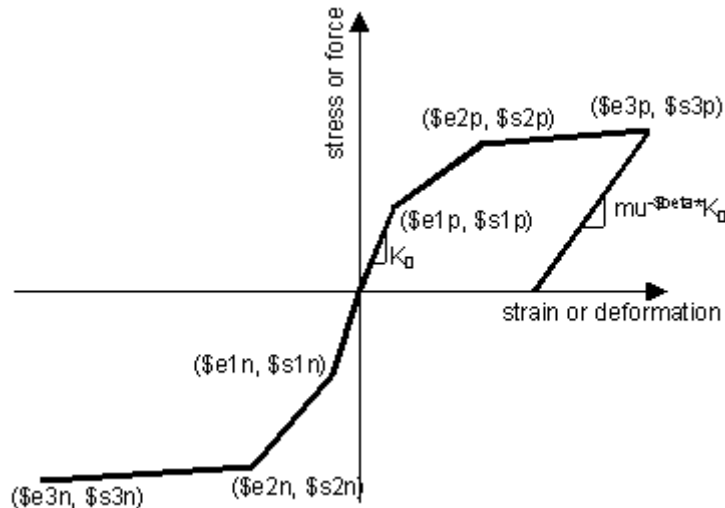


Figure 6.34- Hysteretic Material in OpenSees

Parameters obtained from the software *Cumbia* referring to yielding and ultimate moments and curvatures were used for the definition of the material “Hysteretic” for moment-curvature response of plastic hinge column sections.

For linear elastic central height of columns, moment-curvature response was calculated using the *OpenSees* uniaxial material “Elastic” with an elastic stiffness equal to  $E_c \cdot J$  (with  $E_c$  concrete elastic modulus,  $J$  area moment of inertia of the column) calculated for cracked sections as described at the beginning of this section.

Structural elements performing a nonlinear behaviour were modelled in *OpenSees* using a force-based beam-column element object for each column segment, based on the iterative force-based formulation.

The arguments for the *OpenSees* command “Force-Based Beam-Column Element” are:

```
element forceBeamColumn $eleTag $iNode $jNode $transfTag "IntegrationType arg1
arg2 ..." <-mass $massDens> <-iter $maxIters $tol>
```

\$eleTag	unique element object tag
\$iNode \$jNode	end nodes
\$transfTag	identifier for previously-defined coordinate-transformation (CrdTransf) object

---

IntegrationType arg1 arg2 ...	specifies locations and weights of integration points and their associated section force-deformation models
\$massDens	element mass density (per unit length), from which a lumped-mass matrix is formed (optional, default=0.0)
\$maxIters	maximum number of iterations to undertake to satisfy element compatibility (optional, default=10)
\$tol	tolerance for satisfaction of element compatibility (optional, default=10-12)

A variety of numerical integration options can be used in the element state determination for plastic hinge integration. Plastic hinge integration methods confine material yielding to regions of the element of specified length while the remainder of the element is linear elastic. In the model the “Radau Hinge Integration” method was used. Two-point Gauss-Radau integration over each hinge region places an integration point at the element ends and at  $2/3$  the hinge length inside the element. This approach represents linear curvature distributions exactly; however, the characteristic length for softening plastic hinges is not equal to the assumed plastic hinge length.

*set integration “HingeRadauTwo \$secTagI \$lpI \$secTagJ \$lpJ \$secTagE”*

The plastic hinge length at ends I and J is equal to respectively  $lpI$  and  $lpJ$  and the associated force-deformation response is defined by the section with tag  $secTagI$  and  $secTagJ$ . The force-deformation response of the element interior is defined by the section with tag  $secTagE$ .

In the model the two different section typologies defined with the command “Section Aggregator” and described above were associated to plastic hinges at the ends of the column and to linear elastic central height of columns.

The code for the creation of the structural model was written in order to have the possibility to vary the constraints and to control the nodal degrees of freedom choosing different kinds of beam-column connection when performing analyses and taking into account or excluding friction mechanism and/or the dissipative devices.

Three combinations of connection typologies were considered:

- hinged connection;
- friction connection;
- dissipative connection with different values of friction coefficient.

The *OpenSees* command for the control of constraints between nodes “EqualDOF” is:

*equalDOF \$rNodeTag \$cNodeTag \$dof1 \$dof2 ...*

$rNodeTag$  integer tag identifying the retained, or master node (rNode)

---

\$cNodeTag	integer tag identifying the constrained, or slave node (cNode)
\$dof1 \$dof2 ...	nodal degrees-of-freedom that are constrained at the cNode to be the same as those at the rNode; valid range is from 1 through ndf, the number of nodal degrees-of-freedom.

The *OpenSees* “Recorder” command was used to generate a recorder object to monitor what is happening during the analysis and generate output data about nodes and elements. Particularly, concerning nodes, response in terms of nodal reactions, displacement, velocity, acceleration and damping forces was collected.

Concerning elements, in case of “ZeroLength” elements and “Force-Based Beam-Column” elements, response in terms of force and deformation was recorded, while in case of “Elastic Beam Column” elements only in terms of force.

Vertical load applied was divided into a number of subsequent load increments, until reaching the total load value. The *OpenSees* “Load Control” static integrator was used.

The Newton-Raphson algorithm (*OpenSees* command “Newton Algorithm”) was used to solve the nonlinear residual equation.

The limitation of the norm of displacement increments vector of the matrix equation below a determined tolerance ( $1 \times 10^{-12}$ ) was used to determine if convergence has been achieved at the end of an iteration step for models with column performing linear elastic behaviour.

The limitation of the dot product of the solution vector and norm of the right hand side of the matrix equation below a determined tolerance ( $1 \times 10^{-10}$ ) was used to determine if convergence has been achieved at the end of an iteration step for models with column performing nonlinear behaviour.

Acceleration time history is applied to the structure after vertical static load application.

The Hilber-Hughes-Taylor method (also called the  $\alpha$  method) was used for the direct integration of the equations of motion. The HHT method is a one-step implicit method for solving the transient problem which allows for energy dissipation and second order accuracy, because it attempts to increase the amount of numerical damping present without degrading the order of accuracy.

An algorithm which takes one iteration to solve the system of equations (*OpenSees* command “Linear Algorithm”) was used.

In the model Rayleigh damping was considered, with the damping matrix for elements or nodes specified as a combination of stiffness- and mass-proportional damping matrices.

Factors applied to mass matrix and to initial stiffness matrix have been defined according to Rayleigh damping rules illustrated in Chopra (2006).

---

Considering Rayleigh damping as:

$$c = a_0 m + a_1 k$$

with  $a_0$  [sec<sup>-1</sup>] and  $a_1$  [sec] constants for mass-proportional and stiffness-proportional damping

The modal damping ratio for a system with mass-proportional damping is inversely proportional to the natural frequency. The modal damping ratio for a system with stiffness-proportional damping increases linearly with the natural frequency.

The damping ratio for the  $n$ th mode of such a system is:

$$\zeta_n = \frac{a_0}{2} \frac{1}{\omega_n} + \frac{a_1}{2} \omega_n$$

with  $\omega_n$  natural frequency for the  $n^{\text{th}}$  mode

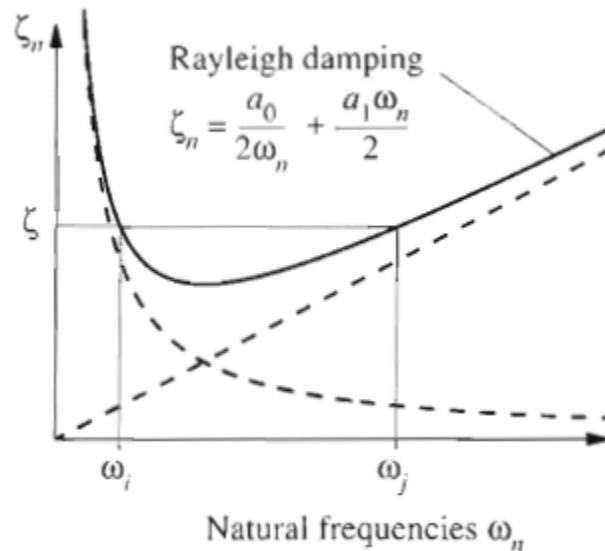


Figure 6.35- Variation of modal damping ratios with natural frequency (Chopra 2006)

The coefficients  $a_0$  and  $a_1$  can be determined from specified damping ratios  $\zeta_i$  and  $\zeta_j$  for the  $i$ th and the  $j$ th modes, respectively. If both modes are assumed to have the same damping ratio  $\zeta$ , then:

$$a_0 = \zeta \frac{2\omega_i\omega_j}{\omega_i + \omega_j} a_1 = \zeta \frac{2}{\omega_i + \omega_j}$$

The modes  $i$  and  $j$  with specified damping ratios should be chosen to ensure reasonable values for the damping ratios in all the modes contributing significantly to the response.

The *OpenSees* command to assign damping to all previously-defined elements and nodes “Rayleigh” is:

```
rayleigh $alphaM $betaK $betaKinit $betaKcomm
```

\$alphaM	factor applied to elements or nodes mass matrix
\$betaK	factor applied to elements current stiffness matrix.
\$betaKinit	factor applied to elements initial stiffness matrix.
\$betaKcomm	factor applied to elements committed stiffness matrix.

In the *OpenSees* command *\$alphaM* and *\$betaK* factors, coincide respectively to coefficients  $a_0$  and  $a_1$ , computed as indicated above.

In the model, coefficients  $a_0$  and  $a_1$  were applied to mass matrix and initial stiffness matrix, while other factors requested by the command were applied equal to zero.

A 5% Rayleigh damping ratio was adopted in all the analyses.

## 7. EVALUATION OF BEHAVIOUR FACTOR USING IDA

The purpose of numerical analyses described in this chapter is to evaluate an equivalent behaviour factor for structures equipped with the dissipative devices by comparing the behaviour of portal frames with dissipative connections with equivalent elastic systems. To reach this goal Incremental Dynamic Analyses (IDA) have been performed.

Referring to the IDA methodology illustrated by Vamvatsikos and Cornell (2002), the ground motion Intensity Measure considered (IM) is the 5% damped spectral acceleration at the structure's natural period, while two different Damage Measure (DM) depending on columns behaviour (linear elastic or nonlinear) were considered. For columns performing linear elastic behaviour the Damage Measure (DM) is the deformation of the dissipative device, i.e. the beam-column relative displacement; for columns performing nonlinear behaviour the Damage Measure (DM) is the chord rotation at the base of the columns.

Assuming maximum deformation capacity  $S_{max}$  of the device as target damage permits to control the entire range of behaviour of the dissipative device, from elastic to inelastic, until the end of its deformation capacity and consequently the end of its dissipative capacity. The maximum deformation capacity  $S_{max}$  of the device is coincident to the maximum relative displacement value between the beam and the column.

The ultimate chord rotation of columns, assumed as target damage for columns performing nonlinear behaviour, was computed for the three different models following recommendations by Priestley et al. (2007) using the software *Cumbia*, as described in Section 6.2.1.

An algorithm that uses IDA and bisection was adopted in order to identify, for each acceleration time history considered, the scaling factor required in order to achieve the target damage, i.e. the maximum deformation of the dissipative devices or the ultimate chord rotation at the base of the columns. The so obtained scaling factor was then used to perform dynamic analyses on an equivalent elastic system, i.e. the model with linear elastic behaviour of columns without the devices and therefore with simple hinges at the ends of the beam.

The equivalent behaviour factor for structures equipped with the dissipative devices was then computed as the ratio between the maximum base shear value in the equivalent elastic system and the one in the system with dissipative devices.

## 7.1 Columns performing linear elastic behaviour

As introduced in previous sections, the choice of the dissipative device is related to the capacity of the column and its reinforcement steel bars. The value of the equivalent force of plasticization  $F_{eq}$  of the device is designed as the maximum value of force that, added to friction forces, can be transferred to the top of the column before reaching the yield moment at its base. Therefore, if the target damage for IDA analyses is the maximum deformation of the dissipative device itself, columns perform a linear elastic behaviour.

The aim of these analyses is to evaluate only the contribution of the devices to dissipative capacity of the structure.

The value of the equivalent force of plasticization  $F_{eq}$  of the device is equal to 10, 30 and 50 kN, respectively for Model A, B and C. The first branch of the trilinear model of force-deformation relationship of the devices has a stiffness of 20, 30 and 50 kN/mm, respectively for Model A, B and C.

The following Table 7.1 resumes main parameters of the three models used in *OpenSees* for analyses performing linear elastic behaviour of columns.

		<b>Model A</b>	<b>Model B</b>	<b>Model C</b>
Span Length $L$	m	12	20	25
Column Height $H$	m	8	7	6
Column Section	m	0.5 x 0.5	0.5 x 0.5	0.45 x 0.45
Beam Section	m	0.3 x 1.1	0.3 x 1.1	0.3 x 1.1
Total Beam Load (dead + variable)	kN/m	41.58	38.25	56.25
Total Joint Load (dead +variable)	kN	249	383	703
Device $F_{eq}$	kN	10	30	50

*Table 7.1- Parameters of Model A, B and C with columns performing linear elastic behaviour*

The fundamental period of vibration  $T_1$  of the structural models is equal to 1.19, 1.18 and 1.54 seconds, respectively for Model A, B and C.

### 7.1.1 IDA results – 2012 Emilia earthquakes ground motions

Firstly, recorded acceleration time histories from 2012 Emilia earthquakes were considered as seismic input for numerical analyses on structural models created with the software *OpenSees*. In the analyses carried out, only the horizontal component of acceleration was considered.

These analyses were performed not introducing friction models in the beam-column simply supported joint. Such a choice was made in order to take into account the effect of vertical

component of acceleration that can reduce or nullify the friction effect, as shown by records of 2012 Emilia earthquakes, determining losses of support of structural elements without mechanical connections (see Section 6.2 for more details about the choice of not considering friction mechanism contribution).

Two different maximum deformation values  $S_{max}$  for dissipative devices were considered as target damage for IDA analyses: 70 mm and 120 mm.

For each performed analysis with recorded acceleration time histories from 2012 Emilia earthquakes on the three models *A*, *B* and *C* the following parameters have been collected: scaling factor required reaching target damage (70 or 120 mm), maximum base shear of the system with dissipative devices and maximum base shear of the equivalent elastic system, behaviour factor  $q$ .

IDA analyses results are reported in Table 7.2, Table 7.3 and Table 7.4, respectively for Model *A*, *B* and *C*.

<b>MODEL A</b>					
<b>TH-ID</b>		<b>20May-MRN</b>	<b>29May-MRN</b>	<b>29May-SAN0</b>	<b>29May-SMS0</b>
<b><math>S_{max}</math> 70 mm – no friction</b>					
<b><math>SF_1</math></b>		0.43	0.33	0.64	1.49
<b>Base Shear</b>	N	40082	39505	37859	45068
<b>Base Shear Elastic</b>	N	98004	67458	43768	77219
<b><math>q_1</math></b>		2.45	1.71	1.16	1.71
<b><math>S_{max}</math> 120 mm – no friction</b>					
<b><math>SF_2</math></b>		1.00	0.62	0.97	1.99
<b>Base Shear</b>	N	45637	48405	45359	44923
<b>Base Shear Elastic</b>	N	229356	128797	66706	102997
<b><math>q_2</math></b>		5.03	2.66	1.47	2.29
<b><math>SF_2/SF_1</math></b>	%	<b>134%</b>	<b>91%</b>	<b>52%</b>	<b>33%</b>
<b><math>q_2/q_1</math></b>	%	<b>106%</b>	<b>56%</b>	<b>27%</b>	<b>34%</b>

Table 7.2- IDA analyses results for Model A, 2012 Emilia records,  $S_{max}$  of 70 and 120 mm (no friction)

<b>MODEL B</b>					
<b>TH-ID</b>		<b>20May-MRN</b>	<b>29May-MRN</b>	<b>29May-SAN0</b>	<b>29May-SMS0</b>
<b><math>S_{max}</math> 70 mm – no friction</b>					
<b><math>SF_1</math></b>		0.52	0.49	0.96	2.12
<b>Base Shear</b>	N	85242	92522	86556	97853
<b>Base Shear Elastic</b>	N	180482	147749	95950	172229
<b><math>q_1</math></b>		2.12	1.60	1.11	1.76
<b><math>S_{max}</math> 120 mm – no friction</b>					
<b><math>SF_2</math></b>		0.77	0.59	1.17	2.83
<b>Base Shear</b>	N	100333	101665	95346	111595
<b>Base Shear Elastic</b>	N	267320	178537	116195	230040
<b><math>q_2</math></b>		2.66	1.76	1.22	2.06
<b><math>SF_2/SF_1</math></b>	%	<b>48%</b>	<b>21%</b>	<b>21%</b>	<b>34%</b>
<b><math>q_2/q_1</math></b>	%	<b>26%</b>	<b>10%</b>	<b>10%</b>	<b>17%</b>

Table 7.3- IDA analyses results for Model B, 2012 Emilia records,  $S_{max}$  of 70 and 120 mm (no friction)

<b>MODEL C</b>					
<b>TH-ID</b>		<b>20May-MRN</b>	<b>29May-MRN</b>	<b>29May-SAN0</b>	<b>29May-SMS0</b>
<b><math>S_{max}</math> 70 mm – no friction</b>					
<b><math>SF_1</math></b>		0.58	0.42	0.83	2.00
<b>Base Shear</b>	N	124125	127590	133526	139847
<b>Base Shear Elastic</b>	N	279734	261550	248178	215714
<b><math>q_1</math></b>		2.25	2.05	1.86	1.54
<b><math>S_{max}</math> 120 mm – no friction</b>					
<b><math>SF_2</math></b>		0.97	0.65	1.13	2.55
<b>Base Shear</b>	N	148731	140230	139306	153813
<b>Base Shear Elastic</b>	N	471270	407036	337114	274312
<b><math>q_2</math></b>		3.17	2.90	2.42	1.78
<b><math>SF_2/SF_1</math></b>	%	<b>68%</b>	<b>56%</b>	<b>36%</b>	<b>27%</b>
<b><math>q_2/q_1</math></b>	%	<b>41%</b>	<b>42%</b>	<b>30%</b>	<b>16%</b>

Table 7.4- IDA analyses results for Model C, 2012 Emilia records,  $S_{max}$  of 70 and 120 mm (no friction)

As expected, the scaling factor  $SF$  required in order to achieve the target damage increases for a target deformation of dissipative devices of 120 mm respect to 70 mm.

In all performed analyses the maximum value of base shear of the model reinforced with the devices is lower than the maximum value of base shear of the equivalent elastic model with hinges at the ends of the beam, proving the fuse effect of the devices.

The plastic behaviour of the force-deformation relationship of the devices permits to have a well-defined shear value at base joints of the column, much lower than the one of the scheme with hinged beam-column joints.

As an example, the following figures illustrate the results of the nonlinear dynamic analysis performed on the N-S acceleration time history recorded in the station of Mirandola (MRN)

during the 29<sup>th</sup> May earthquake, with the scaling factor required to reach a target device deformation of 70 mm for Model C.

Figure 7.1 shows IDA curve with scaling factor required to reach target damage, i.e. maximum deformation capacity of dissipative device.

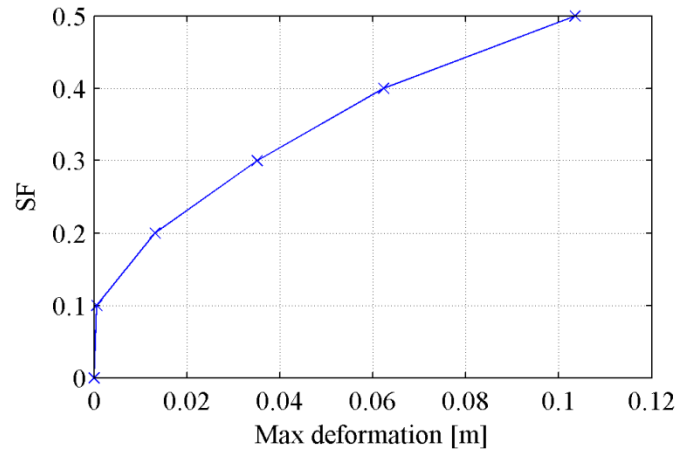


Figure 7.1- IDA curve (Model C - 29May-MRN record –  $S_{max}$  70 mm)

Comparing the results of dynamic analyses for the models with and without the dissipative devices allows to evaluate the effectiveness of the dissipation system. The difference in base shear values between the model with dissipative devices and the equivalent elastic system is shown in Figure 7.2.

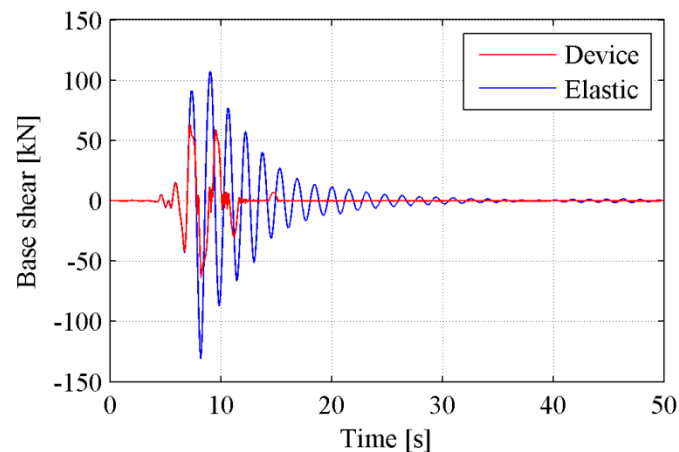


Figure 7.2- Base shear values for the system with dissipative devices and the equivalent elastic system (Model C - 29May-MRN record –  $S_{max}$  70 mm)

Figure 7.3 shows the relative beam-column displacement time history and forces on the dissipative devices. The deformation of the devices and consequently the relative beam-

column displacement takes place, as expected, only for the highest values of seismic acceleration.

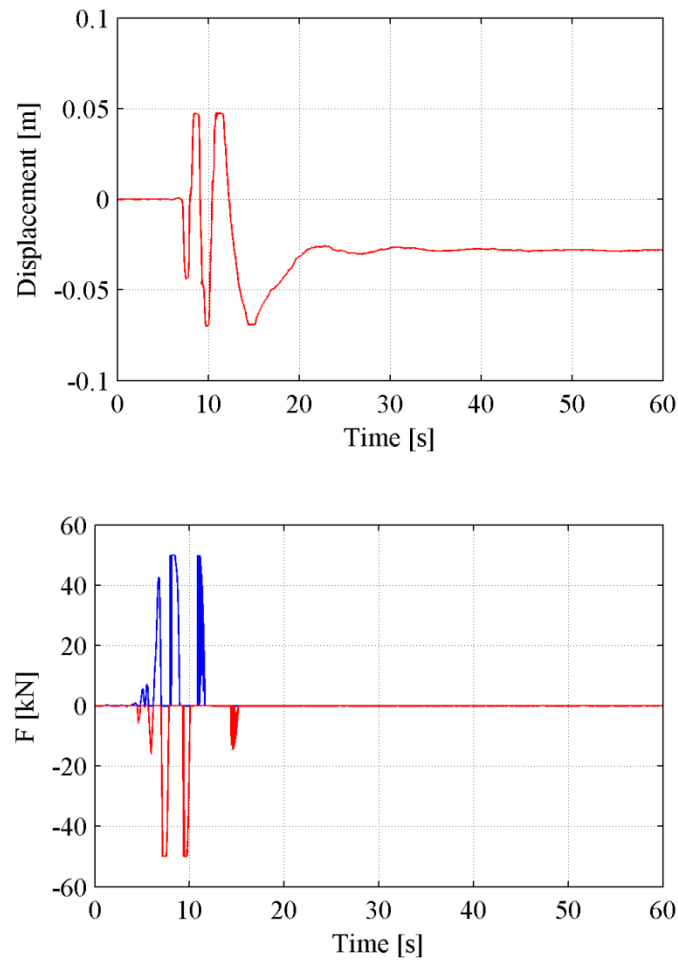


Figure 7.3- Relative beam-column displacement and forces on the dissipative devices (Model C - 29May-MRN record -  $S_{max}$  70 mm)

Figure 7.4 shows the hysteresis cycle of the dissipative devices.

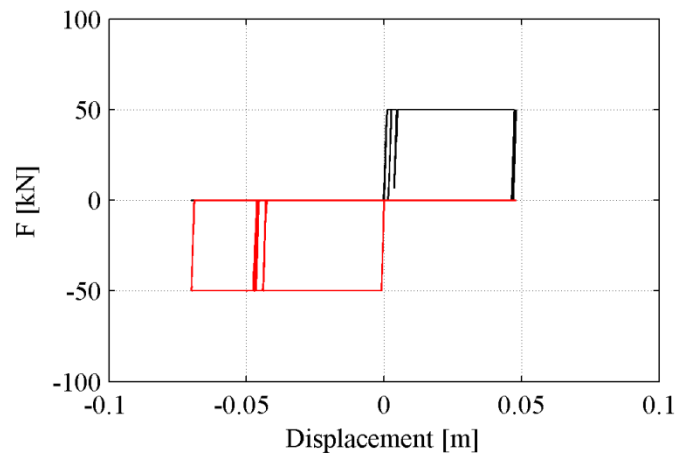


Figure 7.4- Hysteresis cycle of the dissipative devices (Model C - 29May-MRN record -  $S_{max}$  70 mm)

Table 7.5 shows behaviour factors, computed as the ratio between the maximum base shear value in the equivalent elastic system and the one in the system with dissipative devices, for each analysis performed to reach a target deformation of dissipative devices of 70 mm and 120 mm for Model A, B and C.

The behaviour factor for a target device deformation of 70 mm is indicated as  $q_1$ , the one for a target device deformation of 120 mm as  $q_2$ . The reduction of base shear values is significant: the range of behaviour factor  $q$  values is 1.16 – 2.45 for  $q_1$  and 1.22 - 5.03 for  $q_2$ .

As expected, behaviour factor  $q$  values increase for a target deformation of dissipative devices of 120 mm respect to 70 mm.

recorded acceleration time history	Model A		Model B		Model C	
	$q_1$	$q_2$	$q_1$	$q_2$	$q_1$	$q_2$
20May-MRN	2.45	5.03	2.12	2.66	2.25	3.17
29May-MRN	1.71	2.66	1.60	1.76	2.05	2.90
29May-SAN0	1.16	1.47	1.11	1.22	1.86	2.42
29May-SMS0	1.71	2.29	1.76	2.06	1.54	1.78
<b>mean values</b>	<b>1.76</b>	<b>2.86</b>	<b>1.65</b>	<b>1.93</b>	<b>1.93</b>	<b>2.57</b>

Table 7.5- Behaviour factor for target device deformation of 70 mm and 120 mm (no friction) for Model A, B and C

The behaviour factor  $q$  values listed in Table 7.5 are linked only to the effect of the introduction of the dissipative devices, since column in the models have a linear elastic behaviour.

### 7.1.2 IDA results - PEER database ground motions

Numerical investigation continued on structural models created with the software *OpenSees* considering as seismic input recorded acceleration time histories from *PEER* database.

As illustrated in Section 6.3, records of *PEER* database were selected in order to have three classes of motions belonging to three different Magnitude-Distance scenarios:

- Large Magnitude – Large Distance (35 ground motions);
- Large Magnitude – Small Distance (33 ground motions);
- Small Magnitude – Small Distance (29 ground motions).

The aim of the definition of three different Magnitude-Distance scenarios is to evaluate the dependence of dynamic behaviour of dissipative devices from the characteristics of the seismic input.

In the analyses carried out, only the horizontal component of acceleration was considered. These analyses were performed with beams simply supported on the column tops, both without introducing friction models and assuming a friction coefficient value of 0.05 for the beam-column joint.

A maximum deformation value  $S_{max}$  of 75 mm for dissipative devices was considered as target damage for IDA analyses.

For each performed analysis on the three models *A*, *B* and *C* the following parameters have been collected: scaling factor required to reach target damage (75 mm), maximum base shear of the system with dissipative devices and maximum base shear of the equivalent elastic system, behaviour factor  $q$ .

The behaviour factor  $q$  is computed as the ratio between the maximum base shear value in the equivalent elastic system and the one in the system with dissipative devices.

As an example, the following figures illustrate the results of the nonlinear dynamic analysis performed on Model *B*, considering TH-ID 7 acceleration time history of PEER database belonging to Small Magnitude – Small Distance scenario, with the scaling factor required to reach the target device deformation of 75 mm and with friction coefficient equal to 0.05.

Figure 7.5 shows IDA curve with scaling factor required to reach target damage, i.e. maximum deformation capacity of dissipative device.

Comparing the results of dynamic analyses for the models with and without the dissipative devices allows to evaluate the effectiveness of the dissipation system. The difference in base shear values between the model with dissipative devices and the equivalent elastic system is shown in Figure 7.6.

Figure 7.7 shows friction forces time history, while Figure 7.8 shows the relative beam-column displacement time history and forces on the dissipative devices. The deformation of the devices and consequently the relative beam-column displacement takes place, as expected, only for the highest values of seismic acceleration.

Figure 7.9 shows the hysteresis cycle of the dissipative devices.

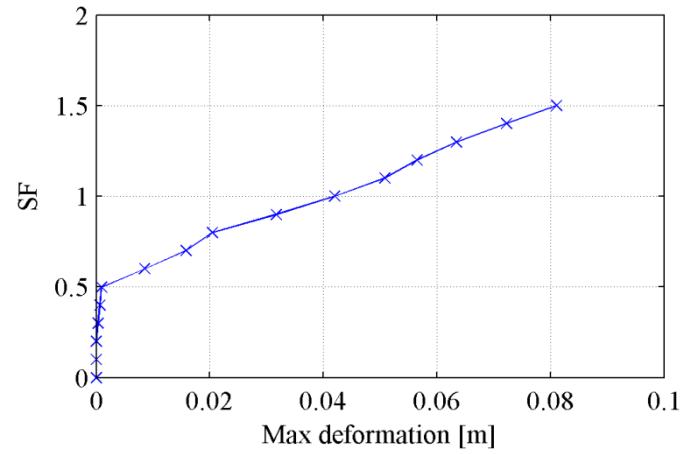


Figure 7.5- IDA curve (Model B – TH-ID 7 Large Magnitude – Large Distance scenario –friction 0.05 -  $S_{max}$  75 mm)

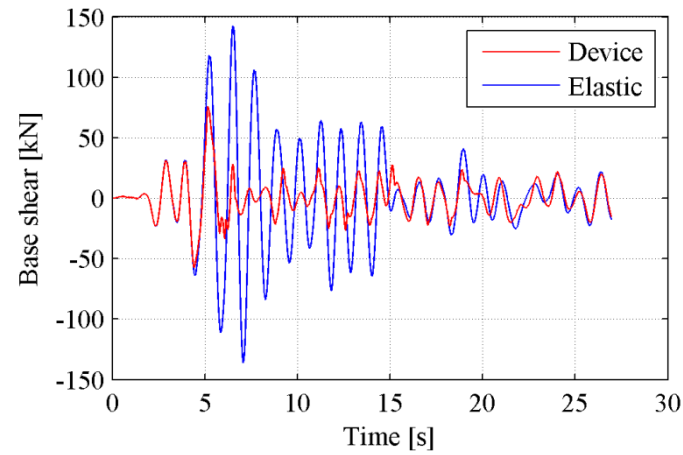


Figure 7.6- Base shear values for the system with dissipative devices and the equivalent elastic system (Model B – TH-ID 7 Large Magnitude – Large Distance scenario –friction 0.05 -  $S_{max}$  75 mm)

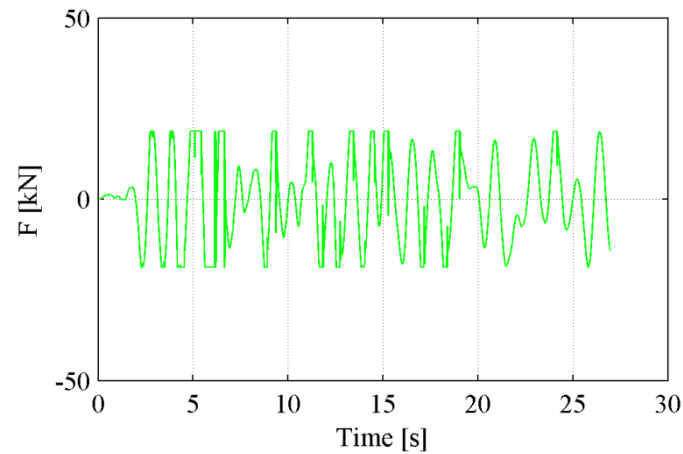


Figure 7.7- Beam-column friction forces (Model B – TH-ID 7 Large Magnitude – Large Distance scenario –friction 0.05 -  $S_{max}$  75 mm)

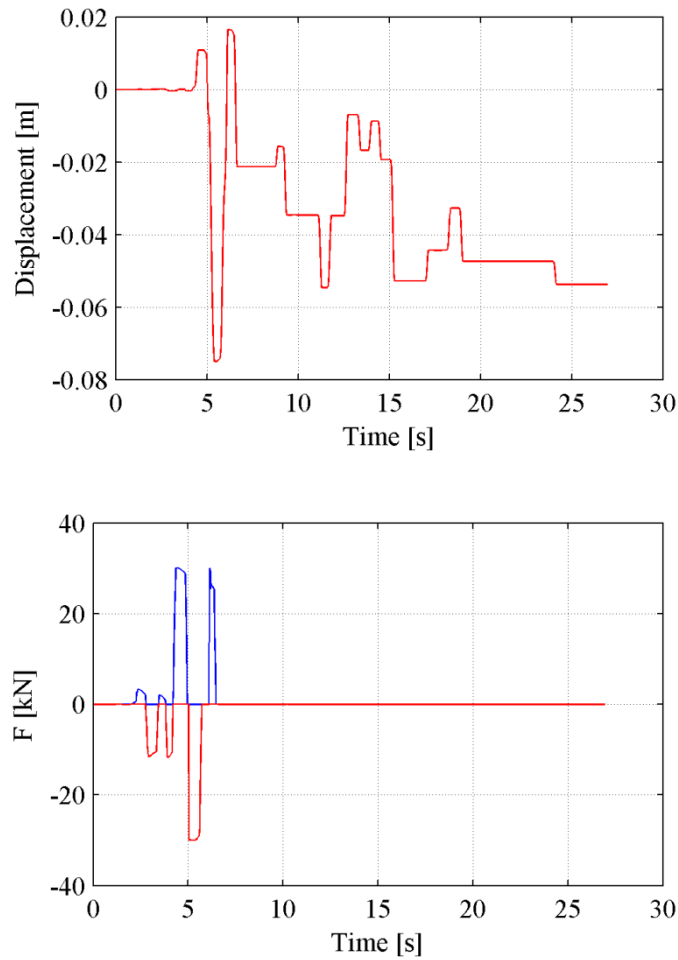


Figure 7.8- Relative beam-column displacement and forces on the dissipative devices (Model B – TH-ID 7 Large Magnitude – Large Distance scenario – friction 0.05 -  $S_{max}$  75 mm)

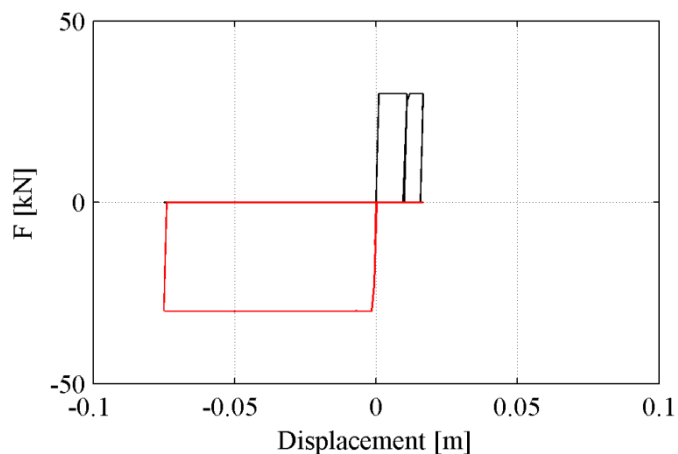


Figure 7.9- Hysteresis cycle of the dissipative devices (Model B – TH-ID 7 Large Magnitude – Large Distance scenario – friction 0.05 -  $S_{max}$  75 mm)

Table 7.6 shows mean values of the behaviour factor  $q$ , computed as the ratio between the maximum base shear value in the equivalent elastic system and the one in the system with dissipative devices, for analyses performed to reach a target deformation of 75 mm with

friction coefficient value equal to zero and 0.05 for Model A, B and C for the three different Magnitude-Distance scenarios. For each of the three different Magnitude-Distance scenarios mean values of behaviour factor  $q$  values reported in the table are also divided for impulsive ( $q_{imp}$ ) and non-impulsive ( $q_{noimp}$ ) ground motions.

Behaviour factor  $q$  values reported in the following Table 7.6 are mean values of a total of 582 IDA analyses performed.

Model	friction coefficient	MLarge-DLarge			MLarge-DSmall			MSmall-DSmall		
		$q_{tot}$	$q_{imp}$	$q_{noimp}$	$q_{tot}$	$q_{imp}$	$q_{noimp}$	$q_{tot}$	$q_{imp}$	$q_{noimp}$
A	0.05	<b>2.72</b>	3.46	2.65	<b>2.50</b>	2.20	2.67	<b>2.57</b>	1.96	2.73
	0	<b>2.93</b>	3.65	2.86	<b>2.97</b>	2.82	3.05	<b>3.33</b>	2.29	3.60
B	0.05	<b>2.22</b>	2.93	2.15	<b>2.13</b>	1.94	2.23	<b>2.30</b>	1.83	2.42
	0	<b>2.15</b>	2.31	2.14	<b>2.23</b>	2.06	2.33	<b>2.58</b>	2.09	2.71
C	0.05	<b>2.18</b>	1.74	2.22	<b>1.88</b>	1.83	1.91	<b>2.04</b>	1.86	2.08
	0	<b>2.28</b>	1.58	2.35	<b>2.12</b>	1.99	2.20	<b>2.36</b>	2.06	2.43

Table 7.6- Behaviour factor (mean values) for a target device deformation of 75 mm for three different Magnitude-Distance scenarios for Model A, B and C

Findings of analyses show that behaviour factor  $q$  values are not dependent from the Magnitude-Distance scenario and from the impulsivity of ground motion.

As for previous analyses, the behaviour factor  $q$  values listed in Table 7.6 are linked only to the effect of the introduction of the dissipative devices, since column in the model have a linear elastic behaviour.

In structural models in which inelastic deformation in the column are allowed we expect to find a larger behaviour factor.

As expected, the scaling factor required in order to achieve the target damage increases considering a friction coefficient value of 0.05, respect to not introducing friction.

In all performed analyses the maximum value of base shear of the model reinforced with the devices is lower than the maximum value of base shear of the equivalent elastic model with hinges at the ends of the beam, proving the fuse effect of the devices.

The plastic behaviour of the force-deformation relationship of the devices permits to have a well-defined shear value at base joints of the column, much lower than the one of the scheme with hinged beam-column joints.

Some considerations on how friction mechanisms influence the behaviour factor of the structure are made in the following:

- if friction coefficient increases, maximum base shear value in the system with dissipative devices increases because the contribution of friction beam-column forces is added to column shear.

This contribution would determine lower behaviour factor  $q$  values, but on the other side:

- if friction coefficient increases, also the scaling factor required in order to achieve the target deformation of dissipative devices increases, determining an higher maximum base shear value of the equivalent elastic system.

This aspect would determine higher behaviour factor  $q$  values.

Generally, in analyses with column performing linear elastic behaviour, the first effect is prevailing, so behaviour factor  $q$  values generally increase not considering friction in beam-column joints.

Finally, the behaviour factor  $q$  values resulting from performed analyses were plotted versus peak ground displacement ( $PGD$ ), peak ground velocity ( $PGV$ ), peak ground acceleration ( $PGA$ ) and Arias Intensity ( $I_A$ ) for each of the three different Magnitude-Distance scenarios in order to evaluate the dependence of dynamic behaviour of dissipative devices from the characteristics of the seismic input.

As an example, the following figures (Figure 7.10 - Figure 7.13) illustrate behaviour factor  $q$  values plotted versus  $PGD$ ,  $PGV$ ,  $PGA$  and  $I_A$  for Model A, friction coefficient of 0.05, Large Magnitude – Large Distance scenario.

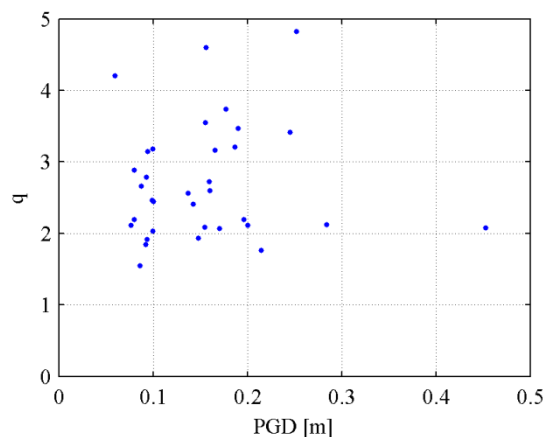


Figure 7.10- Behaviour factor  $q$  versus  $PGD$  (Model A, Large Magnitude – Large Distance scenario)

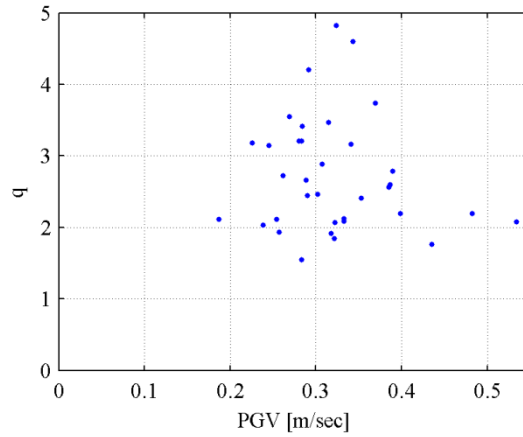


Figure 7.11- Behaviour factor  $q$  versus PGV (Model A, Large Magnitude – Large Distance scenario)

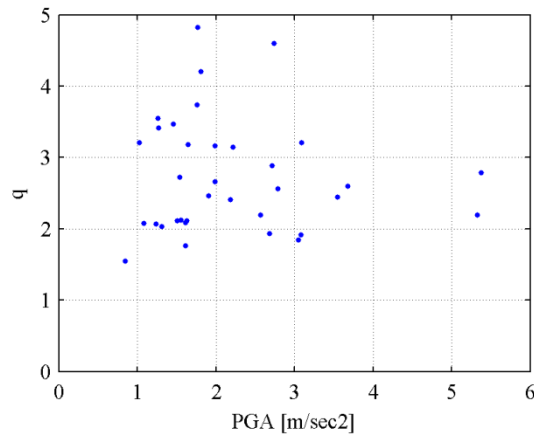


Figure 7.12- Behaviour factor  $q$  versus PGA (Model A, Large Magnitude – Large Distance scenario)

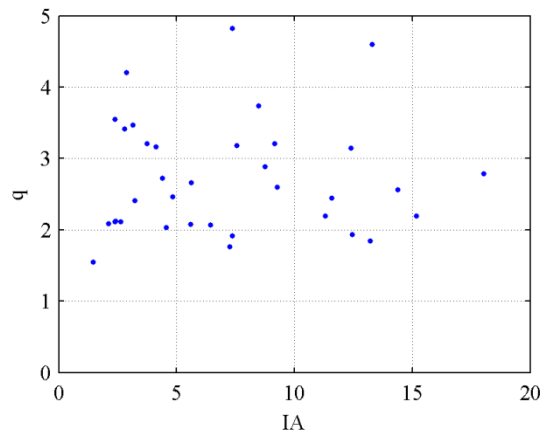


Figure 7.13- Behaviour factor  $q$  versus  $I_A$  (Model A, Large Magnitude – Large Distance scenario)

Findings of analyses show that behaviour factor  $q$  values are not dependent from the characteristics of ground motions considered above:  $PGD$ ,  $PGV$ ,  $PGA$  and  $I_A$ .

## 7.2 Columns performing nonlinear behaviour

If the target damage for IDA analyses is the ultimate chord rotation at the base of the columns in order to take into account also the inelastic resources of the structure, columns perform a nonlinear behaviour.

The aim of these analyses is to evaluate the equivalent behaviour factor for structures equipped with the dissipative devices.

As introduced above, the value of the equivalent force of plasticization  $F_{eq}$  of the device is designed as the maximum value of force that, added to friction forces, can be transferred to the top of the column before reaching the yield moment at its base. This choice is made in order to have columns performing linear elastic behaviour until the devices have not reached their maximum deformation capacity. The value of the equivalent force of plasticization  $F_{eq}$  of the device is equal to 10, 20 and 30 kN, respectively for Model A, B and C. The first branch of the trilinear model of force-deformation relationship of the devices has a stiffness of 20, 20 and 30 kN/mm, respectively for Model A, B and C.

The following Table 7.7 resumes main parameters of the three models used in *OpenSees* for analyses performing nonlinear behaviour of columns. Ultimate capacity, ductility and dissipative characteristics of the three models are also reported.

		Model A	Model B	Model C
Span Length $L$	m	12	20	25
Column Height $H$	m	8	7	6
Column Section	m	0.5 x 0.5	0.5 x 0.5	0.5 x 0.5
Beam Section	m	0.3 x 1.1	0.3 x 1.1	0.3 x 1.1
Total Beam Load (dead + variable)	kN/m	41.58	38.25	56.25
Total Joint Load (dead +variable)	kN	249	383	703
Device $F_{eq}$	kN	10	20	30
Friction coefficient	-	0.05	0.05	0.05
Friction Force	kN	12	19	35
Moment for First Yield $M_y$	kNm	300	393	535
Ultimate Moment $M_u$	kNm	348	464	682
First Yielding Force $F_y$	kN	38	56	89
Ultimate Force $F_u$	kN	43	66	114
First Yielding Chord Rotation $\theta_y$	%	1.72	1.57	1.49
Ultimate Chord Rotation $\theta_u$	%	4.49	4.16	4.80

Table 7.7- Parameters of Model A, B and C with columns performing nonlinear behaviour

The fundamental period of vibration  $T_1$  of the structural models is equal to 2.04, 1.80 and 1.71 seconds, respectively for Model A, B and C (flexural stiffness of cracked sections was considered as described in Section 6.5).

### ***7.2.1 IDA results – PEER database ground motions***

In this section further numerical investigations on structural models with columns performing nonlinear behaviour, varying maximum deformation capacity  $S_{max}$  of dissipative devices, are presented. As introduced above, analyses presented in this section have been performed taking into account inelastic response of columns.

The aim of these analyses is to evaluate the dependence of the behaviour factor of the structure with dissipative connections from maximum deformation capacity  $S_{max}$  of dissipative devices.

Analyses have been performed considering as seismic input recorded acceleration time histories of PEER database, with records of Large Magnitude – Small Distance scenario (33 ground motions).

In the analyses carried out, only the horizontal component of acceleration was considered.

A friction coefficient value of 0.05 was considered for beam-column joints.

Concerning maximum deformation value  $S_{max}$  for dissipative devices, five different values were considered: 25, 50, 75, 100 and 125 mm.

Two different values of chord rotation  $\theta_u$  for columns were considered as target damage for IDA analyses: 3% and 4.5%.

For each performed analysis on the three models A, B and C with dissipative connections the following parameters have been collected: scaling factor required to reach target damage (3% or 4.5% chord rotation), maximum total base shear ( $F_{u,col}$ ) of the system with dissipative devices at target damage and maximum total base shear ( $T_{el,col+dev}$ ) of the equivalent elastic system, behaviour factor  $q_{col+dev}$ .

The behaviour factor  $q_{col+dev}$  is computed as the ratio between the maximum total base shear ( $T_{el,col+dev}$ ) in the equivalent elastic system and the one in the system with nonlinear behaviour of columns and dissipative connections ( $F_{u,col}$ ).

As an example, in the following Table 7.8 parameters collected for each of the 990 IDA analyses performed on systems with dissipative connections are reported for the 33 IDA

analyses performed on Model A with a target chord rotation of 4.5% and maximum deformation capacity of dissipative devices  $S_{max}$  of 75 mm.

A complete report of results of the 990 IDA analyses performed on systems with dissipative connections is provided in Appendix A, where all parameters collected are listed in different tables.

<b>TH-ID</b>	<b><math>q_{col+dev}</math></b>	<b><math>F_{u,col}</math> [N]</b>	<b><math>T_{el,col+dev}</math> [N]</b>	<b><math>SF_{col+dev}</math></b>
1	4.02	69563	279420	2.34
2	3.50	69498	243272	0.99
3	2.30	69586	160013	1.69
4	4.22	69599	293392	1.04
5	5.04	69603	350654	3.84
6	2.96	69566	205784	0.74
7	2.79	69584	194368	0.81
8	3.77	69637	262688	2.28
9	3.59	69488	249346	2.28
10	2.37	69637	165267	3.24
11	3.36	69594	234144	4.49
12	3.83	69621	266354	0.63
13	3.67	69579	255454	2.80
14	3.12	69539	216880	0.63
15	3.33	69608	231908	1.11
16	3.88	69488	269392	0.81
17	2.85	69585	198419	0.98
18	2.73	69529	189494	1.55
19	2.12	69624	147743	0.85
20	3.26	69658	227264	2.48
21	3.46	69515	240646	0.87
22	4.33	69591	301484	0.94
23	4.50	69632	313310	0.91
24	4.25	69581	295844	1.47
25	5.42	69629	377188	1.90
26	2.14	69632	148870	1.17
27	6.34	69577	441142	0.77
28	4.12	69579	286840	0.67
29	3.94	69571	274248	1.16
30	6.63	69568	461548	2.90
31	5.18	69578	360128	1.51
32	5.68	69587	395214	3.54
33	3.28	69622	228408	0.73
<b>mean</b>	<b>3.82</b>	<b>69583</b>	<b>265640</b>	<b>1.64</b>

Table 7.8- IDA results for Model A, target column chord rotation 4.5%,  $S_{max}$  75 mm

As an example, the following figures illustrate the results of the nonlinear dynamic analysis performed on Model A, considering *TH-ID 1* acceleration time history of PEER database belonging to Large Magnitude – Small Distance scenario, with the scaling factor required to reach a target column chord rotation of 4.5 % with maximum deformation capacity of dissipative devices of 75 mm.

Figure 7.14 shows IDA curve with scaling factor required to reach target damage, i.e. ultimate column chord rotation. Observing IDA curves for the system with dissipative devices it is possible to notice a discontinuity in the curve, with scale factor values increasing in correspondence of almost the same value of column chord rotation (see red dashed lines in Figure 7.14). This trend of IDA curves identifies the range of working of dissipative devices and highlights their positive effects in terms of seismic protection of columns, postponing the achievement of ultimate capacity of columns. As expected, this trend of IDA curves is more evident for higher values of maximum deformation capacity of dissipative devices.

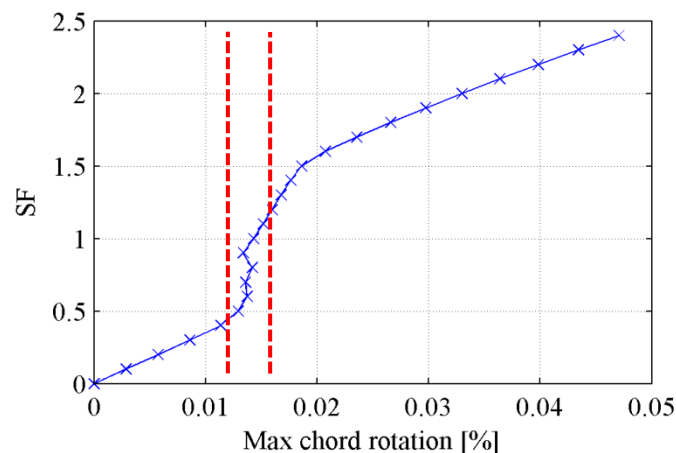


Figure 7.14- IDA curve (Model A – *TH-ID 1* -  $S_{max}$  75 mm – column chord rotation 4.5%)

Comparing the results of dynamic analyses for the models with dissipative devices and equivalent elastic systems allows to evaluate the effectiveness of the dissipation system. The difference in base shear values between the model with dissipative devices and the equivalent elastic system is shown in Figure 7.15.

Figure 7.16 shows the relative beam-column displacement time history. The deformation of the devices and consequently the relative beam-column displacement takes place, as expected, only for the highest values of seismic acceleration.

Figure 7.17 shows friction forces time history, Figure 7.18 the moment-curvature relation at column base while Figure 7.19 shows the hysteresis cycle of the dissipative devices.

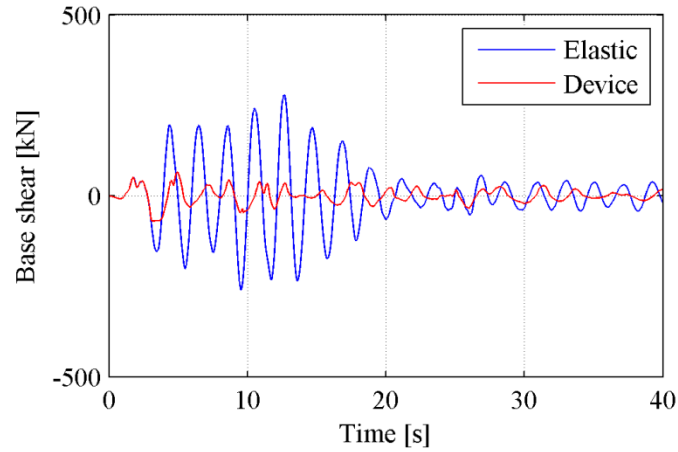


Figure 7.15- Base shear values for the system with dissipative devices and the equivalent elastic system (Model A – TH-ID 1 -  $S_{max}$  75 mm – column chord rotation 4.5%)

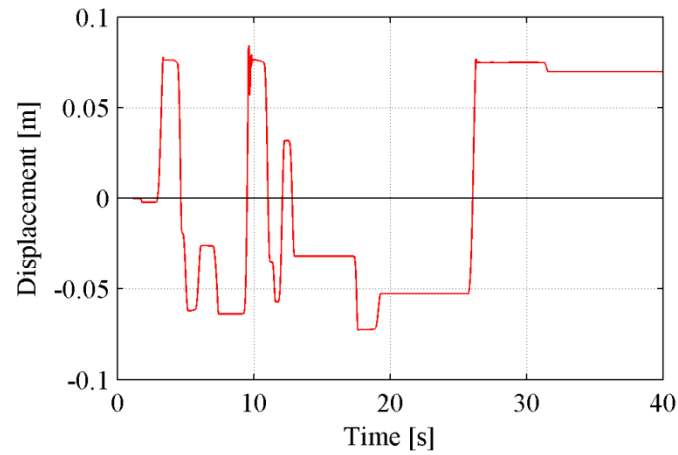


Figure 7.16- Relative beam-column displacement (Model A – TH-ID 1 -  $S_{max}$  75 mm – column chord rotation 4.5%)

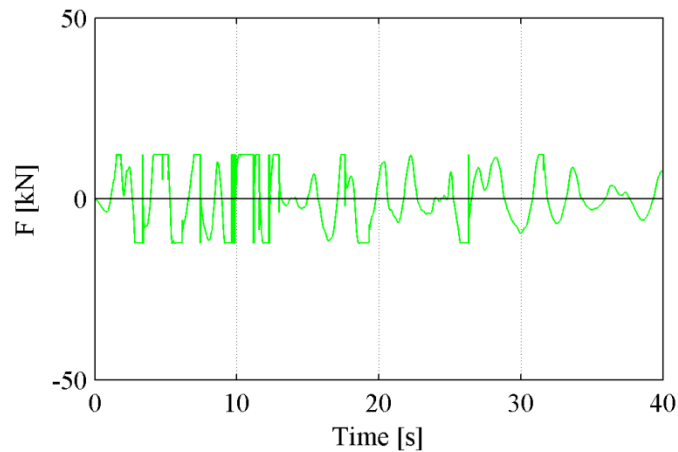


Figure 7.17- Beam-column friction forces (Model A – TH-ID 1 -  $S_{max}$  75 mm – column chord rotation 4.5%)

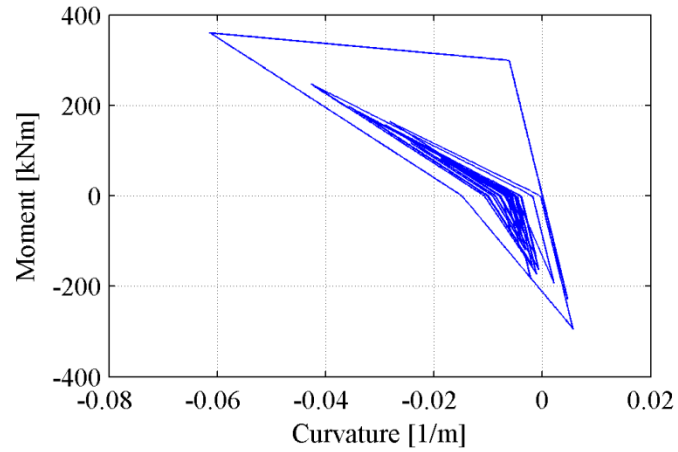


Figure 7.18- Moment-curvature relation of column (Model A – TH-ID 1 -  $S_{max}$  75 mm – column chord rotation 4.5%)

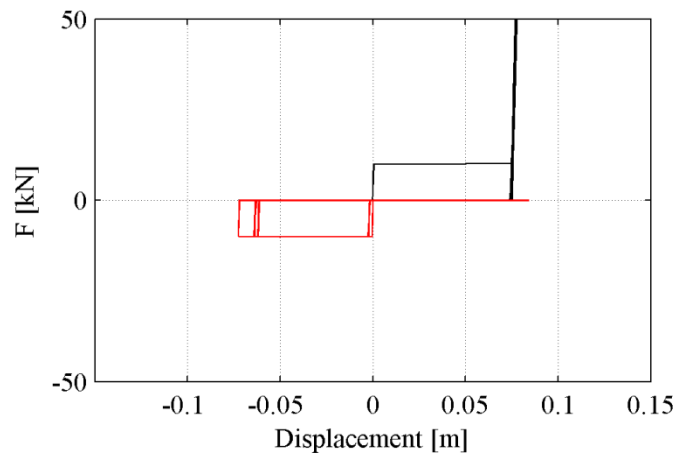


Figure 7.19- Hysteresis cycle of the dissipative devices (Model A – TH-ID 1 -  $S_{max}$  75 mm – column chord rotation 4.5%)

Table 7.9 resumes mean values of the behaviour factor  $q_{col+dev}$  for analyses performed on Model A, B and C considering the 33 ground motions of Large Magnitude – Small Distance scenario to reach the target chord rotation of columns (3% or 4.5%), with friction coefficient equal to 0.05 and considering 5 different maximum deformation values  $S_{max}$  for dissipative devices from 25 mm to 125 mm.

Each value listed in the table is the mean of 33 IDA analyses for a total of 990 IDA analyses performed (see Appendix A for a detailed review of results).

Model	Target damage (column chord rotation)	$q_{col+dev}$				
		$S_{max}$				
		25 mm	50 mm	75 mm	100 mm	125 mm
A	3%	2.32	2.68	2.92	3.07	3.26
	4.5%	3.25	3.57	3.82	4.05	4.28
B	3%	2.51	2.86	3.20	3.44	3.67
	4.5%	3.46	3.81	4.10	4.36	4.64
C	3%	2.72	3.10	3.49	3.78	4.06
	4.5%	3.66	4.02	4.35	4.70	5.06

Table 7.9- Behaviour factor (mean values) for different maximum device deformation capacities and target column chord rotation for Model A, B and C

The behaviour factor  $q_{col+dev}$  is due both to the effect of dissipative devices and to plastic hinges developing at the base of the columns.

As expected, behaviour factor  $q_{col+dev}$  values are higher for a target column chord rotation of 4.5% respect to 3%.

As expected, behaviour factor  $q_{col+dev}$  values increase increasing maximum deformation capacity of dissipative devices from 25 mm to 125 mm.

### 7.2.2 Comparison between dissipative and hinged connections

IDA analyses were performed then on the same models with nonlinear column behaviour, but with hinged connections, i.e. without dissipative devices in beam-column joints. The same seismic input and the same values of target columns chord rotation were considered.

For each performed analysis on the three models A, B and C with hinged connections the following parameters have been collected: scaling factor required to reach target damage (3% or 4.5% chord rotation), maximum total base shear ( $F_{u,col}$ ) of the system with hinged connections at target damage and maximum total base shear ( $T_{el,col}$ ) of the equivalent elastic system, behaviour factor  $q_{col}$ .

The behaviour factor  $q_{col}$  is computed as the ratio between the maximum total base shear ( $T_{el,col}$ ) in the equivalent elastic system and the one in the system with nonlinear behaviour of columns and hinged connections ( $F_{u,col}$ ).

As an example, in the following Table 7.10 parameters collected for each of the 198 IDA analyses performed on system with hinged connections are reported for the 33 IDA analyses

performed on Model A with a target chord rotation of 4.5%. A complete report of results of the 198 IDA analyses performed on systems with hinged connections is provided in Appendix A, where all parameters collected are listed in different tables.

<i>TH-ID</i>	$q_{col}$	$F_{u,col} [N]$	$T_{el,col} [N]$	$SF_{col}$
1	3.60	69585	250472	2.10
2	3.04	69488	211564	0.86
3	2.21	69620	153911	1.62
4	3.05	69479	211810	0.75
5	3.84	69502	266564	2.92
6	2.13	69632	148194	0.54
7	2.14	69597	149273	0.62
8	2.15	69563	149661	1.30
9	3.14	69621	218886	2.00
10	2.20	69512	152807	2.99
11	2.51	69508	174600	3.35
12	2.68	69583	186458	0.44
13	2.56	69576	178301	1.95
14	2.17	69649	150913	0.44
15	2.29	69647	159242	0.76
16	3.40	69486	236526	0.72
17	2.62	69458	182210	0.90
18	2.30	69555	159718	1.31
19	1.99	69651	138631	0.80
20	2.17	69549	151133	1.65
21	2.98	69628	207544	0.75
22	2.64	69548	183553	0.57
23	3.75	69640	260900	0.76
24	3.03	69475	210206	1.05
25	4.73	69497	328910	1.65
26	1.79	69585	124761	0.98
27	6.20	69605	431378	0.75
28	2.89	69557	201254	0.47
29	2.62	69579	182172	0.77
30	4.29	69533	298612	1.87
31	3.15	69598	218962	0.92
32	3.74	69521	259908	2.33
33	2.29	69540	159416	0.51
<b>mean</b>	<b>2.92</b>	<b>69563</b>	<b>202983</b>	<b>1.25</b>

Table 7.10- IDA results for Model A with hinged connections, target column chord rotation 4.5%

Table 7.11 resumes mean values of the behaviour factor  $q_{col}$  for analyses performed on Model A, B and C with hinged connections considering the 33 ground motions of Large Magnitude – Small Distance scenario to reach the target chord rotation of columns (3% or 4.5%), with friction coefficient equal to 0.05.

Each value listed in the table is the mean of 33 IDA analyses for a total of 198 IDA analyses performed (see Appendix A for a detailed review of results).

Model	Target damage (column chord rotation)	$q_{col}$
A	3%	1.94
	4.5%	2.92
B	3%	2.05
	4.5%	3.07
C	3%	2.14
	4.5%	3.23

*Table 7.11- Behaviour factor (mean values) for different target column chord rotation for Model A, B and C with hinged connections*

Maximum total base shear value of the system with dissipative devices at target damage is equal to maximum total base shear value of the system with hinged connections at target damage, because they both coincide to the ultimate base shear ( $F_{u,col}$ ) for the considered value of column chord rotation, depending only on the force-deformation relationship of columns.

The behaviour factor  $q_{col}$  is only linked to the development of plastic hinges at the base of the columns, while the behaviour factor  $q_{col+dev}$  is due both to the effect of dissipative devices and to plastic hinges developing at the base of the columns. The difference between the two behaviour factor values  $q_{col+dev}$  and  $q_{col}$  is due to the contribution of dissipative devices.

The same contribution of the devices can be evaluated also from the difference between the scaling factor required to reach the same target damage of column chord rotation in the system with dissipative connections and in the one with hinged connections, and consequently between the two values of maximum total base shear  $T_{el,col}$  and  $T_{el,col+dev}$  of the equivalent elastic systems.

A comparison between results of IDA analyses for the systems with hinged and dissipative beam-column connections was made in order to evaluate only the contribution of the devices in terms of behaviour factor of the structure.

As an example, in Table 7.12 a comparison of parameters collected for each of the 1188 IDA analyses performed on systems with dissipative and hinged connections is reported for the 33 IDA analyses performed on Model A with a target chord rotation of 4.5% with dissipative connections (maximum deformation capacity of dissipative devices  $S_{max}$  of 75 mm) and hinged connections.

A complete report of results of the 1188 IDA analyses performed (990 IDA analyses on systems with dissipative connections, 198 IDA analyses on systems with hinged connections) is provided in Appendix A, where all parameters collected are listed in different tables, comparing systems with dissipative and hinged connections.

To reach the same target damage of column chord rotation in the system with dissipative devices in beam-column connections, it is necessary to use a scaling factor for acceleration records higher than in the system with hinged beam-column connections. Consequently the behaviour factor, computed as the ratio between the maximum base shear in the equivalent elastic system and the one in the system with nonlinear behaviour of columns, for the system with dissipative connections ( $q_{col+dev}$ ) is higher than for the system with hinged connections ( $q_{col}$ ).

## 7. EVALUATION OF BEHAVIOUR FACTOR USING IDA

TH-ID	Dissipative connections				Hinged connections				Comparison	
	$q_{col+dev}$	$F_{u,col}$ [N]	$T_{el,col+dev}$ [N]	$SF_{col+dev}$	$q_{col}$	$F_{u,col}$ [N]	$T_{el,col}$ [N]	$SF_{col}$	$\frac{SF_{col+dev}}{SF_{col}}$	$\frac{q_{col+dev}}{q_{col}}$
1	4.02	69563	279420	2.34	3.60	69585	250472	2.10	12%	1.12
2	3.50	69498	243272	0.99	3.04	69488	211564	0.86	15%	1.15
3	2.30	69586	160013	1.69	2.21	69620	153911	1.62	4%	1.04
4	4.22	69599	293392	1.04	3.05	69479	211810	0.75	39%	1.38
5	5.04	69603	350654	3.84	3.84	69502	266564	2.92	32%	1.31
6	2.96	69566	205784	0.74	2.13	69632	148194	0.54	39%	1.39
7	2.79	69584	194368	0.81	2.14	69597	149273	0.62	30%	1.30
8	3.77	69637	262688	2.28	2.15	69563	149661	1.30	76%	1.75
9	3.59	69488	249346	2.28	3.14	69621	218886	2.00	14%	1.14
10	2.37	69637	165267	3.24	2.20	69512	152807	2.99	8%	1.08
11	3.36	69594	234144	4.49	2.51	69508	174600	3.35	34%	1.34
12	3.83	69621	266354	0.63	2.68	69583	186458	0.44	43%	1.43
13	3.67	69579	255454	2.80	2.56	69576	178301	1.95	43%	1.43
14	3.12	69539	216880	0.63	2.17	69649	150913	0.44	44%	1.44
15	3.33	69608	231908	1.11	2.29	69647	159242	0.76	46%	1.46
16	3.88	69488	269392	0.81	3.40	69486	236526	0.72	14%	1.14
17	2.85	69585	198419	0.98	2.62	69458	182210	0.90	9%	1.09
18	2.73	69529	189494	1.55	2.30	69555	159718	1.31	19%	1.19
19	2.12	69624	147743	0.85	1.99	69651	138631	0.80	7%	1.07
20	3.26	69658	227264	2.48	2.17	69549	151133	1.65	50%	1.50
21	3.46	69515	240646	0.87	2.98	69628	207544	0.75	16%	1.16
22	4.33	69591	301484	0.94	2.64	69548	183553	0.57	64%	1.64
23	4.50	69632	313310	0.91	3.75	69640	260900	0.76	20%	1.20
24	4.25	69581	295844	1.47	3.03	69475	210206	1.05	41%	1.41
25	5.42	69629	377188	1.90	4.73	69497	328910	1.65	15%	1.14
26	2.14	69632	148870	1.17	1.79	69585	124761	0.98	19%	1.19
27	6.34	69577	441142	0.77	6.20	69605	431378	0.75	2%	1.02
28	4.12	69579	286840	0.67	2.89	69557	201254	0.47	43%	1.42
29	3.94	69571	274248	1.16	2.62	69579	182172	0.77	51%	1.51
30	6.63	69568	461548	2.90	4.29	69533	298612	1.87	55%	1.54
31	5.18	69578	360128	1.51	3.15	69598	218962	0.92	64%	1.65
32	5.68	69587	395214	3.54	3.74	69521	259908	2.33	52%	1.52
33	3.28	69622	228408	0.73	2.29	69540	159416	0.51	43%	1.43
<b>mean</b>	<b>3.82</b>	<b>69583</b>	<b>265640</b>	<b>1.64</b>	<b>2.92</b>	<b>69563</b>	<b>202983</b>	<b>1.25</b>	<b>32%</b>	<b>1.32</b>

Table 7.12- Comparison between IDA results for Model A, target column chord rotation of 4.5% with dissipative connections ( $S_{max}$  75 mm) and hinged connections

The difference in scaling factor and behaviour factor values between dissipative and hinged systems depends on the maximum deformation capacity  $S_{max}$  of the dissipative devices according to a linear rule, as shown in following Table 7.13 and Table 7.14.

Table 7.13 and Table 7.14 report the increase in mean values of the behaviour factor  $q_{col+dev}$  respect to  $q_{col}$  values due to the introduction of dissipative devices for analyses performed on Model A, B and C respectively to reach a target column chord rotation of 3% and 4.5% for different maximum device deformation values  $S_{max}$  considered.

Each value listed in the table is the mean of 33 IDA analyses for a total of 1188 different IDA analyses performed (see Appendix A for a detailed review of results).

Model	IDA results	column chord rotation 3%				
		$S_{max}$				
		25 mm	50 mm	75 mm	100 mm	125 mm
A	$q_{col+dev}$	2.32	2.68	2.92	3.07	3.26
	$q_{col}$	1.94	1.94	1.94	1.94	1.94
	$q_{col+dev} / q_{col} [\%]$	19%	37%	50%	58%	67%
B	$q_{col+dev}$	2.51	2.86	3.20	3.44	3.67
	$q_{col}$	2.05	2.05	2.05	2.05	2.05
	$q_{col+dev} / q_{col} [\%]$	22%	39%	55%	67%	78%
C	$q_{col+dev}$	2.72	3.10	3.49	3.78	4.06
	$q_{col}$	2.14	2.14	2.14	2.14	2.14
	$q_{col+dev} / q_{col} [\%]$	26%	45%	63%	76%	89%

Table 7.13- Difference in behaviour factor values between dissipative and hinged connections for Model A, B and C for different maximum device deformation values  $S_{max}$  for target column chord rotation of 3%

Model	IDA results	column chord rotation 4.5%				
		$S_{max}$				
		25 mm	50 mm	75 mm	100 mm	125 mm
A	$q_{col+dev}$	3.25	3.57	3.82	4.05	4.28
	$q_{col}$	2.92	2.92	2.92	2.92	2.92
	$q_{col+dev} / q_{col} [\%]$	12%	23%	32%	40%	48%
B	$q_{col+dev}$	3.46	3.81	4.10	4.36	4.64
	$q_{col}$	3.07	3.07	3.07	3.07	3.07
	$q_{col+dev} / q_{col} [\%]$	13%	25%	34%	42%	51%
C	$q_{col+dev}$	3.66	4.02	4.35	4.70	5.06
	$q_{col}$	3.23	3.23	3.23	3.23	3.23
	$q_{col+dev} / q_{col} [\%]$	14%	26%	36%	47%	58%

Table 7.14- Difference in behaviour factor values between dissipative and hinged connections for Model A, B and C for different maximum device deformation values  $S_{max}$  for target column chord rotation of 4.5%

Finally, further analyses were performed in order to evaluate the dependence of behaviour factor values for structures equipped with the dissipative devices on the equivalent force of plasticization value  $F_{eq}$  of dissipative devices. Findings of analyses performed varying  $F_{eq}$  values showed how the influence of  $F_{eq}$  value of dissipative device is negligible if columns perform linear elastic behaviour until the devices reach their maximum deformation capacity and target damage for IDA analyses is ultimate chord rotation of columns.

In the following section a simplified approach to compute an equivalent behaviour factor for a structure with dissipative beam-column connections is proposed.

### **7.3 Simplified approach for behaviour factor evaluation**

As introduced in previous sections, the proposed design criterion for the dissipative connection is to choose a force of activation for the dissipative devices lower than capacity of existing columns, in order to have columns performing linear elastic behaviour until the devices have not reached their maximum deformation capacity. For this reason, the value of the equivalent force of plasticization  $F_{eq}$  of the device is designed as the maximum value of force that, added to friction forces, can be transferred to the top of the column before reaching the yield moment at its base.

With the hypothesis that  $F_{eq} < F_{y,col}$ , until the dissipative devices have not reached their maximum deformation capacity columns perform linear elastic behaviour.

A simplified approach to evaluate an equivalent behaviour factor for a structure equipped with dissipative devices in friction-based beam-column joints is proposed and compared with results of IDA analyses performed. The following considerations refer to force-displacement relationships for elastic and inelastic response of the system shown in Figure 7.20.

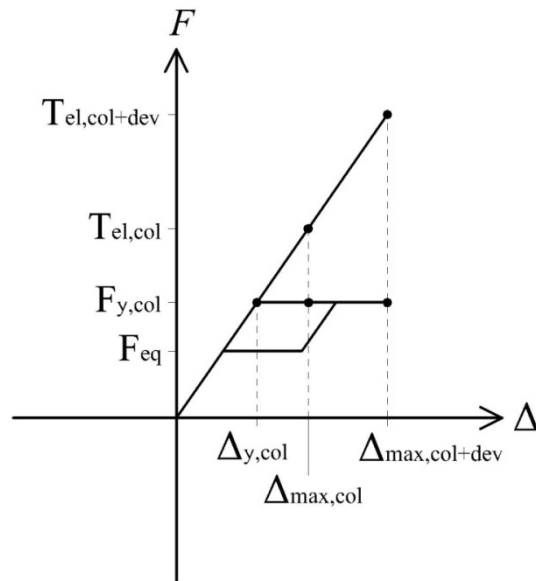


Figure 7.20- Force-displacement relation for elastic and inelastic response of the systems with and without dissipative connections

Main parameters introduced in Figure 7.20 are:

$T_{el,col}$	maximum force developed at peak displacement for equivalent elastic system of the structure without dissipative devices (hinged connections)
$T_{el,col+dev}$	maximum force developed at peak displacement for equivalent elastic system of the structure equipped with dissipative devices
$F_{y,col}$	column maximum force developed at first yielding and at peak displacement for inelastic response of the structure
$\Delta_{max,col}$	maximum displacement of the structure without dissipative devices (hinged connections)
$\Delta_{max,col+dev}$	maximum displacement of the structure equipped with dissipative devices
$\Delta_{y,col}$	column first yielding displacement
$F_{eq}$	equivalent force of plasticization of the dissipative device

For each performed analysis on the three models *A*, *B* and *C*, the maximum column displacement value  $\Delta_{max,col}$  for the equivalent elastic system of the structure with hinged connections and the maximum column displacement value  $\Delta_{max,col+dev}$  for the equivalent elastic system of the structure with dissipative devices have been calculated as follows, basing on equal displacement approximation:

$$\Delta_{max,col} = \frac{T_{el,col}}{2 \cdot K_{col}}$$

$$\Delta_{\max, col+dev} = \frac{T_{el, col+dev}}{2 \cdot K_{col}}$$

with column stiffness  $K_{col}$  computed as:

$$K_{col} = 3 \cdot \frac{E_c \cdot J_{col}}{H^3}$$

with

- $E_c$  concrete elastic modulus  
 $J_{col}$  area moment of inertia of the column  
 $E_c \cdot J_{col}$  flexural stiffness of cracked section of columns  
 $H$  column height

For each performed analysis on the three models *A*, *B* and *C*, the difference between the maximum column displacement  $\Delta_{\max, col+dev}$  for the equivalent elastic system of the structure with dissipative devices and the maximum column displacement  $\Delta_{\max, col}$  for the equivalent elastic system of the structure with hinged connections has been calculated.

Mean values of  $\Delta_{\max, col+dev} - \Delta_{\max, col}$  for each performed analysis are close, not exactly coincident probably because of equal displacement approximation, to the maximum deformation capacity  $S_{\max}$  of the dissipative device considered in the analysis, as reported in following Table 7.15 and Table 7.16.

Model	Displacement	column chord rotation 3%				
		$S_{\max}$				
		25 mm	50 mm	75 mm	100 mm	125 mm
<b>A</b>	$\Delta_{\max, col+dev} [m]$	0.31	0.36	0.39	0.41	0.44
	$\Delta_{\max, col} [m]$	0.26	0.26	0.26	0.26	0.26
	$\Delta_{\max, col+dev} - \Delta_{\max, col} [m]$	0.050	0.099	0.131	0.151	0.176
<b>B</b>	$\Delta_{\max, col+dev} [m]$	0.27	0.31	0.34	0.37	0.40
	$\Delta_{\max, col} [m]$	0.22	0.22	0.22	0.22	0.22
	$\Delta_{\max, col+dev} - \Delta_{\max, col} [m]$	0.049	0.087	0.124	0.150	0.174
<b>C</b>	$\Delta_{\max, col+dev} [m]$	0.24	0.27	0.30	0.33	0.35
	$\Delta_{\max, col} [m]$	0.19	0.19	0.19	0.19	0.19
	$\Delta_{\max, col+dev} - \Delta_{\max, col} [m]$	0.050	0.084	0.117	0.143	0.167

*Table 7.15- Difference in maximum displacement values between the equivalent elastic systems of the structure with dissipative and hinged connections for Model A, B and C for different maximum device deformation values  $S_{\max}$  for target column chord rotation of 3%*

Model	Displacement	column chord rotation 4.5%				
		$S_{max}$				
		25 mm	50 mm	75 mm	100 mm	125 mm
A	$\Delta_{max,col+dev} [m]$	0.44	0.48	0.51	0.54	0.57
	$\Delta_{max,col} [m]$	0.39	0.39	0.39	0.39	0.39
	$\Delta_{max,col+dev} - \Delta_{max,col} [m]$	0.045	0.088	0.121	0.152	0.183
B	$\Delta_{max,col+dev} [m]$	0.38	0.41	0.45	0.47	0.50
	$\Delta_{max,col} [m]$	0.33	0.33	0.33	0.33	0.33
	$\Delta_{max,col+dev} - \Delta_{max,col} [m]$	0.042	0.080	0.112	0.139	0.170
C	$\Delta_{max,col+dev} [m]$	0.32	0.35	0.38	0.41	0.44
	$\Delta_{max,col} [m]$	0.28	0.28	0.28	0.28	0.28
	$\Delta_{max,col+dev} - \Delta_{max,col} [m]$	0.038	0.070	0.099	0.129	0.161

Table 7.16- Difference in maximum displacement values between the equivalent elastic systems of the structure with dissipative and hinged connections for Model A, B and C for different maximum device deformation values  $S_{max}$  for target column chord rotation of 4.5%

Therefore, assuming the maximum displacement of the structure equipped with dissipative devices  $\Delta_{max,col+dev}$  as the sum of ultimate column displacement  $\Delta_{max,col}$  and the maximum deformation capacity of the dissipative device  $S_{max}$ :

$$\Delta_{max,col+dev} = \Delta_{max,col} + S_{max}$$

$$\frac{T_{el,col}}{\Delta_{max,col}} = \frac{T_{el,col+dev}}{\Delta_{max,col+dev}}$$

$$T_{el,col+dev} = T_{el,col} \cdot \frac{\Delta_{max,col+dev}}{\Delta_{max,col}} = T_{el,col} \cdot \left( 1 + \frac{S_{max}}{\Delta_{max,col}} \right)$$

For the equal displacement approximation, the displacement ductility factor is equal to the force reduction factor:

$$q_{col} = \frac{\Delta_{max,col}}{\Delta_{y,col}} = \frac{T_{el,col}}{F_{y,col}}$$

$$q_{col+dev}^* = \frac{\Delta_{max,col+dev}}{\Delta_{y,col}} = \frac{T_{el,col+dev}}{F_{y,col}}$$

Therefore:

$$q_{col+dev}^* = \frac{T_{el,col+dev}}{F_{y,col}} = \frac{T_{el,col}}{F_{y,col}} \cdot \left( 1 + \frac{S_{max}}{\Delta_{max,col}} \right) = q_{col} \cdot \left( 1 + \frac{S_{max}}{\Delta_{max,col}} \right)$$

with

$T_{el,col}$	maximum force developed at peak displacement for equivalent elastic system of the structure without dissipative devices (hinged connections)
$T_{el,col+dev}$	maximum force developed at peak displacement for equivalent elastic system of the structure equipped with dissipative devices
$F_{y,col}$	column maximum force developed at first yielding and at peak displacement for inelastic response of the structure
$\Delta_{max,col}$	maximum displacement of the structure without dissipative devices (hinged connections)
$\Delta_{max,col+dev}$	maximum displacement of the structure equipped with dissipative devices
$\Delta_{y,col}$	column first yielding displacement
$F_{eq}$	equivalent force of plasticization of the dissipative device
$S_{max}$	maximum deformation capacity of the dissipative device

The simplified formula proposed above was verified by comparing behaviour factor  $q_{col+dev}^*$  values computed using the simplified formula with behaviour factor  $q_{col+dev}$  values found as results of IDA analyses (Section 7.2.1), as resumed in following Table 7.17 and Table 7.18.

Model	Behaviour factor	column chord rotation 3%				
		$S_{max}$				
		25 mm	50 mm	75 mm	100 mm	125 mm
A	$q_{col+dev}^*$	2.13	2.32	2.50	2.69	2.88
	$q_{col+dev}$	2.32	2.68	2.92	3.07	3.26
	$q_{col+dev}^* / q_{col} [\%]$	10%	20%	30%	40%	49%
	$q_{col+dev} / q_{col} [\%]$	19%	37%	50%	58%	67%
B	$q_{col+dev}^*$	2.28	2.52	2.75	2.98	3.21
	$q_{col+dev}$	2.51	2.86	3.20	3.44	3.67
	$q_{col+dev}^* / q_{col} [\%]$	12%	23%	35%	47%	58%
	$q_{col+dev} / q_{col} [\%]$	22%	39%	55%	67%	78%
C	$q_{col+dev}^*$	2.43	2.71	3.00	3.29	3.58
	$q_{col+dev}$	2.72	3.10	3.49	3.78	4.06
	$q_{col+dev}^* / q_{col} [\%]$	14%	28%	41%	55%	69%
	$q_{col+dev} / q_{col} [\%]$	26%	45%	63%	76%	89%

Table 7.17- Comparison between behaviour factor values computed using the simplified formula and found as results of IDA analyses for Model A, B and C for different maximum device deformation values  $S_{max}$  for target column chord rotation of 3%

Model	Behaviour factor	column chord rotation 4.5%				
		$S_{max}$				
		25 mm	50 mm	75 mm	100 mm	125 mm
A	$q^*_{col+dev}$	3.10	3.29	3.48	3.66	3.85
	$q_{col+dev}$	3.25	3.57	3.82	4.05	4.28
	$q^*_{col+dev} / q_{col} [\%]$	7%	14%	21%	28%	34%
	$q_{col+dev} / q_{col} [\%]$	12%	23%	32%	40%	48%
B	$q^*_{col+dev}$	3.30	3.53	3.77	4.00	4.23
	$q_{col+dev}$	3.46	3.81	4.10	4.36	4.64
	$q^*_{col+dev} / q_{col} [\%]$	8%	16%	24%	32%	40%
	$q_{col+dev} / q_{col} [\%]$	13%	25%	34%	42%	52%
C	$q^*_{col+dev}$	3.51	3.79	4.08	4.36	4.65
	$q_{col+dev}$	3.66	4.02	4.35	4.70	5.06
	$q^*_{col+dev} / q_{col} [\%]$	9%	19%	28%	38%	47%
	$q_{col+dev} / q_{col} [\%]$	14%	26%	36%	47%	58%

Table 7.18- Comparison between behaviour factor values computed using the simplified formula and found as results of IDA analyses for Model A, B and C for different maximum device deformation values  $S_{max}$  for target column chord rotation of 4.5%

For each model and for different target column chord rotation values, the ratio between behaviour factor values  $q_{col+dev}$  and  $q_{col}$  found as results of IDA analyses considering different maximum deformation capacities  $S_{max}$  of the dissipative device was plotted. The ratio between behaviour factor values  $q_{col+dev}$  and  $q_{col}$  permits to evaluate the contribution due to the introduction of dissipative devices.

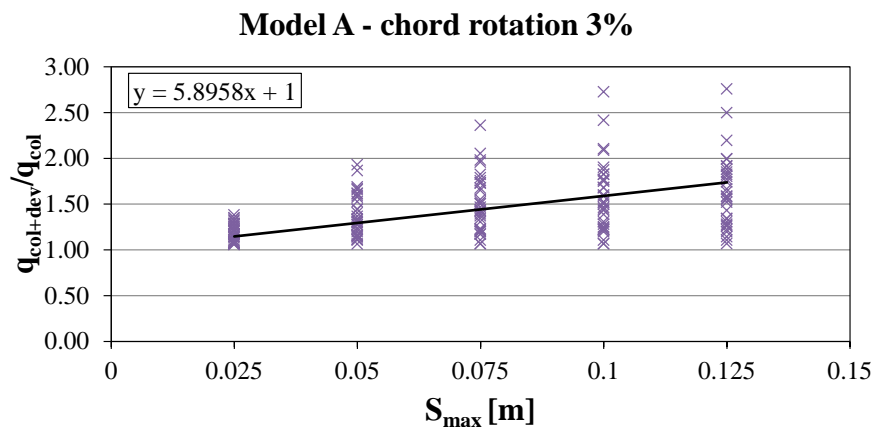


Figure 7.21- Ratio between behaviour factor values resulting from IDA analyses for the systems with dissipative and hinged connections for different maximum device deformation values  $S_{max}$  for Model A and a target column chord rotation of 3%

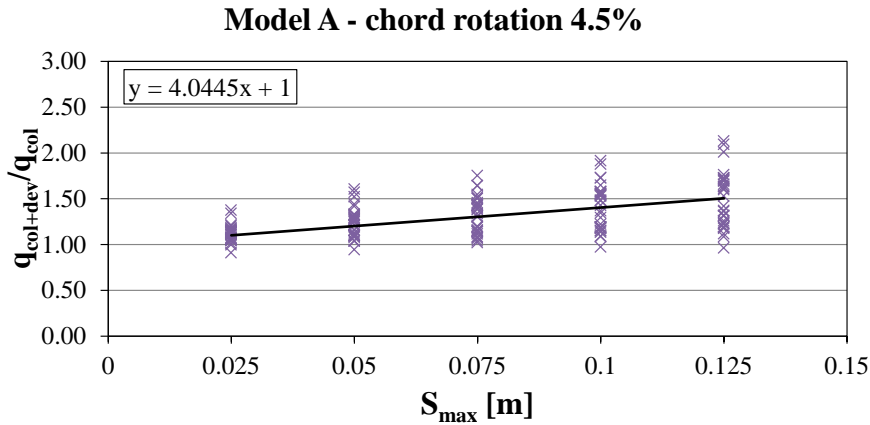


Figure 7.22- Ratio between behaviour factor values resulting from IDA analyses for the systems with dissipative and hinged connections for different maximum device deformation values  $S_{max}$  for Model A and a target column chord rotation of 4.5%

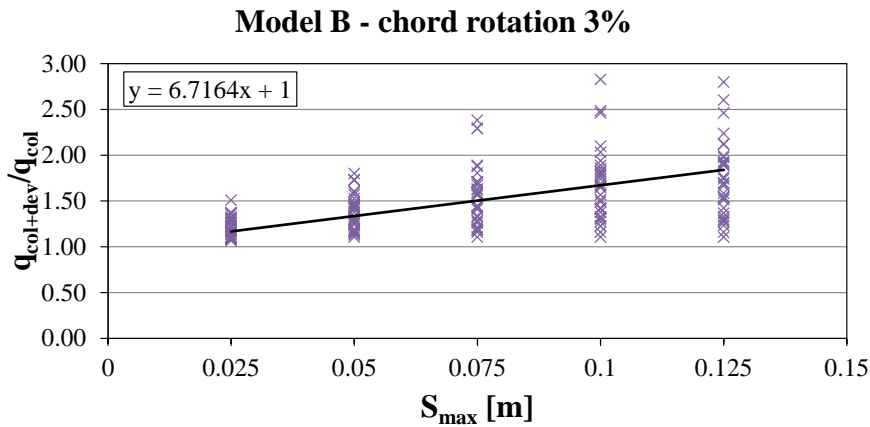


Figure 7.23- Ratio between behaviour factor values resulting from IDA analyses for the systems with dissipative and hinged connections for different maximum device deformation values  $S_{max}$  for Model B and a target column chord rotation of 3%

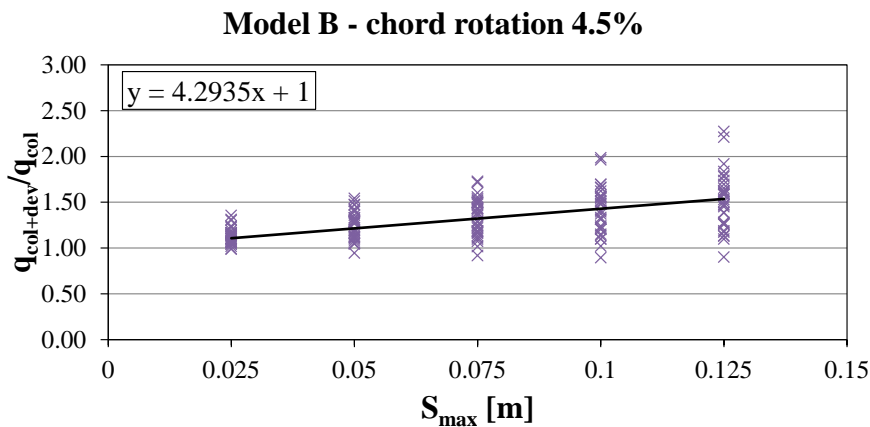


Figure 7.24- Ratio between behaviour factor values resulting from IDA analyses for the systems with dissipative and hinged connections for different maximum device deformation values  $S_{max}$  for Model B and a target column chord rotation of 4.5%

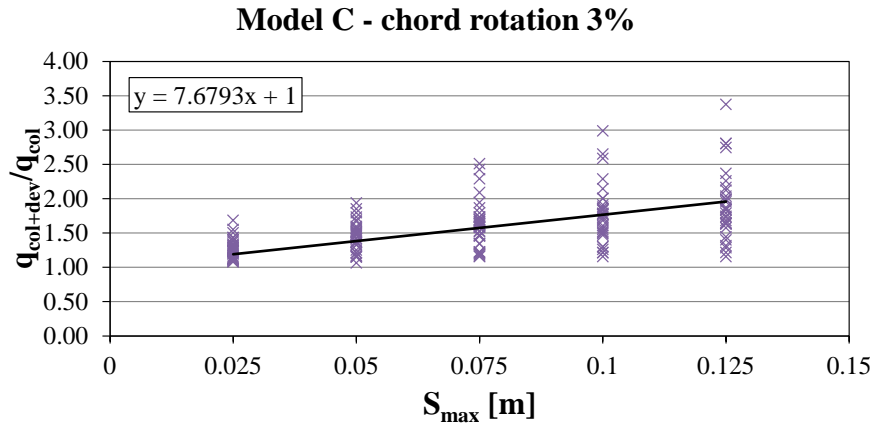


Figure 7.25- Ratio between behaviour factor values resulting from IDA analyses for the systems with dissipative and hinged connections for different maximum device deformation values  $S_{max}$  for Model C and a target column chord rotation of 3%

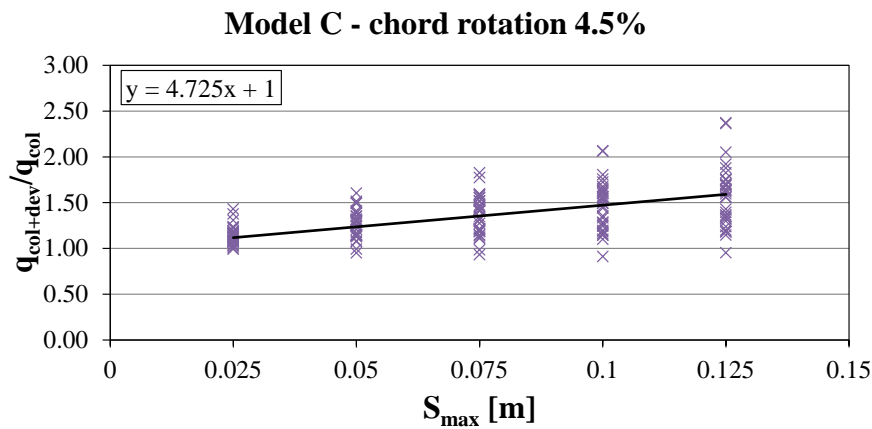


Figure 7.26- Ratio between behaviour factor values resulting from IDA analyses for the systems with dissipative and hinged connections for different maximum device deformation values  $S_{max}$  for Model C and a target column chord rotation of 4.5%

For each graph, a linear trend line using the method of least squares was calculated and compared with the ratio between behaviour factor values  $q_{col+dev}^*$  and  $q_{col}$  calculated using the simplified formula proposed above:

$$q_{col+dev}^* = q_{col} \cdot \left( 1 + \frac{S_{max}}{\Delta_{max,col}} \right)$$

Therefore, considering the ratio between behaviour factor values  $q_{col+dev}^*$  and  $q_{col}$ :

$$\frac{q_{col+dev}^*}{q_{col}} = 1 + \frac{S_{max}}{\Delta_{max,col}}$$

The comparison between the equation of the linear trend line of  $\frac{q_{col+dev}}{q_{col}}$  values resulting from

IDA analyses and the simplified formula shows a good approximation, as highlighted in the following.

In order to have a good approximation, in trend line equation, i.e.  $y = 5.9x + 1$  for Model A – column chord rotation 3%, the factor that multiplies the  $x$  value of  $S_{max}$  should be close to the

factor  $\frac{1}{\Delta_{max,col}}$  of the simplified formula, i.e.  $\frac{1}{0.26} = 3.85$  for Model A – column chord

rotation 3%.

The following Table 7.19 resumes the comparison between these factors, assuming  $x = S_{max}$

and  $y = \frac{q_{col+dev}}{q_{col}}$ .

	Model A		Model B		Model C	
	Chord rotation 3%	Chord rotation 4.5%	Chord rotation 3%	Chord rotation 4.5%	Chord rotation 3%	Chord rotation 4.5%
<b>Trend line equation</b>	$y=1+5.90x$	$y=1+4.04x$	$y=1+6.71x$	$y=1+4.29x$	$y=1+7.68x$	$y=1+4.73x$
<b>Simplified equation</b>	$y=1+3.85x$	$y=1+2.56x$	$y=1+4.55x$	$y=1+3.03x$	$y=1+5.26x$	$y=1+3.57x$

*Table 7.19- Comparison between trend line equation of IDA analyses results and simplified formula proposed for Model A, B and C for target column chord rotation of 3 and 4.5%*

In following figures behaviour factor  $q_{col+dev}$  (IDA analyses results) and  $q_{col+dev}^*$  (simplified approach) values, corresponding to different maximum deformation capacities  $S_{max}$  of the dissipative device, were plotted in the same graph for each model and for each target column chord rotation value.

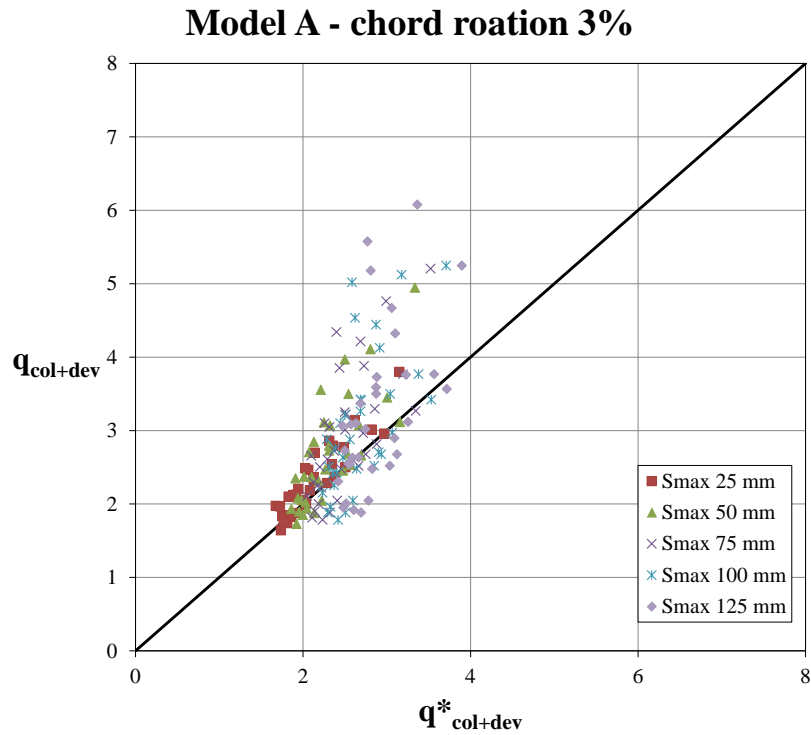


Figure 7.27- Comparison between behaviour factor values resulting from IDA analyses and calculated with the simplified approach for different maximum device deformation values  $S_{max}$  for Model A and a target column chord rotation of 3%

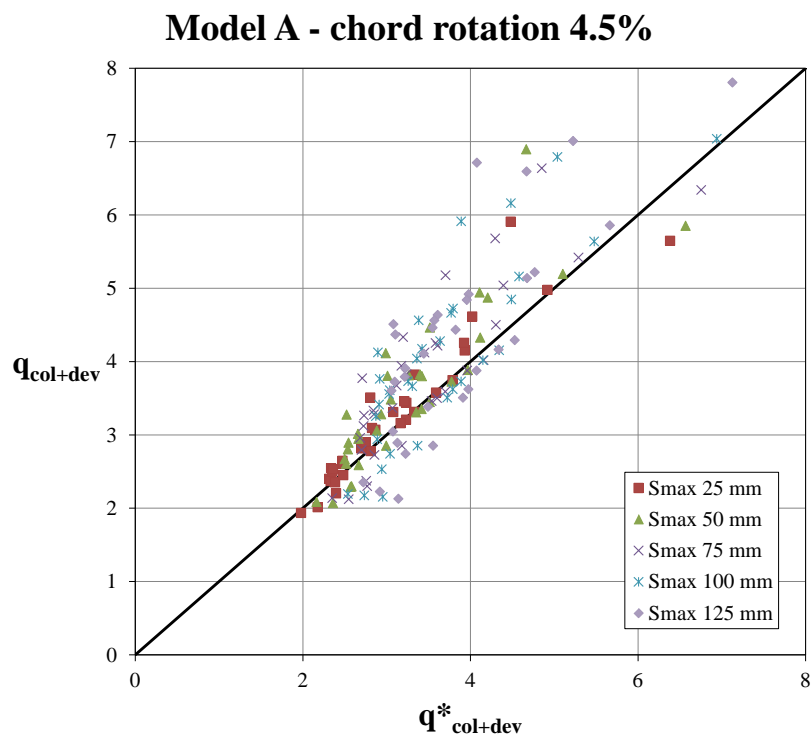


Figure 7.28- Comparison between behaviour factor values resulting from IDA analyses and calculated with the simplified approach for different maximum device deformation values  $S_{max}$  for Model A and a target column chord rotation of 4.5%

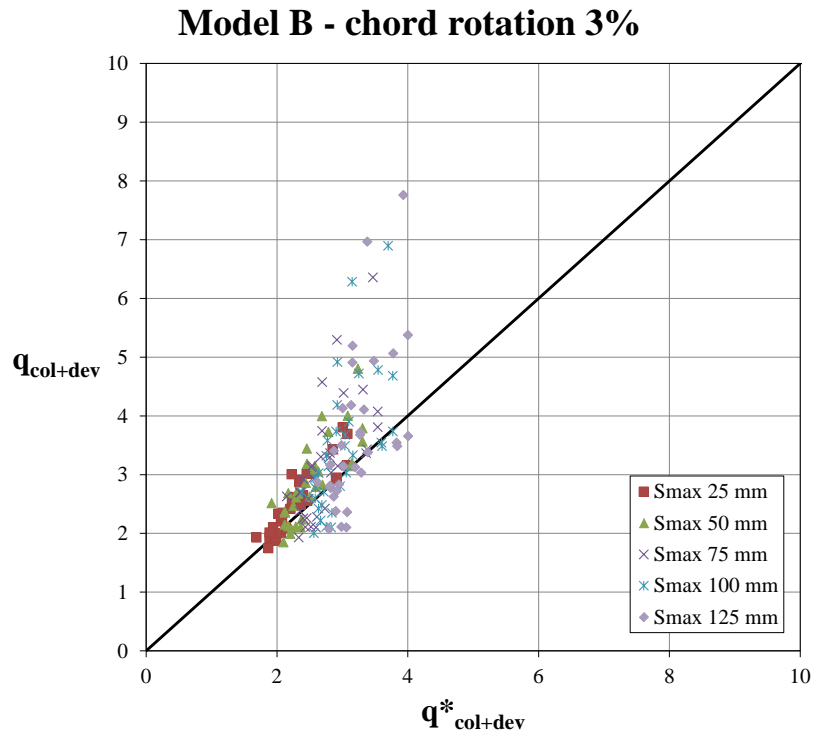


Figure 7.29- Comparison between behaviour factor values resulting from IDA analyses and calculated with the simplified approach for different maximum device deformation values  $S_{max}$  for Model B and a target column chord rotation of 3%

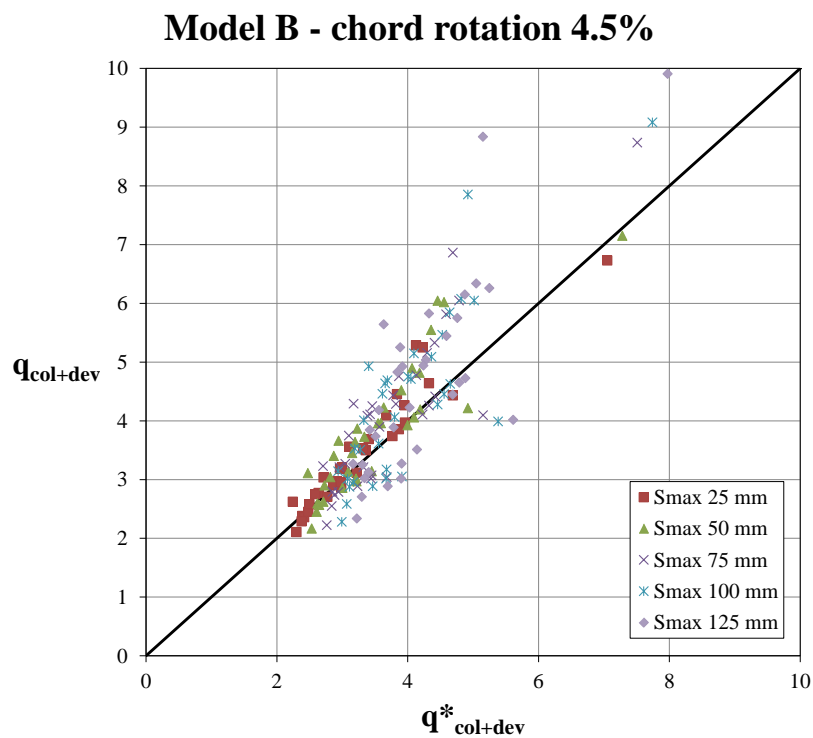


Figure 7.30- Comparison between behaviour factor values resulting from IDA analyses and calculated with the simplified approach for different maximum device deformation values  $S_{max}$  for Model B and a target column chord rotation of 4.5%

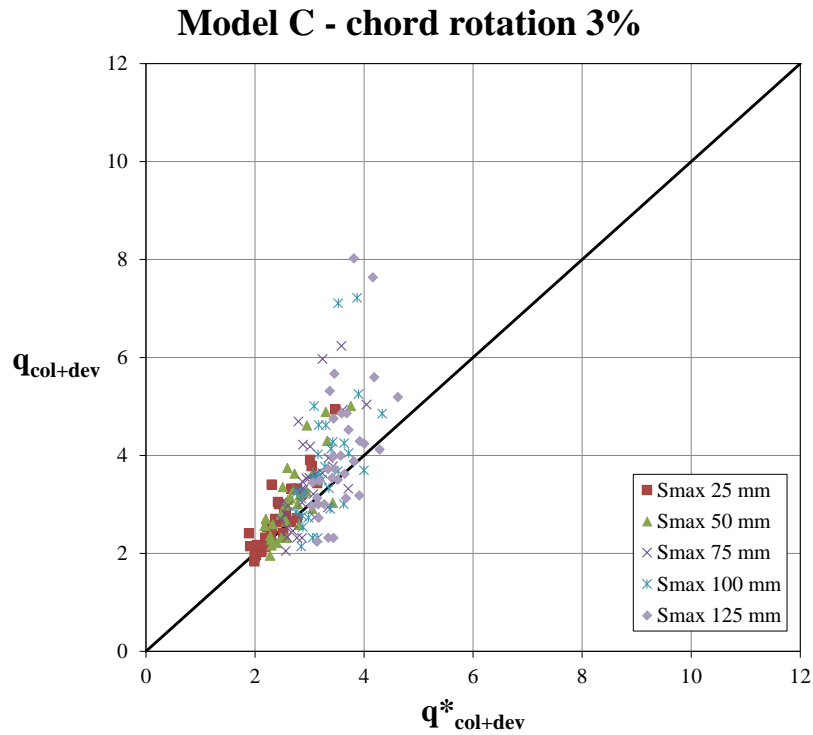


Figure 7.31- Comparison between behaviour factor values resulting from IDA analyses and calculated with the simplified approach for different maximum device deformation values  $S_{max}$  for Model C and a target column chord rotation of 3%

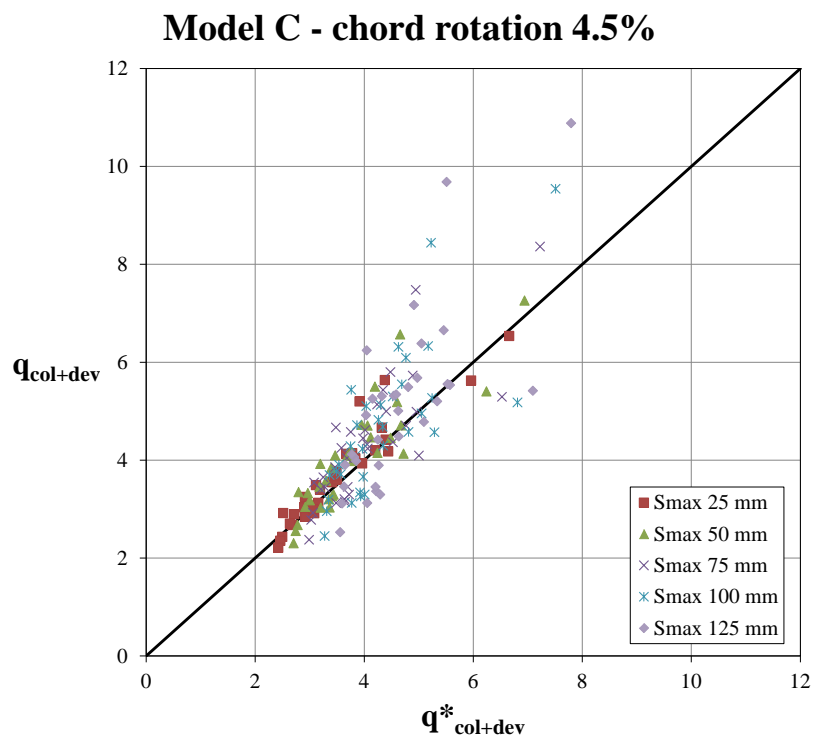


Figure 7.32- Comparison between behaviour factor values resulting from IDA analyses and calculated with the simplified approach for different maximum device deformation values  $S_{max}$  for Model C and a target column chord rotation of 4.5%

Figures show how behaviour factor  $q_{col+dev}^*$  values calculated with the simplified formula proposed well approximate behaviour factor  $q_{col+dev}$  values calculated with IDA analyses.

The approximation is particular good for behaviour factor values of systems with dissipative connections with maximum device deformation capacity  $S_{max}$  in the range 25 mm to 75 mm.

The difference between behaviour factor values calculated with the simplified formula proposed and resulting from IDA analyses is probably due to the equal displacement hypothesis for elastic and inelastic response of the system that is not completely satisfied.

Table 7.15 and Table 7.16 show how mean values of  $\Delta_{max,col+dev} - \Delta_{max,col}$  for each performed analysis are close but not exactly coincident to the maximum deformation capacity  $S_{max}$  of the dissipative device considered in the analysis.

## 8. CONCLUSIONS

The research presents innovative anti-seismic devices, based on carbon-wrapped steel tubes, proposed as low-damage retrofitting solution for friction-based beam column-joints of existing precast RC structures. The dissipative devices provide that, up to a target value, the relative displacement between structural elements, occurring once overcome friction forces, determines the compression of the devices, dissipating energy during their plastic deformation and reducing the effects of the seismic action on structural elements.

Based on experimental results and numerical analyses performed, the following conclusions can be drawn:

- Energy absorption capacity of presented devices was evaluated by means of quasi-static monotonic and cyclic experimental tests (75 tests performed on three different specimen types). Experimental tests exhibited a very regular behaviour of the devices during buckling process and a very good repeatability of energy dissipation performances.
- A simple trilinear model, based on an energy equivalence criterion, was proposed to represent the monotonic experimental behaviour of the device.
- Results obtained from quasi-static tests were extended to dynamic loading by performing dynamic drop tests also.
- The specific hysteretic behaviour of the device, which features an increasing gap because of progressive plasticization, does not allow to use traditional design criteria. Effective design criteria are being defined and validated by means of an extensive set of nonlinear dynamic analyses.
- The effectiveness of the introduction of dissipative devices in beam-column friction connections of precast structures was evaluated performing nonlinear dynamic analyses considering different seismic input.
- Nonlinear dynamic analyses performed permitted to investigate the dynamic behaviour of the device during ground motions and its effects in terms of reduction of relative beam-

column displacement and forces transmitted to the column. Results of preliminary analyses on simple portal frame structures equipped with dissipative devices were compared with those provided by equivalent elastic systems with simple hinged beam-column connections. A significant reduction of base shear was recorded, respectively of 31% and 47% in case of friction coefficient equal to 0.1 and 0.0.

- Until maximum deformation of the devices is reached, the dissipative fuse behaviour of the devices permits to have a well-defined shear value at base joints of the column, much lower than the one of the scheme with hinged beam-column joints. Equivalent force of plasticization  $F_{eq}$  of the device is set according to existing column capacity in order to make the dissipative device work with columns performing linear elastic behaviour.
- In all performed analyses the maximum value of base shear of the model reinforced with the dissipative devices is lower than the maximum value of base shear of the equivalent elastic model with hinges at the ends of the beam, proving the dissipative fuse effect of the devices.
- An equivalent behaviour factor for structures equipped with the dissipative devices was evaluated performing Incremental Dynamic Analyses (IDA). IDA analyses have been performed considering a high number of acceleration time histories and assuming as target damage different maximum device deformation values and different column chord rotation values for a total of 1188 different IDA analyses performed.
- The behaviour factor of the structure was investigated comparing the seismic response of a portal frame equipped with dissipative devices with the response of equivalent elastic systems. Behaviour factor values were computed as the ratio between the maximum base shear in the equivalent elastic system and the one in the system with dissipative devices.
- Findings of analyses showed that behaviour factor values are not dependent from the Magnitude-Distance scenario, the impulsivity and other characteristics of ground motions ( $PGD$ ,  $PGV$ ,  $PGA$  and  $I_A$ ).
- Further analyses were performed to evaluate the dependence of the behaviour factor of structures with dissipative connections on maximum deformation capacity  $S_{max}$  of

dissipative devices. Considering as target damage ultimate chord rotation of columns (4.5% for the three investigated models), behaviour factor values increase, with mean values varying from 3.25 to 5.06, increasing maximum deformation capacity of dissipative devices from 25 mm to 125 mm.

- A comparison between results of IDA analyses for the systems with hinged and dissipative beam-column connections was made in order to evaluate the contribution of the devices to dissipative capacity of the structure.
- IDA analyses showed how the introduction of the dissipative devices produces a significant improvement of the behaviour factor of the structure respect to systems with hinged connections, strongly depending on maximum deformation capacity of dissipative devices. Considering as target damage ultimate chord rotation of columns (4.5% for the three investigated models), mean values of behaviour factor improvement vary from 12% to 58%, with maximum deformation capacity of dissipative devices varying from 25 mm to 125 mm.
- A simplified approach to evaluate an equivalent behaviour factor for a structure equipped with dissipative devices in friction-based beam-column joints was proposed and compared with results of IDA analyses performed. The approximation of the simplified formula proposed is particular good for behaviour factor values of systems with dissipative connections with maximum device deformation capacity in the range 25 mm - 75 mm.
- Numerical investigations could continue including friction mechanism and vertical component of seismic acceleration in order to provide a more complete model of dynamic behaviour of precast connections and to better understand the effectiveness of the introduction of the devices.
- Even though the behaviour of devices has not yet been experimentally validated in a relevant environment (i.e. full scale actual beam-column joints), numerical findings showed that the dissipative devices seem to be a good retrofitting solution for friction joints to combine the need to connect elements and to maintain a low level of shear forces in existing structural elements.

## APPENDIX A

A complete report of results of the 1188 IDA analyses (990 IDA analyses on systems with dissipative connections, 198 IDA analyses on systems with hinged connections) discussed in Section 7.2 is provided, comparing systems with dissipative and hinged connections.

For each performed analysis on the three models *A*, *B* and *C*, both with dissipative and hinged connections, the following parameters have been collected:

- scaling factor required to reach target damage ( $SF_{col+dev}$  or  $SF_{col}$ );
- maximum total base shear of the system at target damage ( $F_{u,col}$ );
- maximum base shear of the equivalent elastic system ( $T_{el,col+dev}$  or  $T_{el,col}$ );
- behaviour factor ( $q_{col+dev}$  or  $q_{col}$ ).

For systems with dissipative connections, the behaviour factor  $q_{col+dev}$  is computed as the ratio between maximum total base shear ( $T_{el,col+dev}$ ) in the equivalent elastic system and the one in the system with nonlinear behaviour of columns and dissipative connections ( $F_{u,col}$ ).

For systems with hinged connections, the behaviour factor  $q_{col}$  is computed as the ratio between maximum total base shear ( $T_{el,col}$ ) in the equivalent elastic system and the one in the system with nonlinear behaviour of columns and hinged connections ( $F_{u,col}$ ).

All parameters collected and compared are listed in the following tables.

<i>Model A – target chord rotation 3% - <math>S_{max}</math> 25 mm</i>										
	<i>Dissipative connections</i>				<i>Hinged connections</i>				<i>Comparison</i>	
<i>TH-ID</i>	$q_{col+dev}$	$F_{u,col}$ [N]	$T_{el,col+dev}$ [N]	$SF_{col+dev}$	$q_{col}$	$F_{u,col}$ [N]	$T_{el,col}$ [N]	$SF_{col}$	$\frac{SF_{col+dev}}{SF_{col}}$	$\frac{q_{col+dev}}{q_{col}}$
1	2.96	69607	205974	1.73	2.79	69598	193907	1.63	6%	1.06
2	2.37	69556	164639	0.67	2.19	69559	152326	0.62	8%	1.08
3	1.82	69598	126906	1.34	1.67	69636	116596	1.23	9%	1.09
4	2.12	69573	147559	0.52	1.70	69655	118365	0.42	25%	1.25
5	3.01	69568	209592	2.30	2.63	69580	183238	2.01	14%	1.14
6	1.84	69578	127749	0.46	1.57	69581	108984	0.39	17%	1.17
7	1.85	69645	128723	0.54	1.61	69566	112063	0.47	15%	1.15
8	2.05	69585	142644	1.24	1.81	69593	126248	1.09	13%	1.13
9	2.50	69635	174031	1.59	2.32	69557	161449	1.48	8%	1.08
10	1.97	69536	137317	2.69	1.49	69620	103634	2.03	33%	1.33
11	2.19	69608	152101	2.92	1.90	69607	131911	2.53	15%	1.15
12	2.33	69621	162188	0.38	1.94	69586	135091	0.32	20%	1.20
13	2.54	69553	176541	1.93	2.16	69596	150292	1.64	17%	1.18
14	1.74	69620	121128	0.35	1.63	69566	113075	0.33	7%	1.07
15	1.84	69567	127728	0.61	1.66	69524	115241	0.55	11%	1.11
16	2.20	69572	153390	0.46	1.76	69661	122391	0.37	25%	1.25
17	2.01	69579	139623	0.69	1.85	69538	128632	0.64	9%	1.08
18	1.88	69590	130620	1.07	1.76	69578	122575	1.00	7%	1.07
19	1.64	69541	114126	0.66	1.55	69581	107898	0.62	6%	1.06
20	2.10	69642	146184	1.59	1.64	69627	114283	1.25	28%	1.28
21	2.28	69557	158930	0.57	2.10	69570	146396	0.53	9%	1.09
22	2.13	69547	147830	0.46	1.73	69620	120552	0.37	23%	1.23
23	2.79	69608	194389	0.56	2.17	69624	151111	0.44	29%	1.29
24	2.77	69625	193079	0.96	2.30	69541	159704	0.80	21%	1.21
25	2.86	69616	199192	1.00	2.13	69591	148027	0.74	35%	1.35
26	1.75	69631	121786	0.96	1.58	69623	110156	0.86	11%	1.11
27	3.14	69485	218206	0.38	2.43	69597	169324	0.30	29%	1.29
28	2.36	69603	164591	0.39	1.94	69632	135096	0.32	22%	1.22
29	2.70	69589	187695	0.79	1.95	69591	135740	0.57	38%	1.38
30	3.80	69607	264378	1.66	2.96	69611	206358	1.30	28%	1.28
31	2.46	69627	171583	0.72	1.88	69644	130745	0.55	31%	1.31
32	2.48	69592	172895	1.55	1.84	69635	128135	1.15	35%	1.35
33	1.97	69602	136805	0.44	1.54	69616	107050	0.34	28%	1.28
<b>mean</b>	<b>2.32</b>	<b>69590</b>	<b>161216</b>	<b>1.04</b>	<b>1.94</b>	<b>69597</b>	<b>135351</b>	<b>0.88</b>	<b>19%</b>	<b>1.19</b>

*Table A.1- Comparison between IDA results for Model A, target column chord rotation of 3% with dissipative connections ( $S_{max}$  25 mm) and hinged connections*

<i>Model A – target chord rotation 3% - <math>S_{max}</math> 50 mm</i>										
	<i>Dissipative connections</i>				<i>Hinged connections</i>				<i>Comparison</i>	
<i>TH-ID</i>	$q_{col+dev}$	$F_{u,col}$ [N]	$T_{el,col+dev}$ [N]	$SF_{col+dev}$	$q_{col}$	$F_{u,col}$ [N]	$T_{el,col}$ [N]	$SF_{col}$	$\frac{SF_{col+dev}}{SF_{col}}$	$\frac{q_{col+dev}}{q_{col}}$
1	3.11	69612	216834	1.82	2.79	69598	193907	1.63	12%	1.12
2	2.53	69548	176138	0.72	2.19	69559	152326	0.62	16%	1.16
3	1.94	69583	134846	1.42	1.67	69636	116596	1.23	16%	1.16
4	2.70	69599	188250	0.67	1.70	69655	118365	0.42	59%	1.59
5	3.45	69565	240044	2.63	2.63	69580	183238	2.01	31%	1.31
6	2.08	69571	144620	0.52	1.57	69581	108984	0.39	33%	1.33
7	2.05	69645	143059	0.59	1.61	69566	112063	0.47	28%	1.28
8	2.31	69632	160833	1.39	1.81	69593	126248	1.09	27%	1.27
9	2.66	69571	185189	1.70	2.32	69557	161449	1.48	15%	1.15
10	1.93	69604	134447	2.63	1.49	69620	103634	2.03	30%	1.30
11	2.47	69538	171794	3.29	1.90	69607	131911	2.53	30%	1.30
12	2.73	69497	189612	0.45	1.94	69586	135091	0.32	40%	1.41
13	2.68	69573	186310	2.04	2.16	69596	150292	1.64	24%	1.24
14	1.85	69609	128909	0.37	1.63	69566	113075	0.33	14%	1.14
15	2.02	69562	140801	0.67	1.66	69524	115241	0.55	22%	1.22
16	2.85	69576	197972	0.60	1.76	69661	122391	0.37	62%	1.62
17	2.05	69487	142202	0.70	1.85	69538	128632	0.64	11%	1.11
18	1.88	69625	130620	1.07	1.76	69578	122575	1.00	7%	1.06
19	1.73	69656	120390	0.69	1.55	69581	107898	0.62	12%	1.11
20	2.37	69621	165194	1.80	1.64	69627	114283	1.25	45%	1.45
21	2.45	69550	170670	0.62	2.10	69570	146396	0.53	17%	1.17
22	2.37	69543	164478	0.51	1.73	69620	120552	0.37	36%	1.37
23	3.50	69568	243344	0.71	2.17	69624	151111	0.44	61%	1.61
24	3.08	69533	213840	1.07	2.30	69541	159704	0.80	34%	1.34
25	3.97	69646	276388	1.39	2.13	69591	148027	0.74	87%	1.87
26	1.89	69647	131957	1.04	1.58	69623	110156	0.86	20%	1.20
27	4.11	69397	285000	0.50	2.43	69597	169324	0.30	68%	1.69
28	2.80	69637	194721	0.46	1.94	69632	135096	0.32	44%	1.44
29	3.07	69596	213706	0.90	1.95	69591	135740	0.57	57%	1.57
30	4.95	69431	343394	2.16	2.96	69611	206358	1.30	66%	1.67
31	3.11	69575	216406	0.91	1.88	69644	130745	0.55	66%	1.66
32	3.55	69547	247186	2.21	1.84	69635	128135	1.15	93%	1.93
33	2.35	69617	163378	0.52	1.54	69616	107050	0.34	53%	1.53
<b>mean</b>	<b>2.68</b>	<b>69575</b>	<b>186743</b>	<b>1.17</b>	<b>1.94</b>	<b>69597</b>	<b>135351</b>	<b>0.88</b>	<b>37%</b>	<b>1.37</b>

Table A.2- Comparison between IDA results for Model A, target column chord rotation of 3% with dissipative connections ( $S_{max}$  50 mm) and hinged connections

<i>Model A – target chord rotation 3% - <math>S_{max}</math> 75 mm</i>										
	<i>Dissipative connections</i>				<i>Hinged connections</i>				<i>Comparison</i>	
<i>TH-ID</i>	$q_{col+dev}$	$F_{u,col}$ [N]	$T_{el,col+dev}$ [N]	$SF_{col+dev}$	$q_{col}$	$F_{u,col}$ [N]	$T_{el,col}$ [N]	$SF_{col}$	$\frac{SF_{col+dev}}{SF_{col}}$	$\frac{q_{col+dev}}{q_{col}}$
1	3.27	69604	227470	1.91	2.79	69598	193907	1.63	17%	1.17
2	2.68	69555	186129	0.76	2.19	69559	152326	0.62	22%	1.22
3	1.79	69594	124242	1.31	1.67	69636	116596	1.23	7%	1.07
4	3.10	69548	215594	0.77	1.70	69655	118365	0.42	82%	1.82
5	3.77	69553	261978	2.87	2.63	69580	183238	2.01	43%	1.43
6	2.30	69575	159772	0.58	1.57	69581	108984	0.39	47%	1.47
7	2.25	69656	156399	0.65	1.61	69566	112063	0.47	40%	1.39
8	2.72	69597	189495	1.64	1.81	69593	126248	1.09	50%	1.50
9	2.82	69556	195885	1.79	2.32	69557	161449	1.48	21%	1.21
10	2.11	69558	146650	2.87	1.49	69620	103634	2.03	42%	1.42
11	2.48	69558	172353	3.30	1.90	69607	131911	2.53	31%	1.31
12	3.01	69598	209468	0.50	1.94	69586	135091	0.32	55%	1.55
13	2.96	69592	206176	2.26	2.16	69596	150292	1.64	37%	1.37
14	2.00	69621	139437	0.40	1.63	69566	113075	0.33	23%	1.23
15	2.22	69568	154703	0.74	1.66	69524	115241	0.55	34%	1.34
16	3.05	69591	212050	0.64	1.76	69661	122391	0.37	73%	1.73
17	2.05	69487	142202	0.70	1.85	69538	128632	0.64	11%	1.11
18	1.88	69386	130620	1.07	1.76	69578	122575	1.00	7%	1.07
19	1.81	69637	126320	0.73	1.55	69581	107898	0.62	17%	1.17
20	2.50	69626	174355	1.90	1.64	69627	114283	1.25	53%	1.53
21	2.52	69518	175159	0.63	2.10	69570	146396	0.53	20%	1.20
22	2.61	69569	181450	0.56	1.73	69620	120552	0.37	51%	1.51
23	3.88	69575	270010	0.78	2.17	69624	151111	0.44	79%	1.79
24	3.30	69568	229226	1.14	2.30	69541	159704	0.80	44%	1.43
25	4.21	69564	293060	1.47	2.13	69591	148027	0.74	98%	1.98
26	1.90	69479	132182	1.04	1.58	69623	110156	0.86	20%	1.20
27	4.76	69448	330730	0.58	2.43	69597	169324	0.30	95%	1.96
28	3.25	69618	226238	0.53	1.94	69632	135096	0.32	67%	1.68
29	3.22	69591	224038	0.95	1.95	69591	135740	0.57	65%	1.65
30	5.20	69654	362480	2.28	2.96	69611	206358	1.30	76%	1.76
31	3.85	69619	268220	1.13	1.88	69644	130745	0.55	105%	2.05
32	4.34	69536	301954	2.70	1.84	69635	128135	1.15	136%	2.36
33	2.66	69605	184955	0.59	1.54	69616	107050	0.34	73%	1.73
<b>mean</b>	<b>2.92</b>	<b>69570</b>	<b>203364</b>	<b>1.27</b>	<b>1.94</b>	<b>69597</b>	<b>135351</b>	<b>0.88</b>	<b>50%</b>	<b>1.50</b>

*Table A.3- Comparison between IDA results for Model A, target column chord rotation of 3% with dissipative connections ( $S_{max}$  75 mm) and hinged connections*

<i>Model A – target chord rotation 3% - <math>S_{max}</math> 100 mm</i>										
	<i>Dissipative connections</i>				<i>Hinged connections</i>				<i>Comparison</i>	
<i>TH-ID</i>	$q_{col+dev}$	$F_{u,col}$ [N]	$T_{el,col+dev}$ [N]	$SF_{col+dev}$	$q_{col}$	$F_{u,col}$ [N]	$T_{el,col}$ [N]	$SF_{col}$	$\frac{SF_{col+dev}}{SF_{col}}$	$\frac{q_{col+dev}}{q_{col}}$
1	3.42	69580	237944	2.00	2.79	69598	193907	1.63	23%	1.23
2	2.68	69555	186130	0.76	2.19	69559	152326	0.62	22%	1.22
3	1.78	69613	124154	1.31	1.67	69636	116596	1.23	6%	1.07
4	3.10	69548	215594	0.77	1.70	69655	118365	0.42	82%	1.82
5	3.77	69542	261978	2.87	2.63	69580	183238	2.01	43%	1.43
6	2.51	69571	174416	0.63	1.57	69581	108984	0.39	60%	1.60
7	2.41	69641	168134	0.70	1.61	69566	112063	0.47	50%	1.50
8	2.88	69548	200118	1.74	1.81	69593	126248	1.09	59%	1.59
9	2.97	69534	206474	1.89	2.32	69557	161449	1.48	28%	1.28
10	2.15	69543	149623	2.93	1.49	69620	103634	2.03	44%	1.45
11	2.48	69558	172353	3.30	1.90	69607	131911	2.53	31%	1.31
12	3.26	69602	226940	0.54	1.94	69586	135091	0.32	68%	1.68
13	2.70	69625	188250	2.06	2.16	69596	150292	1.64	25%	1.25
14	2.25	69611	156965	0.45	1.63	69566	113075	0.33	39%	1.39
15	2.43	69578	168769	0.81	1.66	69524	115241	0.55	46%	1.46
16	3.21	69579	223320	0.68	1.76	69661	122391	0.37	82%	1.83
17	2.05	69487	142202	0.70	1.85	69538	128632	0.64	11%	1.11
18	1.88	69386	130620	1.07	1.76	69578	122575	1.00	7%	1.07
19	1.89	69625	131291	0.76	1.55	69581	107898	0.62	22%	1.22
20	2.76	69577	191830	2.09	1.64	69627	114283	1.25	68%	1.68
21	2.52	69518	175159	0.63	2.10	69570	146396	0.53	20%	1.20
22	2.63	69564	183186	0.57	1.73	69620	120552	0.37	52%	1.52
23	4.13	69655	287438	0.83	2.17	69624	151111	0.44	90%	1.90
24	3.50	69539	243272	1.21	2.30	69541	159704	0.80	52%	1.52
25	4.44	69649	309392	1.55	2.13	69591	148027	0.74	109%	2.09
26	1.96	69588	136478	1.07	1.58	69623	110156	0.86	24%	1.24
27	5.12	69641	356708	0.62	2.43	69597	169324	0.30	111%	2.11
28	3.42	69620	238216	0.56	1.94	69632	135096	0.32	76%	1.76
29	3.41	69579	237456	1.00	1.95	69591	135740	0.57	75%	1.75
30	5.25	69648	365372	2.29	2.96	69611	206358	1.30	77%	1.77
31	4.53	69644	315812	1.32	1.88	69644	130745	0.55	142%	2.42
32	5.02	69584	349096	3.13	1.84	69635	128135	1.15	172%	2.73
33	2.88	69613	200456	0.64	1.54	69616	107050	0.34	87%	1.87
<b>mean</b>	<b>3.07</b>	<b>69580</b>	<b>213792</b>	<b>1.32</b>	<b>1.94</b>	<b>69597</b>	<b>135351</b>	<b>0.88</b>	<b>58%</b>	<b>1.58</b>

*Table A.4- Comparison between IDA results for Model A, target column chord rotation of 3% with dissipative connections ( $S_{max}$  100 mm) and hinged connections*

<i>Model A – target chord rotation 3% - <math>S_{max}</math> 125 mm</i>										
	<i>Dissipative connections</i>				<i>Hinged connections</i>				<i>Comparison</i>	
<i>TH-ID</i>	$q_{col+dev}$	$F_{u,col}$ [N]	$T_{el,col+dev}$ [N]	$SF_{col+dev}$	$q_{col}$	$F_{u,col}$ [N]	$T_{el,col}$ [N]	$SF_{col}$	$\frac{SF_{col+dev}}{SF_{col}}$	$\frac{q_{col+dev}}{q_{col}}$
1	3.57	69565	248044	2.08	2.79	69598	193907	1.63	28%	1.28
2	2.68	69555	186130	0.76	2.19	69559	152326	0.62	22%	1.22
3	1.92	69586	133355	1.40	1.67	69636	116596	1.23	14%	1.14
4	3.10	69548	215594	0.77	1.70	69655	118365	0.42	82%	1.82
5	3.77	69542	261978	2.87	2.63	69580	183238	2.01	43%	1.43
6	2.73	69561	189751	0.69	1.57	69581	108984	0.39	74%	1.74
7	2.55	69632	177424	0.74	1.61	69566	112063	0.47	58%	1.58
8	3.02	69540	209926	1.82	1.81	69593	126248	1.09	66%	1.66
9	3.12	69528	216724	1.98	2.32	69557	161449	1.48	34%	1.34
10	2.31	69620	160571	3.15	1.49	69620	103634	2.03	55%	1.55
11	2.48	69558	172353	3.30	1.90	69607	131911	2.53	31%	1.31
12	3.50	69621	243666	0.58	1.94	69586	135091	0.32	80%	1.80
13	2.90	69652	201734	2.21	2.16	69596	150292	1.64	34%	1.34
14	2.54	69532	176690	0.51	1.63	69566	113075	0.33	56%	1.56
15	2.63	69576	183018	0.88	1.66	69524	115241	0.55	59%	1.59
16	3.37	69521	234270	0.71	1.76	69661	122391	0.37	91%	1.92
17	2.05	69487	142202	0.70	1.85	69538	128632	0.64	11%	1.11
18	1.88	69386	130620	1.07	1.76	69578	122575	1.00	7%	1.07
19	1.95	69633	135802	0.78	1.55	69581	107898	0.62	26%	1.26
20	3.08	69644	214708	2.34	1.64	69627	114283	1.25	88%	1.88
21	2.52	69518	175159	0.63	2.10	69570	146396	0.53	20%	1.20
22	2.63	69564	183186	0.57	1.73	69620	120552	0.37	52%	1.52
23	4.32	69630	301010	0.87	2.17	69624	151111	0.44	99%	1.99
24	3.76	69647	261734	1.30	2.30	69541	159704	0.80	64%	1.64
25	4.67	69618	325008	1.63	2.13	69591	148027	0.74	120%	2.19
26	2.01	69628	139686	1.10	1.58	69623	110156	0.86	27%	1.27
27	6.08	69292	421122	0.74	2.43	69597	169324	0.30	149%	2.50
28	3.59	69625	249902	0.59	1.94	69632	135096	0.32	85%	1.85
29	3.73	69542	259264	1.09	1.95	69591	135740	0.57	91%	1.91
30	5.25	69648	365372	2.29	2.96	69611	206358	1.30	77%	1.77
31	5.18	69605	360470	1.51	1.88	69644	130745	0.55	176%	2.76
32	5.57	69476	387324	3.47	1.84	69635	128135	1.15	202%	3.03
33	3.07	69581	213466	0.68	1.54	69616	107050	0.34	99%	2.00
<b>mean</b>	<b>3.26</b>	<b>69565</b>	<b>226584</b>	<b>1.39</b>	<b>1.94</b>	<b>69597</b>	<b>135351</b>	<b>0.88</b>	<b>67%</b>	<b>1.67</b>

*Table A.5- Comparison between IDA results for Model A, target column chord rotation of 3% with dissipative connections ( $S_{max}$  125 mm) and hinged connections*

<i>Model A – target chord rotation 4.5% - <math>S_{max}</math> 25 mm</i>										
	<i>Dissipative connections</i>				<i>Hinged connections</i>				<i>Comparison</i>	
<i>TH-ID</i>	$q_{col+dev}$	$F_{u,col}$ [N]	$T_{el,col+dev}$ [N]	$SF_{col+dev}$	$q_{col}$	$F_{u,col}$ [N]	$T_{el,col}$ [N]	$SF_{col}$	$\frac{SF_{col+dev}}{SF_{col}}$	$\frac{q_{col+dev}}{q_{col}}$
1	3.75	69616	260734	2.19	3.60	69585	250472	2.10	4%	1.04
2	3.21	69549	223070	0.91	3.04	69488	211564	0.86	5%	1.05
3	2.20	69575	153197	1.61	2.21	69620	153911	1.62	0%	1.00
4	3.44	69512	238898	0.85	3.05	69479	211810	0.75	13%	1.13
5	4.61	69448	320344	3.51	3.84	69502	266564	2.92	20%	1.20
6	2.40	69623	167088	0.60	2.13	69632	148194	0.54	13%	1.13
7	2.37	69576	164942	0.69	2.14	69597	149273	0.62	10%	1.11
8	2.55	69590	177119	1.54	2.15	69563	149661	1.30	18%	1.18
9	3.31	69508	230250	2.11	3.14	69621	218886	2.00	5%	1.05
10	2.35	69538	163499	3.20	2.20	69512	152807	2.99	7%	1.07
11	2.82	69567	195919	3.75	2.51	69508	174600	3.35	12%	1.12
12	3.07	69660	213856	0.51	2.68	69583	186458	0.44	15%	1.15
13	2.90	69602	201642	2.21	2.56	69576	178301	1.95	13%	1.13
14	2.50	69557	173886	0.50	2.17	69649	150913	0.44	15%	1.15
15	2.65	69550	184008	0.88	2.29	69647	159242	0.76	16%	1.16
16	3.58	69521	248564	0.75	3.40	69486	236526	0.72	5%	1.05
17	2.78	69483	193070	0.96	2.62	69458	182210	0.90	6%	1.06
18	2.45	69534	170354	1.39	2.30	69555	159718	1.31	7%	1.07
19	2.01	69623	140125	0.81	1.99	69651	138631	0.80	1%	1.01
20	2.53	69653	176233	1.92	2.17	69549	151133	1.65	17%	1.16
21	3.16	69526	219642	0.79	2.98	69628	207544	0.75	6%	1.06
22	3.09	69520	215090	0.67	2.64	69548	183553	0.57	17%	1.17
23	4.15	69469	288334	0.84	3.75	69640	260900	0.76	11%	1.11
24	3.46	69291	239536	1.19	3.03	69475	210206	1.05	14%	1.14
25	4.98	69560	346136	1.74	4.73	69497	328910	1.65	5%	1.05
26	1.93	69601	134596	1.06	1.79	69585	124761	0.98	8%	1.08
27	5.65	69590	392940	0.69	6.20	69605	431378	0.75	-9%	0.91
28	3.31	69612	230424	0.54	2.89	69557	201254	0.47	14%	1.14
29	3.51	69629	244344	1.03	2.62	69579	182172	0.77	34%	1.34
30	5.91	69582	410970	2.58	4.29	69533	298612	1.87	38%	1.38
31	3.82	69589	265946	1.12	3.15	69598	218962	0.92	21%	1.21
32	4.25	69584	296030	2.65	3.74	69521	259908	2.33	14%	1.14
33	2.60	69557	180996	0.58	2.29	69540	159416	0.51	14%	1.14
<b>mean</b>	<b>3.25</b>	<b>69557</b>	<b>226115</b>	<b>1.40</b>	<b>2.92</b>	<b>69563</b>	<b>202983</b>	<b>1.25</b>	<b>12%</b>	<b>1.12</b>

*Table A.6- Comparison between IDA results for Model A, target column chord rotation of 4.5% with dissipative connections ( $S_{max}$  25 mm) and hinged connections*

<i>Model A – target chord rotation 4.5% - <math>S_{max}</math> 50 mm</i>										
	<i>Dissipative connections</i>				<i>Hinged connections</i>				<i>Comparison</i>	
<i>TH-ID</i>	$q_{col+dev}$	$F_{u,col}$ [N]	$T_{el,col+dev}$ [N]	$SF_{col+dev}$	$q_{col}$	$F_{u,col}$ [N]	$T_{el,col}$ [N]	$SF_{col}$	$\frac{SF_{col+dev}}{SF_{col}}$	$\frac{q_{col+dev}}{q_{col}}$
1	3.88	69568	270212	2.27	3.60	69585	250472	2.10	8%	1.08
2	3.35	69523	233014	0.95	3.04	69488	211564	0.86	10%	1.10
3	2.30	69558	159832	1.68	2.21	69620	153911	1.62	4%	1.04
4	3.80	69484	264020	0.94	3.05	69479	211810	0.75	25%	1.25
5	4.87	69630	339260	3.72	3.84	69502	266564	2.92	27%	1.27
6	2.67	69615	185819	0.67	2.13	69632	148194	0.54	25%	1.25
7	2.61	69614	181404	0.75	2.14	69597	149273	0.62	22%	1.21
8	3.28	69620	228022	1.98	2.15	69563	149661	1.30	52%	1.52
9	3.45	69499	239688	2.20	3.14	69621	218886	2.00	10%	1.10
10	2.29	69642	159520	3.13	2.20	69512	152807	2.99	4%	1.04
11	3.06	69658	213030	4.08	2.51	69508	174600	3.35	22%	1.22
12	3.48	69630	242466	0.57	2.68	69583	186458	0.44	30%	1.30
13	3.28	69648	228442	2.50	2.56	69576	178301	1.95	28%	1.28
14	2.80	69556	194837	0.56	2.17	69649	150913	0.44	29%	1.29
15	3.01	69591	209654	1.00	2.29	69647	159242	0.76	32%	1.32
16	3.73	69484	258958	0.78	3.40	69486	236526	0.72	9%	1.09
17	2.85	69560	198419	0.98	2.62	69458	182210	0.90	9%	1.09
18	2.59	69544	179909	1.47	2.30	69555	159718	1.31	13%	1.13
19	2.07	69655	144108	0.83	1.99	69651	138631	0.80	4%	1.04
20	2.89	69598	201366	2.19	2.17	69549	151133	1.65	33%	1.33
21	3.31	69515	229830	0.83	2.98	69628	207544	0.75	11%	1.11
22	3.80	69518	264448	0.82	2.64	69548	183553	0.57	44%	1.44
23	4.33	69509	300706	0.87	3.75	69640	260900	0.76	15%	1.15
24	3.82	69654	266408	1.33	3.03	69475	210206	1.05	27%	1.26
25	5.19	69645	361710	1.82	4.73	69497	328910	1.65	10%	1.10
26	2.08	69644	145131	1.14	1.79	69585	124761	0.98	16%	1.16
27	5.85	69440	406210	0.71	6.20	69605	431378	0.75	-6%	0.94
28	3.81	69585	265236	0.62	2.89	69557	201254	0.47	32%	1.32
29	4.11	69609	286248	1.21	2.62	69579	182172	0.77	57%	1.57
30	6.89	69546	479500	3.01	4.29	69533	298612	1.87	61%	1.61
31	4.46	69588	310564	1.30	3.15	69598	218962	0.92	42%	1.42
32	4.94	69601	343870	3.08	3.74	69521	259908	2.33	32%	1.32
33	2.95	69483	204696	0.66	2.29	69540	159416	0.51	28%	1.29
<b>mean</b>	<b>3.57</b>	<b>69576</b>	<b>248380</b>	<b>1.54</b>	<b>2.92</b>	<b>69563</b>	<b>202983</b>	<b>1.25</b>	<b>23%</b>	<b>1.23</b>

*Table A.7- Comparison between IDA results for Model A, target column chord rotation of 4.5% with dissipative connections ( $S_{max}$  50 mm) and hinged connections*

<i>Model A – target chord rotation 4.5% - <math>S_{max}</math> 75 mm</i>										
	<i>Dissipative connections</i>				<i>Hinged connections</i>				<i>Comparison</i>	
<i>TH-ID</i>	$q_{col+dev}$	$F_{u,col}$ [N]	$T_{el,col+dev}$ [N]	$SF_{col+dev}$	$q_{col}$	$F_{u,col}$ [N]	$T_{el,col}$ [N]	$SF_{col}$	$\frac{SF_{col+dev}}{SF_{col}}$	$\frac{q_{col+dev}}{q_{col}}$
1	4.02	69563	279420	2.34	3.60	69585	250472	2.10	12%	1.12
2	3.50	69498	243272	0.99	3.04	69488	211564	0.86	15%	1.15
3	2.30	69586	160013	1.69	2.21	69620	153911	1.62	4%	1.04
4	4.22	69599	293392	1.04	3.05	69479	211810	0.75	39%	1.38
5	5.04	69603	350654	3.84	3.84	69502	266564	2.92	32%	1.31
6	2.96	69566	205784	0.74	2.13	69632	148194	0.54	39%	1.39
7	2.79	69584	194368	0.81	2.14	69597	149273	0.62	30%	1.30
8	3.77	69637	262688	2.28	2.15	69563	149661	1.30	76%	1.75
9	3.59	69488	249346	2.28	3.14	69621	218886	2.00	14%	1.14
10	2.37	69637	165267	3.24	2.20	69512	152807	2.99	8%	1.08
11	3.36	69594	234144	4.49	2.51	69508	174600	3.35	34%	1.34
12	3.83	69621	266354	0.63	2.68	69583	186458	0.44	43%	1.43
13	3.67	69579	255454	2.80	2.56	69576	178301	1.95	43%	1.43
14	3.12	69539	216880	0.63	2.17	69649	150913	0.44	44%	1.44
15	3.33	69608	231908	1.11	2.29	69647	159242	0.76	46%	1.46
16	3.88	69488	269392	0.81	3.40	69486	236526	0.72	14%	1.14
17	2.85	69585	198419	0.98	2.62	69458	182210	0.90	9%	1.09
18	2.73	69529	189494	1.55	2.30	69555	159718	1.31	19%	1.19
19	2.12	69624	147743	0.85	1.99	69651	138631	0.80	7%	1.07
20	3.26	69658	227264	2.48	2.17	69549	151133	1.65	50%	1.50
21	3.46	69515	240646	0.87	2.98	69628	207544	0.75	16%	1.16
22	4.33	69591	301484	0.94	2.64	69548	183553	0.57	64%	1.64
23	4.50	69632	313310	0.91	3.75	69640	260900	0.76	20%	1.20
24	4.25	69581	295844	1.47	3.03	69475	210206	1.05	41%	1.41
25	5.42	69629	377188	1.90	4.73	69497	328910	1.65	15%	1.14
26	2.14	69632	148870	1.17	1.79	69585	124761	0.98	19%	1.19
27	6.34	69577	441142	0.77	6.20	69605	431378	0.75	2%	1.02
28	4.12	69579	286840	0.67	2.89	69557	201254	0.47	43%	1.42
29	3.94	69571	274248	1.16	2.62	69579	182172	0.77	51%	1.51
30	6.63	69568	461548	2.90	4.29	69533	298612	1.87	55%	1.54
31	5.18	69578	360128	1.51	3.15	69598	218962	0.92	64%	1.65
32	5.68	69587	395214	3.54	3.74	69521	259908	2.33	52%	1.52
33	3.28	69622	228408	0.73	2.29	69540	159416	0.51	43%	1.43
<b>mean</b>	<b>3.82</b>	<b>69583</b>	<b>265640</b>	<b>1.64</b>	<b>2.92</b>	<b>69563</b>	<b>202983</b>	<b>1.25</b>	<b>32%</b>	<b>1.32</b>

*Table A.8- Comparison between IDA results for Model A, target column chord rotation of 4.5% with dissipative connections ( $S_{max}$  75 mm) and hinged connections*

<i>Model A – target chord rotation 4.5% - <math>S_{max}</math> 100 mm</i>										
	<i>Dissipative connections</i>				<i>Hinged connections</i>				<i>Comparison</i>	
<i>TH-ID</i>	$q_{col+dev}$	$F_{u,col}$ [N]	$T_{el,col+dev}$ [N]	$SF_{col+dev}$	$q_{col}$	$F_{u,col}$ [N]	$T_{el,col}$ [N]	$SF_{col}$	$\frac{SF_{col+dev}}{SF_{col}}$	$\frac{q_{col+dev}}{q_{col}}$
1	4.15	69554	288798	2.42	3.60	69585	250472	2.10	15%	1.15
2	3.62	69489	251712	1.03	3.04	69488	211564	0.86	19%	1.19
3	2.15	69598	149958	1.58	2.21	69620	153911	1.62	-3%	0.97
4	4.72	69501	328240	1.17	3.05	69479	211810	0.75	55%	1.55
5	5.16	69585	359034	3.93	3.84	69502	266564	2.92	35%	1.35
6	3.25	69651	226688	0.82	2.13	69632	148194	0.54	53%	1.53
7	2.94	69570	204492	0.85	2.14	69597	149273	0.62	37%	1.37
8	4.12	69590	286956	2.49	2.15	69563	149661	1.30	92%	1.92
9	3.73	69481	259132	2.37	3.14	69621	218886	2.00	18%	1.19
10	2.53	69628	176132	3.45	2.20	69512	152807	2.99	15%	1.15
11	3.73	69594	259580	4.98	2.51	69508	174600	3.35	49%	1.48
12	4.18	69613	290642	0.69	2.68	69583	186458	0.44	56%	1.56
13	3.66	69520	254480	2.79	2.56	69576	178301	1.95	43%	1.43
14	3.41	69656	237808	0.69	2.17	69649	150913	0.44	58%	1.58
15	3.56	69572	247372	1.18	2.29	69647	159242	0.76	55%	1.56
16	4.02	69626	279670	0.85	3.40	69486	236526	0.72	18%	1.18
17	2.85	69585	198419	0.98	2.62	69458	182210	0.90	9%	1.09
18	2.74	69516	190526	1.56	2.30	69555	159718	1.31	19%	1.19
19	2.17	69618	151364	0.87	1.99	69651	138631	0.80	9%	1.09
20	3.76	69572	261816	2.85	2.17	69549	151133	1.65	73%	1.73
21	3.51	69508	243768	0.88	2.98	69628	207544	0.75	17%	1.18
22	4.56	69625	317550	0.99	2.64	69548	183553	0.57	73%	1.73
23	4.85	69592	337208	0.98	3.75	69640	260900	0.76	29%	1.29
24	4.66	69606	324670	1.62	3.03	69475	210206	1.05	54%	1.54
25	5.64	69631	392486	1.97	4.73	69497	328910	1.65	19%	1.19
26	2.19	69610	152721	1.20	1.79	69585	124761	0.98	22%	1.22
27	7.04	69565	489570	0.86	6.20	69605	431378	0.75	13%	1.14
28	4.28	69591	297672	0.70	2.89	69557	201254	0.47	48%	1.48
29	4.04	69631	281232	1.19	2.62	69579	182172	0.77	54%	1.54
30	6.79	69569	472322	2.97	4.29	69533	298612	1.87	58%	1.58
31	5.91	69646	411732	1.73	3.15	69598	218962	0.92	88%	1.88
32	6.16	69475	427942	3.83	3.74	69521	259908	2.33	65%	1.65
33	3.61	69574	251080	0.80	2.29	69540	159416	0.51	57%	1.57
<b>mean</b>	<b>4.05</b>	<b>69580</b>	<b>281902</b>	<b>1.73</b>	<b>2.92</b>	<b>69563</b>	<b>202983</b>	<b>1.25</b>	<b>40%</b>	<b>1.40</b>

*Table A.9- Comparison between IDA results for Model A, target column chord rotation of 4.5% with dissipative connections ( $S_{max}$  100 mm) and hinged connections*

<i>Model A – target chord rotation 4.5% - <math>S_{max}</math> 125 mm</i>										
	<i>Dissipative connections</i>				<i>Hinged connections</i>				<i>Comparison</i>	
<i>TH-ID</i>	$q_{col+dev}$	$F_{u,col}$ [N]	$T_{el,col+dev}$ [N]	$SF_{col+dev}$	$q_{col}$	$F_{u,col}$ [N]	$T_{el,col}$ [N]	$SF_{col}$	$\frac{SF_{col+dev}}{SF_{col}}$	$\frac{q_{col+dev}}{q_{col}}$
1	4.29	69542	298390	2.50	3.60	69585	250472	2.10	19%	1.19
2	3.62	69489	251712	1.03	3.04	69488	211564	0.86	19%	1.19
3	2.13	69620	148178	1.56	2.21	69620	153911	1.62	-4%	0.96
4	4.92	69526	341980	1.21	3.05	69479	211810	0.75	61%	1.61
5	5.22	69580	363066	3.98	3.84	69502	266564	2.92	36%	1.36
6	3.60	69617	250740	0.91	2.13	69632	148194	0.54	69%	1.69
7	3.05	69557	211886	0.88	2.14	69597	149273	0.62	42%	1.42
8	4.51	69561	313596	2.72	2.15	69563	149661	1.30	110%	2.10
9	3.88	69482	269318	2.47	3.14	69621	218886	2.00	23%	1.23
10	2.89	69629	201302	3.94	2.20	69512	152807	2.99	32%	1.32
11	4.11	69549	285666	5.48	2.51	69508	174600	3.35	64%	1.64
12	4.64	69591	322582	0.76	2.68	69583	186458	0.44	73%	1.73
13	3.38	69497	235154	2.57	2.56	69576	178301	1.95	32%	1.32
14	3.72	69510	258800	0.75	2.17	69649	150913	0.44	71%	1.72
15	3.79	69564	263736	1.26	2.29	69647	159242	0.76	66%	1.66
16	4.16	69620	289834	0.88	3.40	69486	236526	0.72	23%	1.22
17	2.85	69585	198419	0.98	2.62	69458	182210	0.90	9%	1.09
18	2.74	69516	190526	1.56	2.30	69555	159718	1.31	19%	1.19
19	2.23	69621	154976	0.89	1.99	69651	138631	0.80	12%	1.12
20	4.37	69613	304010	3.31	2.17	69549	151133	1.65	101%	2.01
21	3.51	69508	243768	0.88	2.98	69628	207544	0.75	17%	1.18
22	4.56	69625	317550	0.99	2.64	69548	183553	0.57	73%	1.73
23	5.14	69567	357352	1.04	3.75	69640	260900	0.76	37%	1.37
24	4.84	69618	336838	1.68	3.03	69475	210206	1.05	60%	1.60
25	5.86	69609	407684	2.05	4.73	69497	328910	1.65	24%	1.24
26	2.35	69594	163750	1.28	1.79	69585	124761	0.98	31%	1.31
27	7.80	69539	542740	0.95	6.20	69605	431378	0.75	26%	1.26
28	4.43	69619	308558	0.72	2.89	69557	201254	0.47	53%	1.53
29	4.46	69562	310290	1.31	2.62	69579	182172	0.77	70%	1.70
30	7.01	69566	487514	3.06	4.29	69533	298612	1.87	63%	1.63
31	6.71	69579	466914	1.96	3.15	69598	218962	0.92	113%	2.13
32	6.59	69367	457304	4.09	3.74	69521	259908	2.33	76%	1.76
33	3.91	69558	271792	0.87	2.29	69540	159416	0.51	70%	1.70
<b>mean</b>	<b>4.28</b>	<b>69563</b>	<b>297755</b>	<b>1.83</b>	<b>2.92</b>	<b>69563</b>	<b>202983</b>	<b>1.25</b>	<b>48%</b>	<b>1.48</b>

*Table A.10- Comparison between IDA results for Model A, target column chord rotation of 4.5% with dissipative connections ( $S_{max}$  125 mm) and hinged connections*

<i>Model B – target chord rotation 3% - <math>S_{max}</math> 25 mm</i>										
	<i>Dissipative connections</i>				<i>Hinged connections</i>				<i>Comparison</i>	
<i>TH-ID</i>	$q_{col+dev}$	$F_{u,col}$ [N]	$T_{el,col+dev}$ [N]	$SF_{col+dev}$	$q_{col}$	$F_{u,col}$ [N]	$T_{el,col}$ [N]	$SF_{col}$	$\frac{SF_{col+dev}}{SF_{col}}$	$\frac{q_{col+dev}}{q_{col}}$
1	2.33	106011	247320	1.87	1.79	106012	189631	1.44	30%	1.30
2	2.92	106014	309508	0.65	2.67	106014	283022	0.60	9%	1.09
3	3.69	106011	391364	1.45	2.85	106012	301670	1.12	30%	1.30
4	1.96	106031	207382	0.53	1.66	106011	176098	0.45	18%	1.18
5	2.90	106003	307358	2.03	2.11	106013	224202	1.48	37%	1.37
6	1.92	106013	203856	0.49	1.66	106018	175532	0.42	16%	1.16
7	1.94	106014	205366	0.56	1.71	106014	181117	0.50	13%	1.13
8	2.55	106011	270468	1.25	2.23	106014	236708	1.10	14%	1.14
9	2.87	106013	303956	1.54	2.11	106013	223900	1.13	36%	1.36
10	2.62	106012	277390	2.69	2.04	106015	215958	2.10	28%	1.28
11	2.48	106002	263204	2.52	2.13	106012	225820	2.16	17%	1.17
12	2.42	106011	256246	0.32	1.98	106014	209480	0.27	22%	1.22
13	2.10	106014	223104	1.63	1.71	106015	181252	1.32	23%	1.23
14	1.87	106013	198457	0.38	1.74	106013	184504	0.35	8%	1.08
15	1.92	106013	203806	0.56	1.76	106014	186407	0.51	9%	1.09
16	2.20	106014	233514	0.45	1.83	106014	193892	0.37	20%	1.20
17	2.00	105986	212442	0.66	1.83	106016	193488	0.61	10%	1.10
18	2.10	106028	222710	0.95	1.90	106002	201474	0.86	11%	1.11
19	1.75	106013	185097	0.66	1.64	106013	173497	0.62	7%	1.07
20	3.00	106013	318544	1.48	1.99	106016	211382	0.98	51%	1.51
21	2.95	106012	312632	0.57	2.68	106011	284122	0.52	10%	1.10
22	2.35	106014	249090	0.44	1.86	106013	197212	0.35	26%	1.26
23	3.04	106015	322546	0.54	2.32	106013	246310	0.41	31%	1.31
24	3.43	106016	363558	0.90	2.62	106013	277650	0.69	31%	1.31
25	2.52	106013	267520	0.81	2.00	106014	211692	0.64	26%	1.26
26	2.07	106014	219824	0.97	1.91	106014	202962	0.90	8%	1.08
27	3.80	106011	403360	0.33	2.77	106014	293952	0.24	37%	1.37
28	2.65	106015	280422	0.39	2.17	106015	230042	0.32	22%	1.22
29	1.93	106014	204492	0.71	1.46	106015	154291	0.54	33%	1.33
30	3.16	106011	335006	1.47	2.84	106014	301508	1.32	11%	1.11
31	2.26	106007	239582	0.71	1.85	106013	195654	0.58	22%	1.22
32	3.02	106011	319858	1.38	2.22	106013	235576	1.02	36%	1.36
33	2.01	106014	213364	0.43	1.65	106016	175429	0.35	22%	1.22
<b>mean</b>	<b>2.51</b>	<b>106012</b>	<b>265829</b>	<b>0.98</b>	<b>2.05</b>	<b>106013</b>	<b>217437</b>	<b>0.80</b>	<b>22%</b>	<b>1.22</b>

*Table A.11- Comparison between IDA results for Model B, target column chord rotation of 3% with dissipative connections ( $S_{max}$  25 mm) and hinged connections*

<i>Model B – target chord rotation 3% - <math>S_{max}</math> 50 mm</i>										
	<i>Dissipative connections</i>				<i>Hinged connections</i>				<i>Comparison</i>	
<i>TH-ID</i>	$q_{col+dev}$	$F_{u,col}$ [N]	$T_{el,col+dev}$ [N]	$SF_{col+dev}$	$q_{col}$	$F_{u,col}$ [N]	$T_{el,col}$ [N]	$SF_{col}$	$\frac{SF_{col+dev}}{SF_{col}}$	$\frac{q_{col+dev}}{q_{col}}$
1	2.47	106015	261374	1.98	1.79	106012	189631	1.44	38%	1.38
2	3.15	106014	333418	0.70	2.67	106014	283022	0.60	18%	1.18
3	3.79	106008	401442	1.49	2.85	106012	301670	1.12	33%	1.33
4	2.35	106013	249562	0.64	1.66	106011	176098	0.45	42%	1.42
5	3.15	106006	333484	2.20	2.11	106013	224202	1.48	49%	1.49
6	2.15	106012	227988	0.55	1.66	106018	175532	0.42	30%	1.30
7	2.12	106014	224924	0.62	1.71	106014	181117	0.50	24%	1.24
8	2.83	106016	299754	1.39	2.23	106014	236708	1.10	27%	1.27
9	3.08	106014	327028	1.65	2.11	106013	223900	1.13	46%	1.46
10	2.62	106013	277882	2.70	2.04	106015	215958	2.10	29%	1.29
11	2.79	106013	295914	2.83	2.13	106012	225820	2.16	31%	1.31
12	2.86	106018	303126	0.38	1.98	106014	209480	0.27	45%	1.45
13	2.68	106014	284398	2.07	1.71	106015	181252	1.32	57%	1.57
14	1.99	106013	210982	0.40	1.74	106013	184504	0.35	14%	1.14
15	2.07	106016	219440	0.60	1.76	106014	186407	0.51	18%	1.18
16	2.61	106015	276894	0.53	1.83	106014	193892	0.37	43%	1.43
17	2.11	106016	223974	0.70	1.83	106016	193488	0.61	16%	1.16
18	2.10	106028	222710	0.95	1.90	106002	201474	0.86	11%	1.11
19	1.85	106014	195840	0.70	1.64	106013	173497	0.62	13%	1.13
20	3.44	106003	364932	1.70	1.99	106016	211382	0.98	73%	1.73
21	3.19	106010	338402	0.62	2.68	106011	284122	0.52	19%	1.19
22	2.68	106018	283742	0.50	1.86	106013	197212	0.35	44%	1.44
23	3.73	106014	394916	0.66	2.32	106013	246310	0.41	60%	1.60
24	4.00	106004	424060	1.05	2.62	106013	277650	0.69	53%	1.53
25	3.18	106012	337450	1.02	2.00	106014	211692	0.64	59%	1.59
26	2.24	106012	237190	1.05	1.91	106014	202962	0.90	17%	1.17
27	4.80	106012	509102	0.42	2.77	106014	293952	0.24	73%	1.73
28	3.06	106013	323914	0.45	2.17	106015	230042	0.32	41%	1.41
29	2.51	106012	266576	0.93	1.46	106015	154291	0.54	73%	1.73
30	3.56	106016	377788	1.66	2.84	106014	301508	1.32	25%	1.25
31	2.71	106024	287778	0.85	1.85	106013	195654	0.58	47%	1.47
32	4.00	106013	423594	1.83	2.22	106013	235576	1.02	80%	1.80
33	2.37	106012	251552	0.50	1.65	106016	175429	0.35	43%	1.43
<b>mean</b>	<b>2.86</b>	<b>106014</b>	<b>302762</b>	<b>1.10</b>	<b>2.05</b>	<b>106013</b>	<b>217437</b>	<b>0.80</b>	<b>39%</b>	<b>1.39</b>

*Table A.12- Comparison between IDA results for Model B, target column chord rotation of 3% with dissipative connections ( $S_{max}$  50 mm) and hinged connections*

<i>Model B – target chord rotation 3% - <math>S_{max}</math> 75 mm</i>										
	<i>Dissipative connections</i>				<i>Hinged connections</i>				<i>Comparison</i>	
<i>TH-ID</i>	$q_{col+dev}$	$F_{u,col}$ [N]	$T_{el,col+dev}$ [N]	$SF_{col+dev}$	$q_{col}$	$F_{u,col}$ [N]	$T_{el,col}$ [N]	$SF_{col}$	$\frac{SF_{col+dev}}{SF_{col}}$	$\frac{q_{col+dev}}{q_{col}}$
1	2.59	106013	274426	2.08	1.79	106012	189631	1.44	45%	1.45
2	3.36	106015	356708	0.75	2.67	106014	283022	0.60	26%	1.26
3	3.81	106012	403542	1.50	2.85	106012	301670	1.12	34%	1.34
4	2.69	106013	285068	0.73	1.66	106011	176098	0.45	62%	1.62
5	3.37	106006	356882	2.35	2.11	106013	224202	1.48	59%	1.59
6	2.37	106014	251646	0.60	1.66	106018	175532	0.42	43%	1.43
7	2.26	106017	239228	0.66	1.71	106014	181117	0.50	32%	1.32
8	3.15	106013	333464	1.55	2.23	106014	236708	1.10	41%	1.41
9	3.29	106014	349246	1.77	2.11	106013	223900	1.13	56%	1.56
10	2.42	106011	256646	2.49	2.04	106015	215958	2.10	19%	1.19
11	3.03	106025	321484	3.07	2.13	106012	225820	2.16	42%	1.42
12	3.30	106013	350006	0.44	1.98	106014	209480	0.27	67%	1.67
13	2.92	106019	309346	2.26	1.71	106015	181252	1.32	71%	1.71
14	2.11	106014	223306	0.42	1.74	106013	184504	0.35	21%	1.21
15	2.26	106014	239596	0.66	1.76	106014	186407	0.51	29%	1.29
16	3.13	106015	331610	0.63	1.83	106014	193892	0.37	71%	1.71
17	2.11	106016	223974	0.70	1.83	106016	193488	0.61	16%	1.16
18	2.10	106028	222710	0.95	1.90	106002	201474	0.86	11%	1.11
19	1.93	106016	204526	0.73	1.64	106013	173497	0.62	18%	1.18
20	3.74	106026	396922	1.85	1.99	106016	211382	0.98	88%	1.88
21	3.43	106010	363696	0.67	2.68	106011	284122	0.52	28%	1.28
22	2.94	106007	311924	0.55	1.86	106013	197212	0.35	58%	1.58
23	4.39	106017	465168	0.77	2.32	106013	246310	0.41	89%	1.89
24	4.45	105994	471200	1.17	2.62	106013	277650	0.69	70%	1.70
25	4.57	106012	484840	1.46	2.00	106014	211692	0.64	129%	2.29
26	2.28	106013	241752	1.07	1.91	106014	202962	0.90	19%	1.19
27	6.36	106012	673910	0.55	2.77	106014	293952	0.24	129%	2.29
28	3.43	106015	363106	0.50	2.17	106015	230042	0.32	58%	1.58
29	2.63	106012	278566	0.97	1.46	106015	154291	0.54	81%	1.81
30	4.07	106006	431828	1.89	2.84	106014	301508	1.32	43%	1.43
31	3.15	106018	334180	0.99	1.85	106013	195654	0.58	71%	1.71
32	5.29	106010	561090	2.43	2.22	106013	235576	1.02	138%	2.38
33	2.70	106013	286142	0.57	1.65	106016	175429	0.35	63%	1.63
<b>mean</b>	<b>3.20</b>	<b>106014</b>	<b>339325</b>	<b>1.21</b>	<b>2.05</b>	<b>106013</b>	<b>217437</b>	<b>0.80</b>	<b>55%</b>	<b>1.55</b>

*Table A.13- Comparison between IDA results for Model B, target column chord rotation of 3% with dissipative connections ( $S_{max}$  75 mm) and hinged connections*

<i>Model B – target chord rotation 3% - <math>S_{max}</math> 100 mm</i>										
	<i>Dissipative connections</i>				<i>Hinged connections</i>				<i>Comparison</i>	
<i>TH-ID</i>	$q_{col+dev}$	$F_{u,col}$ [N]	$T_{el,col+dev}$ [N]	$SF_{col+dev}$	$q_{col}$	$F_{u,col}$ [N]	$T_{el,col}$ [N]	$SF_{col}$	$\frac{SF_{col+dev}}{SF_{col}}$	$\frac{q_{col+dev}}{q_{col}}$
1	2.71	106013	287342	2.18	1.79	106012	189631	1.44	52%	1.52
2	3.54	106010	375788	0.79	2.67	106014	283022	0.60	33%	1.33
3	3.73	106014	395960	1.47	2.85	106012	301670	1.12	31%	1.31
4	2.77	106014	293726	0.75	1.66	106011	176098	0.45	67%	1.67
5	3.68	106027	389874	2.57	2.11	106013	224202	1.48	74%	1.74
6	2.59	106010	275018	0.66	1.66	106018	175532	0.42	57%	1.57
7	2.42	106012	256608	0.71	1.71	106014	181117	0.50	42%	1.42
8	3.33	106013	352852	1.64	2.23	106014	236708	1.10	49%	1.49
9	3.49	106014	369986	1.87	2.11	106013	223900	1.13	65%	1.65
10	2.80	106006	296954	2.88	2.04	106015	215958	2.10	38%	1.38
11	3.03	106025	321484	3.07	2.13	106012	225820	2.16	42%	1.42
12	3.73	106017	395956	0.50	1.98	106014	209480	0.27	89%	1.89
13	3.02	106018	320546	2.34	1.71	106015	181252	1.32	77%	1.77
14	2.22	106013	235050	0.45	1.74	106013	184504	0.35	27%	1.27
15	2.48	106013	263318	0.72	1.76	106014	186407	0.51	41%	1.41
16	3.32	106013	352108	0.67	1.83	106014	193892	0.37	82%	1.82
17	2.11	106016	223974	0.70	1.83	106016	193488	0.61	16%	1.16
18	2.10	106028	222710	0.95	1.90	106002	201474	0.86	11%	1.11
19	2.00	106011	212176	0.76	1.64	106013	173497	0.62	22%	1.22
20	4.18	105955	443352	2.06	1.99	106016	211382	0.98	110%	2.10
21	3.48	106011	369392	0.68	2.68	106011	284122	0.52	30%	1.30
22	3.14	106015	333044	0.59	1.86	106013	197212	0.35	69%	1.69
23	4.72	106018	500372	0.83	2.32	106013	246310	0.41	103%	2.03
24	4.78	105979	506686	1.26	2.62	106013	277650	0.69	82%	1.83
25	4.92	106011	521160	1.57	2.00	106014	211692	0.64	146%	2.46
26	2.35	106016	248984	1.10	1.91	106014	202962	0.90	23%	1.23
27	6.89	106010	730756	0.60	2.77	106014	293952	0.24	149%	2.49
28	3.90	106014	413616	0.57	2.17	106015	230042	0.32	80%	1.80
29	2.70	106012	286268	1.00	1.46	106015	154291	0.54	86%	1.86
30	4.68	106010	496318	2.17	2.84	106014	301508	1.32	65%	1.65
31	3.58	106020	379462	1.12	1.85	106013	195654	0.58	94%	1.94
32	6.28	106010	665978	2.88	2.22	106013	235576	1.02	183%	2.83
33	2.94	106016	311800	0.62	1.65	106016	175429	0.35	78%	1.78
<b>mean</b>	<b>3.44</b>	<b>106012</b>	<b>365110</b>	<b>1.30</b>	<b>2.05</b>	<b>106013</b>	<b>217437</b>	<b>0.80</b>	<b>67%</b>	<b>1.67</b>

*Table A.14- Comparison between IDA results for Model B, target column chord rotation of 3% with dissipative connections ( $S_{max}$  100 mm) and hinged connections*

<i>Model B – target chord rotation 3% - <math>S_{max}</math> 125 mm</i>										
	<i>Dissipative connections</i>				<i>Hinged connections</i>				<i>Comparison</i>	
<i>TH-ID</i>	$q_{col+dev}$	$F_{u,col}$ [N]	$T_{el,col+dev}$ [N]	$SF_{col+dev}$	$q_{col}$	$F_{u,col}$ [N]	$T_{el,col}$ [N]	$SF_{col}$	$\frac{SF_{col+dev}}{SF_{col}}$	$\frac{q_{col+dev}}{q_{col}}$
1	2.83	106012	300104	2.27	1.79	106012	189631	1.44	58%	1.58
2	3.54	106010	375788	0.79	2.67	106014	283022	0.60	33%	1.33
3	3.65	106020	387442	1.44	2.85	106012	301670	1.12	28%	1.28
4	2.77	106014	293726	0.75	1.66	106011	176098	0.45	67%	1.67
5	3.72	106008	394646	2.60	2.11	106013	224202	1.48	76%	1.76
6	2.81	106012	298132	0.72	1.66	106018	175532	0.42	70%	1.70
7	2.63	106016	278434	0.77	1.71	106014	181117	0.50	54%	1.54
8	3.38	106013	358348	1.66	2.23	106014	236708	1.10	51%	1.51
9	3.68	106014	389812	1.97	2.11	106013	223900	1.13	74%	1.74
10	3.13	106012	331378	3.22	2.04	106015	215958	2.10	53%	1.53
11	3.03	106025	321484	3.07	2.13	106012	225820	2.16	42%	1.42
12	4.18	106008	443464	0.56	1.98	106014	209480	0.27	112%	2.12
13	3.40	106014	360866	2.63	1.71	106015	181252	1.32	99%	1.99
14	2.38	106014	251974	0.48	1.74	106013	184504	0.35	37%	1.37
15	2.72	106014	288704	0.79	1.76	106014	186407	0.51	55%	1.55
16	3.50	106014	371070	0.71	1.83	106014	193892	0.37	91%	1.91
17	2.11	106016	223974	0.70	1.83	106016	193488	0.61	16%	1.16
18	2.10	106028	222710	0.95	1.90	106002	201474	0.86	11%	1.11
19	2.08	106010	219972	0.79	1.64	106013	173497	0.62	27%	1.27
20	4.91	105858	519486	2.42	1.99	106016	211382	0.98	146%	2.46
21	3.48	106011	369392	0.68	2.68	106011	284122	0.52	30%	1.30
22	3.14	106015	333044	0.59	1.86	106013	197212	0.35	69%	1.69
23	4.93	106015	523160	0.87	2.32	106013	246310	0.41	112%	2.12
24	5.06	106008	536658	1.33	2.62	106013	277650	0.69	93%	1.93
25	5.19	106011	550446	1.66	2.00	106014	211692	0.64	160%	2.60
26	2.36	106009	250294	1.11	1.91	106014	202962	0.90	23%	1.23
27	7.76	106018	822438	0.67	2.77	106014	293952	0.24	180%	2.80
28	4.11	106013	435446	0.60	2.17	106015	230042	0.32	89%	1.89
29	2.87	106012	304732	1.06	1.46	106015	154291	0.54	98%	1.98
30	5.37	105970	569514	2.50	2.84	106014	301508	1.32	89%	1.89
31	4.13	106015	437842	1.29	1.85	106013	195654	0.58	124%	2.24
32	6.96	106014	738352	3.19	2.22	106013	235576	1.02	213%	3.13
33	3.16	106013	335358	0.67	1.65	106016	175429	0.35	91%	1.91
<b>mean</b>	<b>3.67</b>	<b>106008</b>	<b>389036</b>	<b>1.38</b>	<b>2.05</b>	<b>106013</b>	<b>217437</b>	<b>0.80</b>	<b>78%</b>	<b>1.78</b>

*Table A.15- Comparison between IDA results for Model B, target column chord rotation of 3% with dissipative connections ( $S_{max}$  125 mm) and hinged connections*

<i>Model B – target chord rotation 4.5% - <math>S_{max}</math> 25 mm</i>										
	<i>Dissipative connections</i>				<i>Hinged connections</i>				<i>Comparison</i>	
<i>TH-ID</i>	$q_{col+dev}$	$F_{u,col}$ [N]	$T_{el,col+dev}$ [N]	$SF_{col+dev}$	$q_{col}$	$F_{u,col}$ [N]	$T_{el,col}$ [N]	$SF_{col}$	$\frac{SF_{col+dev}}{SF_{col}}$	$\frac{q_{col+dev}}{q_{col}}$
1	2.87	106758	306086	2.32	2.76	106756	294256	2.23	4%	1.04
2	3.86	106758	411698	0.87	3.64	106759	388142	0.82	6%	1.06
3	4.43	106761	473278	1.76	4.46	106759	476256	1.77	-1%	0.99
4	2.77	106752	295934	0.76	2.41	106758	257174	0.66	15%	1.15
5	4.09	106760	436866	2.88	3.44	106758	367438	2.42	19%	1.19
6	2.38	106761	254174	0.61	2.16	106759	230562	0.55	10%	1.10
7	2.36	106760	251912	0.69	2.19	106758	233626	0.64	8%	1.08
8	2.97	106759	316766	1.47	2.69	106759	287442	1.33	10%	1.10
9	3.74	106759	399122	2.02	3.54	106759	377622	1.91	6%	1.06
10	3.12	106758	332844	3.23	2.99	106756	319252	3.10	4%	1.04
11	3.50	106755	373358	3.57	3.13	106755	334024	3.19	12%	1.12
12	3.18	106758	339774	0.43	2.74	106760	292012	0.37	16%	1.16
13	2.90	106757	309734	2.26	2.63	106759	281122	2.05	10%	1.10
14	2.45	106759	261636	0.50	2.25	106758	240376	0.46	9%	1.09
15	2.75	106758	293620	0.81	2.36	106759	251546	0.69	17%	1.17
16	3.56	106760	380194	0.73	2.88	106759	307264	0.59	24%	1.24
17	2.71	106749	288798	0.90	2.54	106757	271428	0.85	6%	1.06
18	2.95	106767	315452	1.34	2.75	106771	293534	1.25	7%	1.07
19	2.11	106757	224882	0.80	2.07	106757	221120	0.79	2%	1.02
20	3.69	106757	393700	1.83	3.17	106755	338898	1.58	16%	1.16
21	3.97	106755	423754	0.78	3.73	106753	398200	0.73	6%	1.06
22	3.21	106750	342738	0.61	2.77	106760	295570	0.53	16%	1.16
23	4.46	106764	475672	0.79	3.61	106759	385056	0.64	24%	1.24
24	4.26	106730	455202	1.13	3.72	106757	397272	0.99	15%	1.15
25	5.28	106758	564150	1.70	3.90	106758	416050	1.26	36%	1.36
26	2.29	106758	244270	1.08	2.15	106763	229344	1.02	7%	1.07
27	6.73	106757	718288	0.59	6.82	106756	728178	0.60	-1%	0.99
28	3.53	106762	376908	0.52	3.09	106762	329652	0.45	14%	1.14
29	2.62	106757	279948	0.97	2.01	106760	215102	0.75	30%	1.30
30	4.64	106760	495184	2.17	4.10	106760	437276	1.92	13%	1.13
31	3.04	106767	324178	0.96	2.48	106762	265058	0.78	22%	1.22
32	5.25	106759	560114	2.42	4.00	106760	426928	1.85	31%	1.31
33	2.58	106760	275288	0.55	2.27	106761	242212	0.48	14%	1.14
<b>mean</b>	<b>3.46</b>	<b>106758</b>	<b>369561</b>	<b>1.33</b>	<b>3.07</b>	<b>106759</b>	<b>328151</b>	<b>1.19</b>	<b>13%</b>	<b>1.13</b>

*Table A.16- Comparison between IDA results for Model B, target column chord rotation of 4.5% with dissipative connections ( $S_{max}$  25 mm) and hinged connections*

<i>Model B – target chord rotation 4.5% - <math>S_{max}</math> 50 mm</i>										
	<i>Dissipative connections</i>				<i>Hinged connections</i>				<i>Comparison</i>	
<i>TH-ID</i>	$q_{col+dev}$	$F_{u,col}$ [N]	$T_{el,col+dev}$ [N]	$SF_{col+dev}$	$q_{col}$	$F_{u,col}$ [N]	$T_{el,col}$ [N]	$SF_{col}$	$\frac{SF_{col+dev}}{SF_{col}}$	$\frac{q_{col+dev}}{q_{col}}$
1	2.97	106758	317022	2.40	2.76	106756	294256	2.23	8%	1.08
2	4.06	106757	433224	0.91	3.64	106759	388142	0.82	12%	1.12
3	4.21	106761	449958	1.67	4.46	106759	476256	1.77	-6%	0.94
4	3.40	106745	363224	0.93	2.41	106758	257174	0.66	41%	1.41
5	4.52	106765	482592	3.18	3.44	106758	367438	2.42	31%	1.31
6	2.59	106759	276776	0.66	2.16	106759	230562	0.55	20%	1.20
7	2.57	106760	274166	0.75	2.19	106758	233626	0.64	17%	1.17
8	3.45	106758	368552	1.71	2.69	106759	287442	1.33	28%	1.28
9	3.92	106759	418946	2.12	3.54	106759	377622	1.91	11%	1.11
10	3.14	106760	335414	3.26	2.99	106756	319252	3.10	5%	1.05
11	3.96	106771	422612	4.04	3.13	106755	334024	3.19	27%	1.27
12	3.64	106759	388350	0.49	2.74	106760	292012	0.37	33%	1.33
13	3.13	106761	334596	2.44	2.63	106759	281122	2.05	19%	1.19
14	2.62	106757	279992	0.53	2.25	106758	240376	0.46	16%	1.16
15	3.04	106758	324528	0.89	2.36	106759	251546	0.69	29%	1.29
16	3.73	106758	397914	0.76	2.88	106759	307264	0.59	30%	1.30
17	2.86	106754	305304	0.96	2.54	106757	271428	0.85	12%	1.12
18	3.02	106729	321806	1.37	2.75	106771	293534	1.25	10%	1.10
19	2.17	106758	231288	0.83	2.07	106757	221120	0.79	5%	1.05
20	4.23	106773	451122	2.10	3.17	106755	338898	1.58	33%	1.33
21	4.19	106753	447592	0.82	3.73	106753	398200	0.73	12%	1.12
22	3.87	106769	412786	0.73	2.77	106760	295570	0.53	40%	1.40
23	4.90	106764	522618	0.87	3.61	106759	385056	0.64	36%	1.36
24	4.82	106761	514300	1.28	3.72	106757	397272	0.99	29%	1.29
25	5.55	106756	592086	1.79	3.90	106758	416050	1.26	42%	1.42
26	2.45	106760	261598	1.16	2.15	106763	229344	1.02	14%	1.14
27	7.15	106758	763344	0.63	6.82	106756	728178	0.60	5%	1.05
28	3.96	106762	422300	0.58	3.09	106762	329652	0.45	28%	1.28
29	3.11	106759	331784	1.16	2.01	106760	215102	0.75	54%	1.54
30	6.02	106752	642692	2.82	4.10	106760	437276	1.92	47%	1.47
31	3.66	106756	390752	1.16	2.48	106762	265058	0.78	47%	1.47
32	6.04	106762	645266	2.79	4.00	106760	426928	1.85	51%	1.51
33	2.90	106760	309480	0.62	2.27	106761	242212	0.48	28%	1.28
<b>mean</b>	<b>3.81</b>	<b>106758</b>	<b>407090</b>	<b>1.47</b>	<b>3.07</b>	<b>106759</b>	<b>328151</b>	<b>1.19</b>	<b>25%</b>	<b>1.25</b>

*Table A.17- Comparison between IDA results for Model B, target column chord rotation of 4.5% with dissipative connections ( $S_{max}$  50 mm) and hinged connections*

<i>Model B – target chord rotation 4.5% - <math>S_{max}</math> 75 mm</i>										
	<i>Dissipative connections</i>				<i>Hinged connections</i>				<i>Comparison</i>	
<i>TH-ID</i>	$q_{col+dev}$	$F_{u,col}$ [N]	$T_{el,col+dev}$ [N]	$SF_{col+dev}$	$q_{col}$	$F_{u,col}$ [N]	$T_{el,col}$ [N]	$SF_{col}$	$\frac{SF_{col+dev}}{SF_{col}}$	$\frac{q_{col+dev}}{q_{col}}$
1	3.07	106759	327730	2.48	2.76	106756	294256	2.23	11%	1.11
2	4.26	106755	454570	0.96	3.64	106759	388142	0.82	17%	1.17
3	4.10	106758	437296	1.62	4.46	106759	476256	1.77	-8%	0.92
4	3.75	106772	399996	1.02	2.41	106758	257174	0.66	56%	1.56
5	4.77	106760	509710	3.36	3.44	106758	367438	2.42	39%	1.39
6	2.79	106759	298062	0.72	2.16	106759	230562	0.55	29%	1.29
7	2.74	106760	292212	0.80	2.19	106758	233626	0.64	25%	1.25
8	4.09	106759	436294	2.02	2.69	106759	287442	1.33	52%	1.52
9	4.11	106758	438254	2.22	3.54	106759	377622	1.91	16%	1.16
10	3.04	106758	324596	3.15	2.99	106756	319252	3.10	2%	1.02
11	4.29	106746	457576	4.38	3.13	106755	334024	3.19	37%	1.37
12	4.11	106763	438694	0.56	2.74	106760	292012	0.37	50%	1.50
13	3.21	106755	342754	2.50	2.63	106759	281122	2.05	22%	1.22
14	2.79	106760	297782	0.56	2.25	106758	240376	0.46	24%	1.24
15	3.27	106757	349028	0.96	2.36	106759	251546	0.69	39%	1.39
16	3.90	106758	415982	0.80	2.88	106759	307264	0.59	35%	1.35
17	2.89	106752	308190	0.96	2.54	106757	271428	0.85	14%	1.14
18	3.02	106729	321806	1.37	2.75	106771	293534	1.25	10%	1.10
19	2.22	106757	237188	0.85	2.07	106757	221120	0.79	7%	1.07
20	4.76	106742	507720	2.36	3.17	106755	338898	1.58	50%	1.50
21	4.41	106758	471164	0.86	3.73	106753	398200	0.73	18%	1.18
22	4.25	106749	453752	0.81	2.77	106760	295570	0.53	54%	1.54
23	5.16	106763	550366	0.92	3.61	106759	385056	0.64	43%	1.43
24	5.33	106751	568864	1.41	3.72	106757	397272	0.99	43%	1.43
25	5.81	106756	620562	1.87	3.90	106758	416050	1.26	49%	1.49
26	2.55	106762	272140	1.21	2.15	106763	229344	1.02	19%	1.19
27	8.73	106749	932286	0.76	6.82	106756	728178	0.60	28%	1.28
28	4.43	106760	473138	0.65	3.09	106762	329652	0.45	44%	1.44
29	3.23	106757	344698	1.20	2.01	106760	215102	0.75	60%	1.60
30	6.05	106741	645366	2.83	4.10	106760	437276	1.92	48%	1.48
31	4.29	106767	457988	1.35	2.48	106762	265058	0.78	73%	1.73
32	6.86	106757	732640	3.17	4.00	106760	426928	1.85	72%	1.72
33	3.21	106760	342742	0.68	2.27	106761	242212	0.48	42%	1.42
<b>mean</b>	<b>4.10</b>	<b>106756</b>	<b>438217</b>	<b>1.56</b>	<b>3.07</b>	<b>106759</b>	<b>328151</b>	<b>1.19</b>	<b>34%</b>	<b>1.34</b>

*Table A.18- Comparison between IDA results for Model B, target column chord rotation of 4.5% with dissipative connections ( $S_{max}$  75 mm) and hinged connections*

<i>Model B – target chord rotation 4.5% - <math>S_{max}</math> 100 mm</i>										
	<i>Dissipative connections</i>				<i>Hinged connections</i>				<i>Comparison</i>	
<i>TH-ID</i>	$q_{col+dev}$	$F_{u,col}$ [N]	$T_{el,col+dev}$ [N]	$SF_{col+dev}$	$q_{col}$	$F_{u,col}$ [N]	$T_{el,col}$ [N]	$SF_{col}$	$\frac{SF_{col+dev}}{SF_{col}}$	$\frac{q_{col+dev}}{q_{col}}$
1	3.17	106758	338486	2.56	2.76	106756	294256	2.23	15%	1.15
2	4.45	106751	475520	1.00	3.64	106759	388142	0.82	23%	1.23
3	3.99	106758	425958	1.58	4.46	106759	476256	1.77	-11%	0.89
4	4.01	106723	427778	1.09	2.41	106758	257174	0.66	66%	1.66
5	5.09	106755	543348	3.58	3.44	106758	367438	2.42	48%	1.48
6	3.01	106758	321550	0.77	2.16	106759	230562	0.55	39%	1.39
7	2.87	106759	306856	0.84	2.19	106758	233626	0.64	31%	1.31
8	4.46	106758	475940	2.21	2.69	106759	287442	1.33	66%	1.66
9	4.28	106758	456638	2.31	3.54	106759	377622	1.91	21%	1.21
10	3.05	106757	325854	3.16	2.99	106756	319252	3.10	2%	1.02
11	4.71	106749	502712	4.81	3.13	106755	334024	3.19	51%	1.51
12	4.64	106760	494976	0.63	2.74	106760	292012	0.37	70%	1.70
13	3.61	106757	385472	2.81	2.63	106759	281122	2.05	37%	1.37
14	2.96	106758	315602	0.60	2.25	106758	240376	0.46	31%	1.31
15	3.50	106758	374100	1.03	2.36	106759	251546	0.69	49%	1.49
16	4.06	106758	433600	0.83	2.88	106759	307264	0.59	41%	1.41
17	2.89	106752	308190	0.96	2.54	106757	271428	0.85	14%	1.14
18	3.02	106729	321806	1.37	2.75	106771	293534	1.25	10%	1.10
19	2.28	106758	243270	0.87	2.07	106757	221120	0.79	10%	1.10
20	5.15	106722	549416	2.56	3.17	106755	338898	1.58	62%	1.62
21	4.63	106756	494140	0.90	3.73	106753	398200	0.73	24%	1.24
22	4.69	106760	500710	0.89	2.77	106760	295570	0.53	69%	1.69
23	5.47	106759	583494	0.97	3.61	106759	385056	0.64	52%	1.52
24	5.85	106773	624258	1.55	3.72	106757	397272	0.99	57%	1.57
25	6.08	106756	648652	1.96	3.90	106758	416050	1.26	56%	1.56
26	2.58	106761	275910	1.22	2.15	106763	229344	1.02	20%	1.20
27	9.08	106752	969350	0.80	6.82	106756	728178	0.60	33%	1.33
28	4.75	106757	507236	0.70	3.09	106762	329652	0.45	54%	1.54
29	3.14	106758	335450	1.17	2.01	106760	215102	0.75	56%	1.56
30	6.05	106757	645626	2.83	4.10	106760	437276	1.92	48%	1.48
31	4.93	106757	526004	1.56	2.48	106762	265058	0.78	98%	1.98
32	7.85	106756	838030	3.62	4.00	106760	426928	1.85	96%	1.96
33	3.53	106760	376708	0.75	2.27	106761	242212	0.48	56%	1.56
<b>mean</b>	<b>4.36</b>	<b>106755</b>	<b>465232</b>	<b>1.65</b>	<b>3.07</b>	<b>106759</b>	<b>328151</b>	<b>1.19</b>	<b>42%</b>	<b>1.42</b>

*Table A.19- Comparison between IDA results for Model B, target column chord rotation of 4.5% with dissipative connections ( $S_{max}$  100 mm) and hinged connections*

<i>Model B – target chord rotation 4.5% - <math>S_{max}</math> 125 mm</i>										
	<i>Dissipative connections</i>				<i>Hinged connections</i>				<i>Comparison</i>	
<i>TH-ID</i>	$q_{col+dev}$	$F_{u,col}$ [N]	$T_{el,col+dev}$ [N]	$SF_{col+dev}$	$q_{col}$	$F_{u,col}$ [N]	$T_{el,col}$ [N]	$SF_{col}$	$\frac{SF_{col+dev}}{SF_{col}}$	$\frac{q_{col+dev}}{q_{col}}$
1	3.27	106758	349216	2.64	2.76	106756	294256	2.23	19%	1.19
2	4.65	106760	496432	1.05	3.64	106759	388142	0.82	28%	1.28
3	4.02	106739	428640	1.59	4.46	106759	476256	1.77	-10%	0.90
4	4.18	106776	446462	1.14	2.41	106758	257174	0.66	74%	1.74
5	5.44	106758	581010	3.83	3.44	106758	367438	2.42	58%	1.58
6	3.25	106760	347244	0.83	2.16	106759	230562	0.55	51%	1.51
7	3.03	106757	323020	0.89	2.19	106758	233626	0.64	38%	1.38
8	4.83	106758	515494	2.39	2.69	106759	287442	1.33	79%	1.79
9	4.45	106758	474734	2.40	3.54	106759	377622	1.91	26%	1.26
10	3.51	106754	374768	3.64	2.99	106756	319252	3.10	17%	1.17
11	5.04	106755	537650	5.14	3.13	106755	334024	3.19	61%	1.61
12	5.25	106762	560528	0.71	2.74	106760	292012	0.37	92%	1.92
13	3.89	106759	415138	3.03	2.63	106759	281122	2.05	48%	1.48
14	3.12	106759	333564	0.63	2.25	106758	240376	0.46	39%	1.39
15	3.74	106757	398830	1.10	2.36	106759	251546	0.69	59%	1.59
16	4.22	106759	451028	0.86	2.88	106759	307264	0.59	47%	1.47
17	2.89	106752	308190	0.96	2.54	106757	271428	0.85	14%	1.14
18	3.02	106729	321806	1.37	2.75	106771	293534	1.25	10%	1.10
19	2.34	106756	249400	0.89	2.07	106757	221120	0.79	13%	1.13
20	5.83	106726	621884	2.89	3.17	106755	338898	1.58	84%	1.84
21	4.73	106758	504638	0.92	3.73	106753	398200	0.73	27%	1.27
22	4.92	106754	525534	0.93	2.77	106760	295570	0.53	78%	1.78
23	5.75	106758	613948	1.02	3.61	106759	385056	0.64	59%	1.59
24	6.15	106762	656672	1.63	3.72	106757	397272	0.99	65%	1.65
25	6.34	106756	676488	2.04	3.90	106758	416050	1.26	63%	1.63
26	2.71	106760	288934	1.28	2.15	106763	229344	1.02	26%	1.26
27	9.91	106757	1057516	0.87	6.82	106756	728178	0.60	45%	1.45
28	4.94	106757	527284	0.73	3.09	106762	329652	0.45	60%	1.60
29	3.27	106758	348800	1.21	2.01	106760	215102	0.75	62%	1.62
30	6.26	106747	668158	2.93	4.10	106760	437276	1.92	53%	1.53
31	5.64	106727	602250	1.78	2.48	106762	265058	0.78	127%	2.27
32	8.84	106748	943248	4.08	4.00	106760	426928	1.85	121%	2.21
33	3.85	106757	410542	0.82	2.27	106761	242212	0.48	69%	1.70
<b>mean</b>	<b>4.64</b>	<b>106754</b>	<b>495729</b>	<b>1.76</b>	<b>3.07</b>	<b>106759</b>	<b>328151</b>	<b>1.19</b>	<b>51%</b>	<b>1.52</b>

*Table A.20- Comparison between IDA results for Model B, target column chord rotation of 4.5% with dissipative connections ( $S_{max}$  125 mm) and hinged connections*

<i>Model C – target chord rotation 3% - <math>S_{max}</math> 25 mm</i>										
	<i>Dissipative connections</i>				<i>Hinged connections</i>				<i>Comparison</i>	
<i>TH-ID</i>	$q_{col+dev}$	$F_{u,col}$ [N]	$T_{el,col+dev}$ [N]	$SF_{col+dev}$	$q_{col}$	$F_{u,col}$ [N]	$T_{el,col}$ [N]	$SF_{col}$	$\frac{SF_{col+dev}}{SF_{col}}$	$\frac{q_{col+dev}}{q_{col}}$
1	2.41	168712	406506	1.71	1.60	168710	270688	1.14	50%	1.50
2	3.21	168706	542108	0.58	2.57	168707	433426	0.47	25%	1.25
3	4.94	168704	833040	1.36	3.19	168706	537510	0.88	55%	1.55
4	1.93	168711	325098	0.48	1.71	168723	287972	0.42	13%	1.13
5	2.50	168679	421012	1.64	2.03	168716	342602	1.33	23%	1.23
6	2.01	168711	338566	0.45	1.72	168711	290424	0.39	17%	1.17
7	1.96	168712	331142	0.52	1.73	168713	291902	0.45	13%	1.13
8	2.64	168708	444888	1.14	2.21	168711	372780	0.95	19%	1.19
9	3.05	168709	514308	1.38	2.13	168709	360192	0.97	43%	1.43
10	3.43	168702	579174	2.29	2.85	168713	481158	1.90	20%	1.20
11	2.70	168664	455860	2.40	2.08	168708	351390	1.85	30%	1.30
12	2.29	168718	386784	0.29	2.00	168711	337352	0.25	15%	1.15
13	2.64	168711	445276	1.47	2.37	168712	400638	1.32	11%	1.11
14	2.42	168709	407692	0.35	2.23	168709	376730	0.33	8%	1.08
15	2.03	168717	343084	0.50	1.83	168711	309116	0.45	11%	1.11
16	2.32	168713	391702	0.41	1.90	168714	321148	0.34	22%	1.22
17	2.13	168716	359182	0.60	1.91	168702	321906	0.54	12%	1.12
18	2.27	168569	381900	0.82	2.00	168627	337674	0.72	13%	1.13
19	1.84	168709	309922	0.57	1.70	168708	287160	0.53	8%	1.08
20	3.41	168604	574194	1.32	2.02	168708	340928	0.78	68%	1.69
21	3.32	168706	560696	0.52	2.49	168714	419654	0.39	34%	1.34
22	2.54	168718	427852	0.40	1.98	168718	333908	0.31	28%	1.28
23	3.01	168710	507004	0.49	2.15	168715	363042	0.35	40%	1.40
24	3.78	168669	637440	0.81	2.75	168717	463992	0.59	37%	1.37
25	2.55	168709	429674	0.72	1.94	168708	326664	0.55	32%	1.32
26	2.72	168713	458582	0.87	2.48	168716	418052	0.80	10%	1.10
27	3.91	168712	659860	0.30	2.72	168712	459460	0.21	44%	1.44
28	2.81	168717	474296	0.35	2.28	168715	384498	0.29	23%	1.23
29	2.15	168713	362254	0.64	1.62	168716	273972	0.48	32%	1.32
30	2.85	168688	481118	1.38	2.25	168712	379050	1.09	27%	1.27
31	2.50	168693	422226	0.65	2.01	168717	338648	0.52	25%	1.25
32	3.32	168704	560392	1.25	2.38	168703	401182	0.89	40%	1.40
33	2.17	168718	366338	0.39	1.75	168721	295084	0.31	24%	1.24
<b>mean</b>	<b>2.72</b>	<b>168699</b>	<b>458763</b>	<b>0.88</b>	<b>2.14</b>	<b>168709</b>	<b>360906</b>	<b>0.69</b>	<b>26%</b>	<b>1.26</b>

*Table A.21- Comparison between IDA results for Model C, target column chord rotation of 3% with dissipative connections ( $S_{max}$  25 mm) and hinged connections*

<i>Model C – target chord rotation 3% - <math>S_{max}</math> 50 mm</i>										
	<i>Dissipative connections</i>				<i>Hinged connections</i>				<i>Comparison</i>	
<i>TH-ID</i>	$q_{col+dev}$	$F_{u,col}$ [N]	$T_{el,col+dev}$ [N]	$SF_{col+dev}$	$q_{col}$	$F_{u,col}$ [N]	$T_{el,col}$ [N]	$SF_{col}$	$\frac{SF_{col+dev}}{SF_{col}}$	$\frac{q_{col+dev}}{q_{col}}$
1	2.56	168710	431650	1.82	1.60	168710	270688	1.14	59%	1.59
2	3.50	168701	590606	0.64	2.57	168707	433426	0.47	36%	1.36
3	5.01	168744	845490	1.38	3.19	168706	537510	0.88	57%	1.57
4	2.36	168672	397878	0.59	1.71	168723	287972	0.42	38%	1.38
5	3.09	168668	521326	2.03	2.03	168716	342602	1.33	52%	1.52
6	2.28	168717	384330	0.51	1.72	168711	290424	0.39	32%	1.32
7	2.16	168706	364906	0.57	1.73	168713	291902	0.45	25%	1.25
8	3.01	168709	507338	1.30	2.21	168711	372780	0.95	36%	1.36
9	3.30	168711	556532	1.50	2.13	168709	360192	0.97	55%	1.55
10	3.03	168709	511494	2.02	2.85	168713	481158	1.90	6%	1.06
11	3.12	168700	527120	2.78	2.08	168708	351390	1.85	50%	1.50
12	2.66	168720	448300	0.34	2.00	168711	337352	0.25	33%	1.33
13	3.26	168718	550678	1.82	2.37	168712	400638	1.32	37%	1.37
14	2.58	168709	435260	0.38	2.23	168709	376730	0.33	16%	1.16
15	2.21	168670	373074	0.55	1.83	168711	309116	0.45	21%	1.21
16	2.80	168705	471646	0.50	1.90	168714	321148	0.34	47%	1.47
17	2.32	168717	390888	0.65	1.91	168702	321906	0.54	21%	1.21
18	2.32	168632	390426	0.83	2.00	168627	337674	0.72	16%	1.16
19	1.95	168711	329466	0.61	1.70	168708	287160	0.53	15%	1.15
20	3.74	168637	631060	1.45	2.02	168708	340928	0.78	85%	1.85
21	3.64	168687	614142	0.57	2.49	168714	419654	0.39	46%	1.46
22	2.98	168697	503360	0.47	1.98	168718	333908	0.31	51%	1.51
23	3.63	168714	612370	0.59	2.15	168715	363042	0.35	69%	1.69
24	4.30	168655	724592	0.92	2.75	168717	463992	0.59	56%	1.56
25	3.35	168706	565464	0.94	1.94	168708	326664	0.55	73%	1.73
26	2.91	168715	490644	0.93	2.48	168716	418052	0.80	17%	1.17
27	4.89	168700	824790	0.38	2.72	168712	459460	0.21	80%	1.80
28	3.24	168713	546234	0.41	2.28	168715	384498	0.29	42%	1.42
29	2.71	168710	456522	0.80	1.62	168716	273972	0.48	67%	1.67
30	3.18	168686	536750	1.54	2.25	168712	379050	1.09	42%	1.42
31	2.98	168677	503396	0.77	2.01	168717	338648	0.52	49%	1.49
32	4.61	168717	777860	1.73	2.38	168703	401182	0.89	94%	1.94
33	2.59	168718	437218	0.47	1.75	168721	295084	0.31	48%	1.48
<b>mean</b>	<b>3.10</b>	<b>168699</b>	<b>522812</b>	<b>0.99</b>	<b>2.14</b>	<b>168709</b>	<b>360906</b>	<b>0.69</b>	<b>45%</b>	<b>1.45</b>

Table A.22- Comparison between IDA results for Model C, target column chord rotation of 3% with dissipative connections ( $S_{max}$  50 mm) and hinged connections

<i>Model C – target chord rotation 3% - <math>S_{max}</math> 75 mm</i>										
	<i>Dissipative connections</i>				<i>Hinged connections</i>				<i>Comparison</i>	
<i>TH-ID</i>	$q_{col+dev}$	$F_{u,col}$ [N]	$T_{el,col+dev}$ [N]	$SF_{col+dev}$	$q_{col}$	$F_{u,col}$ [N]	$T_{el,col}$ [N]	$SF_{col}$	$\frac{SF_{col+dev}}{SF_{col}}$	$\frac{q_{col+dev}}{q_{col}}$
1	2.71	168703	456668	1.92	1.60	168710	270688	1.14	69%	1.69
2	3.78	168702	637194	0.69	2.57	168707	433426	0.47	47%	1.47
3	5.04	168746	850070	1.39	3.19	168706	537510	0.88	58%	1.58
4	2.80	168647	471394	0.70	1.71	168723	287972	0.42	64%	1.64
5	3.31	168631	558202	2.17	2.03	168716	342602	1.33	63%	1.63
6	2.53	168705	426228	0.57	1.72	168711	290424	0.39	47%	1.47
7	2.33	168713	392552	0.61	1.73	168713	291902	0.45	34%	1.34
8	3.21	168709	541084	1.38	2.21	168711	372780	0.95	45%	1.45
9	3.54	168713	597244	1.61	2.13	168709	360192	0.97	66%	1.66
10	3.32	168707	559796	2.21	2.85	168713	481158	1.90	16%	1.16
11	3.53	168698	595320	3.14	2.08	168708	351390	1.85	69%	1.69
12	3.04	168713	512146	0.38	2.00	168711	337352	0.25	52%	1.52
13	3.64	168710	613304	2.02	2.37	168712	400638	1.32	53%	1.53
14	2.74	168716	462066	0.40	2.23	168709	376730	0.33	23%	1.23
15	2.46	168712	414548	0.61	1.83	168711	309116	0.45	34%	1.34
16	3.30	168714	556566	0.59	1.90	168714	321148	0.34	73%	1.73
17	2.32	168717	390910	0.65	1.91	168702	321906	0.54	21%	1.21
18	2.32	168632	390426	0.83	2.00	168627	337674	0.72	16%	1.16
19	2.05	168710	345328	0.64	1.70	168708	287160	0.53	20%	1.20
20	4.22	168689	711796	1.64	2.02	168708	340928	0.78	109%	2.09
21	3.95	168687	665570	0.61	2.49	168714	419654	0.39	59%	1.59
22	3.29	168668	555514	0.52	1.98	168718	333908	0.31	66%	1.66
23	4.18	168717	705336	0.68	2.15	168715	363042	0.35	94%	1.94
24	4.93	168680	831474	1.05	2.75	168717	463992	0.59	79%	1.79
25	4.69	168704	791800	1.32	1.94	168708	326664	0.55	142%	2.42
26	2.94	168713	495568	0.94	2.48	168716	418052	0.80	19%	1.19
27	6.24	168697	1051964	0.48	2.72	168712	459460	0.21	129%	2.29
28	3.63	168715	612624	0.46	2.28	168715	384498	0.29	59%	1.59
29	3.03	168708	510876	0.90	1.62	168716	273972	0.48	86%	1.86
30	3.62	168690	611094	1.76	2.25	168712	379050	1.09	61%	1.61
31	3.47	168705	584820	0.90	2.01	168717	338648	0.52	73%	1.73
32	5.97	168702	1006706	2.24	2.38	168703	401182	0.89	151%	2.51
33	2.97	168717	500962	0.53	1.75	168721	295084	0.31	70%	1.70
<b>mean</b>	<b>3.49</b>	<b>168700</b>	<b>588095</b>	<b>1.11</b>	<b>2.14</b>	<b>168709</b>	<b>360906</b>	<b>0.69</b>	<b>63%</b>	<b>1.63</b>

*Table A.23- Comparison between IDA results for Model C, target column chord rotation of 3% with dissipative connections ( $S_{max}$  75 mm) and hinged connections*

<i>Model C – target chord rotation 3% - <math>S_{max}</math> 100 mm</i>										
	<i>Dissipative connections</i>				<i>Hinged connections</i>				<i>Comparison</i>	
<i>TH-ID</i>	$q_{col+dev}$	$F_{u,col}$ [N]	$T_{el,col+dev}$ [N]	$SF_{col+dev}$	$q_{col}$	$F_{u,col}$ [N]	$T_{el,col}$ [N]	$SF_{col}$	$\frac{SF_{col+dev}}{SF_{col}}$	$\frac{q_{col+dev}}{q_{col}}$
1	2.85	168707	480414	2.02	1.60	168710	270688	1.14	77%	1.77
2	4.05	168704	682662	0.74	2.57	168707	433426	0.47	58%	1.58
3	4.85	168721	818496	1.34	3.19	168706	537510	0.88	52%	1.52
4	3.12	168715	525844	0.78	1.71	168723	287972	0.42	83%	1.83
5	3.59	168674	606282	2.36	2.03	168716	342602	1.33	77%	1.77
6	2.77	168722	466540	0.62	1.72	168711	290424	0.39	61%	1.61
7	2.54	168718	428176	0.67	1.73	168713	291902	0.45	47%	1.47
8	3.33	168716	561470	1.43	2.21	168711	372780	0.95	51%	1.51
9	3.77	168712	636232	1.71	2.13	168709	360192	0.97	77%	1.77
10	3.69	168703	623290	2.46	2.85	168713	481158	1.90	30%	1.30
11	3.50	168721	591120	3.11	2.08	168708	351390	1.85	68%	1.68
12	3.47	168717	585044	0.44	2.00	168711	337352	0.25	73%	1.73
13	3.68	168717	621010	2.05	2.37	168712	400638	1.32	55%	1.55
14	2.91	168714	490522	0.43	2.23	168709	376730	0.33	30%	1.30
15	2.73	168680	460460	0.67	1.83	168711	309116	0.45	49%	1.49
16	3.51	168712	592586	0.62	1.90	168714	321148	0.34	85%	1.85
17	2.32	168717	390910	0.65	1.91	168702	321906	0.54	21%	1.21
18	2.32	168632	390426	0.83	2.00	168627	337674	0.72	16%	1.16
19	2.14	168705	361392	0.67	1.70	168708	287160	0.53	26%	1.26
20	4.62	168690	779234	1.79	2.02	168708	340928	0.78	129%	2.29
21	4.25	168683	716890	0.66	2.49	168714	419654	0.39	71%	1.71
22	3.54	168721	596736	0.56	1.98	168718	333908	0.31	79%	1.79
23	4.62	168716	778940	0.75	2.15	168715	363042	0.35	115%	2.15
24	5.25	168593	885802	1.12	2.75	168717	463992	0.59	91%	1.91
25	5.01	168701	844510	1.41	1.94	168708	326664	0.55	159%	2.59
26	3.00	168701	506926	0.97	2.48	168716	418052	0.80	21%	1.21
27	7.22	168689	1217630	0.56	2.72	168712	459460	0.21	165%	2.65
28	4.28	168705	721392	0.54	2.28	168715	384498	0.29	88%	1.88
29	3.25	168715	548258	0.96	1.62	168716	273972	0.48	100%	2.00
30	4.13	168677	697302	2.01	2.25	168712	379050	1.09	84%	1.84
31	4.02	168717	678452	1.04	2.01	168717	338648	0.52	100%	2.00
32	7.11	168723	1198920	2.67	2.38	168703	401182	0.89	199%	2.99
33	3.23	168717	545098	0.58	1.75	168721	295084	0.31	85%	1.85
<b>mean</b>	<b>3.78</b>	<b>168702</b>	<b>637241</b>	<b>1.19</b>	<b>2.14</b>	<b>168709</b>	<b>360906</b>	<b>0.69</b>	<b>76%</b>	<b>1.76</b>

*Table A.24- Comparison between IDA results for Model C, target column chord rotation of 3% with dissipative connections ( $S_{max}$  100 mm) and hinged connections*

<i>Model C – target chord rotation 3% - <math>S_{max}</math> 125 mm</i>										
	<i>Dissipative connections</i>				<i>Hinged connections</i>				<i>Comparison</i>	
<i>TH-ID</i>	$q_{col+dev}$	$F_{u,col}$ [N]	$T_{el,col+dev}$ [N]	$SF_{col+dev}$	$q_{col}$	$F_{u,col}$ [N]	$T_{el,col}$ [N]	$SF_{col}$	$\frac{SF_{col+dev}}{SF_{col}}$	$\frac{q_{col+dev}}{q_{col}}$
1	2.97	168708	500858	2.11	1.60	168710	270688	1.14	85%	1.85
2	4.24	168707	714940	0.77	2.57	168707	433426	0.47	65%	1.65
3	5.19	168712	875998	1.43	3.19	168706	537510	0.88	63%	1.63
4	3.13	168651	528636	0.78	1.71	168723	287972	0.42	84%	1.84
5	3.72	168680	628114	2.44	2.03	168716	342602	1.33	83%	1.83
6	3.00	168713	506286	0.68	1.72	168711	290424	0.39	74%	1.74
7	2.73	168718	459968	0.72	1.73	168713	291902	0.45	58%	1.58
8	3.62	168707	611454	1.56	2.21	168711	372780	0.95	64%	1.64
9	3.99	168714	673800	1.81	2.13	168709	360192	0.97	87%	1.87
10	4.12	168695	694620	2.75	2.85	168713	481158	1.90	44%	1.44
11	3.50	168721	591120	3.11	2.08	168708	351390	1.85	68%	1.68
12	3.98	168724	670864	0.50	2.00	168711	337352	0.25	99%	1.99
13	3.88	168711	654738	2.16	2.37	168712	400638	1.32	63%	1.63
14	3.12	168706	526968	0.46	2.23	168709	376730	0.33	40%	1.40
15	3.00	168693	506548	0.74	1.83	168711	309116	0.45	64%	1.64
16	3.72	168708	627518	0.66	1.90	168714	321148	0.34	95%	1.95
17	2.32	168717	390910	0.65	1.91	168702	321906	0.54	21%	1.21
18	2.32	168632	390426	0.83	2.00	168627	337674	0.72	16%	1.16
19	2.24	168702	377950	0.70	1.70	168708	287160	0.53	32%	1.32
20	5.67	169070	958398	2.20	2.02	168708	340928	0.78	181%	2.81
21	4.29	168700	723910	0.67	2.49	168714	419654	0.39	73%	1.73
22	3.54	168721	596736	0.56	1.98	168718	333908	0.31	79%	1.79
23	4.86	168720	819732	0.79	2.15	168715	363042	0.35	126%	2.26
24	5.60	168699	943896	1.19	2.75	168717	463992	0.59	103%	2.03
25	5.32	168700	896934	1.50	1.94	168708	326664	0.55	175%	2.75
26	3.18	168706	536924	1.02	2.48	168716	418052	0.80	28%	1.28
27	7.63	168709	1287912	0.59	2.72	168712	459460	0.21	180%	2.80
28	4.52	168703	762846	0.57	2.28	168715	384498	0.29	98%	1.98
29	3.45	168710	581676	1.02	1.62	168716	273972	0.48	112%	2.12
30	4.86	168596	819088	2.36	2.25	168712	379050	1.09	116%	2.16
31	4.75	168702	801448	1.23	2.01	168717	338648	0.52	137%	2.37
32	8.02	168705	1353578	3.02	2.38	168703	401182	0.89	237%	3.37
33	3.49	168712	588148	0.63	1.75	168721	295084	0.31	99%	1.99
<b>mean</b>	<b>4.06</b>	<b>168711</b>	<b>684938</b>	<b>1.28</b>	<b>2.14</b>	<b>168709</b>	<b>360906</b>	<b>0.69</b>	<b>89%</b>	<b>1.89</b>

*Table A.25- Comparison between IDA results for Model C, target column chord rotation of 3% with dissipative connections ( $S_{max}$  125 mm) and hinged connections*

<i>Model C – target chord rotation 4.5% - <math>S_{max}</math> 25 mm</i>										
	<i>Dissipative connections</i>				<i>Hinged connections</i>				<i>Comparison</i>	
<i>TH-ID</i>	$q_{col+dev}$	$F_{u,col}$ [N]	$T_{el,col+dev}$ [N]	$SF_{col+dev}$	$q_{col}$	$F_{u,col}$ [N]	$T_{el,col}$ [N]	$SF_{col}$	$\frac{SF_{col+dev}}{SF_{col}}$	$\frac{q_{col+dev}}{q_{col}}$
1	2.91	170414	496520	2.09	2.80	170413	477190	2.01	4%	1.04
2	4.20	170419	715038	0.77	3.92	170415	667760	0.72	7%	1.07
3	5.62	170420	958418	1.56	5.68	170417	967360	1.58	-1%	0.99
4	2.67	170403	455608	0.67	2.40	170405	408956	0.60	11%	1.11
5	3.76	170386	641062	2.49	3.21	170404	546362	2.12	17%	1.17
6	2.43	170423	414580	0.55	2.21	170421	376916	0.50	10%	1.10
7	2.36	170422	401470	0.62	2.18	170419	370994	0.58	8%	1.08
8	3.06	170420	520876	1.33	2.73	170422	465938	1.19	12%	1.12
9	3.93	170420	669970	1.80	3.68	170420	626704	1.69	7%	1.07
10	4.18	170417	711946	2.81	4.15	170421	708080	2.80	1%	1.01
11	3.55	170423	604454	3.18	3.13	170399	532976	2.81	13%	1.13
12	3.03	170418	517046	0.39	2.62	170421	445872	0.34	16%	1.16
13	3.60	170424	614058	2.03	3.22	170426	548028	1.81	12%	1.12
14	3.07	170423	523678	0.46	2.85	170417	485286	0.42	8%	1.08
15	2.90	170425	493628	0.72	2.44	170418	415000	0.61	19%	1.19
16	3.49	170425	594614	0.63	2.83	170420	482834	0.51	23%	1.23
17	2.84	170396	483784	0.81	2.64	170424	449440	0.75	8%	1.08
18	3.13	170231	532556	1.14	2.87	170431	489830	1.05	9%	1.09
19	2.21	170412	376666	0.70	2.14	170415	364686	0.68	3%	1.03
20	4.14	170338	705318	1.62	3.49	170422	595608	1.37	18%	1.18
21	4.42	170405	752690	0.70	4.11	170405	700426	0.65	7%	1.07
22	3.40	170416	578840	0.54	2.90	170414	494902	0.46	17%	1.17
23	4.13	170399	703456	0.68	3.39	170420	577460	0.55	22%	1.22
24	4.66	170413	794528	1.01	4.04	170411	688236	0.87	15%	1.15
25	5.20	170412	885768	1.48	3.63	170416	618828	1.03	43%	1.43
26	2.99	170409	509898	0.97	2.79	170424	475272	0.91	7%	1.07
27	6.53	170411	1113446	0.51	6.38	170409	1086512	0.50	2%	1.02
28	3.67	170419	625790	0.47	3.17	170423	539968	0.40	16%	1.16
29	2.92	170420	497212	0.87	2.23	170422	380240	0.67	31%	1.31
30	4.03	170424	687446	1.98	3.55	170422	605768	1.74	13%	1.13
31	3.25	170422	553482	0.85	2.63	170426	448036	0.69	24%	1.24
32	5.64	170422	960452	2.14	4.09	170417	697628	1.55	38%	1.38
33	2.70	170420	460524	0.49	2.35	170422	401262	0.43	15%	1.15
<b>mean</b>	<b>3.66</b>	<b>170408</b>	<b>622873</b>	<b>1.18</b>	<b>3.23</b>	<b>170418</b>	<b>549708</b>	<b>1.05</b>	<b>0.14</b>	<b>1.14</b>

*Table A.26- Comparison between IDA results for Model C, target column chord rotation of 4.5% with dissipative connections ( $S_{max}$  25 mm) and hinged connections*

<i>Model C – target chord rotation 4.5% - <math>S_{max}</math> 50 mm</i>										
	<i>Dissipative connections</i>				<i>Hinged connections</i>				<i>Comparison</i>	
<i>TH-ID</i>	$q_{col+dev}$	$F_{u,col}$ [N]	$T_{el,col+dev}$ [N]	$SF_{col+dev}$	$q_{col}$	$F_{u,col}$ [N]	$T_{el,col}$ [N]	$SF_{col}$	$\frac{SF_{col+dev}}{SF_{col}}$	$\frac{q_{col+dev}}{q_{col}}$
1	3.03	170418	516234	2.17	2.80	170413	477190	2.01	8%	1.08
2	4.45	170416	758482	0.82	3.92	170415	667760	0.72	14%	1.14
3	5.40	170428	920260	1.50	5.68	170417	967360	1.58	-5%	0.95
4	3.32	170376	566354	0.84	2.40	170405	408956	0.60	38%	1.39
5	4.15	170389	707284	2.75	3.21	170404	546362	2.12	29%	1.29
6	2.67	170425	454992	0.61	2.21	170421	376916	0.50	21%	1.21
7	2.55	170421	434526	0.68	2.18	170419	370994	0.58	17%	1.17
8	3.58	170413	609666	1.56	2.73	170422	465938	1.19	31%	1.31
9	4.15	170420	706418	1.90	3.68	170420	626704	1.69	13%	1.13
10	4.13	170414	703622	2.78	4.15	170421	708080	2.80	-1%	0.99
11	4.09	170477	697142	3.67	3.13	170399	532976	2.81	31%	1.31
12	3.45	170413	588288	0.44	2.62	170421	445872	0.34	32%	1.32
13	3.98	170417	678034	2.24	3.22	170426	548028	1.81	24%	1.24
14	3.26	170417	555972	0.48	2.85	170417	485286	0.42	15%	1.15
15	3.18	170423	541136	0.79	2.44	170418	415000	0.61	30%	1.30
16	3.84	170420	654616	0.69	2.83	170420	482834	0.51	36%	1.36
17	3.03	170387	515792	0.86	2.64	170424	449440	0.75	15%	1.15
18	3.29	170360	560930	1.20	2.87	170431	489830	1.05	15%	1.15
19	2.30	170417	391516	0.73	2.14	170415	364686	0.68	7%	1.07
20	4.70	170409	801518	1.84	3.49	170422	595608	1.37	35%	1.35
21	4.71	170357	801550	0.74	4.11	170405	700426	0.65	14%	1.14
22	4.09	170374	697466	0.65	2.90	170414	494902	0.46	41%	1.41
23	4.72	170431	804216	0.77	3.39	170420	577460	0.55	39%	1.39
24	5.18	170439	882926	1.12	4.04	170411	688236	0.87	28%	1.28
25	5.50	170413	936938	1.56	3.63	170416	618828	1.03	51%	1.51
26	3.20	170417	545216	1.04	2.79	170424	475272	0.91	15%	1.15
27	7.26	170411	1236424	0.57	6.38	170409	1086512	0.50	14%	1.14
28	4.14	170425	705502	0.53	3.17	170423	539968	0.40	31%	1.31
29	3.34	170418	569438	1.00	2.23	170422	380240	0.67	50%	1.50
30	4.46	170388	760318	2.19	3.55	170422	605768	1.74	26%	1.26
31	3.92	170406	668148	1.02	2.63	170426	448036	0.69	49%	1.49
32	6.57	170416	1118802	2.49	4.09	170417	697628	1.55	60%	1.60
33	3.04	170419	518670	0.55	2.35	170422	401262	0.43	29%	1.29
<b>mean</b>	<b>4.02</b>	<b>170411</b>	<b>685103</b>	<b>1.30</b>	<b>3.23</b>	<b>170418</b>	<b>549708</b>	<b>1.05</b>	<b>0.26</b>	<b>1.26</b>

*Table A.27- Comparison between IDA results for Model C, target column chord rotation of 4.5% with dissipative connections ( $S_{max}$  50 mm) and hinged connections*

<i>Model C – target chord rotation 4.5% - <math>S_{max}</math> 75 mm</i>										
	<i>Dissipative connections</i>				<i>Hinged connections</i>				<i>Comparison</i>	
<i>TH-ID</i>	$q_{col+dev}$	$F_{u,col}$ [N]	$T_{el,col+dev}$ [N]	$SF_{col+dev}$	$q_{col}$	$F_{u,col}$ [N]	$T_{el,col}$ [N]	$SF_{col}$	$\frac{SF_{col+dev}}{SF_{col}}$	$\frac{q_{col+dev}}{q_{col}}$
1	3.14	170424	535646	2.25	2.80	170413	477190	2.01	12%	1.12
2	4.70	170411	800960	0.86	3.92	170415	667760	0.72	20%	1.20
3	5.29	170431	901412	1.47	5.68	170417	967360	1.58	-7%	0.93
4	3.65	170426	621524	0.92	2.40	170405	408956	0.60	52%	1.52
5	4.32	170382	735766	2.86	3.21	170404	546362	2.12	35%	1.35
6	2.92	170412	498170	0.67	2.21	170421	376916	0.50	32%	1.32
7	2.77	170430	472732	0.74	2.18	170419	370994	0.58	27%	1.27
8	4.24	170414	723314	1.85	2.73	170422	465938	1.19	55%	1.55
9	4.36	170419	743060	2.00	3.68	170420	626704	1.69	19%	1.19
10	4.09	170404	696956	2.76	4.15	170421	708080	2.80	-2%	0.98
11	4.44	170394	756754	3.99	3.13	170399	532976	2.81	42%	1.42
12	3.85	170395	656474	0.49	2.62	170421	445872	0.34	47%	1.47
13	4.23	170415	721298	2.38	3.22	170426	548028	1.81	32%	1.32
14	3.45	170417	588158	0.51	2.85	170417	485286	0.42	21%	1.21
15	3.44	170419	585842	0.86	2.44	170418	415000	0.61	41%	1.41
16	4.04	170417	687770	0.72	2.83	170420	482834	0.51	42%	1.42
17	3.12	170425	531604	0.89	2.64	170424	449440	0.75	18%	1.18
18	3.29	170360	560930	1.20	2.87	170431	489830	1.05	15%	1.15
19	2.37	170413	404076	0.75	2.14	170415	364686	0.68	11%	1.11
20	5.43	170424	925326	2.13	3.49	170422	595608	1.37	55%	1.55
21	4.99	170403	849888	0.78	4.11	170405	700426	0.65	21%	1.21
22	4.57	170424	779142	0.73	2.90	170414	494902	0.46	57%	1.57
23	5.13	170415	874734	0.84	3.39	170420	577460	0.55	51%	1.51
24	5.72	170319	974718	1.23	4.04	170411	688236	0.87	42%	1.42
25	5.79	170409	987404	1.65	3.63	170416	618828	1.03	60%	1.60
26	3.20	170420	545134	1.04	2.79	170424	475272	0.91	15%	1.15
27	8.36	170397	1424118	0.65	6.38	170409	1086512	0.50	31%	1.31
28	4.61	170425	785690	0.59	3.17	170423	539968	0.40	46%	1.46
29	3.54	170423	602862	1.06	2.23	170422	380240	0.67	59%	1.59
30	4.99	170388	850686	2.45	3.55	170422	605768	1.74	40%	1.40
31	4.66	170372	794270	1.22	2.63	170426	448036	0.69	77%	1.77
32	7.47	170414	1273470	2.84	4.09	170417	697628	1.55	83%	1.83
33	3.40	170426	579862	0.62	2.35	170422	401262	0.43	45%	1.45
<b>mean</b>	<b>4.35</b>	<b>170408</b>	<b>741508</b>	<b>1.39</b>	<b>3.23</b>	<b>170418</b>	<b>549708</b>	<b>1.05</b>	<b>0.36</b>	<b>1.36</b>

*Table A.28- Comparison between IDA results for Model C target column chord rotation of 4.5% with dissipative connections ( $S_{max}$  75 mm) and hinged connections*

<i>Model C – target chord rotation 4.5% - <math>S_{max}</math> 100 mm</i>										
	<i>Dissipative connections</i>				<i>Hinged connections</i>				<i>Comparison</i>	
<i>TH-ID</i>	$q_{col+dev}$	$F_{u,col}$ [N]	$T_{el,col+dev}$ [N]	$SF_{col+dev}$	$q_{col}$	$F_{u,col}$ [N]	$T_{el,col}$ [N]	$SF_{col}$	$\frac{SF_{col+dev}}{SF_{col}}$	$\frac{q_{col+dev}}{q_{col}}$
1	3.25	170417	554474	2.33	2.80	170413	477190	2.01	16%	1.16
2	4.95	170412	843702	0.91	3.92	170415	667760	0.72	26%	1.26
3	5.17	170461	881902	1.44	5.68	170417	967360	1.58	-9%	0.91
4	3.90	170319	664864	0.98	2.40	170405	408956	0.60	63%	1.63
5	4.68	170458	797376	3.10	3.21	170404	546362	2.12	46%	1.46
6	3.19	170426	543068	0.73	2.21	170421	376916	0.50	44%	1.44
7	2.95	170418	503044	0.78	2.18	170419	370994	0.58	36%	1.36
8	4.71	170417	802876	2.05	2.73	170422	465938	1.19	72%	1.72
9	4.57	170415	779010	2.10	3.68	170420	626704	1.69	24%	1.24
10	4.57	170406	778032	3.08	4.15	170421	708080	2.80	10%	1.10
11	4.82	170417	821122	4.32	3.13	170399	532976	2.81	54%	1.54
12	4.28	170423	729534	0.55	2.62	170421	445872	0.34	64%	1.64
13	4.29	170424	731170	2.41	3.22	170426	548028	1.81	33%	1.33
14	3.65	170418	622874	0.54	2.85	170417	485286	0.42	28%	1.28
15	3.71	170417	631888	0.92	2.44	170418	415000	0.61	52%	1.52
16	4.23	170416	720410	0.76	2.83	170420	482834	0.51	49%	1.49
17	3.12	170425	531604	0.89	2.64	170424	449440	0.75	18%	1.18
18	3.29	170360	560930	1.20	2.87	170431	489830	1.05	15%	1.15
19	2.45	170416	416884	0.77	2.14	170415	364686	0.68	14%	1.14
20	6.31	170065	1073004	2.47	3.49	170422	595608	1.37	80%	1.81
21	5.27	170395	897304	0.83	4.11	170405	700426	0.65	28%	1.28
22	5.10	170408	869206	0.81	2.90	170414	494902	0.46	76%	1.76
23	5.30	170407	902366	0.87	3.39	170420	577460	0.55	56%	1.56
24	6.33	170388	1078022	1.36	4.04	170411	688236	0.87	57%	1.57
25	6.09	170408	1037438	1.73	3.63	170416	618828	1.03	68%	1.68
26	3.34	170422	568576	1.08	2.79	170424	475272	0.91	20%	1.20
27	9.54	170400	1625522	0.74	6.38	170409	1086512	0.50	50%	1.50
28	5.12	170415	873188	0.65	3.17	170423	539968	0.40	62%	1.62
29	3.69	170417	628810	1.10	2.23	170422	380240	0.67	65%	1.65
30	5.54	170367	944298	2.72	3.55	170422	605768	1.74	56%	1.56
31	5.43	170400	925884	1.42	2.63	170426	448036	0.69	107%	2.07
32	8.44	170417	1437992	3.20	4.09	170417	697628	1.55	106%	2.06
33	3.76	170409	641330	0.68	2.35	170422	401262	0.43	60%	1.60
<b>mean</b>	<b>4.70</b>	<b>170400</b>	<b>800536</b>	<b>1.50</b>	<b>3.23</b>	<b>170418</b>	<b>549708</b>	<b>1.05</b>	<b>0.47</b>	<b>1.47</b>

*Table A.29- Comparison between IDA results for Model C, target column chord rotation of 4.5% with dissipative connections ( $S_{max}$  100 mm) and hinged connections*

<i>Model C – target chord rotation 4.5% - <math>S_{max}</math> 125 mm</i>										
	<i>Dissipative connections</i>				<i>Hinged connections</i>				<i>Comparison</i>	
<i>TH-ID</i>	$q_{col+dev}$	$F_{u,col}$ [N]	$T_{el,col+dev}$ [N]	$SF_{col+dev}$	$q_{col}$	$F_{u,col}$ [N]	$T_{el,col}$ [N]	$SF_{col}$	$\frac{SF_{col+dev}}{SF_{col}}$	$\frac{q_{col+dev}}{q_{col}}$
1	3.36	170410	573120	2.41	2.80	170413	477190	2.01	20%	1.20
2	5.20	170392	885614	0.96	3.92	170415	667760	0.72	33%	1.33
3	5.41	170414	922466	1.51	5.68	170417	967360	1.58	-5%	0.95
4	4.06	170429	691948	1.02	2.40	170405	408956	0.60	69%	1.69
5	5.00	170363	852328	3.31	3.21	170404	546362	2.12	56%	1.56
6	3.46	170416	589286	0.79	2.21	170421	376916	0.50	56%	1.56
7	3.11	170430	530306	0.83	2.18	170419	370994	0.58	43%	1.43
8	5.25	170417	894722	2.28	2.73	170422	465938	1.19	92%	1.92
9	4.78	170416	814364	2.19	3.68	170420	626704	1.69	30%	1.30
10	5.53	170415	942598	3.73	4.15	170421	708080	2.80	33%	1.33
11	5.31	170412	905228	4.77	3.13	170399	532976	2.81	70%	1.70
12	4.92	170437	837802	0.63	2.62	170421	445872	0.34	88%	1.88
13	4.48	170422	763630	2.52	3.22	170426	548028	1.81	39%	1.39
14	3.89	170420	663004	0.58	2.85	170417	485286	0.42	37%	1.37
15	3.98	170415	677890	0.99	2.44	170418	415000	0.61	63%	1.63
16	4.42	170416	752552	0.79	2.83	170420	482834	0.51	56%	1.56
17	3.12	170425	531604	0.89	2.64	170424	449440	0.75	18%	1.18
18	3.29	170360	560930	1.20	2.87	170431	489830	1.05	15%	1.15
19	2.52	170411	429816	0.80	2.14	170415	364686	0.68	18%	1.18
20	7.16	170500	1221510	2.81	3.49	170422	595608	1.37	105%	2.05
21	5.55	170405	945990	0.87	4.11	170405	700426	0.65	35%	1.35
22	5.30	170420	903632	0.85	2.90	170414	494902	0.46	83%	1.83
23	5.49	170421	935154	0.90	3.39	170420	577460	0.55	62%	1.62
24	6.65	170434	1133204	1.43	4.04	170411	688236	0.87	65%	1.65
25	6.38	170407	1086944	1.82	3.63	170416	618828	1.03	76%	1.76
26	3.45	170421	587938	1.12	2.79	170424	475272	0.91	24%	1.24
27	10.88	170410	1853880	0.85	6.38	170409	1086512	0.50	71%	1.71
28	5.34	170428	909796	0.68	3.17	170423	539968	0.40	68%	1.68
29	3.90	170423	664920	1.17	2.23	170422	380240	0.67	75%	1.75
30	5.68	170348	966902	2.78	3.55	170422	605768	1.74	60%	1.60
31	6.24	170389	1063004	1.63	2.63	170426	448036	0.69	137%	2.37
32	9.68	170412	1649160	3.68	4.09	170417	697628	1.55	136%	2.36
33	4.12	170415	701486	0.75	2.35	170422	401262	0.43	75%	1.75
<b>mean</b>	<b>5.06</b>	<b>170414</b>	<b>861901</b>	<b>1.62</b>	<b>3.23</b>	<b>170418</b>	<b>549708</b>	<b>1.05</b>	<b>0.58</b>	<b>1.58</b>

*Table A.30- Comparison between IDA results for Model C, target column chord rotation of 4.5% with dissipative connections ( $S_{max}$  125 mm) and hinged connections*

---

## LIST OF FIGURES

Figure 2.1- Distribution map of industrial buildings in Italy (Italian Revenue Agency 2012)..	7
Figure 2.2- Typical configuration of one-storey precast RC industrial buildings (Wood 2006)	8
Figure 2.3- Double-slope roof (Bonfanti et al. 2008) .....	10
Figure 2.4- Continuous plane roof (Bonfanti et al. 2008).....	10
Figure 2.5- Discontinuous plane roof (Bonfanti et al. 2008) .....	10
Figure 2.6- Shed roof (Bonfanti et al. 2008).....	10
Figure 2.7- Multi-storey precast building (Bonfanti et al. 2008).....	11
Figure 2.8- Double-slope roof without and with shed openings (Bonfanti et al. 2008).....	12
Figure 2.9- Plane roof with corrugated tiles (Bonfanti et al. 2008) .....	12
Figure 2.10- Shed roof with knee beams (Bonfanti et al. 2008) .....	13
Figure 2.11- Shed roof with inclined beams (Bonfanti et al. 2008).....	13
Figure 2.12- Classification of roof floor by in-plane stiffness: rigid, flexible and semi-rigid (Nascimbene and Bellotti 2013).....	14
Figure 2.13- Main characteristics of most common beams of current production (Bellotti et al. 2014).....	16
Figure 2.14- Main characteristics of most common roof floor elements of current production (Bellotti et al. 2014) .....	17
Figure 2.15- Different shapes of column tops: a) for rectangular or I-, L-, T-shaped beams; b) and c) with forks for double-slope beams; d) for H-shaped beams (Bellotti et al. 2014).....	18
Figure 2.16- Precast panels: a) horizontal panels fixed to the columns; b) vertical panels supporting on foundation (Bellotti et al. 2014) .....	19
Figure 2.17- Roof element-beam connection using steel angles (Magliulo et al. 2014c).....	20
Figure 2.18- Roof element-beam connections: a) steel angles and bolts; b) steel reinforcement and grout casting in-situ (Bellotti et al. 2014).....	20
Figure 2.19- Most common beam-column connections (Bellotti et al. 2014) .....	21
Figure 2.20- Dowel beam-column connection (Magliulo et al. 2014c).....	21

---

Figure 2.21- Socket column-foundation connection (Magliulo et al. 2014c) .....	22
Figure 2.22- Connection between vertical precast panel and resistant structure (a), channel bar (b), interlock (c) and connector (d) (Magliulo et al. 2014b) .....	22
Figure 2.23- Aerial photos of collapses of industrial precast buildings during 2012 Emilia earthquakes.....	24
Figure 2.24- Typical mode of collapse of single-storey precast structures due to loss of support in beam-column connections based on friction (Bonfanti et al. 2008) .....	27
Figure 2.25- Mode of vibration in absence of rigid-diaphragm effect (Bonfanti et al. 2008) .	27
Figure 2.26- Beam collapse due to absence of adequate lateral restraints (Bonfanti et al. 2008)	28
Figure 2.27- Shear failure due to short-column mechanism (Bonfanti et al. 2008).....	29
Figure 2.28- Framed structure with continuous joints (Circolare n. 617 2009).....	32
Figure 2.29- Framed structure with hinged joints (Circolare n. 617 2009) .....	33
Figure 2.30- Isostatic column structure (Circolare n. 617 2009) .....	33
Figure 3.1- Map of the area affected by Emilia earthquakes of May 2012 showing westward progressive move of epicentres (INGV 2012a).....	36
Figure 3.2- Map of seismic sequence of Emilia earthquakes from 20 <sup>th</sup> May to 20 <sup>th</sup> July 2012 (INGV 2013) .....	36
Figure 3.3- Permanent and temporary (installed after 20 <sup>th</sup> May 2012) stations of Strong Motion Network .....	37
Figure 3.4- Vertical, N-S and E-W recordings at Mirandola station during 20 <sup>th</sup> May 2012 event (Bournas et al. 2013) .....	37
Figure 3.5- Seismic zone classification in Italy (a) in 1984 and (b) in 2003; the black dot indicates the Emilia earthquakes epicentral zone (INGV 2012b) .....	39
Figure 3.6- Number of structures according to the year of construction in Emilia-Romagna (Deyanova et al. 2014) .....	39
Figure 3.7- Spectra of the N-S component of the 20 <sup>th</sup> and 29 <sup>th</sup> May 2012 events compared to the Italian code spectrum (Bournas et al. 2013).....	40

---

---

Figure 3.8- Elastic response spectra recorded on 20th May 2012 in Mirandola: N-S (green) and E-W component (blue) compared to elastic response spectra provided by Italian building code (Magliulo et al. 2014c) .....	41
Figure 3.9- Response spectra at Mirandola station of N-S (green dashed line) and E-W (blue line) components for the earthquakes of (a) 20 <sup>th</sup> May and (b) 29 <sup>th</sup> May 2012 (Bournas et al. 2013).....	42
Figure 3.10- Gross domestic product (GDP) per inhabitant, in purchasing power standard (PPS), by NUTS 2 regions (Eurostat regional yearbook 2011) .....	44
Figure 3.11- Aerial photo of collapses of industrial precast buildings during 2012 Emilia earthquakes.....	48
Figure 3.12- Synopsis of damages observed in more than 30 surveyed industrial buildings (Liberatore et al. 2013).....	50
Figure 3.13- Precast RC structure built during 70s-80s (Type 1) with double-slope beams and masonry infills (Savoia et al. 2012) .....	51
Figure 3.14- Precast RC structure built after 1990 (Type 2) with pre-stressed precast roof elements and precast cladding panels (Savoia et al. 2012) .....	51
Figure 3.15- Lightly damaged regular masonry infills (Savoia et al. 2012) .....	52
Figure 3.16- Damages in head portal frames avoided by regular masonry infills (Savoia et al. 2012).....	52
Figure 3.17- Unseating of the beam due to short-column mechanism because of interaction with partial-height masonry infills (Savoia et al. 2012).....	53
Figure 3.18- Collapses due to unseating of roof precast beams (Bournas et al. 2013) (Liberatore et al. 2013).....	55
Figure 3.19- Unseating of roof beams (Gruppo di Lavoro Agibilità Sismica dei Capannoni Industriali 2012) .....	56
Figure 3.20- Relative beam-column displacements without reaching loss of support.....	56
Figure 3.21- Unseating of main beam and consequent collapse of roof panels (Gruppo di Lavoro Agibilità Sismica dei Capannoni Industriali 2012) .....	57
Figure 3.22- Collapse of precast roof elements due to unseating (Gruppo di Lavoro Agibilità Sismica dei Capannoni Industriali 2012) .....	57

---

---

Figure 3.23- Unseating of the beam due to interaction with partial-height masonry infills and short-column shear failure (red arrow indicates the direction of seismic action) (Bournas et al. 2013).....	58
Figure 3.24- Rotation of the beam in the out-of-plane direction (Gruppo di Lavoro Agibilità Sismica dei Capannoni Industriali 2012) .....	58
Figure 3.25- Rotation of the beam in the out-of-plane direction (Liberatore et al. 2013) .....	59
Figure 3.26- Out-of-plane collapse of a double-slope precast beam after unseating following shear failure of the fork (Bournas et al. 2013) .....	59
Figure 3.27- Out-of-plane collapse of a double-slope precast beam after unseating following shear failure of the fork (Saitta et al. 2012).....	60
Figure 3.28- Collapse due to failure of the pinned beam-column connection (Bournas et al. 2013).....	61
Figure 3.29- Relative beam-column displacement, in spite of probable presence of mechanical connection device but without adequate transverse reinforcement (Gruppo di Lavoro Agibilità Sismica dei Capannoni Industriali 2012) .....	62
Figure 3.30- Loss of verticality of columns (Gruppo di Lavoro Agibilità Sismica dei Capannoni Industriali 2012).....	63
Figure 3.31- Rotation of columns increased by the impact of a fallen roof beam (Liberatore et al. 2013).....	63
Figure 3.32- Loss of verticality of a column and consequent reduction of beam seating length (Gruppo di Lavoro Agibilità Sismica dei Capannoni Industriali 2012).....	63
Figure 3.33- Cracking of the base section of the column (Gruppo di Lavoro Agibilità Sismica dei Capannoni Industriali 2012).....	64
Figure 3.34- Plastic hinge at column base after substantial rotation of the column (Liberatore et al. 2013).....	64
Figure 3.35- Plastic hinge at column base with concrete spalling and longitudinal bar buckling because of the lack of adequate transverse reinforcement in critical region (Gruppo di Lavoro Agibilità Sismica dei Capannoni Industriali 2012) .....	65
Figure 3.36- Short-column failure due to interaction with masonry infills .....	65

---

Figure 3.37- Concrete spalling at beam-column support due to absence of rubber pads (Liberatore et al. 2013).....	66
Figure 3.38- Failure of lateral forks at the top of the column (Liberatore et al. 2013) .....	66
Figure 3.39- Damaged lateral forks at the top of the column (Savoia et al. 2012) (Nascimbene and Bellotti 2013).....	66
Figure 3.40- Collapse of horizontal (a) and vertical precast panels (b) .....	67
Figure 3.41- Failure of horizontal precast panels connections (Magliulo et al. 2014c).....	68
Figure 3.42- Failure of vertical precast panels connections (Magliulo et al. 2014c).....	68
Figure 3.43- In-plane detachment of an exterior cladding element after failure of the connections with the main structure (Bournas et al. 2013) .....	69
Figure 3.44- Out-of-plane detachment of horizontal cladding due to high inertial forces that caused failure of fastenings (Bournas et al. 2013) .....	70
Figure 3.45- Out-of-plane overturning of exterior horizontal claddings (Bournas et al. 2013).....	71
Figure 4.1- Beam-column connections from a database of 40 precast RC industrial buildings from Emilia region in Italy (Deyanova et al. 2014) .....	72
Figure 4.2- Scheme of possible relative displacement between the beam and the column (Saitta et al. 2012) .....	73
Figure 4.3- Structural scheme of typical portal frame with simply supported beam over the columns (Saitta et al. 2012).....	73
Figure 4.4- Acceleration spectral ordinates recorded in Mirandola (Emilia – Italy) during the event of 20 <sup>th</sup> May 2012 compared to the friction coefficient (upper and lower bounds) evaluated by Magliulo et al. (2011) (Magliulo et al. 2014c).....	74
Figure 4.5- Safety factor of loss of support plotted versus fundamental periods for recorded acceleration time histories in Mirandola (Emilia – Italy) during the event of 20 <sup>th</sup> May 2012, assuming $\mu=0.13$ (Magliulo et al. 2014c) .....	75
Figure 4.6- Evaluation of the wind equivalent forces according to past Italian building codes (Magliulo et al. 2014c) .....	76
Figure 4.7- Ratios between the design shear demand $F_v$ in beam-column connection induced by wind, evaluated according to CNR 1967 (CNR67) and D.M. 1996 (DM96), and the	

---

---

connection friction strength $F_f$ , evaluated according friction coefficient $c$ equal to 0.35, 0.13, and 0.09, for the different case studies (Magliulo et al. 2014c).....	77
Figure 4.8- Scheme of a retrofitting solution for beam-column connections using cable restrainers (Bournas et al. 2013) .....	79
Figure 4.9- Retrofitting solution for beam-column connections (Magliulo et al. 2014d).....	79
Figure 4.10- Characteristic mode of collapse of carbon-steel thin section: (a) before buckling, (b) during buckling, (c) final shape .....	83
Figure 4.11- Mode of collapse of steel tubes with and without carbon fibre external wrapping	83
Figure 4.12- Proposed device made of carbon-wrapped steel tubes .....	84
Figure 5.1- Typical configuration of the steel tube wrapped by carbon fibre.....	85
Figure 5.2- Scheme of experimental setup.....	86
Figure 5.3- Sequence of frames of experimental test showing the progression of the plastic deformation of the device.....	87
Figure 5.4- Comparison of load-displacement curves between specimens with and without carbon fibre external wrapping showing contribution of carbon fibres in terms of increasing dissipation capacity .....	87
Figure 5.5- Experimental load-displacement curves of a steel tube simply wrapped with carbon fibre showing a high initial elastic peak load value .....	88
Figure 5.6- Experimental and trilinear equivalent curve in terms of absorbed energy .....	88
Figure 5.7- Specimens after quasi-static tests of compression.....	90
Figure 5.8- Experimental load-displacement curves for specimens of type A, B and C .....	91
Figure 5.9- Frequency distribution for $E_{diss}$ for specimens type C.....	93
Figure 5.10- Cyclic loading experimental test of compression on specimen type A.....	94
Figure 5.11- Shock experimental tests performing using a drop weight impact system .....	95
Figure 6.1- Examples of the introduction of dissipative devices in precast structures with different anchoring elements to the structure .....	98
Figure 6.2- Behaviour of the dissipative connection under seismic action.....	98
Figure 6.3- Subsequent phases of the behaviour of the device under compressive loading ....	99

---

Figure 6.4- Hysteretic cycle of the system composed by two devices.....	100
Figure 6.5- Beam span length and column aspect ratio for 60 precast RC industrial buildings from Italy (40 from the Emilia-Romagna region and 20 from other regions) (Deyanova et al. 2014).....	102
Figure 6.6- Scheme of most widespread typology of one-storey precast buildings .....	102
Figure 6.7- Scheme of typical portal frame of structural models.....	103
Figure 6.8- Force-displacement response of cantilever columns (Priestley et al. 2007) .....	106
Figure 6.9- Moment-curvature response (Priestley et al. 2007).....	106
Figure 6.10- Force-displacement response (Priestley et al. 2007) .....	107
Figure 6.11- Plastic hinge length and idealization of curvature distribution (Priestley et al. 2007).....	108
Figure 6.12- Stress-strain relation for reinforcing steel for Model A, B and C .....	109
Figure 6.13- Stress-strain relation for confined and unconfined concrete for Model A .....	109
Figure 6.14- Stress-strain relation for confined and unconfined concrete for Model B .....	110
Figure 6.15- Stress-strain relation for confined and unconfined concrete for Model C .....	110
Figure 6.16- Moment-curvature relation for Model A.....	110
Figure 6.17- Moment-curvature relation for Model B .....	111
Figure 6.18- Moment-curvature relation for Model C .....	111
Figure 6.19- Force-displacement relation for Model A .....	111
Figure 6.20- Force-displacement relation for Model B.....	112
Figure 6.21- Force-displacement relation for Model C.....	112
Figure 6.22- Set of time histories selected using REXEL spectrum-compatible for the site of Finale Emilia (MO) - Italy .....	114
Figure 6.23- Ground-motion recording stations during Emilia earthquakes (temporary stations were installed after the event of May 20 <sup>th</sup> 2012).....	115
Figure 6.24- Scheme of structural model used for SAP2000 numerical analyses .....	121
Figure 6.25- Modified Takeda hysteretic rule.....	121

---

---

Figure 6.26- Hysteresis cycle of the dissipative device (System b, Time history 42ya) .....	122
Figure 6.27- Relative beam-column displacement (System b, Time history 42ya).....	123
Figure 6.28- Base shear reduction with dissipative connections (Time history 42ya) .....	123
Figure 6.29- Scheme of structural model used for analyses performed using OpenSees .....	125
Figure 6.30- Elastic-Perfectly Plastic Gap Material in OpenSees .....	126
Figure 6.31- Elastic-Perfectly Plastic Material in OpenSees .....	128
Figure 6.32- Geometric coordinate transformation in OpenSees.....	129
Figure 6.33- Section degree-of-freedom for the command “Section Aggregator” in OpenSees	131
Figure 6.34- Hysteretic Material in OpenSees .....	132
Figure 6.35- Variation of modal damping ratios with natural frequency (Chopra 2006) .....	135
Figure 7.1- IDA curve (Model C - 29May-MRN record – $S_{max}$ 70 mm).....	141
Figure 7.2- Base shear values for the system with dissipative devices and the equivalent elastic system (Model C - 29May-MRN record – $S_{max}$ 70 mm) .....	141
Figure 7.3- Relative beam-column displacement and forces on the dissipative devices (Model C - 29May-MRN record – $S_{max}$ 70 mm).....	142
Figure 7.4- Hysteresis cycle of the dissipative devices (Model C - 29May-MRN record – $S_{max}$ 70 mm) .....	142
Figure 7.5- IDA curve (Model B – TH-ID 7 Large Magnitude – Large Distance scenario – friction 0.05 - $S_{max}$ 75 mm) .....	145
Figure 7.6- Base shear values for the system with dissipative devices and the equivalent elastic system (Model B – TH-ID 7 Large Magnitude – Large Distance scenario –friction 0.05 - $S_{max}$ 75 mm) .....	145
Figure 7.7- Beam-column friction forces (Model B – TH-ID 7 Large Magnitude – Large Distance scenario –friction 0.05 - $S_{max}$ 75 mm) .....	145
Figure 7.8- Relative beam-column displacement and forces on the dissipative devices (Model B – TH-ID 7 Large Magnitude – Large Distance scenario –friction 0.05 - $S_{max}$ 75 mm).....	146
Figure 7.9- Hysteresis cycle of the dissipative devices (Model B – TH-ID 7 Large Magnitude – Large Distance scenario –friction 0.05 - $S_{max}$ 75 mm).....	146

---

Figure 7.10- Behaviour factor $q$ versus PGD (Model A, Large Magnitude – Large Distance scenario) .....	148
Figure 7.11- Behaviour factor $q$ versus PGV (Model A, Large Magnitude – Large Distance scenario) .....	149
Figure 7.12- Behaviour factor $q$ versus PGA (Model A, Large Magnitude – Large Distance scenario) .....	149
Figure 7.13- Behaviour factor $q$ versus $I_A$ (Model A, Large Magnitude – Large Distance scenario) .....	149
Figure 7.14- IDA curve (Model A – TH-ID 1 - $S_{max}$ 75 mm – column chord rotation 4.5%)	153
Figure 7.15- Base shear values for the system with dissipative devices and the equivalent elastic system (Model A – TH-ID 1 - $S_{max}$ 75 mm – column chord rotation 4.5%) .....	154
Figure 7.16- Relative beam-column displacement (Model A – TH-ID 1 - $S_{max}$ 75 mm – column chord rotation 4.5%).....	154
Figure 7.17- Beam-column friction forces (Model A – TH-ID 1 - $S_{max}$ 75 mm – column chord rotation 4.5%).....	154
Figure 7.18- Moment-curvature relation of column (Model A – TH-ID 1 - $S_{max}$ 75 mm – column chord rotation 4.5%).....	155
Figure 7.19- Hysteresis cycle of the dissipative devices (Model A – TH-ID 1 - $S_{max}$ 75 mm – column chord rotation 4.5%).....	155
Figure 7.20- Force-displacement relation for elastic and inelastic response of the systems with and without dissipative connections.....	163
Figure 7.21- Ratio between behaviour factor values resulting from IDA analyses for the systems with dissipative and hinged connections for different maximum device deformation values $S_{max}$ for Model A and a target column chord rotation of 3% .....	167
Figure 7.22- Ratio between behaviour factor values resulting from IDA analyses for the systems with dissipative and hinged connections for different maximum device deformation values $S_{max}$ for Model A and a target column chord rotation of 4.5% .....	168
Figure 7.23- Ratio between behaviour factor values resulting from IDA analyses for the systems with dissipative and hinged connections for different maximum device deformation values $S_{max}$ for Model B and a target column chord rotation of 3% .....	168

---

---

Figure 7.24- Ratio between behaviour factor values resulting from IDA analyses for the systems with dissipative and hinged connections for different maximum device deformation values $S_{max}$ for Model B and a target column chord rotation of 4.5% .....	168
Figure 7.25- Ratio between behaviour factor values resulting from IDA analyses for the systems with dissipative and hinged connections for different maximum device deformation values $S_{max}$ for Model C and a target column chord rotation of 3% .....	169
Figure 7.26- Ratio between behaviour factor values resulting from IDA analyses for the systems with dissipative and hinged connections for different maximum device deformation values $S_{max}$ for Model C and a target column chord rotation of 4.5% .....	169
Figure 7.27- Comparison between behaviour factor values resulting from IDA analyses and calculated with the simplified approach for different maximum device deformation values $S_{max}$ for Model A and a target column chord rotation of 3% .....	171
Figure 7.28- Comparison between behaviour factor values resulting from IDA analyses and calculated with the simplified approach for different maximum device deformation values $S_{max}$ for Model A and a target column chord rotation of 4.5% .....	171
Figure 7.29- Comparison between behaviour factor values resulting from IDA analyses and calculated with the simplified approach for different maximum device deformation values $S_{max}$ for Model B and a target column chord rotation of 3% .....	172
Figure 7.30- Comparison between behaviour factor values resulting from IDA analyses and calculated with the simplified approach for different maximum device deformation values $S_{max}$ for Model B and a target column chord rotation of 4.5% .....	172
Figure 7.31- Comparison between behaviour factor values resulting from IDA analyses and calculated with the simplified approach for different maximum device deformation values $S_{max}$ for Model C and a target column chord rotation of 3% .....	173
Figure 7.32- Comparison between behaviour factor values resulting from IDA analyses and calculated with the simplified approach for different maximum device deformation values $S_{max}$ for Model C and a target column chord rotation of 4.5% .....	173

---

---

## LIST OF TABLES

Table 2.1- Distribution of Italian industrial buildings by regions (Italian Revenue Agency 2012).....	7
Table 2.2- Distribution of non-residential buildings by structural typology and use (Nutti and Vanzi 2014).....	8
Table 2.3- Italian Building Code evolution overview (Magliulo et al. 2014c).....	30
Table 3.1- Seismic events with $M_L > 5$ recorded during 2012 Emilia sequence (QUEST INGV Working Group 2012).....	35
Table 3.2- Maximum recorded PGA, PGV and PGD at Mirandola for 20 <sup>th</sup> and 29 <sup>th</sup> May 2012 events (Bournas et al. 2013).....	37
Table 5.1- Dimensions and characteristics of tested specimens of type A, B and C.....	85
Table 5.2- Results of experimental tests on standard and weakened specimens of type C.....	90
Table 5.3- Results of performed tests for specimens of type A, B and C.....	92
Table 6.1- Parameters of the three structural models with columns performing linear elastic behaviour.....	103
Table 6.2- Parameters of the three structural models with columns performing nonlinear behaviour.....	104
Table 6.3- Nonlinear column capacity parameters of Model A, B and C.....	113
Table 6.4- Characteristics of ground motions selected using REXEL.....	114
Table 6.5- Characteristics of records from 2012 Emilia earthquakes.....	115
Table 6.6- Large Magnitude – Large Distance scenario ground motions.....	117
Table 6.7- Large Magnitude – Small Distance scenario ground motions.....	118
Table 6.8- Small Magnitude – Small Distance scenario ground motions.....	119
Table 6.9- Results of time history analyses for Systems a, b and c.....	124
Table 7.1- Parameters of Model A, B and C with columns performing linear elastic behaviour.....	138
Table 7.2- IDA analyses results for Model A, 2012 Emilia records, $S_{max}$ of 70 and 120 mm (no friction).....	139

---

Table 7.3- IDA analyses results for Model B, 2012 Emilia records, $S_{max}$ of 70 and 120 mm (no friction) .....	140
Table 7.4- IDA analyses results for Model C, 2012 Emilia records, $S_{max}$ of 70 and 120 mm (no friction) .....	140
Table 7.5- Behaviour factor for target device deformation of 70 mm and 120 mm (no friction) for Model A, B and C.....	143
Table 7.6- Behaviour factor (mean values) for a target device deformation of 75 mm for three different Magnitude-Distance scenarios for Model A, B and C .....	147
Table 7.7- Parameters of Model A, B and C with columns performing nonlinear behaviour	150
Table 7.8- IDA results for Model A, target column chord rotation 4.5%, $S_{max}$ 75 mm.....	152
Table 7.9- Behaviour factor (mean values) for different maximum device deformation capacities and target column chord rotation for Model A, B and C.....	156
Table 7.10- IDA results for Model A with hinged connections, target column chord rotation 4.5%.....	157
Table 7.11- Behaviour factor (mean values) for different target column chord rotation for Model A, B and C with hinged connections .....	158
Table 7.12- Comparison between IDA results for Model A, target column chord rotation of 4.5% with dissipative connections ( $S_{max}$ 75 mm) and hinged connections.....	160
Table 7.13- Difference in behaviour factor values between dissipative and hinged connections for Model A, B and C for different maximum device deformation values $S_{max}$ for target column chord rotation of 3% .....	161
Table 7.14- Difference in behaviour factor values between dissipative and hinged connections for Model A, B and C for different maximum device deformation values $S_{max}$ for target column chord rotation of 4.5% .....	161
Table 7.15- Difference in maximum displacement values between the equivalent elastic systems of the structure with dissipative and hinged connections for Model A, B and C for different maximum device deformation values $S_{max}$ for target column chord rotation of 3%	164
Table 7.16- Difference in maximum displacement values between the equivalent elastic systems of the structure with dissipative and hinged connections for Model A, B and C for different maximum device deformation values $S_{max}$ for target column chord rotation of 4.5%	165

---

Table 7.17- Comparison between behaviour factor values computed using the simplified formula and found as results of IDA analyses for Model A, B and C for different maximum device deformation values  $S_{max}$  for target column chord rotation of 3% ..... 166

Table 7.18- Comparison between behaviour factor values computed using the simplified formula and found as results of IDA analyses for Model A, B and C for different maximum device deformation values  $S_{max}$  for target column chord rotation of 4.5% ..... 167

Table 7.19- Comparison between trend line equation of IDA analyses results and simplified formula proposed for Model A, B and C for target column chord rotation of 3 and 4.5% .... 170

---

## REFERENCES

- Bellotti D, Casotto C, Crowley H, et al (2014) Capannoni monopiano prefabbricati: distribuzione probabilistica dei sistemi e sottosistemi strutturali dagli anni sessanta ad oggi (in Italian). *Progettazione Sismica* 5:41–70. doi: 10.7414/PS.5.3.41-70
- Biondini F, Titi A, Toniolo G (2013) Prestazioni sismiche di strutture prefabbricate con connessioni trave-pilastro ad attrito (in Italian). In: XV Convegno ANIDIS. Padova, Italy, pp 1–8
- Bonfanti C, Carabellese A, Toniolo G (2008) Strutture prefabbricate: catalogo delle tipologie esistenti (in Italian). Progetto triennale 2005/08-DPC/RELUIS
- Bournas DA, Negro P, Taucer FF (2013) Performance of industrial buildings during the Emilia earthquakes in Northern Italy and recommendations for their strengthening. *Bulletin of Earthquake Engineering* 12:2383–2404. doi: 10.1007/s10518-013-9466-z
- Braga F, Gigliotti R, Monti G, et al (2014) Speedup of post earthquake community recovery: the case of precast industrial buildings after the Emilia 2012 earthquake. *Bulletin of Earthquake Engineering* 12:2405–2418. doi: 10.1007/s10518-014-9583-3
- Chopra AK (2006) *Dynamics of structures*, 3rd Ed. Pearson Prentice Hall
- Circolare M.LL.PP. n. 1422 (1965) Progettazione, calcolo e collaudo, di strutture prefabbricate nelle costruzioni edilizie in zone non sismiche.
- Circolare n. 617 (2009) Istruzioni per l'applicazione delle Nuove norme tecniche per le costruzioni di cui al Decreto Ministeriale 14/01/2008. Circolare Ministero delle Infrastrutture e Trasporti, G.U. n. 47 del 26/2/2009.
- Consiglio Superiore dei Lavori Pubblici (2012) Valutazione della vulnerabilità e interventi per le costruzioni ad uso produttivo in zona sismica (in Italian).
- CSI Computers and Structures Inc. (2013) *Analysis Reference Manual for SAP2000, ETABS, SAFE and CSiBridge*. Berkeley, CA, USA
- D.M. 14/01/2008 Norme tecniche per le costruzioni.
- D.M. 3/12/1987 Norme tecniche per la progettazione, esecuzione e collaudo delle costruzioni prefabbricate.
- Decreto Legge n. 74 6 giugno 2012 Interventi urgenti in favore delle popolazioni colpite dagli eventi sismici che hanno interessato il territorio delle province di Bologna, Modena, Ferrara, Mantova, Reggio Emilia e Rovigo, il 20 e il 29 maggio 2012.
- Deyanova M, Pampanin S, Nascimbene R (2014) Assessment of single-storey precast concrete industrial buildings with hinged beam-column connections with and without dowels. In: *Second European Conference on Earthquake Engineering and Sismology*. Istanbul, Turkey, pp 1–14
- Eurostat regional yearbook (2011) *Gross Domestic Product*.
- Fischinger M, Kramar M, Isaković T (2008) Cyclic response of slender RC columns typical of precast industrial buildings. *Bulletin of Earthquake Engineering* 6:519–534.
- Gruppo di Lavoro Agibilità Sismica dei Capannoni Industriali (2012) *Linee di indirizzo per*
-

- 
- interventi locali e globali su edifici industriali monopiano non progettati con criteri antisismici (in Italian).
- Iervolino I, Galasso C, Cosenza E (2010) REXEL: Computer aided record selection for code-based seismic structural analysis. *Bulletin of Earthquake Engineering* 8:339–362. doi: 10.1007/s10518-009-9146-1
- INGV (2012a) Sequenza pianura padana emiliana. In: INGV Terremoti. <https://ingvterremoti.wordpress.com/>.
- INGV (2013) Sequenza sismica 20 maggio-20 luglio. In: INGV. <http://terremoti.ingv.it/>.
- INGV (2012b) Mappa delle zone sismiche. In: INGV. <http://zonesismiche.mi.ingv.it/>.
- Italian Revenue Agency (2012) Observatory of the real estate market 2012 (in Italian).
- Legge n. 122 1 agosto 2012 Interventi urgenti in favore delle popolazioni colpite dagli eventi sismici che hanno interessato il territorio delle province di Bologna, Modena, Ferrara, Mantova, Reggio Emilia e Rovigo, il 20 e il 29 maggio 2012.
- Legge n. 1224 (1964) Provvedimenti per l'edilizia, con particolari prescrizioni per le zone sismiche.
- Legge n. 1684 (1962) Provvedimenti per l'edilizia, con particolari prescrizioni per le zone sismiche.
- Legge n. 64 (1974) Provvedimenti per le costruzioni con particolari prescrizioni per le zone sismiche.
- Liberatore L, Sorrentino L, Liberatore D, Decanini LD (2013) Failure of industrial structures induced by the Emilia (Italy) 2012 earthquakes. *Engineering Failure Analysis* 34:629–647. doi: 10.1016/j.engfailanal.2013.02.009
- Ligabue V, Bovo M, Savoia M (2014) Connessioni tegolo-trave: studio sperimentale e numerico del comportamento di angolari di collegamento (in Italian). In: Workshop "Tecniche innovative per il miglioramento sismico di edifici prefabbricati." SAIE Bologna, Italy, pp 75–84
- Lima RM, Ismarrubie ZN, Zainudin ES, Tang SH (2011) Axial behavior of steel tube wrapped by composite as energy absorber under compressive load. In: *IEEE Symposium on Business, Engineering and Industrial Applications*. pp 10–15
- Magliulo G, Capozzi V, Fabbrocino G, Manfredi G (2011) Neoprene-concrete friction relationships for seismic assessment of existing precast buildings. *Engineering Structures* 33:535–538. doi: 10.1016/j.engstruct.2010.11.011
- Magliulo G, Cimmino M, Ercolino M, Manfredi G (2014a) Prove cicliche a taglio sulla connessione Sicurlink tra trave e pilastro prefabbricati (in Italian). In: Workshop "Tecniche innovative per il miglioramento sismico di edifici prefabbricati." SAIE Bologna, Italy, pp 43–52
- Magliulo G, Ercolino M, Manfredi G (2014b) Influence of cladding panels on the first period of one-story precast buildings. *Bulletin of Earthquake Engineering*. doi: 10.1007/s10518-014-9657-2
- Magliulo G, Ercolino M, Petrone C, et al (2014c) The Emilia earthquake: seismic performance of precast reinforced concrete buildings. *Earthquake Spectra* 30:891–912. doi: 10.1193/091012EQS285M
-

- 
- Magliulo G, Ercolino M, Petrone C, et al (2014d) Why Did Many Precast Rc Buildings Collapse During the 2012 Emilia Earthquakes? In: Second European Conference on Earthquake Engineering and Seismology. Istanbul, Turkey, pp 1–11
- Magliulo G, Fabbrocino G, Manfredi G (2008) Seismic assessment of existing precast industrial buildings using static and dynamic nonlinear analyses. *Engineering Structures* 30:2580–2588. doi: 10.1016/j.engstruct.2008.02.003
- Mandelli Contegni M, Palermo A, Toniolo G (2008) Strutture prefabbricate: schedario di edifici prefabbricati in c.a. (in Italian). Progetto triennale 2005/08-DPC/RELUIS
- Mandelli Contegni M, Palermo A, Toniolo G (2007) Strutture prefabbricate: schedario dei collegamenti (in Italian). Progetto triennale 2005/08-DPC/RELUIS
- Mander JB, Priestley MJN, Park R (1988) Theoretical Stress-Strain Model for Confined Concrete. *Journal of Structural Engineering* 114:1804–1826.
- Marinini L, Spatti P, Riva P, Nascimbene R (2011) Strutture prefabbricate: moderni sistemi di protezione antisismica (in Italian). *Progettazione Sismica* 3:23–44.
- Mazzoni S, McKenna F, Scott MH, Fenves GL (2006) OpenSees command language manual.
- Muciaccia G, Cervio M, Franzoso M, Veneziano M (2014) Utilizzo di ancoraggi post-inseriti in interventi di recupero di capannoni industriali in zona sismica (in Italian). In: Workshop “Tecniche innovative per il miglioramento sismico di edifici prefabbricati.” SAIE Bologna, Italy, pp 107–118
- Nascimbene R, Bellotti D (2013) Progettazione di interventi di adeguamento per capannoni prefabbricati (in Italian).
- Negro P, Toniolo G (2012) Design Guidelines for Connections of Precast Structures under Seismic Actions. JRC scientific and policy reports
- Nuti C, Vanzi I (2014) Retrofitting of Industrial Structure. In: International Seminar and Exhibition on Recent Developments in Design and Construction for Precast Concrete Technology – REDECON. Bangalore, India - 9-13 November 2014, pp 1–10
- O.P.C.M. n. 3274 (2003) Primi elementi in materia di criteri generali per la classificazione sismica del territorio nazionale e di normative tecniche per le costruzioni in zona sismica.
- O.P.C.M. n. 3431 (2005) Primi elementi in materia di criteri generali per la classificazione sismica del territorio nazionale e di normative tecniche per le costruzioni in zona sismica.
- Olgiati M, Negro P, Bournas D (2011) Literature survey and identification of needs—part two: general survey and design procedures. Contribution of the Joint Research Centre. SAFECast-Deliverable 1.2. Grant agreement no. 218417-2
- Priestley MJN, Calvi GM, Kowalsky MJ (2007) Displacement Based Seismic Design of Structures, IUSS Press. Pavia
- QUEST INGV Working Group (2012) Rapporto macrosismico sui terremoti del 20 (ML 5.9) e del 29 maggio 2012 (ML 5.8 e 5.3) nella pianura padano-emiliana (in Italian).
- Regione Emilia-Romagna (2013) Dossier “A un anno dal terremoto” (in Italian). [www.regione.emilia-romagna.it/a-un-anno-dal-terremoto](http://www.regione.emilia-romagna.it/a-un-anno-dal-terremoto).
- Saitta F, Bongiovanni G, Buffarini G, et al (2012) Behaviour of industrial buildings in the
-

- Pianura Padana Emiliana Earthquake. *Energia, Ambiente e Innovazione* 47–57.
- Savoia M, Mazzotti C, Buratti N, et al (2012) Danneggiamento e crolli negli edifici prefabbricati a seguito del terremoto dell'Emilia (in Italian). *INARCOS* 728:35–45.
- Song H-W, Wan Z-M, Xie Z-M, Du X-W (2000) Axial impact behavior and energy absorption efficiency of composite wrapped metal tubes. *International Journal of Impact Engineering* 24:385–401.
- Toniolo G, Colombo A (2012) Precast concrete structures: the lessons learned from the L'Aquila earthquake. *Structural Concrete* 73–83.
- Vamvatsikos D, Cornell CA (2002) Incremental dynamic analysis. *Earthquake Engineering & Structural Dynamics* 31:491–514. doi: 10.1002/eqe.141
- Wood SL (2006) Seismic rehabilitation of low-rise precast industrial buildings in Turkey. *Advances in earthquake engineering for urban risk reduction (NATO science series: IV: earth and environmental sciences)* 66:167–177.